MULTIDISCIPLINARY ANALYSIS OF THE ENERGETICS AND MECHANISM OF ASSEMBLY OF AMYLOID OLIGOMERIC PRECURSORS

David Ruzafa Ruiz

Abril de 2014

Departamento de Química Física

UNIVERSIDAD DE GRANADA

Directores: Dr. D. Francisco Conejero Lara y Dr. D. Bertrand Morel

El doctorando David Ruzafa Ruiz y los directores de la tesis Francisco Conejero Lara y Bertrand Morel Garantizamos, al firmar esta tesis doctoral, que el trabajo ha sido realizado por el doctorando bajo la dirección de los directores de la tesis y hasta donde nuestro conocimiento alcanza, en la realización del trabajo, se han respetado los derechos de otros autores a ser citados, cuando se han utilizado sus resultados o publicaciones.

Granada a 21 de abril de 2014

Doctorando

Fdo.:   David Ruzafa Ruiz

Directores de la Tesis

Fdo.: Dr. Francisco Conejero Lara   Fdo.: Dr. Bertrand Morel

Contents

II

Chapter 3

Modulation of the Stability of Amyloidogenic Precursors by Anion Binding Strongly Influences the Rate of Amyloid Nucleation

Chapter 4

Mapping the Structure of Amyloid Nucleation Precursors by Protein Engineering Kinetic Analysis

Chapter 5

**N-terminal Acetylation of α–synuclein Reduces the Population of
Partially Folded Oligomers and Inhibits Amyloid Aggregation
Induced by SDS**..**163**

Chapter 6

Appendix

Chapter 1

INTRODUCTION AND OBJECTIVES

INTRODUCTION

The impact of amyloid fibril aggregation in human health

Proteins are very versatile macromolecular polymers consisting of one or more chains constituted by amino acids. Most of the essential structure and functions of cells are mediated by proteins. They are widely implied in the skeleton, control senses, muscles mobility, food digestion, defenses against infections and feeling process. No other macromolecule shows such versatility in their functions. A fundamental principle in protein science is that "protein structure leads to protein function" [1]. The correct folding in proteins is a crucial step in the conversion of genetic information in biologic activity in the living beings. Figure 1 illustrates the different possible fates of a polypeptide chain after its synthesis at the ribosome. A polypeptide of 100 amino acids, if each one only could adopt 2 positions, would have $1.26 \ 10^{30}$ possible different conformations, if we assume that each conformation only takes 10^{-11} s, the folding process would take $\sim 10^{11}$ years. This is the Levinthal paradox, who enounced this problem in 1968[2]. However, this is a wonder of nature is that, after the synthesis of proteins in the cell, most of them are able to natively fold in their biologically active conformation, either in a spontaneous way or assisted by chaperons and other factors.

A small fraction of the proteins are incorrectly folded despite the existence of exigent mechanisms of control of protein aggregation in the cell. Under certain metabolic circumstances (stress, cell aging or the presence of exogenous or infectious agents) some misfolded proteins or peptides form highly-organized aggregates rich in cross-beta sheet, which deposit extracellular aggregates and/or intracellular inclusions commonly known as amyloid. The name amyloid comes from the early mistaken identification by Rudolf Virchow of the substance as starch (amylum in Latin) in 1854. For a period, the scientific community debated whether or not amyloid deposits are fatty or carbohydrate deposits until it was finally found (in 1859) that they are, in fact, deposits of proteinaceous material [3]. Those fibrillar aggregates, structurally and morphologically similar to the amyloid fibrils, also form inside the cells in some diseases. Since in 1907 Alois Alzheimer [4] described for the first time senile plaques

and neurofibrillar tangles in a middle-aged woman affected by memory deficits, the number of diseases related with amyloid aggregates has increased continuously.
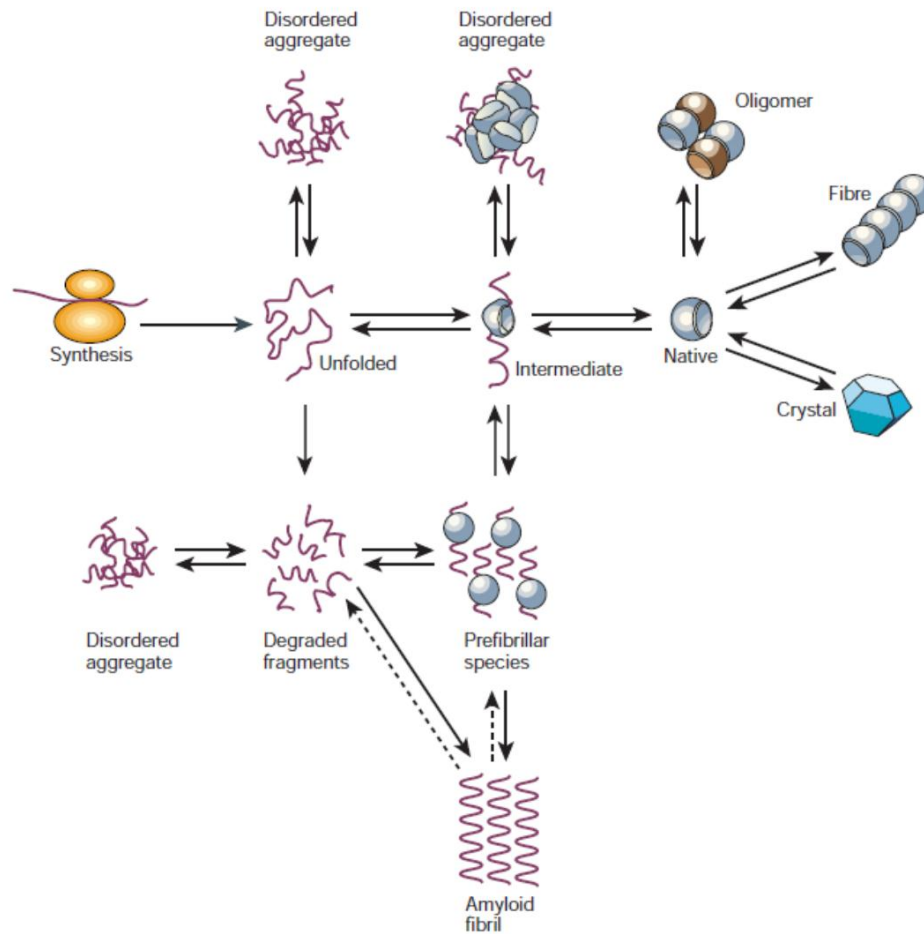
Figure 1. General view of the states accessible of a polypeptide chain after its synthesis in the ribosome. *Image adapted from Dobson et al [5].*

To date there are more than 30 diseases, some sporadic and/or hereditary and some transmissible, associated with amyloid deposits. This type of diseases is known under the generic name of protein deposition diseases. Among these, there are some of the most devastating neurodegenerative diseases, such as Alzheimer, Parkinson and Huntington diseases. Some of those diseases are listed in Table 1. In other diseases

unrelated to the central nervous system, the protein aggregates are deposited in tissues or organs impairing severely their function. This group of diseases infringes an enormous social and personal damage and it is crucial therefore to understand in detail the mechanisms of their genesis and to learn how to treat and prevent them.

Table 1. *Some examples of diseases associated with amyloid deposits. Adapted from Rochet et al[6]*

Disease	Aggregating protein or peptide	References
Alzheimer	Amyloid β peptide (Abeta)	[7,8]
Parkinson	α-Synuclein (aSyn)	[9-11]
Huntington	Huntingtin with poly-Q expansion	[10,12,13]
Frontotemporal dementia	Tau protein	[9,10,14]
Spongiform encephalopathies and Jakob disease	Prions or fragments	[15]
Amyotrophic lateral sclerosis	Superoxide dismutase I	[16]
Primary Systemic AL Amyloidosis	Immunoglobulin light-chain or fragments	[17]
Haemodialysis-related amyloidosis	β2-microglobulin	[18]
Type II diabetes	Amylin or islet amyloid polypeptide	[19]
Cataracts	γ-crystalline	[20]

Hereditary systemic amyloidosis	Lysozyme	[21] [22]
Aortic medial amyloid	Medin	[23]
Familial British dementia	ABri	[24-26]
Finnish-type familial amyloidosis	Gelsolin	[27]
Secondary systemic amyloidosis	Serum amyloid A	[22]
Senile systemic amyloidosis and familial amyloid polyneuropathy	Transthyretin	[21] [22,28]

Morphology and structure of amyloid aggregates and fibrils

Despite the lack of sequence homology or the length of the polypeptide chain of the proteins related to amyloidosis, the extracellular fibrillar deposits associated to these diseases share well-defined properties, such as the external morphology or the highly ordered internal structure. The research based on transmission electron microscopy (TEM) and atomic force microscopy (AFM) shows long and straight fibrils without ramification [29-31] or associated laterally to form ribbons[32]. Those fibrils present a diameter of 6-12 nm and are composed of a number of twisted filaments (Figure 2). According to the X-ray diffraction studies, the protein is arranged in each filament in a highly-ordered cross-β structure, forming β-sheets that extend throughout the entire length of the fibrils [33]. They interact with specific dyes such as Congo red or thioflavin T (ThT) and have a characteristic circular dichroism (CD) and infrared spectra, typical of a high content in β-sheet secondary structure [34]. The most recent advances in magic angle spinning, solid-state nuclear magnetic resonance (NMR) spectroscopy applied to amyloid fibrils [35,36], together with the recent success in growing

nano- and micro-crystals of short peptides with amyloid characteristics[37,38], have allowed to obtain a great level of detail in the internal molecular structure of the fibrils. Detailed information about the structure of amyloid fibrils has also come from amide hydrogen-deuterium studies combined with high-resolution NMR and mass spectrometry[39-42]. Interestingly enough, these methodologies have also established that amyloid fibrils are dynamic structures that can undergo a recycling of molecules in equilibrium between the bulk solution and the fibril ends [40]. This observation has important implications in the design of therapeutic strategies, especially because increasing evidence indicates that the true toxic species to cells are dynamic soluble oligomeric species[43-45], which, as it is described aftherwards, are product of self-association of proteins and act as precursors in the amyloidogenic process.
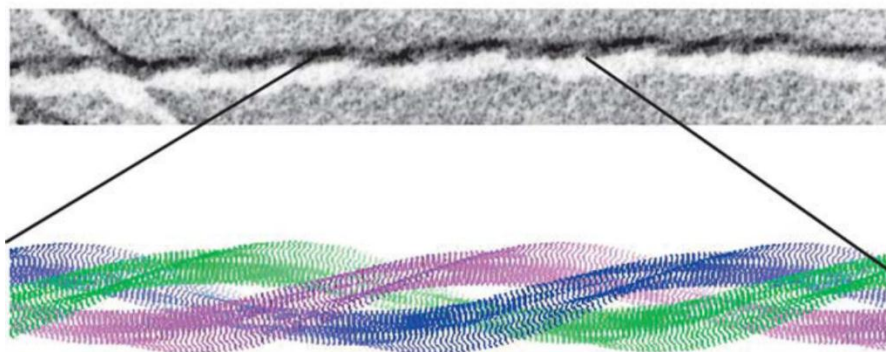
Figure 2. Transmission electron microscopy images of amyloid fibrils of amylin and model of structure of an amyloid fibril formed by filaments of β-sheets. *Image adapted from Goldsbury et al* **[31]**.

The fibrillar structures appear to be stabilized by a high density of hydrogen bonds between the backbound which form the β-sheet. However, the amino acid sequence can also impact on the particular details of each fibril structure, by specific interactions between side chains, within the fibril and change strongly the propensity to fibrillate. Despite the similarity in amyloid fibril structures, there is a significant morphological variability even between the amyloid fibrils formed from the same protein in vitro [46-48]. This is related to a heterogeneity in the nano-scale structure of the fibrils, which is influenced by a variety of factors related to

the environmental conditions of their formation, such as temperature, pH, ionic strength, or mechanical factors such as the presence or absence of agitation [49]. Furthermore, amyloid fibrils can acquire a variety of structures depending on the conditions corresponding to several energy minima in their conformational landscape, being the final conformation simply selected by the thermodynamics or kinetics of the process, where the amyloids are an absolute minimum in the free-energy landscape. It has been proposed that every protein in some conditions could reach this highly ordered structure if submitted to the appropriate conditions[5] (Figure 3). In contrast to the unique native conformation of natural proteins, a number of peptides and proteins, even unrelated to any disease, are able to form amyloid fibrils with similar morphology [48] [5,50]. This fact has promoted the use of model protein system in vitro to study the mechanisms of amyloid fibril formation.
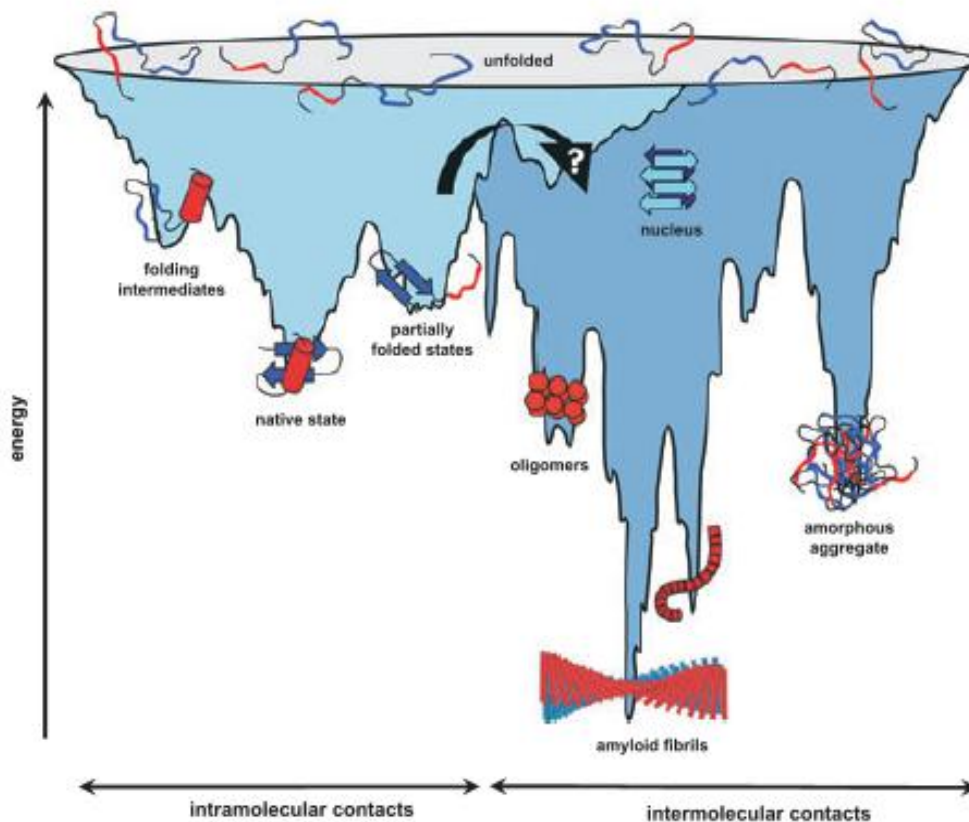
Figure 3. A schematic energy landscape for protein folding and aggregation. Image adapted from Jahn et al [51].

The kinetic of the protein amyloid aggregation

The kinetic and thermodynamic approches on the way to determining the mechanism of protein aggregation began with the work of Oosawa et al [52], where they explore the macromolecular aggregation with a nucleation and growth model, typical of crystallization. This model or some of its modifications has been routinely used over the years by other researchers[53]. Those models presents such a complexity which required some assumptions in order to obtain an analytical solution of the expressions[54]. The typical shape of the time course of fibril formation is sigmoidal. It is characterized by a lag phase of variable length, which is the time required for the formation of the nuclei of aggregation, followed by an exponential growth, that progresses toward the fibrillation by a series of elongation steps with addition of protein molecules to the ends of the fibrils[55]. In some cases has been described using a logistical expression as the simplest solution[56].

Theoretical models usually explain the amyloid aggregation as a succesive process in which a number of consecutive and/or parallel stages occur to convert the soluble protein monomer to large amyloid aggregates [57] [58]. Among these stages models include partial unfolding or refolding, oligomerization, conformational conversion, elongation, condensation, fragmentation, etc. The broad diversity of proposed models of aggregation can be understood in terms of a predominance of one or more of these stages in the overall aggregation kinetics, which results in a variety of kinetic behaviors, depending on the protein and/or the experimental conditions studied in each case[59]. Despite the large number of proposed models[58], a detailed description of the process at the molecular level remains in large part elusive because it is challenging to describe experimentally the early stages of aggregation of polypeptide chains. This is primarily due to the difficulties in detecting and characterizing the small, structurally heterogeneous, and transient species that are involved. The aggregation process leading to amyloid fibrils involves a common pathway generally triggered by protein misfolding, followed by oligomeric precursors to fibrils [43].

Aggregation precursors may be the toxic species to cells

In recent years strong evidence has identified the soluble oligomers and pre-fibrillar protein aggregates, as the main causative agents of cell toxicity and cell dysfunction. These species could be defined as precursors or key intermediates in the amyloid fibril formation[43-45,60-62]. The general toxic nature of prefibrillar aggregates has been further underlined by the finding that oligomeric species of proteins unrelated to disease, such as HypF-N from *E. coli*, the SH3 domain of PI3 kinase or equine lysozyme, are highly toxic in fibroblast and neuron cultures [63-65]. Supporting this hypothesis, some studies have established a significant correlation between the levels of soluble A-beta peptide, including its oligomeric forms, and the degree of synaptic alteration, neurodegeneration and cognitive decline in Alzheimer patients [66]. Furthermore, the neurotoxicity of A-beta oligomers has been demonstrated in animal brains by injection of purified oligomers into rat hippocampus [67]. Also for α-synuclein increasing evidence suggests that nonfibrillar dimers or oligomers play a major role in the disease progress of Parkinson's disease [68]. These are some examples from the increasingly abundant literature. In contrast, the amyloid fibrils of the same proteins show relatively low toxicity [65,66,69] and it can be possible even to reduce the toxicity of A-beta accelerating the fibrillation, limiting the amount of oligomers[70].

The reasons of the toxic behaviour of these prefibrillar aggregates to cells are currently at the front of research. However, this investigation is very limited by the lack of structural information available for the toxic oligomeric species and also the mechanism of their pathological action remains unclear. For instance, it is possible that A-beta neurotoxic effects are the result of an interaction between oligomers and neurotransmitter receptors, interfering with signaling patways in the synaptic plasma membranes [71]. Other hypotheses imply formation of specific ion channels or the non-selective permeabilization of the plasmatic membrane [72]. The main difficulty is that these oligomeric states are relatively short-lived and rapidly convert into the amyloid fibril state and are therefore difficult to detect or study. Consequently, understanding the stability of toxic oligomers under physiological conditions could turn out to be a key factor in amyloid-related diseases. It is therefore of great necessity

to understand the nature, structural and dynamic, of these oligomers and the reasons of their genesis.

Characteristics of the pre-fibrillar oligomeric precursors

These oligomeric precursors, similarly to the amyloid aggregates, present distinct morphologies visible by TEM or AFM depending on the conditions. Non-fibrillar globular beads of 2-6 nm of diameter, chains of beads or annular structures have been described [73-75] (Table 2). These metastable oligomers appear to be relatively disordered initially but then convert into species containing extensive β-sheet structure[43], which are often capable of stimulating efficiently the formation of amyloid fibrils, reducing the lag phase of aggregation [76,77]. All these prefibrillar species also possess high content in β-sheet structure and interact with Congo red and ThT, which suggest a degree of structural regularity. Some of these disordered oligomers appear to be key precursors of protofibrils and fibrils. The elucidation of their conformational properties is of crucial importance in understanding the determinants of amyloid aggregation in order to design therapeutic strategies to inhibit their formation [75].

Table2. *Properties of identified oligomeric intermediates. The dimensions were determined by AFM, table adapted from Rochet et al[6]*

Protein	Prefibrilar species	Dimensions (nm)	References
α-Synuclein (aSyn)	Spheres	4	[78]
	Protofibrils	5	
islet amyloid polypeptide	Protofibrils	2.4-3.7	[79]
Amyloid β peptide	Spheres	2.5-3.9	[74,80]
(Abeta 40)	Protofibrils	3.9	
Amyloid β peptide	Spheres	4-5	[73,81]
(Abeta 42)	Protofibrils	8.7-11.3	

The conformational events triggering the aggregation cascade

The scientific comunity is doing a great effort to understand the early stages of the aggregation cascade, the factors triggering it and the nature of the species implied. The way in which proteins could achieve the partially-folded conformations prone to aggregation is clearly related to the highly dynamic nature of proteins, which undergo a large variety of structural transitions even under native conditions [82-84]. In fact, recent studies have proposed that the destabilization of the native fold results in the modulation of the protein conformational ensemble, disfavoring structural cooperativity and increasing the sampling of partially-folded amyloidogenic conformations [85]. Peptides and proteins that are natively unfolded, as well as fragments of proteins generated by proteolysis athat are unable to fold in the absence of the remainder of the polypeptide chain, can also adopt conformations that are susceptible to form intermolecular interactions triggering aggregation under some circumstances, for example, if their concentrations become elevated. Although amyloid aggregation usually involves a conformational change, there are some cases in which the formation of amyloid fibrils is preceded by an assembly of quasi-native or native-like structures into aggregates. Then, a structural conversion takes place within the aggregates to transform into pre-fibrillar species that may not yet be fibrillar in their morphologies but have some of the characteristics of amyloid-like structures, such as CD or FT-IR spectra typical of β-sheet structure or binding to Congo-red and ThT dyes [86,87]. It is increasely evident that natural sequences in proteins have evolved to avoid this type of conformations[88].

 Amyloid aggregation propensity is stroghly dependent on sequence

There is a profound ignorance about the molecular basis of the amyloid aggregation. In this way, a large body of research has been focused on obtain rules and patterns, which allow us to predict the propensity to form aggregates from the protein sequence[89] [90] [91]. In particular, hydrophobic side chains at key positions in the sequence [92] , net charge and β-sheet propensity of the sequence are factors that can influence strongly the rate of aggregation [93,94]. Remarkably, the changes in the rate of aggregation of unstructured peptides and proteins

following a series of mutations could be rationalized using a phenomenological equation, based on simple physicochemical principles [72]. This provides strong support to the idea that aggregation of polypeptide chains reflects the typical behavior of a simple polymer, in contrast to the process of folding of globular proteins, where the folding rates are strongly coupled to the specific structures of the native states determined by highly evolved sequences. The increasing knowledge about the sequence effects on aggregation has led to the development of algorithms to identify the regions of the sequence that promote aggregation within an unstructured polypeptide chain[95,96].

The SH3 domain of α-spectrin: a model protein to study the mechanism of amyloid fibril formation

Usually the proteins related to diseases have been shown to be difficult to handle because of their intrinsic properties and high aggregation propensity, making it extremely difficult to obtain reproducible quantitative information about the aggregation kinetics. In addition, the use of well-characterized model proteins[97], even though it is unrelated to any known disease, is a potent approach to investigate the mechanisms of formation of amyloid fibrils due to the extended information available about their folding mechanism and conformational stability.

The SH3 domains are small globular protein domains very extended in the proteome being part of a wide variety of proteins and generally are implied in molecular recognition, signal transduction or protein-protein interaction [98]. They are composed by a single polypeptide chain composed between 60 and 85 amino acids and share a similar tridimensional structure.

Many groups, including ours, have studied for many years the structural stability and folding of the SH3 domains[99-103]. Therefore, a vast amount of data about the biophysics and structure of amyloid fibrils has been generated with this model system. The folding transition state of this domain is organized around the distal β-hairpin and the subsequent 3_{10}-helix, and the formation of the tight distal β-turn has been described as a compulsory step in the folding pathway [104]. Those kinetics and equilibrium studies have considered this small domain as an archetypical two-state folding protein, without partially populated intermediates. Although

this apparent two-state folding behavior, H/D exchange studies monitored by NMR with the α-Spectrin SH3 domain (Spc-SH3) indicate that under native conditions is in a statistical conformational equilibrium with transient local or partial unfolded conformations [105-107]. Therefore, since the Spc-SH3 cooperativity is local, the conformational movements and fluctuations of the elements of its structure could be partially coupled between them [108], making it possible the formation of partially folded states which can be populated under native or slightly denaturalizing conditions.

During the course of previous research in our group, it was found that the single mutation N47A, placed within the folding nucleus of the Spc-SH3, favors the rapid formation of curly amyloid fibrils under mild acid conditions favored by the presence of salts [109] [46]. Under these aggregating conditions, the majority of the protein is natively folded. The effects of the N47A mutation on the folding, stability and structural cooperativity of the Spc-SH3 domain have been studied previously[105,110]. This mutation produces a destabilization of the native state by about 2 kJ mol^{-1}. The amyloidogenic character of this mutation is mainly due to an increase in the rate of formation of amyloid nuclei [98] and recent computational studies have proposed that it enhances the population of a partially unfolded intermediate, which may be crucial in triggering the aggregation cascade [111].

During the research that gives rise to this thesis project, this model protein has been used to characterize the molecular and physicochemical details of the intermediate steps leading to the conversion of a soluble and folded protein into amyloid nuclei that further assemble into fibrillar aggregates. We concentrated ourselves particularly on the early stages of the aggregation process. The results obtained with this model protein domain could help to increase our understanding of the aggregation mechanisms of other proteins related to amyloid diseases, such as α-Synuclein, which has been subject of study in the thesis project.

The α-Synuclein

The α-Synuclein (aSyn) is cytoplasmatic protein from the synuclein family [112]. Synucleins are small proteins (between 113-143 amino acids), natively unfolded, highly evolutionarily

conserved and abundantly expressed in the nervous system of vertebrates. aSyn is expressed within glia and neurons, where it is particularly abundant at presynaptic terminals [113]. The precise physiological function of aSyn has yet to be established although different studies suggest a function related to a range of interactions of aSyn with lipids. Such as: binding and stabilizing fatty acid droplets and micelles[114], transporting polyunsaturated fatty acids in dopaminergic neurons[115,116], modulating presynaptic vesicle pool size and vesicle recycling[117], inducing curvature in vesicles and membranes[118] and membrane remodeling[119,120].

A considerable number of neurodegenerative diseases are associated with the aSyn, such as, Parkinson's disease, dementia with Lewy body, Lewy body variant of Alzheimer's disease, multiple system atrophy, and Hallervorden-Spatz disease, implicating a crucial role of aggregated forms of alpha-synuclein in their pathogenesis [121]. The early stages of aSyn fibril formation involve the partial folding of soluble unstructured aSyn into a highly fibrillation-prone, pre-molten globule-like conformation, which represents a key intermediate on the fibrillation pathway[122].

The aggregation process typically described in many studies for the aSyn, as a natively unfolded protein, is a kinetic mechanism of nucleation and growth, typical of crystallization. The time course of fibril formation generally shows a typical lag phase of variable length followed by an exponential growth [55]. The lag phase or "nucleation" phase is the time required for the formation of the nuclei of aggregation, being the rate limiting step of the aggregation process. Once a nucleus is formed, it progresses toward the fibrillation by a series of elongation steps with addition of protein molecules to the ends of the fibrils[123]. Many factors affect the aggregation process. Indeed, it has been previously reported that the addition of seeds[124,125], a variation in the pH[126], salt presence in solution[127,128], chemical modifications (nitration[129], oxidation[130], phosphorylation[131], acetylation [132]....) , shaking[133] and also the addition of anionic surfactants[134-137] could accelerate the fibrillation rate.

As mentioned above, our aim is to contribute to the molecular and physicochemical understanding of the earliest stages of the amyloidogenesis cascade, with special focus on the early oligomeric species, due to their toxic nature. However, under conditions where

aggregation takes place with long lag phases early aggregation nuclei and oligomeric species are very low populated and difficult to describe and characterize. In addition, considering that our aim is to contribute in the biological relevance of the model and given the implication of aSyn ina variety of interactions with lipids and membranes in its normal function, we focus our efforts in the study of the process in presence of a widely used, simple model for membrane environment [135] such as sodium dodecyl sulfate(SDS), which has also been reported to accelerate the amyloid formation of aSyn in vitro [124] .

OBJECTIVES OF THE THESIS

This thesis project was aimed to contribute to the progress in the understanding of the molecular and physicochemical determinants of amyloid fibril formation. Our main general goal was to characterize the structural, thermodynamic and kinetic properties of the main species that participate in the earliest stages of the mechanism of amyloid aggregation.

To achieve this goal, we used a wide variety of biophysical methods and techniques to explore the different stages of amyloid fibrillation. On the basis of previous research perfomed in our group and using a well-characterized model system such as the Spc-SH3 domain, a detailed kinetic and thermodynamic study of the amyloid fibril formation and their precursors was undertaken, in order to establish new methodologies to analyze aggregation that would be applicable to other disease-related protein systems. Futher, we aimed to extend our experimental and theroretical procedures to study the amyloid aggregation of alpha-synuclein, related to Parkinson's disease. This would lead to obtention of energetic information that may be of extraordinary interest in future development of therapeutic strategies for neurodegenerative diseases.

The specific objectives of this work include:

1- To elucidate the details of the mechanism of the earlist stages of amyloid fibril formation using the Spc-SH3 domain as model system. Understanding the earliest molecular events during primary nucleation of the amyloid aggregation cascade is of fundamental significance to prevent amyloid related disorders.

2- On the basis of the mechanistic information obtained, to develop mathematical model of analysis of the early aggregation kinetics in order to extract meaningful thermodynamic and kinetic information about the species involved.

3- To understand the effects of environmental variables, such as the presence of salt ions, on the amyloid fibrillation kinetics of the Spc-SH3 domain and to identify their influence on the derived thermodynamic magnitudes of the amyloidogenic precusor states.

4- To analyze structurally the conformational changes triggering fibril formation using a site-directed mutagenesis approach probing all secondary structure elements in the Spc-SH3 backbone and to obtain structural information about the precursor states of amyloid nucleation of the N47A Spc-SH3 domain.

5- To characterize the biophysical properties and and structure of the aSyn in presence and in absence of SDS and to compare the amyloidogenic propensity between the unmodified and the N-acetylated natural variant of this protein. We will put special effort in identifying the amyloidogenic precursor species for this protein under the selected conditions in order to clarify the mechanism of aggregation.

REFERENCES

(1)   Brändén, C.-I.; Tooze, J.: *Introduction to protein structure*; Garland Pub.: New York, 1991.

(2)   Karplus, M. The Levinthal paradox: yesterday and today. *Folding & design* **1997**, *2*, S69-75.

(3)   Kyle, R. A. Amyloidosis: a convoluted story. *British journal of haematology* **2001**, *114*, 529-538.

(4)   Alois, A. About a peculiar disease of the cerebral cortex. By Alois Alzheimer, 1907 (Translated by L. Jarvik and H. Greenson). *Alzheimer disease and associated disorders* **1987**, *1*, 3-8.

(5)   Dobson, C. M. Protein folding and misfolding. *Nature* **2003**, *426*, 884-890.

(6)   Rochet, J. C.; Lansbury, P. T., Jr. Amyloid fibrillogenesis: themes and variations. *Current opinion in structural biology* **2000**, *10*, 60-68.

(7)   Teplow, D. B. Structural and kinetic features of amyloid beta-protein fibrillogenesis. *Amyloid : the international journal of experimental and clinical investigation : the official journal of the International Society of Amyloidosis* **1998**, *5*, 121-142.

(8)   Selkoe, D. J. Translating cell biology into therapeutic advances in Alzheimer's disease. *Nature* **1999**, *399*, A23-31.

(9)   Goedert, M.; Spillantini, M. G.; Davies, S. W. Filamentous nerve cell inclusions in neurodegenerative diseases. *Current opinion in neurobiology* **1998**, *8*, 619-632.

(10)   Goedert, M. Filamentous nerve cell inclusions in neurodegenerative diseases: tauopathies and alpha-synucleinopathies. *Philosophical transactions of the Royal Society of London. Series B, Biological sciences* **1999**, *354*, 1101-1118.

(11)   Galvin, J. E.; Lee, V. M.; Schmidt, M. L.; Tu, P. H.; Iwatsubo, T.; Trojanowski, J. Q. Pathobiology of the Lewy body. *Advances in neurology* **1999**, *80*, 313-324.

(12)   Perutz, M. F. Glutamine repeats and neurodegenerative diseases: molecular aspects. *Trends in biochemical sciences* **1999**, *24*, 58-63.

(13)   Ross, C. A. Intranuclear neuronal inclusions: a common pathogenic mechanism for glutamine-repeat neurodegenerative diseases? *Neuron* **1997**, *19*, 1147-1150.

(14)   Goedert, M.; Crowther, R. A.; Spillantini, M. G. Tau mutations cause frontotemporal dementias. *Neuron* **1998**, *21*, 955-958.

(15)   Eigen, M. Prionics or the kinetic basis of prion diseases. *Biophysical chemistry* **1996**, *63*, A1-18.

(16)   Miklossy, J.; Steele, J. C.; Yu, S.; McCall, S.; Sandberg, G.; McGeer, E. G.; McGeer, P. L. Enduring involvement of tau, beta-amyloid, alpha-synuclein, ubiquitin and TDP-43 pathology in the amyotrophic lateral sclerosis/parkinsonism-dementia complex of Guam (ALS/PDC). *Acta neuropathologica* **2008**, *116*, 625-637.

(17)   Wetzel, R. Domain stability in immunoglobulin light chain deposition disorders. *Advances in protein chemistry* **1997**, *50*, 183-242.

(18)   Shimizu, M.; Manabe, T.; Matsumoto, T.; Monobe, Y.; Hirokawa, M.; Moriya, T.; Iida, M. Beta 2 microglobulin haemodialysis related amyloidosis: distinctive

gross features of gastrointestinal involvement. *Journal of clinical pathology* **1997**, *50*, 873-875.

(19)   Clark, A.; Charge, S. B.; Badman, M. K.; MacArthur, D. A.; de Koning, E. J. Islet amyloid polypeptide: actions and role in the pathogenesis of diabetes. *Biochemical Society transactions* **1996**, *24*, 594-599.

(20)   Brooks, A. M.; Drewe, R. H.; Grant, G. B.; Billington, T.; Gillies, W. E. Crystalline nature of the iridescent particles in hypermature cataracts. *The British journal of ophthalmology* **1994**, *78*, 581-582.

(21)   Dobson, C. M. Protein misfolding, evolution and disease. *Trends in biochemical sciences* **1999**, *24*, 329-332.

(22)   Kelly, J. W. Alternative conformations of amyloidogenic proteins govern their behavior. *Current opinion in structural biology* **1996**, *6*, 11-17.

(23)   Haggqvist, B.; Naslund, J.; Sletten, K.; Westermark, G. T.; Mucchiano, G.; Tjernberg, L. O.; Nordstedt, C.; Engstrom, U.; Westermark, P. Medin: an integral fragment of aortic smooth muscle cell-produced lactadherin forms the most common human amyloid. *Proceedings of the National Academy of Sciences of the United States of America* **1999**, *96*, 8669-8674.

(24)   Vidal, R.; Frangione, B.; Rostagno, A.; Mead, S.; Revesz, T.; Plant, G.; Ghiso, J. A stop-codon mutation in the BRI gene associated with familial British dementia. *Nature* **1999**, *399*, 776-781.

(25)   Lansbury, P. T., Jr.; Kosik, K. S. Neurodegeneration: new clues on inclusions. *Chemistry & biology* **2000**, *7*, R9-R12.

(26)   Gibson, G.; El-Agnaf, O. M.; Anwar, Z.; Sidera, C.; Isbister, A.; Austen, B. M. Structure and neurotoxicity of novel amyloids derived from the BRI gene. *Biochemical Society transactions* **2005**, *33*, 1111-1112.

(27)   Kiuru, S. Gelsolin-related familial amyloidosis, Finnish type (FAF), and its variants found worldwide. *Amyloid : the international journal of experimental and clinical investigation : the official journal of the International Society of Amyloidosis* **1998**, *5*, 55-66.

(28)   Kelly, J. W.; Colon, W.; Lai, Z.; Lashuel, H. A.; McCulloch, J.; McCutchen, S. L.; Miroy, G. J.; Peterson, S. A. Transthyretin quaternary and tertiary structural changes facilitate misassembly into amyloid. *Advances in protein chemistry* **1997**, *50*, 161-181.

(29)   Serpell, L. C. Alzheimer's amyloid fibrils: structure and assembly. *Biochimica et biophysica acta* **2000**, *1502*, 16-30.

(30)   Stromer, T.; Serpell, L. C. Structure and morphology of the Alzheimer's amyloid fibril. *Microscopy research and technique* **2005**, *67*, 210-217.

(31)   Goldsbury, C.; Baxa, U.; Simon, M. N.; Steven, A. C.; Engel, A.; Wall, J. S.; Aebi, U.; Muller, S. A. Amyloid structure and assembly: insights from scanning transmission electron microscopy. *Journal of structural biology* **2011**, *173*, 1-13.

(32)   Saiki, M.; Honda, S.; Kawasaki, K.; Zhou, D.; Kaito, A.; Konakahara, T.; Morii, H. Higher-order molecular packing in amyloid-like fibrils constructed with linear arrangements of hydrophobic and hydrogen-bonding side-chains. *Journal of molecular biology* **2005**, *348*, 983-998.

(33)   Makin, O. S.; Atkins, E.; Sikorski, P.; Johansson, J.; Serpell, L. C. Molecular basis for amyloid fibril formation and stability. *Proceedings of the National Academy of Sciences of the United States of America* **2005**, *102*, 315-320.

(34)   Sabate, R.; Ventura, S. Cross-beta-sheet supersecondary structure in amyloid folds: techniques for detection and characterization. *Methods in molecular biology* **2013**, *932*, 237-257.

(35)   Comellas, G.; Rienstra, C. M. Protein structure determination by magic-angle spinning solid-state NMR, and insights into the formation, structure, and stability of amyloid fibrils. *Annual review of biophysics* **2013**, *42*, 515-536.

(36)   Heise, H. Solid-state NMR spectroscopy of amyloid proteins. *Chembiochem : a European journal of chemical biology* **2008**, *9*, 179-189.

(37)   Sawaya, M. R.; Sambashivan, S.; Nelson, R.; Ivanova, M. I.; Sievers, S. A.; Apostol, M. I.; Thompson, M. J.; Balbirnie, M.; Wiltzius, J. J.; McFarlane, H. T.; Madsen, A. O.; Riekel, C.; Eisenberg, D. Atomic structures of amyloid cross-beta spines reveal varied steric zippers. *Nature* **2007**, *447*, 453-457.

(38)   Nelson, R.; Sawaya, M. R.; Balbirnie, M.; Madsen, A. O.; Riekel, C.; Grothe, R.; Eisenberg, D. Structure of the cross-beta spine of amyloid-like fibrils. *Nature* **2005**, *435*, 773-778.

(39)   Del Mar, C.; Greenbaum, E. A.; Mayne, L.; Englander, S. W.; Woods, V. L., Jr. Structure and properties of alpha-synuclein and other amyloids determined at the amino acid level. *Proceedings of the National Academy of Sciences of the United States of America* **2005**, *102*, 15477-15482.

(40)   Carulla, N.; Caddy, G. L.; Hall, D. R.; Zurdo, J.; Gairi, M.; Feliz, M.; Giralt, E.; Robinson, C. V.; Dobson, C. M. Molecular recycling within amyloid fibrils. *Nature* **2005**, *436*, 554-558.

(41)   Ma, B.; Nussinov, R. Polymorphic triple beta-sheet structures contribute to amide hydrogen/deuterium (H/D) exchange protection in the Alzheimer amyloid beta42 peptide. *The Journal of biological chemistry* **2011**, *286*, 34244-34253.

(42)   Whittemore, N. A.; Mishra, R.; Kheterpal, I.; Williams, A. D.; Wetzel, R.; Serpersu, E. H. Hydrogen-deuterium (H/D) exchange mapping of Abeta 1-40 amyloid fibril secondary structure using nuclear magnetic resonance spectroscopy. *Biochemistry* **2005**, *44*, 4434-4441.

(43)   Chiti, F.; Dobson, C. M. Protein misfolding, functional amyloid, and human disease. *Annual review of biochemistry* **2006**, *75*, 333-366.

(44)   Baglioni, S.; Casamenti, F.; Bucciantini, M.; Luheshi, L. M.; Taddei, N.; Chiti, F.; Dobson, C. M.; Stefani, M. Prefibrillar amyloid aggregates could be generic toxins in higher organisms. *The Journal of neuroscience : the official journal of the Society for Neuroscience* **2006**, *26*, 8160-8167.

(45)   Campioni, S.; Mannini, B.; Zampagni, M.; Pensalfini, A.; Parrini, C.; Evangelisti, E.; Relini, A.; Stefani, M.; Dobson, C. M.; Cecchi, C.; Chiti, F. A causative link between the structure of aberrant protein oligomers and their toxicity. *Nature chemical biology* **2010**, *6*, 140-147.

(46)   Morel, B.; Varela, L.; Azuaga, A. I.; Conejero-Lara, F. Environmental conditions affect the kinetics of nucleation of amyloid fibrils and determine their morphology. *Biophysical journal* **2010**, *99*, 3801-3810.

(47)   Jimenez, J. L.; Tennent, G.; Pepys, M.; Saibil, H. R. Structural diversity of ex vivo amyloid fibrils studied by cryo-electron microscopy. *Journal of molecular biology* **2001**, *311*, 241-247.

(48)	Jimenez, J. L.; Guijarro, J. I.; Orlova, E.; Zurdo, J.; Dobson, C. M.; Sunde, M.; Saibil, H. R. Cryo-electron microscopy structure of an SH3 amyloid fibril and model of the molecular packing. *The EMBO journal* **1999**, *18*, 815-821.

(49)	Pedersen, J. S.; Otzen, D. E. Amyloid-a state in many guises: survival of the fittest fibril fold. *Protein science : a publication of the Protein Society* **2008**, *17*, 2-10.

(50)	Vendruscolo, M.; Dobson, C. M. Towards complete descriptions of the free-energy landscapes of proteins. *Philosophical transactions. Series A, Mathematical, physical, and engineering sciences* **2005**, *363*, 433-450; discussion 450-432.

(51)	Jahn, T. R.; Radford, S. E. The Yin and Yang of protein folding. *The FEBS journal* **2005**, *272*, 5962-5970.

(52)	Oosawa, F.; Kasai, M. A theory of linear and helical aggregations of macromolecules. *Journal of molecular biology* **1962**, *4*, 10-21.

(53)	Frieden, C.; Goddette, D. W. Polymerization of actin and actin-like systems: evaluation of the time course of polymerization in relation to the mechanism. *Biochemistry* **1983**, *22*, 5836-5843.

(54)	Goldstein, R. F.; Stryer, L. Cooperative polymerization reactions. Analytical approximations, numerical examples, and experimental strategy. *Biophysical journal* **1986**, *50*, 583-599.

(55)	Ferrone, F. Analysis of protein aggregation kinetics. *Methods in enzymology* **1999**, *309*, 256-274.

(56)	Bader, R.; Bamford, R.; Zurdo, J.; Luisi, B. F.; Dobson, C. M. Probing the mechanism of amyloidogenesis through a tandem repeat of the PI3-SH3 domain suggests a generic model for protein aggregation and fibril formation. *Journal of molecular biology* **2006**, *356*, 189-208.

(57)	Roberts, C. J. Non-native protein aggregation kinetics. *Biotechnology and bioengineering* **2007**, *98*, 927-938.

(58)	Morris, A. M.; Watzky, M. A.; Finke, R. G. Protein aggregation kinetics, mechanism, and curve-fitting: a review of the literature. *Biochimica et biophysica acta* **2009**, *1794*, 375-397.

(59)	Andrews, J. M.; Roberts, C. J. A Lumry-Eyring nucleated polymerization model of protein aggregation kinetics: 1. Aggregation with pre-equilibrated unfolding. *The journal of physical chemistry. B* **2007**, *111*, 7897-7913.

(60)	Bucciantini, M.; Giannoni, E.; Chiti, F.; Baroni, F.; Formigli, L.; Zurdo, J.; Taddei, N.; Ramponi, G.; Dobson, C. M.; Stefani, M. Inherent toxicity of aggregates implies a common mechanism for protein misfolding diseases. *Nature* **2002**, *416*, 507-511.

(61)	Koffie, R. M.; Meyer-Luehmann, M.; Hashimoto, T.; Adams, K. W.; Mielke, M. L.; Garcia-Alloza, M.; Micheva, K. D.; Smith, S. J.; Kim, M. L.; Lee, V. M.; Hyman, B. T.; Spires-Jones, T. L. Oligomeric amyloid beta associates with postsynaptic densities and correlates with excitatory synapse loss near senile plaques. *Proceedings of the National Academy of Sciences of the United States of America* **2009**, *106*, 4012-4017.

(62)	Yuan, B.; Sierks, M. R. Intracellular targeting and clearance of oligomeric alpha-synuclein alleviates toxicity in mammalian cells. *Neuroscience letters* **2009**, *459*, 16-18.

(63)	Bucciantini, M.; Rigacci, S.; Berti, A.; Pieri, L.; Cecchi, C.; Nosi, D.; Formigli, L.; Chiti, F.; Stefani, M. Patterns of cell death triggered in two different cell lines

by HypF-N prefibrillar aggregates. *FASEB journal : official publication of the Federation of American Societies for Experimental Biology* **2005**, *19*, 437-439.

(64)   Ventura, S.; Lacroix, E.; Serrano, L. Insights into the origin of the tendency of the PI3-SH3 domain to form amyloid fibrils. *Journal of molecular biology* **2002**, *322*, 1147-1158.

(65)   Malisauskas, M.; Ostman, J.; Darinskas, A.; Zamotin, V.; Liutkevicius, E.; Lundgren, E.; Morozova-Roche, L. A. Does the cytotoxic effect of transient amyloid oligomers from common equine lysozyme in vitro imply innate amyloid toxicity? *The Journal of biological chemistry* **2005**, *280*, 6269-6275.

(66)   McLean, C. A.; Cherny, R. A.; Fraser, F. W.; Fuller, S. J.; Smith, M. J.; Beyreuther, K.; Bush, A. I.; Masters, C. L. Soluble pool of Abeta amyloid as a determinant of severity of neurodegeneration in Alzheimer's disease. *Annals of neurology* **1999**, *46*, 860-866.

(67)   Shankar, G. M.; Li, S.; Mehta, T. H.; Garcia-Munoz, A.; Shepardson, N. E.; Smith, I.; Brett, F. M.; Farrell, M. A.; Rowan, M. J.; Lemere, C. A.; Regan, C. M.; Walsh, D. M.; Sabatini, B. L.; Selkoe, D. J. Amyloid-beta protein dimers isolated directly from Alzheimer's brains impair synaptic plasticity and memory. *Nature medicine* **2008**, *14*, 837-842.

(68)   El-Agnaf, O. M.; Salem, S. A.; Paleologou, K. E.; Cooper, L. J.; Fullwood, N. J.; Gibson, M. J.; Curran, M. D.; Court, J. A.; Mann, D. M.; Ikeda, S.; Cookson, M. R.; Hardy, J.; Allsop, D. Alpha-synuclein implicated in Parkinson's disease is present in extracellular biological fluids, including human plasma. *FASEB journal : official publication of the Federation of American Societies for Experimental Biology* **2003**, *17*, 1945-1947.

(69)   Sousa, M. M.; Cardoso, I.; Fernandes, R.; Guimaraes, A.; Saraiva, M. J. Deposition of transthyretin in early stages of familial amyloidotic polyneuropathy: evidence for toxicity of nonfibrillar aggregates. *The American journal of pathology* **2001**, *159*, 1993-2000.

(70)   Cheng, I. H.; Scearce-Levie, K.; Legleiter, J.; Palop, J. J.; Gerstein, H.; Bien-Ly, N.; Puolivali, J.; Lesne, S.; Ashe, K. H.; Muchowski, P. J.; Mucke, L. Accelerating amyloid-beta fibrillization reduces oligomer levels and functional deficits in Alzheimer disease mouse models. *The Journal of biological chemistry* **2007**, *282*, 23818-23828.

(71)   Bitan, G.; Kirkitadze, M. D.; Lomakin, A.; Vollers, S. S.; Benedek, G. B.; Teplow, D. B. Amyloid beta -protein (Abeta) assembly: Abeta 40 and Abeta 42 oligomerize through distinct pathways. *Proceedings of the National Academy of Sciences of the United States of America* **2003**, *100*, 330-335.

(72)   Chiti, F.; Stefani, M.; Taddei, N.; Ramponi, G.; Dobson, C. M. Rationalization of the effects of mutations on peptide and protein aggregation rates. *Nature* **2003**, *424*, 805-808.

(73)   Nybo, M.; Svehag, S. E.; Holm Nielsen, E. An ultrastructural study of amyloid intermediates in A beta1-42 fibrillogenesis. *Scandinavian journal of immunology* **1999**, *49*, 219-223.

(74)   Blackley, H. K.; Patel, N.; Davies, M. C.; Roberts, C. J.; Tendler, S. J.; Wilkinson, M. J.; Williams, P. M. Morphological development of beta(1-40) amyloid fibrils. *Experimental neurology* **1999**, *158*, 437-443.

(75)   Harper, J. D.; Lieber, C. M.; Lansbury, P. T., Jr. Atomic force microscopic imaging of seeded fibril formation and fibril branching by the Alzheimer's disease amyloid-beta protein. *Chemistry & biology* **1997**, *4*, 951-959.

(76)   Harper, J. D.; Lansbury, P. T., Jr. Models of amyloid seeding in Alzheimer's disease and scrapie: mechanistic truths and physiological consequences of the time-dependent solubility of amyloid proteins. *Annual review of biochemistry* **1997**, *66*, 385-407.

(77)   Uversky, V. N.; Li, J.; Souillac, P.; Millett, I. S.; Doniach, S.; Jakes, R.; Goedert, M.; Fink, A. L. Biophysical properties of the synucleins and their propensities to fibrillate: inhibition of alpha-synuclein assembly by beta- and gamma-synucleins. *The Journal of biological chemistry* **2002**, *277*, 11970-11978.

(78)   Conway, K. A.; Harper, J. D.; Lansbury, P. T. Accelerated in vitro fibril formation by a mutant alpha-synuclein linked to early-onset Parkinson disease. *Nature medicine* **1998**, *4*, 1318-1320.

(79)   Goldsbury, C.; Kistler, J.; Aebi, U.; Arvinte, T.; Cooper, G. J. Watching amyloid fibrils grow by time-lapse atomic force microscopy. *Journal of molecular biology* **1999**, *285*, 33-39.

(80)   Harper, J. D.; Wong, S. S.; Lieber, C. M.; Lansbury, P. T., Jr. Assembly of A beta amyloid protofibrils: an in vitro model for a possible early event in Alzheimer's disease. *Biochemistry* **1999**, *38*, 8972-8980.

(81)   Kowalewski, T.; Holtzman, D. M. In situ atomic force microscopy study of Alzheimer's beta-amyloid peptide on different substrates: new insights into mechanism of beta-sheet formation. *Proceedings of the National Academy of Sciences of the United States of America* **1999**, *96*, 3688-3693.

(82)   Lindorff-Larsen, K.; Best, R. B.; Depristo, M. A.; Dobson, C. M.; Vendruscolo, M. Simultaneous determination of protein structure and dynamics. *Nature* **2005**, *433*, 128-132.

(83)   Sadqi, M.; Casares, S.; Abril, M. A.; Lopez-Mayorga, O.; Conejero-Lara, F.; Freire, E. The native state conformational ensemble of the SH3 domain from alpha-spectrin. *Biochemistry* **1999**, *38*, 8899-8906.

(84)   Hilser, V. J.; Dowdy, D.; Oas, T. G.; Freire, E. The structural distribution of cooperative interactions in proteins: analysis of the native state ensemble. *Proceedings of the National Academy of Sciences of the United States of America* **1998**, *95*, 9903-9908.

(85)   Dumoulin, M.; Canet, D.; Last, A. M.; Pardon, E.; Archer, D. B.; Muyldermans, S.; Wyns, L.; Matagne, A.; Robinson, C. V.; Redfield, C.; Dobson, C. M. Reduced global cooperativity is a common feature underlying the amyloidogenicity of pathogenic lysozyme mutations. *Journal of molecular biology* **2005**, *346*, 773-788.

(86)   Bouchard, M.; Zurdo, J.; Nettleton, E. J.; Dobson, C. M.; Robinson, C. V. Formation of insulin amyloid fibrils followed by FTIR simultaneously with CD and electron microscopy. *Protein science : a publication of the Protein Society* **2000**, *9*, 1960-1967.

(87)   Plakoutsi, G.; Taddei, N.; Stefani, M.; Chiti, F. Aggregation of the Acylphosphatase from Sulfolobus solfataricus: the folded and partially unfolded states can both be precursors for amyloid formation. *The Journal of biological chemistry* **2004**, *279*, 14111-14119.

(88)   Dobson, C. M. The structural basis of protein folding and its links with human disease. *Philosophical transactions of the Royal Society of London. Series B, Biological sciences* **2001**, *356*, 133-145.

(89)   Yoon, S.; Welsh, W. J. Detecting hidden sequence propensity for amyloid fibril formation. *Protein science : a publication of the Protein Society* **2004**, *13*, 2149-2160.

(90)   Bemporad, F.; Calloni, G.; Campioni, S.; Plakoutsi, G.; Taddei, N.; Chiti, F. Sequence and structural determinants of amyloid fibril formation. *Accounts of chemical research* **2006**, *39*, 620-627.

(91)   Iconomidou, V. A.; Chryssikos, G. D.; Gionis, V.; Galanis, A. S.; Cordopatis, P.; Hoenger, A.; Hamodrakas, S. J. Amyloid fibril formation propensity is inherent into the hexapeptide tandemly repeating sequence of the central domain of silkmoth chorion proteins of the A-family. *Journal of structural biology* **2006**, *156*, 480-488.

(92)   Otzen, D. E.; Kristensen, O.; Oliveberg, M. Designed protein tetramer zipped together with a hydrophobic Alzheimer homology: a structural clue to amyloid assembly. *Proceedings of the National Academy of Sciences of the United States of America* **2000**, *97*, 9907-9912.

(93)   Chiti, F.; Calamai, M.; Taddei, N.; Stefani, M.; Ramponi, G.; Dobson, C. M. Studies of the aggregation of mutant proteins in vitro provide insights into the genetics of amyloid diseases. *Proceedings of the National Academy of Sciences of the United States of America* **2002**, *99 Suppl 4*, 16419-16426.

(94)   Lopez De La Paz, M.; Goldie, K.; Zurdo, J.; Lacroix, E.; Dobson, C. M.; Hoenger, A.; Serrano, L. De novo designed peptide-based amyloid fibrils. *Proceedings of the National Academy of Sciences of the United States of America* **2002**, *99*, 16052-16057.

(95)   Fernandez-Escamilla, A. M.; Rousseau, F.; Schymkowitz, J.; Serrano, L. Prediction of sequence-dependent and mutational effects on the aggregation of peptides and proteins. *Nature biotechnology* **2004**, *22*, 1302-1306.

(96)   Pawar, A. P.; Dubay, K. F.; Zurdo, J.; Chiti, F.; Vendruscolo, M.; Dobson, C. M. Prediction of "aggregation-prone" and "aggregation-susceptible" regions in proteins associated with neurodegenerative diseases. *Journal of molecular biology* **2005**, *350*, 379-392.

(97)   Eisenberg, D.; Jucker, M. The amyloid state of proteins in human diseases. *Cell* **2012**, *148*, 1188-1203.

(98)   Varela, L.; Morel, B.; Azuaga, A. I.; Conejero-Lara, F. A single mutation in an SH3 domain increases amyloid aggregation by accelerating nucleation, but not by destabilizing thermodynamically the native state. *FEBS letters* **2009**, *583*, 801-806.

(99)   Sadqi, M.; Casares, S.; Abril, M. A.; Lopez-Mayorga, O.; Conejero-Lara, F.; Freire, E. The native state conformational ensemble of the SH3 domain from alpha-spectrin. *Biochemistry* **1999**, *38*, 8899-8906.

(100)   Viguera, A. R.; Martinez, J. C.; Filimonov, V. V.; Mateo, P. L.; Serrano, L. Thermodynamic and kinetic analysis of the SH3 domain of spectrin shows a two-state folding transition. *Biochemistry* **1994**, *33*, 2142-2150.

(101)   Casares, S.; Sadqi, M.; Lopez-Mayorga, O.; Conejero-Lara, F.; van Nuland, N. A. J. Detection and characterization of partially unfolded oligomers of the SH3 domain of alpha-spectrin. *Biophysical journal* **2004**, *86*, 2403-2413.

(102) Kortemme, T.; Kelly, M. J.; Kay, L. E.; Forman-Kay, J.; Serrano, L. Similarities between the spectrin SH3 domain denatured state and its folding transition state. *Journal of molecular biology* **2000**, *297*, 1217-1229.

(103) Cobos, E. S.; Filimonov, V. V.; Vega, M. C.; Mateo, P. L.; Serrano, L.; Martinez, J. C. A thermodynamic and kinetic analysis of the folding pathway of an SH3 domain entropically stabilised by a redesigned hydrophobic core. *Journal of molecular biology* **2003**, *328*, 221-233.

(104) Martinez, J. C.; Pisabarro, M. T.; Serrano, L. Obligatory steps in protein folding and the conformational diversity of the transition state. *Nature structural biology* **1998**, *5*, 721-729.

(105) Casares, S.; Sadqi, M.; Lopez-Mayorga, O.; Martinez, J. C.; Conejero-Lara, F. Structural cooperativity in the SH3 domain studied by site-directed mutagenesis and amide hydrogen exchange. *FEBS letters* **2003**, *539*, 125-130.

(106) Sadqi, M.; Casares, S.; Lopez-Mayorga, O.; Conejero-Lara, F. The temperature dependence of the hydrogen exchange in the SH3 domain of alpha-spectrin. *FEBS letters* **2002**, *527*, 86-90.

(107) Sadqi, M.; Casares, S.; Lopez-Mayorga, O.; Martinez, J. C.; Conejero-Lara, F. pH dependence of the hydrogen exchange in the SH3 domain of alpha-spectrin. *FEBS letters* **2002**, *514*, 295-299.

(108) Casares, S.; Sadqi, M.; Lopez-Mayorga, O.; Conejero-Lara, F.; van Nuland, N. A. Detection and characterization of partially unfolded oligomers of the SH3 domain of alpha-spectrin. *Biophysical journal* **2004**, *86*, 2403-2413.

(109) Morel, B.; Casares, S.; Conejero-Lara, F. A single mutation induces amyloid aggregation in the alpha-spectrin SH3 domain: analysis of the early stages of fibril formation. *Journal of molecular biology* **2006**, *356*, 453-468.

(110) Casares, S.; Lopez-Mayorga, O.; Vega, M. C.; Camara-Artigas, A.; Conejero-Lara, F. Cooperative propagation of local stability changes from low-stability and high-stability regions in a SH3 domain. *Proteins* **2007**, *67*, 531-547.

(111) Krobath, H.; Estacio, S. G.; Faisca, P. F.; Shakhnovich, E. I. Identification of a conserved aggregation-prone intermediate state in the folding pathways of Spc-SH3 amyloidogenic variants. *Journal of molecular biology* **2012**, *422*, 705-722.

(112) Clayton, D. F.; George, J. M. The synucleins: a family of proteins involved in synaptic function, plasticity, neurodegeneration and disease. *Trends in neurosciences* **1998**, *21*, 249-254.

(113) Mori, F.; Tanji, K.; Yoshimoto, M.; Takahashi, H.; Wakabayashi, K. Demonstration of alpha-synuclein immunoreactivity in neuronal and glial cytoplasm in normal human brain tissue using proteinase K and formic acid pretreatment. *Experimental neurology* **2002**, *176*, 98-104.

(114) De Franceschi, G.; Frare, E.; Bubacco, L.; Mammi, S.; Fontana, A.; de Laureto, P. P. Molecular insights into the interaction between alpha-synuclein and docosahexaenoic acid. *Journal of molecular biology* **2009**, *394*, 94-107.

(115) Sharon, R.; Goldberg, M. S.; Bar-Josef, I.; Betensky, R. A.; Shen, J.; Selkoe, D. J. alpha-Synuclein occurs in lipid-rich high molecular weight complexes, binds fatty acids, and shows homology to the fatty acid-binding proteins. *Proceedings of the National Academy of Sciences of the United States of America* **2001**, *98*, 9110-9115.

(116)   Sharon, R.; Bar-Joseph, I.; Mirick, G. E.; Serhan, C. N.; Selkoe, D. J. Altered fatty acid composition of dopaminergic neurons expressing alpha-synuclein and human brains with alpha-synucleinopathies. *The Journal of biological chemistry* **2003**, *278*, 49874-49881.

(117)   Darios, F.; Ruiperez, V.; Lopez, I.; Villanueva, J.; Gutierrez, L. M.; Davletov, B. Alpha-synuclein sequesters arachidonic acid to modulate SNARE-mediated exocytosis. *EMBO reports* **2010**, *11*, 528-533.

(118)   Perlmutter, J. D.; Braun, A. R.; Sachs, J. N. Curvature dynamics of alpha-synuclein familial Parkinson disease mutants: molecular simulations of the micelle- and bilayer-bound forms. *The Journal of biological chemistry* **2009**, *284*, 7177-7189.

(119)   Rao, J. N.; Kim, Y. E.; Park, L. S.; Ulmer, T. S. Effect of pseudorepeat rearrangement on alpha-synuclein misfolding, vesicle binding, and micelle binding. *Journal of molecular biology* **2009**, *390*, 516-529.

(120)   Ouberai, M. M.; Wang, J.; Swann, M. J.; Galvagnion, C.; Guilliams, T.; Dobson, C. M.; Welland, M. E. alpha-Synuclein senses lipid packing defects and induces lateral expansion of lipids leading to membrane remodeling. *The Journal of biological chemistry* **2013**, *288*, 20883-20895.

(121)   Uversky, V. N.; Lee, H. J.; Li, J.; Fink, A. L.; Lee, S. J. Stabilization of partially folded conformation during alpha-synuclein oligomerization in both purified and cytosolic preparations. *The Journal of biological chemistry* **2001**, *276*, 43495-43498.

(122)   Uversky, V. N.; Li, J.; Fink, A. L. Evidence for a partially folded intermediate in alpha-synuclein fibril formation. *The Journal of biological chemistry* **2001**, *276*, 10737-10744.

(123)   Wetzel, R. Kinetics and thermodynamics of amyloid fibril assembly. *Accounts of chemical research* **2006**, *39*, 671-679.

(124)   Ahmad, M. F.; Ramakrishna, T.; Raman, B.; Rao Ch, M. Fibrillogenic and non-fibrillogenic ensembles of SDS-bound human alpha-synuclein. *Journal of molecular biology* **2006**, *364*, 1061-1072.

(125)   Hong, D. P.; Han, S.; Fink, A. L.; Uversky, V. N. Characterization of the non-fibrillar alpha-synuclein oligomers. *Protein and peptide letters* **2011**, *18*, 230-240.

(126)   Bernstein, S. L.; Liu, D.; Wyttenbach, T.; Bowers, M. T.; Lee, J. C.; Gray, H. B.; Winkler, J. R. Alpha-synuclein: stable compact and extended monomeric structures and pH dependence of dimer formation. *Journal of the American Society for Mass Spectrometry* **2004**, *15*, 1435-1443.

(127)   Uversky, V. N.; Li, J.; Fink, A. L. Metal-triggered structural transformations, aggregation, and fibrillation of human alpha-synuclein. A possible molecular NK between Parkinson's disease and heavy metal exposure. *The Journal of biological chemistry* **2001**, *276*, 44284-44296.

(128)   Ahmad, A.; Burns, C. S.; Fink, A. L.; Uversky, V. N. Peculiarities of copper binding to alpha-synuclein. *Journal of biomolecular structure & dynamics* **2012**, *29*, 825-842.

(129)   Uversky, V. N.; Yamin, G.; Munishkina, L. A.; Karymov, M. A.; Millett, I. S.; Doniach, S.; Lyubchenko, Y. L.; Fink, A. L. Effects of nitration on the structure and aggregation of alpha-synuclein. *Brain research. Molecular brain research* **2005**, *134*, 84-102.

(130)   Uversky, V. N.; Yamin, G.; Souillac, P. O.; Goers, J.; Glaser, C. B.; Fink, A. L. Methionine oxidation inhibits fibrillation of human alpha-synuclein in vitro. *FEBS letters* **2002**, *517*, 239-244.

(131)   Fujiwara, H.; Hasegawa, M.; Dohmae, N.; Kawashima, A.; Masliah, E.; Goldberg, M. S.; Shen, J.; Takio, K.; Iwatsubo, T. alpha-Synuclein is phosphorylated in synucleinopathy lesions. *Nature cell biology* **2002**, *4*, 160-164.

(132)   Trexler, A. J.; Rhoades, E. N-Terminal acetylation is critical for forming alpha-helical oligomer of alpha-synuclein. *Protein science : a publication of the Protein Society* **2012**, *21*, 601-605.

(133)   Uversky, V. N.; Eliezer, D. Biophysics of Parkinson's disease: structure and aggregation of alpha-synuclein. *Current protein & peptide science* **2009**, *10*, 483-499.

(134)   Dikiy, I.; Eliezer, D. N-terminal acetylation stabilizes N-terminal helicity in lipid- and micelle-bound alpha-synuclein and increases its affinity for physiological membranes. *The Journal of biological chemistry* **2014**, *289*, 3652-3665.

(135)   Necula, M.; Chirita, C. N.; Kuret, J. Rapid anionic micelle-mediated alpha-synuclein fibrillization in vitro. *The Journal of biological chemistry* **2003**, *278*, 46674-46680.

(136)   Jo, E.; Darabie, A. A.; Han, K.; Tandon, A.; Fraser, P. E.; McLaurin, J. alpha-Synuclein-synaptosomal membrane interactions: implications for fibrillogenesis. *European journal of biochemistry / FEBS* **2004**, *271*, 3180-3189.

(137)   Perrin, R. J.; Woods, W. S.; Clayton, D. F.; George, J. M. Exposure to long chain polyunsaturated fatty acids triggers rapid multimerization of synucleins. *The Journal of biological chemistry* **2001**, *276*, 41958-41962.

Chapter 2

CHARACTERIZATION OF OLIGOMERS OF HETEROGENEOUS SIZE AS PRECURSORS OF AMYLOID FIBRIL NUCLEATION OF AN SH3 DOMAIN: AN EXPERIMENTAL KINETICS STUDY

ABSTRACT

Understanding the earliest molecular events during nucleation of the amyloid aggregation cascade is of fundamental significance to prevent amyloid related disorders. We report here an experimental kinetic analysis of the amyloid aggregation of the N47A mutant of the α-spectrin SH3 domain (N47A Spc-SH3) under mild acid conditions, where it is governed by rapid formation of amyloid nuclei. The initial rates of formation of amyloid structures, monitored by thioflavine T fluorescence at different protein concentrations, agree quantitatively with high-order kinetics, suggesting an oligomerization pre-equilibrium preceding the rate-limiting step of amyloid nucleation. The curves of native state depletion also follow high-order irreversible kinetics. The analysis is consistent with the existence of low-populated and heterogeneous oligomeric precursors of fibrillation that form by association of partially unfolded protein monomers. An increase in NaCl concentration accelerates fibrillation but reduces the apparent order of the nucleation kinetics; and a double mutant (K43A, N47A) Spc-SH3 domain, largely unfolded under native conditions and prone to oligomerize, fibrillates with apparent first order kinetics. On the light of these observations, we propose a simple kinetic model for the nucleation event, in which the monomer conformational unfolding and the oligomerization of an amyloidogenic intermediate are rapidly pre-equilibrated. A conformational change of the polypeptide chains within any of the oligomers, irrespective of their size, is the rate-limiting step leading to the amyloid nuclei. This model is able to explain quantitatively the initial rates of aggregation and the observed variations in the apparent order of the kinetics and, more importantly, provides crucial thermodynamic magnitudes of the processes preceding the nucleation. This kinetic approach is simple to use and may be of general applicability to characterize the amyloidogenic intermediates and oligomeric precursors of other disease-related proteins.

INTRODUCTION

Protein amyloid aggregation is intimately associated with a wide range of disorders, among which there are some devastating human diseases such as Alzheimer's, Huntington's, Parkinson's, prion diseases or type II diabetes [1]. Protein aggregation is also a general problem

in biotechnological applications of proteins and in some cases plays a biologically relevant role, such as for instance in the polymerization of actin [2]. For these reasons, experimental kinetics studies of protein aggregation have been of general interest since several decades ago [3]. Quantitative aggregation kinetics analysis can help to infer the detailed mechanism and provide insight into the identity and properties of key intermediates in the aggregation pathway. Understanding the mechanisms of protein aggregation is a key step to control protein aggregation and to delineate effective therapeutic strategies for protein aggregation disorders.

An increasingly large body of experimental and theoretical examples of protein aggregation kinetic studies can be found in the recently reviewed literature [4,5]. Theoretical models usually treat protein aggregation as a multi-stage process, in which a number of consecutive and/or parallel stages occur to convert the soluble protein monomer to large amyloid aggregates [4]. These stages may include partial unfolding or refolding, oligomerization, conformational conversion, elongation, condensation, fragmentation, etc. The broad diversity of proposed models of aggregation can be understood in terms of a predominance of one or more of these stages in the overall aggregation kinetics, which results in a variety of kinetic behaviors, depending on the protein and/or the experimental conditions studied in each case [6].

Almost invariably, the formation of oligomeric species, normally soluble and sometimes structurally unstable or metastable, is a key step in the nucleation of amyloid structures. For example, the 40- or 42-residue forms of amyloid-beta peptide (Abeta) give rise to different oligomeric species with a relatively disordered structure in rapid equilibrium with the monomeric forms [7,8]. Likewise, similar oligomers featuring dynamic structures have been identified during amyloid fibril formation of the yeast prion Sup35p, phosphoglycerate kinase or the SH3 domain of the PI3 kinase [9-11]. Nucleation is then completed by structural conversion of these intermediate species into small amyloid-like structures that act subsequently as templates triggering rapid growth of fibrils. Sometimes, native or native-like structures are forming the oligomeric aggregates and then conversion to amyloid structures takes place within the aggregates [12,13].

The investigation of the mechanism of formation of soluble oligomers during the initial stages of aggregation is of vital importance because these species appear to constitute the main toxic agents in neurodegenerative diseases [14]. Supporting this hypothesis, a significant correlation was found between the levels of soluble Abeta peptide, including its oligomeric forms, and the degree of synaptic alteration, neurodegeneration and cognitive decline in Alzheimer's disease patients, whereas a similar correlation was not observed for the insoluble deposits [15]. Also for α-synuclein, increasing evidence suggests that non-fibrillar dimers or oligomers play a major role in the progress of Parkinson's disease [16]. Similarly, it has been shown with neuronal cell cultures that there is less cell death in the presence of large aggregates of poly-Q-rich Huntingtin than when the soluble fraction is present [17]. Certain non-fibrillar aggregates of transthyretin have also been shown to be toxic to neuronal cells under the conditions where the native tetramers and the mature fibrils have no significant toxicity [18].

The general toxic nature of prefibrillar aggregates has been further underlined by the finding that oligomeric species of proteins unrelated to disease, such as HypF-N from E. coli, the SH3 domain of PI3 kinase or equine lysozyme, are highly toxic in fibroblast and neuron cultures, whereas the amyloid fibrils of the same proteins show low toxicity [19,20]. These and many other studies have emphasized on the importance of using well-characterized model proteins, even unrelated to disease, to investigate the mechanisms of amyloid aggregation.

In previous work, we have reported that the wild type form and several mutants of the SH3 domain of α-spectrin (Spc-SH3) are rapidly converted to amyloid fibrils at mild acid pH [21,22]. We found that the rate of nucleation is strongly affected by sequence mutations and experimental conditions, in particular temperature, pH and the concentrations of protein and salt, resulting in considerable changes in the governing kinetics and also in the morphological properties of the finally assembled fibrils [23]. For instance, at low salt concentration the aggregation shows a considerable lag phase, as usually observed for nucleation-dependent polymerization, resulting in well-ordered straight and twisted amyloid fibrils. An increase in salt concentration removes the lag phase due to an increase in the rate of nucleation, which is no longer rate-limiting in the formation of fibrils. Under these conditions, a higher

accumulation of amyloid nuclei results in curly and relatively disordered fibrils. Salt ions appear to act by lowering the apparent activation energy of fibril nucleation [23]. These results implied that the molecular events taking place prior to and during the nucleation of amyloid structures determine the fate of the protein chain along the subsequent aggregation cascade. Therefore, a more detailed knowledge of the molecular mechanism of nucleation could give additional insight upon the physicochemical factors governing the process and offer more opportunities to its manipulation and control.

In this work we analyzed quantitatively the kinetics of formation of amyloid nuclei of the N47A Spc-SH3 mutant using a range of biophysical techniques. Although most amyloid fibrillation studies with both disease-related and unrelated proteins have observed significant lag phases in the kinetics, typical of nucleation-dependent processes, during these lag phases the formation of amyloid nuclei is a rare process, difficult to observe experimentally, and the aggregation kinetics are mainly governed by the elongation of few preformed nuclei accompanied by other secondary processes. For this reason, we decided to work under conditions of fast nucleation, i.e., in the absence of a lag phase, so that amyloid nuclei are abundantly formed and the observed kinetics are mainly representative of the nucleation process itself, whereas subsequent processes such as fibril elongation or fragmentation can be neglected during the initial stages of the kinetics. Under the selected conditions the nucleation kinetics can be quantitatively described as an irreversible high-order reaction, suggesting that nucleation of amyloid structures is preceded by formation of oligomeric precursors in rapid equilibrium with the monomer. Using a battery of biophysical methods we showed that these oligomers occur at very low population, have a heterogeneous size and form by rapid association of partially unfolded protein monomers. We proposed a mathematical kinetic model in which stable amyloid nuclei form by a conformational change of the protein within the oligomers. The model explained very well the observed initial rates of aggregation and allowed us to derive thermodynamic magnitudes characterizing the amyloidogenic intermediate and its oligomerization, as well as the rate constants of conformational change that forms the amyloid nuclei.

MATERIALS AND METHODS

Protein sample preparation

The Spc-SH3 domain mutants studied were overexpressed in *E. coli* and purified as described elsewhere [24]. ^{15}N-labelled protein was produced in *E. coli* cultures using M9 minimal media with ^{15}N-ammonium sulfate as the sole nitrogen source. For aggregation experiments the lyophilized protein was dissolved, unless stated, in the appropriate buffer at 4°C, centrifuged for 2 minutes and filtered through a 0.2 μm filter. Protein concentration was determined by measurement of absorbance at 280 nm using an extinction coefficient of 15220 $M^{-1} cm^{-1}$.

ThT and ANS fluorescence

Thioflavine T (ThT) or 1-Anilino-8-naphthalene sulfonate (ANS) fluorescence was continuously monitored during amyloid fibril formation at 37°C in a Varian Cary Eclipse spectrofluorimeter (Agilent Technologies, Santa Clara, CA) equipped with a Peltier-controlled thermostatic cell holder. To start aggregation, a freshly prepared protein solution was mixed with a concentrated stock solution of each dye previously prepared in the same buffer (100 mM glycine, pH 3.2, 100 mM NaCl). The sample was then placed into a fluorescence cuvette, which was previously thermostatized at 37°C, and covered with mineral oil to avoid evaporation. Fluorescence intensity of ThT at 10 μM was monitored at 485 nm using an excitation wavelength of 440 nm and the ANS fluorescence was measured at 470 nm with excitation at 370 nm using various ANS concentrations. Previous control experiments allowed us to establish the appropriate concentration of each dye for the experiments. A linear relationship between the ThT fluorescence and the mass amount of amyloid fibrils was established using preformed amyloid fibrils (Figure S1).

Initial rates of growth of amyloid structure were calculated by fitting the initial region of the ThT kinetics curves, corresponding to an approximate signal growth of less than 50% of the maximum, using a double exponential function:

$$y = y_0 + A_1 \cdot \left(1 - e^{-k_1 t}\right) + A_2 \cdot \left(1 - e^{-k_2 t}\right) \qquad (1)$$

The initial slope is then calculated from the resulting fitting parameters as:

$$r_0 = \left(\frac{dy}{dt}\right)_{t \to 0} = A_1 \cdot k_1 + A_2 \cdot k_2 \qquad (2)$$

This operational extrapolation procedure allowed us an accurate determination of the initial slopes of the ThT curves and avoided the assumption of any time interval in the kinetics to define an initial aggregation rate.

Circular dichroism (CD)

CD measurements were made in a Jasco J-715 spectropolarimeter (Tokyo, Japan) equipped with a thermostatic cell holder. Near UV CD spectra of the native N47A Spc-SH3 domain and the preformed amyloid fibrils were acquired at 4°C between 260 nm and 320 nm at a protein concentration of 8 mg mL^{-1} in a 1 mm path length cuvette (Figure S2). This short path length was necessary to avoid instrument saturation due to the high protein concentration of the samples. Far-UV CD measurements with the K43A-N47A double mutant were done at a protein concentration of 0.2 mg mL^{-1} using a 1 mm path length cuvette. For kinetic experiments monitored by near-UV CD, a fresh protein sample was placed into a 1 or 2 mm cuvette, depending on the protein concentration of the experiment. The CD signal at 295 nm was then monitored at 37°C during the time course of aggregation. Data were averaged for 20 s using a band width of 1 nm and a response time of 4 s.

Nuclear Magnetic Resonance

To follow the amyloid aggregation by two-dimensional NMR in real time, 4 mg of ^{15}N-labelled protein was dissolved in 500 μL of cold buffer (100 mM d$_6$-Gly, 100 mM NaCl, pH 3.2) containing 10 % D$_2$O and placed into the NMR tube. The final protein concentration was 1.1 mM (8 mg mL^{-1}). The temperature in the NMR probe was set to 37°C and,

immediately after temperature equilibration, a series of ^{1}H-^{15}N HSQC two-dimensional spectra were acquired during the time course of aggregation in a 600 MHz Varian NMRsystem spectrometer (Agilent Technologies, Santa Clara, CA). Each spectrum consisted of 512x32 complex points recorded using a relaxation delay of 1 s and resulting in a total experiment time of 2 minutes and 28 seconds. The spectral widths were 12.04 ppm for ^{1}H and 30.00 ppm for ^{15}N. Spectra were processed using NMRPipe [25]. The assignment of the ^{1}H-^{15}N crosspeaks of the HSQC spectrum was performed using as a reference the previously published assignment of the WT Spc-SH3 domain [26]. To obtain the aggregation kinetics, the signal intensities were evaluated using NMRview [27] and represented versus the incubation time.

Dynamic light scattering (DLS)

Aggregation was monitored at 37°C by DLS in a DynaPro MS-X instrument (Wyatt, Santa Barbara, CA, USA) using a thermostatized 30 μL quartz cuvette. The protein solution and the buffer were centrifuged and filtered through a 0.02 μm filters before the measurements. During the time course of the aggregation the DLS data were acquired every 45 seconds until saturation of the signal. The laser power was adjusted to avoid early saturation. Dynamics v.6 software was used in data collection and processing of the correlation function to finally obtain the particle size distributions during the course of aggregation.

Attenuated total reflectance Fourier-transform infrared (ATR-FTIR) spectroscopy

Infrared spectra were recorded from 4000 cm^{-1} to 900 cm^{-1} on a Bruker IFS-66 FTIR spectrophotometer (Brucker, Ettlingen, Germany) equipped with a BioATR-II cell. For each sample, 128 interferograms were coadded and Fourier transformed with a zero filling factor of 4 to yield spectra with a nominal resolution of 2 cm^{-1}. The sample temperature was controlled and set to 37°C by means of a thermostatic cell jacket. FTIR measurements were taken at 37°C every 90 seconds for the first 120 minutes of incubation and thereafter every

30 minutes. Buffer spectra were recorded under identical conditions and subtracted from the spectra of the protein sample (Figure S3). Spectral contributions from residual water vapor were reduced using the atmospheric compensation filter built in the Bruker OPUS software. Difference FTIR spectra were then calculated by subtracting the first measurement from all subsequent spectra. The change in the area of the difference band (from 1635 cm^{-1} to 1591 cm^{-1}) was calculated and plotted versus time.

Differential scanning calorimetry

The thermal unfolding of the K43A-N47A Spc-SH3 double mutant was monitored in a Auto-Cap VP-DSC instrument (Microcal, Northampton, MA) at a scan rate of 1.5°C min^{-1} and a protein concentration of about 1 mg mL^{-1}. The molar partial heat capacity curve (C_p) was calculated from the DSC data and analyzed using Origin 6.1 (OriginLab, Northampton, MA) according to the two-state unfolding model.

Size-exclusion chromatography

Size-exclusion chromatography (SEC) experiments were performed at 37°C using a thermostatized Superdex 75 HR 10/30 column connected to an ÄKTA prime plus FPLC chromatograph (GE Healthcare, Tokyo). N47A Spc-SH3 samples were prepared in the aggregation buffer at the appropriate concentration and were incubated at 37°C in a water bath during different times. The same buffer was used for the elution at a flow rate of 1 mL min^{-1}. A volume of 100 μL was loaded onto the column. The elution profiles were recorded by monitoring the absorbance at 280 nm. The column was previously calibrated using protein standards.

RESULTS

Kinetics of formation of amyloid structure observed by thioflavine T fluorescence

The kinetics of growth of amyloid fibrils of N47A Spc-SH3 was followed at 37°C at several protein concentrations by continuously monitoring ThT fluorescence at pH 3.2 in 100 mM glycine buffer, 100 mM NaCl. Under these experimental conditions, the development of amyloid structures takes place very rapidly without any significant lag phase, indicating a fast formation of amyloid nuclei (Figure 1A). No stirring or shaking of the samples was necessary to obtain rapid and reliable aggregation kinetics and we observed no significant sedimentation of the aggregates during the length of our experiments. This allowed us monitoring directly the aggregation kinetics using a variety of biophysical techniques, avoiding irreproducibility arising from the control of stirring.

The appearance of a significant amount of fibrils visible by electron microscopy is delayed under these conditions for at least 30 min (see Figure 10 in ref. [21]). Therefore, initial growth of ThT fluorescence could be attributed to the formation of small amyloid nuclei. The aggregation process does not follow first-order kinetics and its rate is strongly dependent of the initial concentration of protein. In addition, the ThT signal does not reach a plateau within the time of the experiments. Initial rates of formation of amyloid nuclei were estimated from initial slopes of the kinetic traces as described in Material and Methods. Using a double logarithmic plot, we found that the initial rates scale approximately with the fourth power of the initial protein concentration, indicating a high order for the nucleation of amyloid structure (Figure 1B, Table 1). Nevertheless, there is a slight but significant sigmoidal shape in this plot.
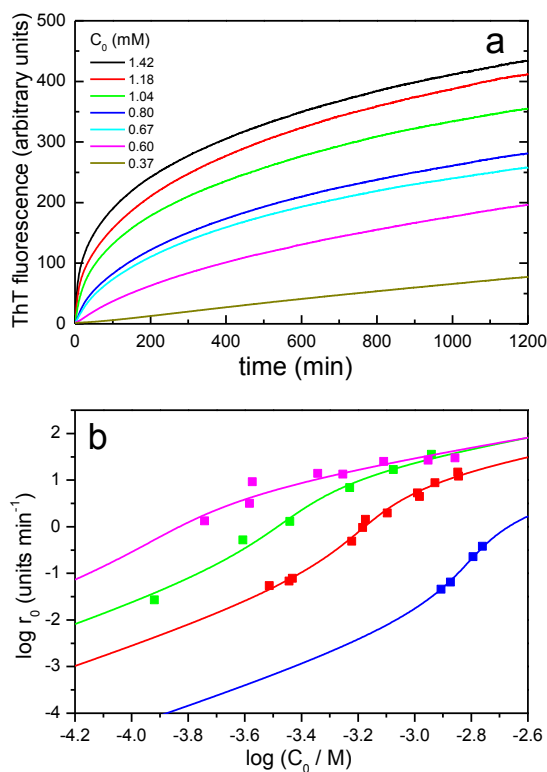
Figure 1. Kinetics of formation of amyloid fibrils followed by ThT fluorescence at 37ºC. *A: Kinetic curves of amyloid fibrillation of N47A Spc-SH3 in the presence of 100 mM NaCl at different initial protein concentrations as indicated. B: Double logarithmic plot of the initial rates of amyloid fibrillation of N47A Spc-SH3 versus the initial protein concentration in presence of different NaCl concentrations: 50 mM (blue); 100 mM (red) and 200 mM (green). The initial rates of the double mutant K43A-N47A Spc-SH3 in the presence of 100 mM NaCl are shown in magenta. Symbols correspond to the experimental rates and continuous lines represent the best fits according to equations 4 to 8 of the model as described in the text.*

Kinetics of depletion of native protein

We monitored the aggregation under the same experimental conditions by acquiring a series of ^{15}N-^{1}H HSQC NMR experiments during the course of the fibrillation process at 37°C using a 1.1 mM (8 mg mL^{-1}) sample of ^{15}N-labelled protein. This experiment was aimed at the detection of any early soluble intermediates of the protein, which may become populated

prior to the formation of the fibrils. All spectra looked, however, identical to that of the native protein except for a rapid and continuous decrease in intensity (Figure S4). No significant shifts of the HSQC signals were observed during the whole process and the intensity decays of all the signals are virtually identical. These observations may suggest that the native protein is converted to large aggregates without accumulation of any intermediate visible by NMR. It is possible that interconversion of intermediates taking place in the NMR time scale could result in extreme line broadening, which renders invisible the signals. A plot of the normalized and averaged intensities of all the native HSQC peaks does not follow a single exponential decay (Figure 2). The kinetics could instead be very well fitted using the integrated equation of an n-order irreversible kinetics:

$$[N] = \frac{C_0}{\left(1 + C_0^{n-1}kt\right)^{1/(n-1)}} \qquad (3)$$

Where n is the apparent order of the reaction, C_0 is the initial protein concentration, [N] is the concentration of native protein at time t and k is an apparent n-order rate constant. This fitting resulted in an apparent order of 4.2 ± 0.3 (Table 1).
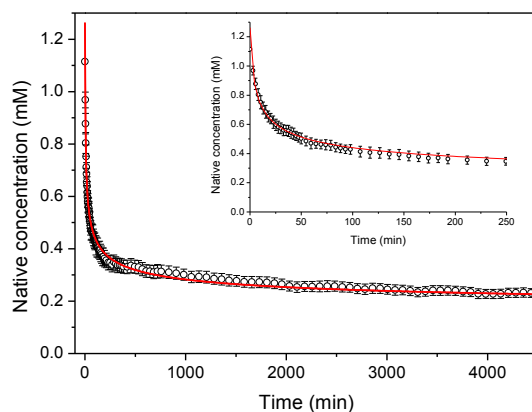
Figure 2. Kinetics of native-state depletion monitored by NMR. *Averaged and normalized intensities of the cross peaks of all residues of N7A Spc-SH3 in a series of ^{15}N-^{1}H-HSQC NMR spectra recorded during the course of aggregation at 37ºC using an initial protein concentration of 1.1 mM. The red continuous line represents the best fit using the integrated equation of an n-order irreversible kinetics. The inset shows an expansion of the early times of the kinetics.*

The rate of disappearance of the native protein during the early stages of fibrillation was also monitored by near-UV CD at several protein concentrations ranging between 0.84 mM and 1.6 mM (Figure 3). In these experiments we took advantage of the absence of CD signal at 295 nm in the near-UV CD spectrum of the amyloid fibrils and we could assume therefore that the CD signal intensity at this wavelength is proportional to the concentration of the native protein monomer during the aggregation process. The kinetic curves are strongly concentration-dependent and in agreement with a high-order process. When normalized by the protein concentration, as expected for this type of kinetics, the curves converge approximately to a common trend. Global fitting of all the kinetic curves using equation 3 did not give fully satisfactory results especially for the curves at the lowest protein concentrations. Individual fittings yielded apparent orders ranging between 4 and 4.7 and relatively similar values for the apparent rate constants (Table 1). The initial rates of native state depletion, estimated by extrapolation of the slopes of the kinetics, are also strongly dependent on protein concentration. Double logarithmic plot of the initial rates versus the protein concentration provides an apparent order of about 6.
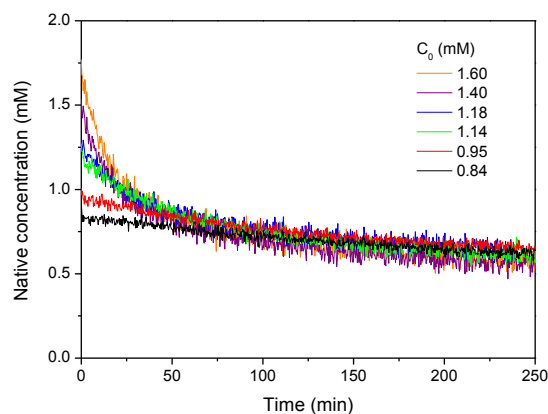
Figure 3. ***Kinetics of native state depletion monitored by near-UV CD.*** *Different initial protein concentrations of N47A Spc-SH3 were analyzed as indicated. The intensity of the native CD signal at 295 nm was monitored as a function of time and normalized using the values of initial protein concentration.*

These results clearly demonstrate that during the early stages of aggregation, both the depletion of native protein and the growth of amyloid structures follow high-order

irreversible kinetics. A simple interpretation of this result would suggest that the precursors of the rate-limiting step for amyloid nucleation are oligomers of about 4 to 6 protein molecules. Formation of these oligomeric precursor species from the native state of the protein seems to be therefore a necessary step preceding the nucleation process. Furthermore, this oligomerization must be sufficiently fast under these conditions to avoid a lag phase in the fibrillation.

Formation of β-sheet structure

Infrared spectra were measured during the aggregation process under the same conditions of the above experiments (Figure S3). The development of a prominent band at 1622 cm^{-1} indicative of the formation of β-sheet structure occurs in a rapid phase within 100-120 min (Figure 4). Further development of β-sheet structure occurs in a slower process as a result of fibril formation.
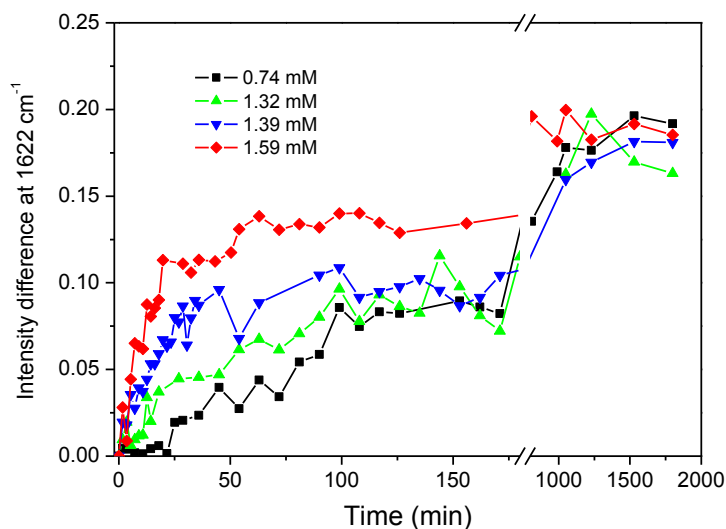
Figure 4. Kinetics of formation of beta-sheet structure during the course of aggregation. *Aggregation of N47A Spc-SH3 was monitored by infrared spectroscopy at different initial protein concentrations as indicated in the figure. The data correspond to the area of the spectral band between 1591 cm^{-1} and 1635 cm^{-1} in the difference spectra obtained by subtracting initial spectrum from that of each time point of the kinetics.*

Table 1*: Kinetic analysis of the apparent order for irreversible aggregation of Spc-SH3 using different biophysical techniques and methods of analysis.*

Method	Type of analysis	Apparent order	log k $(M^{1-n}\,min^{-1})$	Protein concentration (mM)
ThT fluorescence	Initial rates[a]	3.80 ± 0.13	-	0.31 - 1.44
NMR	Non-linear fitting[b]	4.2 ± 0.3	9.2 ± 0.6	1.1
Near-UV CD	Initial rates[a]	6.1 ± 0.5	12.9 ± 1.4	0.84 - 1.6
	Non-linear fitting[b]	4.57 ± 0.07	9.2 ± 0.3	1.6
		4.73 ± 0.08	9.7 ± 0.3	1.4
		4.52 ± 0.08	8.9 ± 0.2	1.18
		4.62 ± 0.06	9.6 ± 0.2	1.14
		4.28 ± 0.06	7.9 ± 0.3	0.95
		4.0 ± 0.1	6.9 ± 0.3	0.84
ANS fluorescence	Initial rates[a]	3.1 ± 0.5	-	0.14 - 1.17
Far-UV CD	Initial rates[a]	1.5 ± 0.3	-	0.36 - 1.11

[a]Initial rates of signal growth were plotted versus the initial protein concentration in a double logarithmic plot. The apparent order is derived from the slope in a linear fit to this representation.

[b]The normalized signal intensity decay was fitted to the integrated equation of an irreversible n-order kinetics.

The rapid conformational change to achieve beta-sheet structure was also observed by far-UV CD in a previous work although these data were presented in a normalized form (mean-residue molar ellipticity, see Figure 2b in ref. [23]). The negative CD signal at 215 nm increases very rapidly in a fast phase within about 100 min, indicating a fast conformational change with β-sheet formation even at the lowest protein concentration analyzed (0.36 mM). The initial rates of CD signal development scale approximately with the 1.5 power of the initial protein concentration, suggesting that the appearance of some β-sheet structure occurs prior to the fibril nucleation and is likely to be concomitant to pre-oligomerization. These results clearly indicate the occurrence of a rapid conformational phase previous to nucleation of the amyloid fibrils, which involves partial unfolding of the protein, formation of β-sheet structure and oligomerization.

Detection of partially-folded species

The formation of oligomers of partially unfolded protein may result in the exposure of hydrophobic surface, which could be monitored using ANS fluorescence. We first followed the process for a protein concentration of 1.26 mM using different ANS concentrations ranging between 10 μM and 400 μM (not shown). The ANS fluorescence intensity develops rapidly in all experiments reaching a plateau. The final ANS fluorescence intensity is approximately proportional to the ANS concentration up to about 100 μM and then tends to saturate. Above 50 μM ANS we found a significant effect of ANS on the rate of aggregation (results not shown). Using 25 μM ANS and varying the protein concentration, we observed considerable dependence of the growth rate of fluorescence intensity and absence of lag phase (Figure 5). The growth of ANS fluorescence intensity occurs earlier than that of ThT fluorescence, indicating rapid exposure of hydrophobic patches preceding nucleation of amyloid structure. Initial rate analysis indicates an apparent order of 3.1 ± 0.5, which is intermediate between the order observed for fibrillation and that of the initial conformational change monitored by far-UV CD. These results suggest that the development of the ANS fluorescence signal is not specific of the appearance of oligomers but it may also report on

the formation of amyloid structures. This is supported by separate experiments, in which we found that ANS co-precipitates with the amyloid fibrils indicating strong ANS binding to amyloid structures (results not shown).
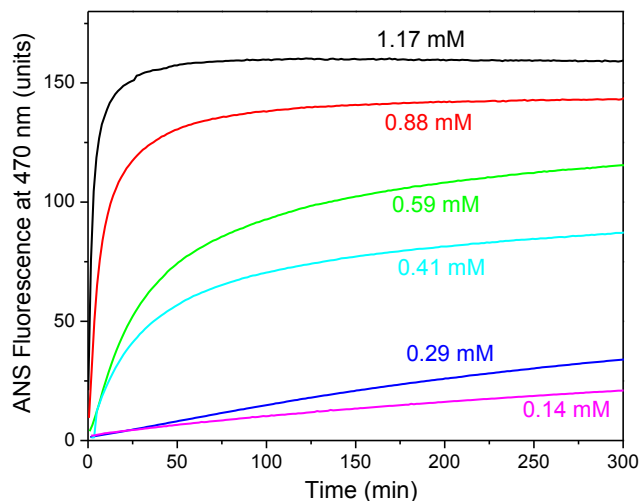
Figure 5. Exposure of hydrophobic surface during the course of aggregation of N47A Spc-SH3. Aggregation was monitored by ANS fluorescence at several initial protein concentrations are indicated along each curve. The concentration of ANS in these experiments was 50 μM.

Direct detection of oligomeric species

To investigate the growth rate of aggregates, DLS measurements were performed during the course of the aggregation at several protein concentrations. Figure 6 shows the time evolution of the scattering intensity and the apparent hydrodynamic radii (R_h) of the smallest particles visible in the size distributions. The changes in the particle size distributions clearly indicate a progressive conversion of the native protein (detected at the early times as a peak with apparent radius of about 1.7 nm) into larger particles (Figure 6A). Growing particles are observed with apparent radii starting from about 10-20 nm and increasing up to 30-50 nm, depending on the initial protein concentration, similarly to that observed for Abeta fibrillation by DLS [28]. In addition, the peak corresponding to the native R_h shifts up to ca. 2.7 to 3.0 nm, which suggests the association of a few protein molecules into small oligomers. This shift is

considerably delayed as the protein concentration is reduced indicating a slower accumulation of oligomers. The delay of oligomerization is coincident with a similar delay in the growth of scattering intensity (Figure 6B). The lag in the development of scattering intensity is not observed in the kinetics monitored by ThT fluorescence at similar concentrations, which indicates that only small-sized amyloid particles, likely amyloid nuclei, form at early times in the kinetics. The fact that the onset of growth in scattering intensity is concurrent with the oligomerization is suggestive of a condensation of nuclei as the process dominating the growth of large amyloid aggregates.
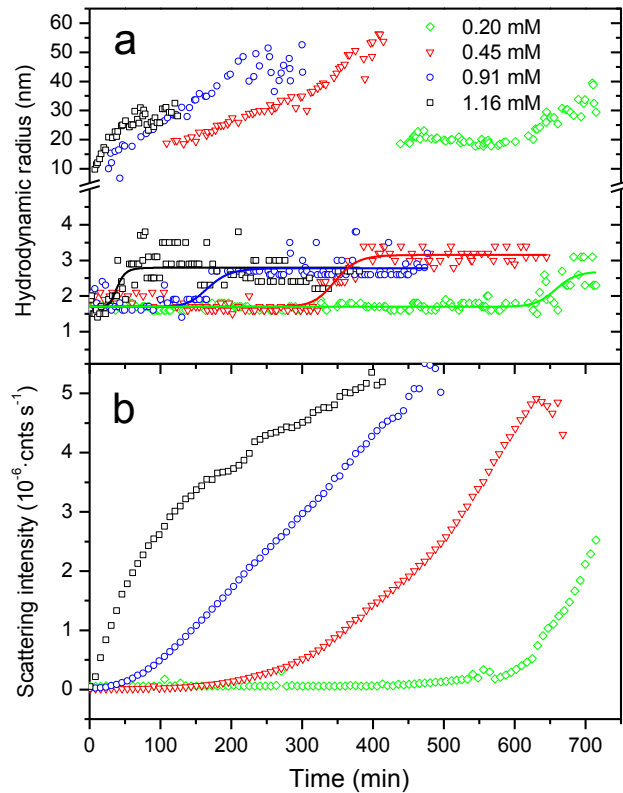
Figure 6. Time course of aggregation of N47A Spc-SH3 monitored by DLS. Several initial protein concentrations were analyzed as indicated. A: Hydrodynamic radii of the two smallest particles visible in the size distributions as a function of the time of incubation. The sigmoidal lines are used only for clarity purposes. B: Time dependence of the scattering intensity.

SEC experiments were also made to analyze the mixtures during the early stages of the fibrillation (Figure 7). Samples of 8 mg mL^{-1} (1.1 mM) of protein were incubated at 37°C for several time periods and analyzed in a Superdex S75 column previously equilibrated in the same aggregation buffer and also thermostatized at 37°C (Figure 7A). The elution profile of a non-incubated sample shows a single peak eluting at 18.5 mL, corresponding to the native monomer. After 30 min of incubation, high-molecular weight particles are already formed eluting at the exclusion volume of the column. The amount of these aggregates increases at longer times of incubation while the amount of monomer decreases concomitantly. These species correspond very likely to stable protofibrils or fibrils. In contrast, for protein samples incubated for only 5 min or 10 min there is still no evidence of formation of the high-molecular weight aggregates and most of the protein eluted as monomer. There is however a non-negligible UV absorption in the elution profiles for elution volumes corresponding to intermediate sized particles, suggesting a low population of oligomeric species (see Figure 7B). These low-molecular-weight oligomers cannot be detected at any elution volume if the SEC analysis of the same samples is made at 4°C or 25°C (not shown), indicating reversibility of the oligomerization at low temperature. When we repeated the same experiment at 37°C and double protein concentration (2.2 mM), the presence of small oligomers is much more evident in the profiles and the formation of high-molecular weight particles is faster (Figure 7C). There is no clear peak corresponding to any particular oligomer size but a broad UV absorption between the monomer and the large aggregate peaks. This suggests the existence of a distribution of interconverting oligomers, very likely in equilibrium with the monomers. Since SEC is a separative technique, the dilution that occurs during the chromatography separation would tend to shift the equilibrium towards the monomer.

From these results, we can conclude that early oligomers form rapidly during the kinetics leading to the early accumulation of small amyloid nuclei. The rate of this process is strongly dependent of the protein concentration and shows apparent high-order kinetics.
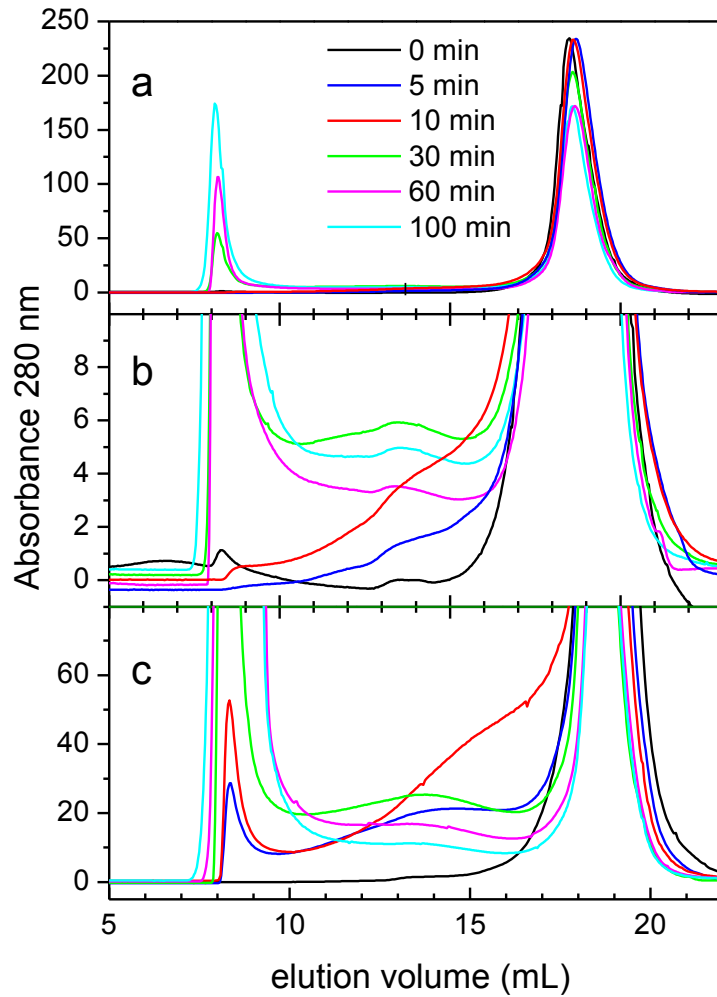
Figure 7. ***Size-exclusion chromatography analysis of N47A Spc-SH3 during the course of aggregation.*** *Samples were incubated at 37ºC during the times indicated along each elution profile prior to the analysis. A: Initial protein concentration of 1.1 mM; B: expansion of the ordinate axis of panel A; C: initial protein concentration of 2.2 mM.*

Influence of the salt concentration on the nucleation kinetics

Previously, we have reported that the concentration of NaCl strongly affects the nucleation of the N47A Spc-SH3 fibrillation [23]. Here we re-investigated the effect of the salt concentration on the nucleation kinetics by measuring the initial rates of fibrillation at 37°C by ThT fluorescence. Initial rates were measured under each condition only at protein concentrations producing an absence of significant lag phase, indicating a fast amyloid nucleation. As observed before, an increase in NaCl concentration accelerates the nucleation but, interestingly, reduces the apparent order of the kinetics from 6.4 ± 0.3 at 50 mM NaCl to 3.2 ± 0.2 at 200 mM NaCl (Figure 1B, Table 1). This might be in principle interpreted as a reduction in the average size of the critical oligomers preceding the nucleation produced by the increase in the concentration of salt ions. This would be contrary however to the increase in size of oligomers produced by a rise in the concentration of NaCl as observed by DLS in our previous work [23].

A simple nucleation model to interpret initial aggregation rates

To understand the observed kinetic effects in terms of a plausible mechanism, we proposed a simple model for amyloid fibril nucleation. This model is based upon previous polymerization models reported in the literature [3] [5,6], in which partial unfolding and/or linear polymerization processes previous to the rate-limiting steps of aggregation were assumed to be pre-equilibrated, i.e., they can be considered sufficiently fast to be under equilibrium during the process. The model is summarized in Figure 8 and mathematically developed in detail in the Supporting Information (Text S1):

In this model, N and U are respectively the native and the unfolded states of the protein. The state I is a monomeric intermediate prone to intermolecular association in equilibrium with the folded and unfolded states. The species A_i are oligomeric aggregates formed by reversible association of intermediate molecules. There is no limit imposed in our model to the maximum size of these oligomers, which will be only determined by the concentration of the associating species and the equilibrium association constants. The nucleation step was

modeled as an irreversible conformational change of the protein when it is part of an oligomer, giving rise to an oligomeric amyloid nucleus F_i of the same size [6]. We did not impose any restriction to the size of the oligomers that may undergo the nucleation change, except for the fact that nucleation can only occur from oligomeric states. This is different to most aggregation models, which usually assume a unique nucleus size. Since we are specifically modeling the initial rates of the amyloid nucleation process, we assumed that further elongation steps are not significant during the very early stages of the kinetics and do not contribute significantly to the accumulation of amyloid structures. This assumption is reasonable since we are extrapolating the aggregation rates to time zero, where no amyloid nuclei are still formed. In addition, as discussed in the Supporting Information (Text S3), a significant contribution of monomer addition to any nuclei or fibrils formed during the early times would result in upwards curvature of the kinetics, which is not observed under our experimental conditions, except for very slow nucleation conditions, such as at low protein and salt concentration (results not shown).

The equilibrium constants governing the conformational equilibrium of the monomeric protein are defined as:

$$K_I = \exp\left(-\frac{\Delta G_I^o}{RT}\right) = \left(\frac{[I]}{[N]}\right)_{eq} \quad (4a)$$

$$K_U = \exp\left(-\frac{\Delta G_U^o}{RT}\right) = \left(\frac{[U]}{[N]}\right)_{eq} \quad (4b)$$

And the equilibrium constant for each oligomerization step:

$$K_{A,i} = \exp\left(-\frac{\Delta G_{A,i}^o}{RT}\right) = \left(\frac{[A_{i+1}]}{[A_i][I]}\right)_{eq} \quad (i = 1 \ldots \infty) \quad (4c)$$

We assumed for simplicity that the equilibrium constants of all oligomerization steps are equal ($K_{A,i} = K_A$) [3]. Using this assumption, it is easy to obtain relatively simple equations relating the total protein concentration, C_0, to the equilibrium constants and the population of every equilibrium state (see Supplementary Material).

Figure 8. Kinetic scheme for amyloid nucleation. *N, I and U represent respectively the native, intermediate and unfolded monomeric states. A_i states represent oligomers of i size, where i can take any value from two to infinite. F_i represent oligomeric amyloid nuclei. Double arrows indicate rapidly-equilibrated reversible processes and the single arrow indicates a rate-limiting irreversible process.*

For instance, the fraction of protein in the native state, x_N, can be obtained solving the following equation:

$$1 = Ax_N + \frac{K_I x_N}{(1 - Bx_N)^2} \qquad (5)$$

The equilibrium constants governing the conformational equilibrium of the monomeric protein are defined as:

$$K_I = \exp\left(-\frac{\Delta G_I^o}{RT}\right) = \left(\frac{[I]}{[N]}\right)_{eq} \qquad (4a)$$

$$K_U = \exp\left(-\frac{\Delta G_U^o}{RT}\right) = \left(\frac{[U]}{[N]}\right)_{eq} \qquad (4b)$$

And the equilibrium constant for each oligomerization step:

$$K_{A,i} = \exp\left(-\frac{\Delta G_{A,i}^o}{RT}\right) = \left(\frac{[A_{i+1}]}{[A_i][I]}\right)_{eq} \qquad (i = 1 \dots \infty) \quad (4c)$$

We assumed for simplicity that the equilibrium constants of all oligomerization steps are equal ($K_{A,i} = K_A$) [3]. Using this assumption, it is easy to obtain relatively simple equations relating the total protein concentration, C_0, to the equilibrium constants and the population of every equilibrium state (see Supplementary Material). For instance, the fraction of protein in the native state, x_N, can be obtained solving the following equation:

$$1 = Ax_N + \frac{K_I x_N}{(1 - Bx_N)^2} \qquad (5)$$

Where $A = 1 + K_U$, and $B = K_I \cdot K_A \cdot C_0$. Similarly, the pre-equilibrated concentration of monomer in oligomeric species prior to the onset of the aggregation process is given by:

$$C_{A,0} = \sum_{i=2}^{\infty} i[A_i]_0 = \frac{(Bx_N)^2(2 - Bx_N)}{K_A(1 - Bx_N)^2} \qquad (6)$$

And the initial rate of conversion of protein to the amyloid state is given by:

$$r_0 = \left(\frac{dC_F}{dt}\right)_{t \to 0} = -\frac{d}{dt}\sum_{i=2}^{\infty} i[A_i]_0 = \sum_{i=2}^{\infty} ik_{F,i}[A_i]_0 \qquad (7)$$

Here C_F stands for the concentration of protein monomers in amyloid states. $k_{F,i}$ is the first-order rate constant for the conformational change of an i-sized oligomer to form an amyloid nucleus of equal size. Also for the sake of simplicity, we assumed that the rate constants are approximately independent of the size of the oligomers, i.e. $k_{F,i} \approx k_F$. Using this assumption eq. 7 becomes:

$$r_0 = k_F C_{A,0} = \frac{k_F(Bx_N)^2(2 - Bx_N)}{K_A(1 - Bx_N)^2} \qquad (8)$$

According to this equation, the initial slopes of the kinetics of amyloid growth –for instance, those measured by ThT fluorescence– will be a function of the first-order rate constant of conformational conversion, the initial protein concentration and the thermodynamic parameters governing the conformational-association equilibrium preceding the rate-limiting nucleation step.

Using equation 8 we simulated the initial rates of amyloid nucleation for an extensive set of values of the model parameters. A summary of the results of these simulations is shown in the Supporting Information (Text S2). First, we simulated the case where the amyloidogenic intermediate is the most stable state under the aggregating conditions ($K_I \gg 1$). In this case there are two limiting nucleation regimes: A) Low protein concentrations: $C_0 \ll K_A^{-1}$. Under these conditions the slope of the plot of log r_0 vs log C_0 is linear with a slope of 2. This means that most of the protein is in the monomeric state and the nucleation takes place via the dimer, with apparent 2nd order (I $\leftrightarrow$ A$_2$ $\to$ F$_2$). B) High protein concentration: $C_0 \gg K_A^{-1}$. In this case, the slope of the double logarithmic plot is 1 because most of the protein pre-equilibrates

as oligomers and the process simplifies to a first-order reaction ($A_i \rightarrow F_i$). The change from second to first order occurs progressively when C_0 approaches to K_A^{-1}.

In the case of a stable folded protein, with a low-populated amyloidogenic intermediate, there are two similar limiting regimes: A) Second order for $C_0 \ll (K_A \cdot K_I)^{-1}$ and B) first order for $C_0 \gg (K_A \cdot K_I)^{-1}$. For protein concentrations around a critical concentration, $C_0 \approx (K_A \cdot K_I)^{-1}$, the plot of log r_0 vs log C_0 undergoes an inflexion with a transient increase in slope. Interestingly, for the same critical concentration, the maximum slope depends on the relative values of K_I and K_A, i.e., on the stability of the monomeric intermediate compared to that of the oligomers. Low values of K_I and high association constant, K_A, give rise to a steep inflexion with high apparent reaction orders. This is due to a quite pronounced shift in the oligomerization pre-equilibrium as the protein concentration rises.

Changes in the values of the rate constant of the conformational change, k_F, result only in a vertical displacement of the double logarithmic plot. The effect of changes in the global unfolding equilibrium constant, K_U, is relatively small because it affects only marginally the relative population of I and the corresponding oligomerization equilibrium.

Using the equations of this model, we have fitted the experimental initial rates of amyloid nucleation measured by ThT fluorescence as a function of the protein concentration. In this analysis we assumed that only the amyloid nuclei are detected by thioflavin T fluorescence. An important problem arising when fitting these data is that the theoretical equations depend on four independent parameters (K_A, K_I, K_U and k_F). To reduce their number, we fixed the values of K_U using the experimental value at 37°C derived from the analysis of the thermal unfolding by DSC at low protein concentration [23]. Another difficulty in this analysis is that the interval of protein concentrations and the range of experimentally accessible initial rates are limited. For instance, at 50 mM NaCl, the fibril nucleation is fast only at high protein concentrations, whereas below 1 mM the aggregation kinetics shows a considerable lag phase [23]. The range of experimental data is therefore quite limited for this condition.

Individual fits at the three different salt concentrations describe very well the data but the dependency between the fitting parameters is high. We found that the fits converge to similar

values for K_A for the different NaCl concentrations and the three sets of initial rates could be globally fitted using a common value for this parameter (Figure 1b), which suggests that the association equilibrium constant does not change much with the concentration of NaCl. The parameters resulting from this analysis are shown in Table 2. The increase in salt concentration stabilizes the amyloidogenic intermediate relative to the native and unfolded states, thus increasing its population. The rate constant of the conformational conversion of oligomers into amyloid nuclei is also considerably increased with salt concentration.

To further validate our nucleation model, we studied the aggregation kinetics of a double mutant of the Spc-SH3 domain (N47A + K43A). The second mutation K43A destabilizes strongly the native state. The far-UV CD spectrum indicates a partially unfolded conformation (Figure S5a) and the DSC thermogram obtained at a low protein concentration shows a weak and broad unfolding transition (Figure S5b), consistent with a low structural cooperativity. This double mutant forms fibrils much faster than the single mutant N47A in the presence of 100 mM NaCl as observed by TEM (results not shown). Initial rates of nucleation were measured by ThT fluorescence (Figure 1b). Under these conditions, there is a rapid growth of ThT fluorescence indicating a fast formation of amyloid nuclei. The plot of log r_0 vs log C_0 has a slope close to one over most of the concentration range explored. This is consistent with a kinetic regime where the amyloid nucleation takes place from the oligomers, i.e., $C_0 \gg (K_A \cdot K_I)^{-1}$. In fact, DLS indicates that this double mutant domain forms oligomers even at 15ºC and at relatively low concentrations (Figure S5c). SEC analysis at 37ºC also shows a considerable population of oligomers prior to the incubation and during the very early times of the aggregation kinetics (Figure S5d). Fitting the initial aggregation rates using our model yielded a considerably higher K_I for this mutant, mainly due to a strong destabilization of the native state. We needed however to fix the K_A value in this fitting because the data did not contain enough information for an accurate determination of all the fitting parameters (Table 2). Nevertheless, these results strongly support the validity of our model and its power to provide thermodynamic and kinetic data characterizing the amyloid nucleation process.

DISCUSSION

Here we have shown that amyloid fibrillation of the N47A Spc-SH3 mutant domain takes place following apparent high-order irreversible kinetics, as a result of oligomeric precursors preceding the fibril nucleation event. This high-order kinetics is confirmed by fitting of aggregation kinetics followed by 2D-NMR or near-UV CD, which selectively monitor the concentration of native monomers. On the other hand, the kinetics followed by far-UV CD and ANS fluorescence show that partial unfolding of the native protein involving secondary structure changes and the exposure of hydrophobic patches takes place significantly faster than nucleation and with lower apparent order. This implies that these early conformational changes are, at least in part, associated to the formation of the pool of oligomeric precursors themselves. These oligomers are likely to be low-populated, unstable and interconverting species. Formation of transient oligomeric intermediates has been previously reported as a crucial event preceding amyloid fibrillation in many proteins. For instance, oligomeric intermediates formed at low pH above a critical concentration of amyloid-beta 1-40 were proposed to have micellar properties and be in equilibrium with the monomeric protein [28]. Using photo-induced cross linking it was observed that the Abeta 1-40 peptide undergoes a rapid oligomerization equilibrium involving monomer, dimer, trimer, and tetramer during the pre-nucleation phase of fibril assembly [8]. Insulin fibrillation takes also place by rapid formation of soluble oligomers followed by a slower transition into a second distinct class of oligomers that lead to amyloid fibrils [29]. Single-molecule fluorescence methods have also shown a rapid and transient increase in the population of oligomeric species during the early stages of PI3–SH3 aggregation [7]. These early oligomers formed a highly heterogeneous size distribution. All these studies and many others show common features for early stages of amyloid formation: i) early oligomers are structurally unstable and interconverting species with heterogeneous sizes; ii) the oligomerization pre-equilibrates rapidly from the monomers prior to the nucleation event; iii) the oligomers then convert into amyloid structures, which is the rate limiting step in fibrillation. These general characteristics are in good agreement with our results and constitute the basis of the presented model of amyloid nucleation.

To monitor the initial aggregation rates we selected deliberately the conditions under which the conversion of native N47A Spc-SH3 into fibrils takes place without a lag phase due to a rapid formation of amyloid nuclei. The advantage of this approach is that the earliest times of the kinetic traces followed by ThT fluorescence are mainly sensitive to the nucleation event. Similar lag-free aggregation kinetics was previously observed by Dobson and coworkers [11] for the PI3-SH3 domain at pH 3.6, whereas fibrillation showing a lag phase occurs at lower pH. These authors invoked a "nucleated conformational conversion" mechanism to explain their fibrillation kinetics in the absence of lag phase, similar to that proposed here. This mechanism was previously proposed for the prion protein Sup35 [9], which was reported to form structurally fluid oligomeric complexes that appear to be crucial intermediates in the *de novo* amyloid nucleation. Fibrillation of β2-microglobulin into disordered worm-like fibrils or short rod-like fibrils has also been shown to occur without a lag-phase by an aggregation pathway, which is different to that of the relatively rigid long-straight fibrils classically associated with amyloid [30]. The partitioning between these different competing pathways is modulated by environmental conditions and occurs during the earliest conformational and association phenomena, which direct subsequent events leading to different types of aggregates.

Since the early work of Oosawa et al. [3] many theoretical models to describe quantitatively the kinetics of protein aggregation have been proposed with the aim to obtain kinetic and thermodynamic parameters characterizing the critical steps of the process (see [5] for a comprehensive review). Models were developed to fit the nucleation-dependent kinetic curves typical of protein aggregation and were usually formulated with the assumption of an aggregation nucleus of a specific size [6] [31] [32] [33]. Recently, Roberts and coworkers have proposed a combined Lumry-Eyring and Nucleated Polymerization (LENP) model [6] [34], in which the aggregation rates are considered slow compared to the folding-unfolding equilibrium. They model the nucleation event as a conformational rearrangement of x-sized oligomers into x-sized nuclei. Interestingly, by exploring different qualitative kinetic regimes, they showed that their model is a generalization of many previously proposed nucleation and growth models for aggregation. One of their main findings is that under the scenarios where nucleation is fast, the apparent kinetics of monomer depletion follows x-

order kinetics. Our finding of high order kinetics is in agreement with the predictions of the LENP model, which supports the validity of our assumption of fast nucleation. Apparent sizes of the dominant amyloid nuclei ranging between 3 and 6 molecules would be derived from the apparent order of the kinetics depending on the conditions.

In spite of this agreement, our nucleation model does not imply any assumption of a specific size for the aggregation nuclei. In fact, we model the nucleation event as a conformational change taking place within any preformed oligomer irrespective of their size. The size distribution of the oligomers is however controlled by the thermodynamic parameters of the process, i.e., the stability of the amyloidogenic intermediate, the equilibrium constant for the oligomerization and the protein concentration.

In a recent work, Vitalis and Pappu [35] have reanalyzed the aggregation mechanism of polyglutamine peptides using a model that also accounts for the possibility of nucleation from a pool of heterogeneous oligomers, similarly to the model proposed here. They clarified previous observations of fractional and/or negative values of estimates of the critical nucleus size arising from the assumption of a homogeneous nucleation model. The model proposed by these authors for early aggregation shares with the nucleation model proposed here two major assumptions: First, a rapidly pre-equilibrated distribution of oligomers is formed by successive monomer addition; second, the nucleation event occurs by a rate-limiting conformational conversion of oligomers into pre-fibrillar species. On the other hand, there are several mathematical and conceptual differences between the two models: Vitalis and Pappu do not analyze the initial aggregation rates but they adapt their model to the analysis of early aggregation kinetics as originally developed by Ferrone [33], in which they analyze the slope of extent of aggregation plotted versus t^2. They also take into account the elongation of the fibrillar aggregates via monomer addition, whereas we neglected its contribution in our model as discussed above and in Text S3 of the Supporting Information. In addition, these authors limited in their analysis the maximum oligomer size and the minimum size of oligomers that are competent for conformational conversion. Finally, they do not consider the existence of a folding-unfolding equilibrium for the monomer.

In spite of these differences, some of their fundamental conclusions are similar to ours. They highlight the importance of the factors controlling the oligomer distribution in determining the apparent oligomer size in the analysis of the kinetics is made assuming a single nucleus size. In particular, if the process nucleates under conditions where large fractions of the aggregating material are present as soluble oligomers that are competent to promote fibril formation, then the apparent nucleus size may results in quite anomalous values (fractional or even negative in their analysis).In fact, using the equations of the model and the parameters of Table 2, we could calculate the average size and the size distributions of the pre-equilibrated oligomers for each concentration of protein (see Figure S6). It is evident that the size of the oligomers and their population depend quite dramatically on the total protein concentration. At low concentrations there are mainly dimers at very low populations. As concentration increases, the overall oligomer population increases and the size distributions become shifted toward larger sizes and considerably broadened. An increase in the NaCl concentration strongly enhances oligomerization. Importantly, the experimental order of the kinetics does not need to be correlated with the average oligomer size, except if the measurements are made near the critical concentration. For instance, at 50 mM NaCl concentration, the N47A Spc-SH3 mutant shows an apparent order of 6.4, which is in very good agreement with the average sizes of the oligomers predicted by our model (between 4 and 8 in the protein concentration interval explored) but, despite this coincidence, the size distributions are quite broad at these protein concentrations. In contrast, the kinetics of the K43A-N47A double mutant were studied well above its critical concentration and even though the aggregation nucleates from a wide variety of oligomer sizes the experimental order is close to one. The observation of concentration-independent nucleation at high protein concentration appears to be a general property of polymerization models due to the fact that under this regime the nuclei are no longer the least thermodynamically unstable species, as described by Powers and Powers [36].

The direct detection of the oligomeric precursors of nucleation has proved extremely difficult, due to their instability and the fact that they are not usually the dominant species in the aggregating solution. Here we used DLS and SEC to analyze the mixtures during the course of the aggregation. DLS shows the formation of oligomeric particles with average

hydrodynamic radii of about 2.7 to 3.0 nm and SEC is also able to detect a low population of oligomeric species at early aggregation times but only when the samples were analyzed at 37°C and at very high protein concentrations. In contrast, the oligomers are clearly present for the K43A-N47A double mutant even prior to aggregation, as demonstrated by DLS and SEC. It is likely, however, that the oligomer fraction detected during aggregation includes also stable amyloid nuclei, which would not dissociate during the SEC analysis. Nevertheless, the existence of this range of oligomeric species is fully consistent with the observed aggregation kinetics.

The possibility of nucleation from oligomers of different sizes, which are modulated by the experimental conditions, could have profound implications in understanding the mechanism of amyloid aggregation. This is schematically illustrated in Figure 9. The conformational conversion of the polypeptide chain into amyloid structure may be constrained differently within oligomers of different sizes, giving rise to a structural variability in the nuclei and a consequent polymorphism of the final amyloid structures modulated by the conditions [23,30,37]. Also, the amount and size distribution of nucleating oligomers would affect strongly all subsequent fibrillation stages. Conditions disfavoring oligomerization, such as low salt or low protein concentration, would promote a slower nucleation via smaller oligomers. As a consequence, less abundant and more homogeneous nuclei would preferentially grow via monomer addition into more ordered filaments that could then assemble into mature twisted fibrils. On the other hand, rapid accumulation of a heterogeneous distribution of amyloid nuclei could promote aggregation via condensation or growth of heterogeneous fibrils via monomer addition to a diversity of structural templates, in any of these cases giving rise to more disordered fibrillar aggregates [11] or even amorphous aggregates as we observe for N47A Spc-SH3 in the presence of 300 mM NaCl (results not shown).

An important advantage of our kinetic approach is its mathematical and experimental simplicity. The measurement of initial aggregation rates are relatively straightforward and do not need the recording of long aggregation kinetics, allowing the exploration of a larger number of experimental variables. Also, the equations describing the initial rates are very simple and complicated numerical integration procedures are not necessary to fit the data.

This method could be applicable to any protein aggregation process as long as the kinetics does not show a lag phase and the initial rates are representative of the formation of the earliest amyloid structures.

Our analysis provides important thermodynamic and kinetic magnitudes allowing us to rationalize the nucleation event. This is of chief importance to understand the factors governing the stability of early amyloidogenic species. The amyloidogenic monomeric intermediate of N47A Spc-SH3 is a very unstable state, likely an ensemble of partially unfolded species. Its stability is much lower even than the fully unfolded state under the aggregation conditions. It has however a very strong propensity to oligomerize, as indicated by the large association constant K_A. As a result, the concentration of I is very low under all conditions, but the factors affecting its stability are key to modulate the amount and distribution of oligomers that are competent to nucleate aggregation. This is crucial to understand the mechanisms by which proteins maintain solubility and avoid deleterious aggregation processes. Protein sequences have evolved to maintain a high structural cooperativity of the native states, favoring either the native or the globally unfolded state under all conditions and reducing the population of aggregation-prone partially unfolded species. A reduction in the global unfolding cooperativity produced by mutations has been shown to enhance amyloidogenicity [38].

Our kinetic approach could be also relevant for the case of intrinsically disordered proteins, such as Abeta or α-synuclein, because their most populated soluble states are not necessarily the amyloidogenic ones. It has been shown that disordered polypeptide chains must partially refold to initiate amyloid aggregation [39] achieving a high-energy, partially-folded conformation, which then is able to oligomerize and aggregate. This is similar to what we observed for the double mutant K43A-N47A Spc-SH3. The soluble monomeric state is probably an ensemble of conformations with low unfolding cooperativity but the amyloidogenic conformation does not need to be the most populated one but just a subfraction of this ensemble.

Another important result is that an increase in the NaCl concentration appears to produce a selective stabilization of the monomeric intermediate, I, and not an enhancement of its

association tendency. NaCl also increases the rate constant of the conformational conversion to amyloid structure. Salt ions may affect protein aggregation by a number of mechanisms but how each specific molecular stage is influenced by ions is still not known. Simple Debye-Hückel screening of electrostatic interactions has been ruled out as a main contributor to aggregation for several systems [40] [41], although it plays a role on fibrillation of α-synuclein at low ionic strengths [42]. Preferential anion binding to the protein groups has been proposed as a main mechanism promoting fibrillation of β2-microglobulin at acid pH, because the aggregation enhancement produced by different ions is ordered according to the electroselectivity series [43]. Similar observations were made for the fibrillation of glucagon [40] and mouse prion protein [44] both at acid pH. In contrast, the effect of ions on α-synuclein fibrillation has been found to follow the Hofmeister series, suggesting an important role of hydration effects [42]. The aggregation of Abeta1-40 at pH 9 seems to depend on a combination of both effects [41]. The result of our analysis ascribes the effect of salt ions mainly to a relative stabilization of the amyloidogenic monomer, which is partially unfolded and exposes a significant amount of hydrophobic surface. Also, at the mildly acid pH of our experiments the protein is positively charged. At the relatively low NaCl concentrations used in these experiments and given that the Na^+ and Cl^- ions are neither strong "salting-out" or "salting-in" ions [45], it is unlikely that the intermediate is primarily stabilized by a Hofmeister effect. In fact, the fully unfolded state exposing more surface area is less stabilized by NaCl than the intermediate. Preferential binding of chloride anions to the intermediate relative to the native state could be playing a role in compensating the net positive charge, reducing electrostatic repulsion and thus favoring oligomerization. A more profound investigation of the effect of different salt ions is however necessary to clarify these effects.

CONCLUSION

We have shown that the amyloid nucleation kinetics of the Spc-SH3 domain obeys to a high-order irreversible kinetics. The analysis of the aggregation kinetics by a variety of biophysical methods has allowed us to infer that the earliest stages of the amyloid nucleation process imply a pre-equilibrium involving oligomerization of a partially-unfolded intermediate followed by a conformational conversion of the polypeptide chain within the oligomers. The latter process leads to formation of the amyloid nuclei. A simple mathematical model can account very well for the experimental initial rates of aggregation and their dependence with the concentration of protein. The model has allowed us to derive thermodynamic magnitudes characterizing the highly unstable amyloidogenic intermediate and its oligomers. It is shown that environmental conditions such as protein or salt concentration can strongly affect the stability and population of the precursors, leading to different nucleation scenarios that may in turn result in diverse aggregation pathways and fibril morphologies. The kinetic approach presented here may be applicable to characterize the amyloidogenic intermediates and oligomeric precursors of amyloid aggregation in disease-related proteins.

ACKNOWLEDGMENTS

REFERENCES

(1)   Chiti, F.; Dobson, C. M. Protein misfolding, functional amyloid, and human disease. *Annual review of biochemistry* **2006**, *75*, 333-366.

(2)   Disanza, A.; Steffen, A.; Hertzog, M.; Frittoli, E.; Rottner, K.; Scita, G. Actin polymerization machinery: the finish line of signaling networks, the starting point of cellular movement. *Cellular and molecular life sciences : CMLS* **2005**, *62*, 955-970.

(3)   Oosawa, F.; Kasai, M. A theory of linear and helical aggregations of macromolecules. *Journal of molecular biology* **1962**, *4*, 10-21.

(4)   Roberts, C. J. Non-native protein aggregation kinetics. *Biotechnology and bioengineering* **2007**, *98*, 927-938.

(5)   Morris, A. M.; Watzky, M. A.; Finke, R. G. Protein aggregation kinetics, mechanism, and curve-fitting: a review of the literature. *Biochimica et biophysica acta* **2009**, *1794*, 375-397.

(6)   Andrews, J. M.; Roberts, C. J. A Lumry-Eyring nucleated polymerization model of protein aggregation kinetics: 1. Aggregation with pre-equilibrated unfolding. *The journal of physical chemistry. B* **2007**, *111*, 7897-7913.

(7)   Orte, A.; Birkett, N. R.; Clarke, R. W.; Devlin, G. L.; Dobson, C. M.; Klenerman, D. Direct characterization of amyloidogenic oligomers by single-molecule fluorescence. *Proceedings of the National Academy of Sciences of the United States of America* **2008**, *105*, 14424-14429.

(8)   Bitan, G.; Kirkitadze, M. D.; Lomakin, A.; Vollers, S. S.; Benedek, G. B.; Teplow, D. B. Amyloid beta -protein (Abeta) assembly: Abeta 40 and Abeta 42 oligomerize through distinct pathways. *Proceedings of the National Academy of Sciences of the United States of America* **2003**, *100*, 330-335.

(9)   Serio, T. R.; Cashikar, A. G.; Kowal, A. S.; Sawicki, G. J.; Moslehi, J. J.; Serpell, L.; Arnsdorf, M. F.; Lindquist, S. L. Nucleated conformational conversion and the replication of conformational information by a prion determinant. *Science* **2000**, *289*, 1317-1321.

(10)   Modler, A. J.; Gast, K.; Lutsch, G.; Damaschun, G. Assembly of amyloid protofibrils via critical oligomers--a novel pathway of amyloid formation. *Journal of molecular biology* **2003**, *325*, 135-148.

(11)   Bader, R.; Bamford, R.; Zurdo, J.; Luisi, B. F.; Dobson, C. M. Probing the mechanism of amyloidogenesis through a tandem repeat of the PI3-SH3 domain suggests a generic model for protein aggregation and fibril formation. *Journal of molecular biology* **2006**, *356*, 189-208.

(12)   Nettleton, E. J.; Tito, P.; Sunde, M.; Bouchard, M.; Dobson, C. M.; Robinson, C. V. Characterization of the oligomeric states of insulin in self-assembly and amyloid fibril formation by mass spectrometry. *Biophysical journal* **2000**, *79*, 1053-1065.

(13)   Plakoutsi, G.; Taddei, N.; Stefani, M.; Chiti, F. Aggregation of the Acylphosphatase from Sulfolobus solfataricus: the folded and partially unfolded states can both be precursors for amyloid formation. *The Journal of biological chemistry* **2004**, *279*, 14111-14119.

(14)   Haass, C.; Selkoe, D. J. Soluble protein oligomers in neurodegeneration: lessons from the Alzheimer's amyloid beta-peptide. *Nature reviews. Molecular cell biology* **2007**, *8*, 101-112.

(15)   McLean, C. A.; Cherny, R. A.; Fraser, F. W.; Fuller, S. J.; Smith, M. J.; Beyreuther, K.; Bush, A. I.; Masters, C. L. Soluble pool of Abeta amyloid as a determinant of severity of neurodegeneration in Alzheimer's disease. *Annals of neurology* **1999**, *46*, 860-866.

(16)   El-Agnaf, O. M.; Salem, S. A.; Paleologou, K. E.; Cooper, L. J.; Fullwood, N. J.; Gibson, M. J.; Curran, M. D.; Court, J. A.; Mann, D. M.; Ikeda, S.; Cookson, M. R.; Hardy, J.; Allsop, D. Alpha-synuclein implicated in Parkinson's disease is present in extracellular biological fluids,

including human plasma. *FASEB journal : official publication of the Federation of American Societies for Experimental Biology* **2003**, *17*, 1945-1947.

(17)   Schaffar, G.; Breuer, P.; Boteva, R.; Behrends, C.; Tzvetkov, N.; Strippel, N.; Sakahira, H.; Siegers, K.; Hayer-Hartl, M.; Hartl, F. U. Cellular toxicity of polyglutamine expansion proteins: mechanism of transcription factor deactivation. *Molecular cell* **2004**, *15*, 95-105.

(18)   Sousa, M. M.; Cardoso, I.; Fernandes, R.; Guimaraes, A.; Saraiva, M. J. Deposition of transthyretin in early stages of familial amyloidotic polyneuropathy: evidence for toxicity of nonfibrillar aggregates. *The American journal of pathology* **2001**, *159*, 1993-2000.

(19)   Malisauskas, M.; Ostman, J.; Darinskas, A.; Zamotin, V.; Liutkevicius, E.; Lundgren, E.; Morozova-Roche, L. A. Does the cytotoxic effect of transient amyloid oligomers from common equine lysozyme in vitro imply innate amyloid toxicity? *The Journal of biological chemistry* **2005**, *280*, 6269-6275.

(20)   Bucciantini, M.; Calloni, G.; Chiti, F.; Formigli, L.; Nosi, D.; Dobson, C. M.; Stefani, M. Prefibrillar amyloid protein aggregates share common features of cytotoxicity. *The Journal of biological chemistry* **2004**, *279*, 31374-31382.

(21)   Morel, B.; Casares, S.; Conejero-Lara, F. A single mutation induces amyloid aggregation in the alpha-spectrin SH3 domain: analysis of the early stages of fibril formation. *Journal of molecular biology* **2006**, *356*, 453-468.

(22)   Varela, L.; Morel, B.; Azuaga, A. I.; Conejero-Lara, F. A single mutation in an SH3 domain increases amyloid aggregation by accelerating nucleation, but not by destabilizing thermodynamically the native state. *FEBS letters* **2009**, *583*, 801-806.

(23)   Morel, B.; Varela, L.; Azuaga, A. I.; Conejero-Lara, F. Environmental conditions affect the kinetics of nucleation of amyloid fibrils and determine their morphology. *Biophysical journal* **2010**, *99*, 3801-3810.

(24)   Sadqi, M.; Casares, S.; Abril, M. A.; Lopez-Mayorga, O.; Conejero-Lara, F.; Freire, E. The native state conformational ensemble of the SH3 domain from alpha-spectrin. *Biochemistry* **1999**, *38*, 8899-8906.

(25)   Delaglio, F.; Grzesiek, S.; Vuister, G. W.; Zhu, G.; Pfeifer, J.; Bax, A. NMRPipe: a multidimensional spectral processing system based on UNIX pipes. *Journal of biomolecular NMR* **1995**, *6*, 277-293.

(26)   Blanco, F. J.; Ortiz, A. R.; Serrano, L. 1H and 15N NMR assignment and solution structure of the SH3 domain of spectrin: comparison of unrefined and refined structure sets with the crystal structure. *Journal of biomolecular NMR* **1997**, *9*, 347-357.

(27)   Johnson, B. A. Using NMRView to visualize and analyze the NMR spectra of macromolecules. *Methods in molecular biology* **2004**, *278*, 313-352.

(28)   Lomakin, A.; Chung, D. S.; Benedek, G. B.; Kirschner, D. A.; Teplow, D. B. On the nucleation and growth of amyloid beta-protein fibrils: detection of nuclei and quantitation of rate constants. *Proceedings of the National Academy of Sciences of the United States of America* **1996**, *93*, 1125-1129.

(29)   Ahmad, A.; Uversky, V. N.; Hong, D.; Fink, A. L. Early events in the fibrillation of monomeric insulin. *The Journal of biological chemistry* **2005**, *280*, 42669-42675.

(30)   Gosal, W. S.; Morten, I. J.; Hewitt, E. W.; Smith, D. A.; Thomson, N. H.; Radford, S. E. Competing pathways determine fibril morphology in the self-assembly of beta2-microglobulin into amyloid. *Journal of molecular biology* **2005**, *351*, 850-864.

(31)   Jarrett, J. T.; Lansbury, P. T., Jr. Seeding "one-dimensional crystallization" of amyloid: a pathogenic mechanism in Alzheimer's disease and scrapie? *Cell* **1993**, *73*, 1055-1058.

(32)   Lomakin, A.; Teplow, D. B.; Kirschner, D. A.; Benedek, G. B. Kinetic theory of fibrillogenesis of amyloid beta-protein. *Proceedings of the National Academy of Sciences of the United States of America* **1997**, *94*, 7942-7947.

(33)   Ferrone, F. Analysis of protein aggregation kinetics. *Methods in enzymology* **1999**, *309*, 256-274.

(34)   Li, Y.; Roberts, C. J. Lumry-Eyring nucleated-polymerization model of protein aggregation kinetics. 2. Competing growth via condensation and chain polymerization. *The journal of physical chemistry. B* **2009**, *113*, 7020-7032.

(35)   Vitalis, A.; Pappu, R. V. Assessing the contribution of heterogeneous distributions of oligomers to aggregation mechanisms of polyglutamine peptides. *Biophysical chemistry* **2011**, *159*, 14-23.

(36)   Powers, E. T.; Powers, D. L. The kinetics of nucleated polymerizations at high concentrations: amyloid fibril formation near and above the "supercritical concentration". *Biophysical journal* **2006**, *91*, 122-132.

(37)   Serpell, L. C. Alzheimer's amyloid fibrils: structure and assembly. *Biochimica et biophysica acta* **2000**, *1502*, 16-30.

(38)   Dumoulin, M.; Canet, D.; Last, A. M.; Pardon, E.; Archer, D. B.; Muyldermans, S.; Wyns, L.; Matagne, A.; Robinson, C. V.; Redfield, C.; Dobson, C. M. Reduced global cooperativity is a common feature underlying the amyloidogenicity of pathogenic lysozyme mutations. *Journal of molecular biology* **2005**, *346*, 773-788.

(39)   Uversky, V. N.; Fink, A. L. Conformational constraints for amyloid fibrillation: the importance of being unfolded. *Biochimica et biophysica acta* **2004**, *1698*, 131-153.

(40)   Pedersen, J. S.; Flink, J. M.; Dikov, D.; Otzen, D. E. Sulfates dramatically stabilize a salt-dependent type of glucagon fibrils. *Biophysical journal* **2006**, *90*, 4181-4194.

(41)   Klement, K.; Wieligmann, K.; Meinhardt, J.; Hortschansky, P.; Richter, W.; Fandrich, M. Effect of different salt ions on the propensity of aggregation and on the structure of Alzheimer's abeta(1-40) amyloid fibrils. *Journal of molecular biology* **2007**, *373*, 1321-1333.

(42)   Munishkina, L. A.; Henriques, J.; Uversky, V. N.; Fink, A. L. Role of protein-water interactions and electrostatics in alpha-synuclein fibril formation. *Biochemistry* **2004**, *43*, 3289-3300.

(43)   Raman, B.; Chatani, E.; Kihara, M.; Ban, T.; Sakai, M.; Hasegawa, K.; Naiki, H.; Rao Ch, M.; Goto, Y. Critical balance of electrostatic and hydrophobic interactions is required for beta 2-microglobulin amyloid fibril growth and stability. *Biochemistry* **2005**, *44*, 1288-1299.

(44)   Jain, S.; Udgaonkar, J. B. Salt-induced modulation of the pathway of amyloid fibril formation by the mouse prion protein. *Biochemistry* **2010**, *49*, 7615-7624.

(45)   Baldwin, R. L. How Hofmeister ion interactions affect protein stability. *Biophysical journal* **1996**, *71*, 2056-2063.

SUPPORTING INFORMATION
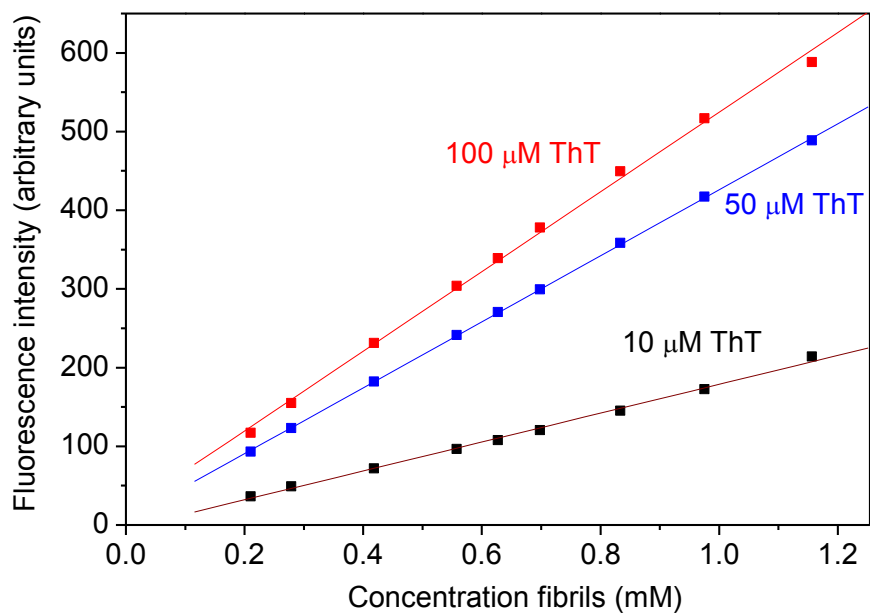
Figure S1. Linearity of the thioflavine T (ThT) fluorescence as a function of the concentration of amyloid fibrils. *Amyloid fibrils of N47A mutant of the Spc-SH3 were prepared by in incubation at 37ºC in 100 mM glycine buffer, 100 mM NaCl pH 3.2, isolated by centrifugation and resuspended in the same buffer for ThT assay.*
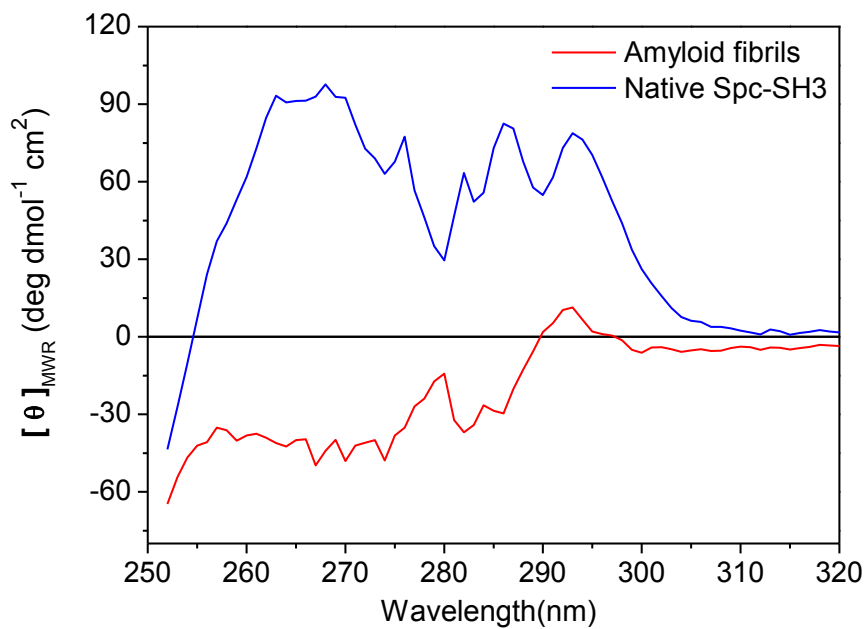
Figure S2: Near-UV CD spectra of N47A Spc-SH3 in the native state and the amyloid fibrillar state. *Spectra were recorded at the same protein concentration at 25ºC in 100 mM glycine buffer, 100 mM NaCl pH 3.2.*
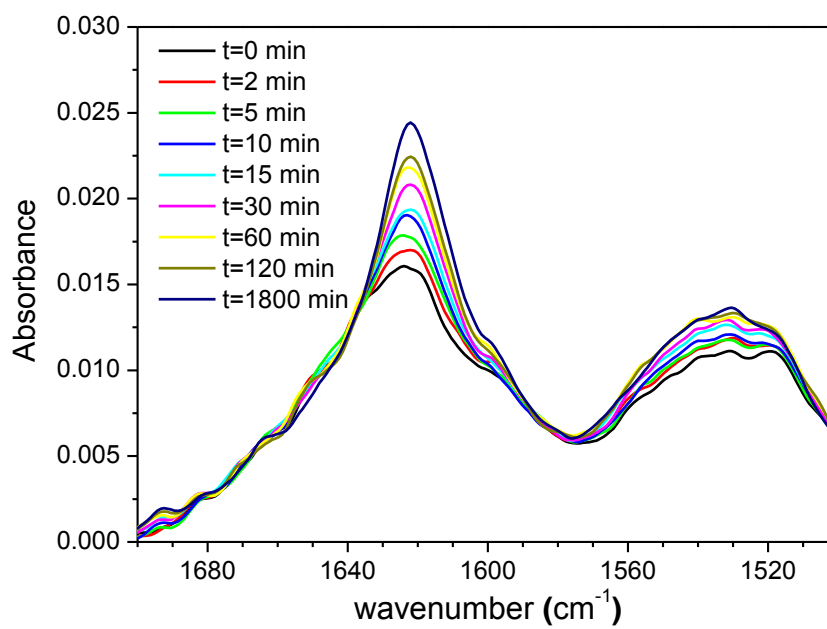
Figure S3: Infrared spectra of N47A Spc-SH3 recorded during the aggregation at 37ºC. *Buffer was 100 mM glycine buffer, 100 mM NaCl pH 3.2 and the protein concentration was 1.59 mM.*
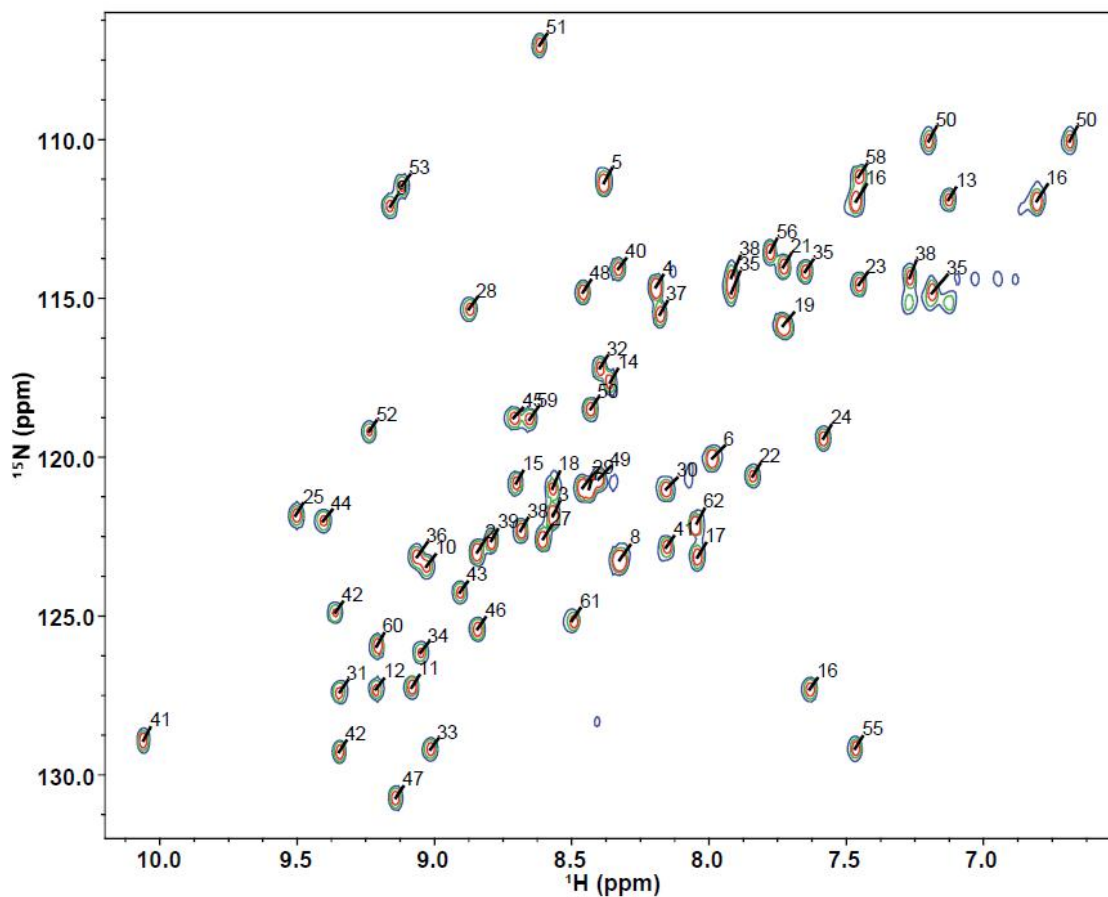
Figure S4: Overlay of ¹⁵N-¹H HSQC NMR spectra of N47A Spc-SH3 at different times of aggregation at 37ºC. *Buffer conditions were the same as in Figure S3, except for the use of per-deuterated glycine and the addition of 10% D₂O for field lock. The concentration of ¹⁵N-labelled protein was 1.1 mM (8 mg mL⁻¹). The three spectra have been plotted using a single contour level and the same intensity threshold. The times of incubation are: 3 min (blue); 50 min (green) and 1957 min (red). The numbers next to each cross-peak indicate the residue number assignment.*
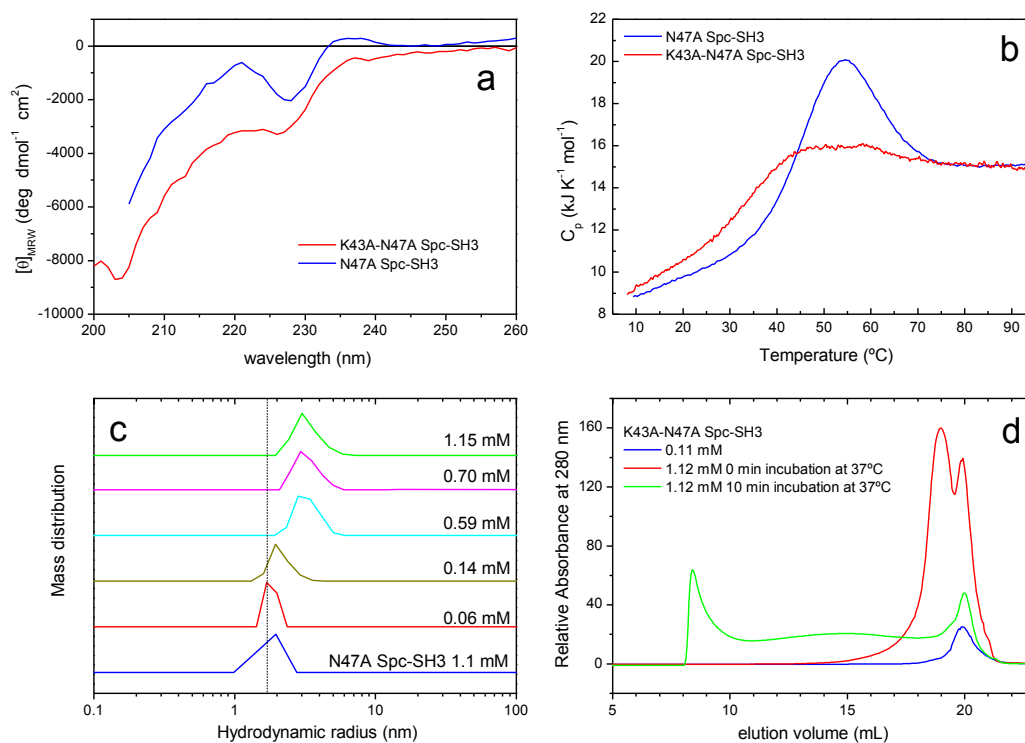
Figure S5: Structure, stability and oligomerization state of the K43A-N47A Spc-SH3 double mutant*. a) Far-UV CD spectrum in comparison with the N47A single mutant; b) thermal unfolding monitored by DSC; c) Apparent hydrodynamic radius determined at 15ºC at different concentrations as indicated. The vertical dashed line indicates the radius of the native Spc-SH3 domain; d) Size-exclusion chromatography at 37ºC at two different concentrations as indicated. The peak eluting at ca. 20 mL corresponds to the monomer and the excluded volume is about 8.5 mL.*
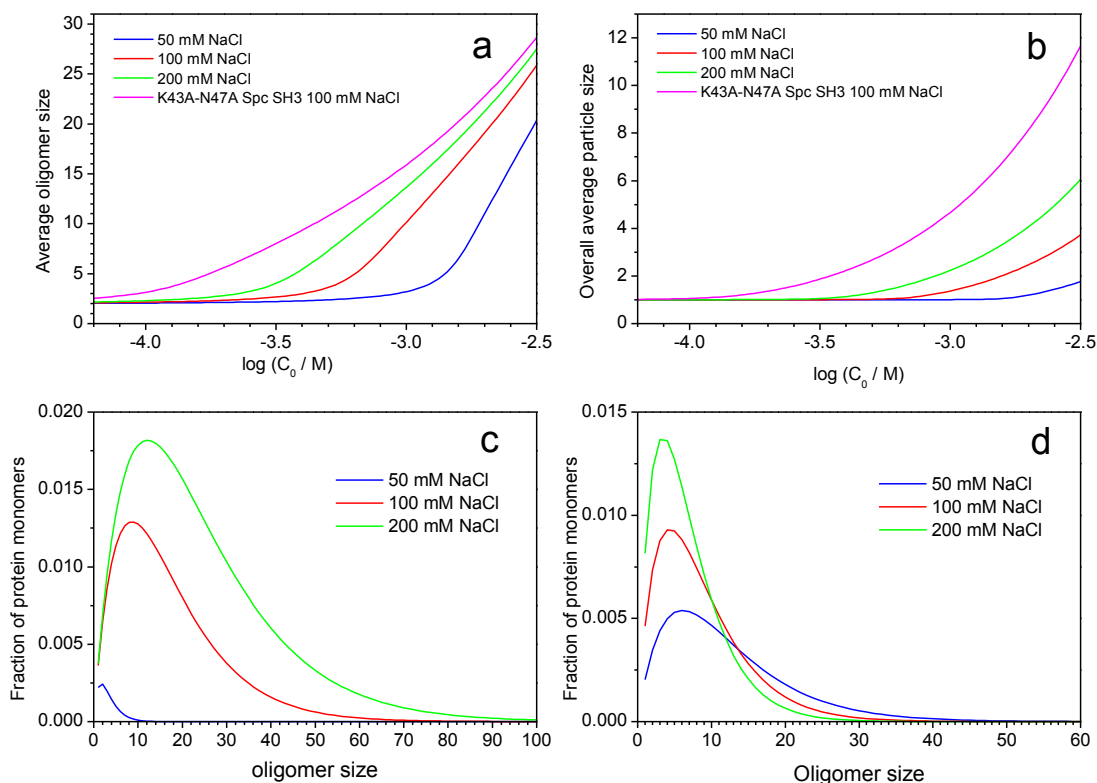
Figure S6: Simulations of oligomer size distributions. *Average size distributions were calculated using the parameters derived from the fitting of the experimental initial rates using the equations of the model (see main manuscript text). (a) Average size of the oligomers as a function of the total protein concentration; (b) Average size of all the particles present in solution; (c) Size distribution of the oligomers at 1 mM of total protein concentration; (d) Size distribution of the oligomers at the critical concentration, $(K_A \cdot K_I)^{-1}$, obtained under each experimental condition.*

Text S1: Model of amyloid nucleation preceded by partial unfolding and oligomerization pre-equilibrium.

$$N$$

$$I \rightleftarrows A_2 \rightleftarrows A_3 \cdots \rightleftarrows A_i \cdots \rightleftarrows \cdots A_N \quad (N \to \infty)$$

$$U$$

$$A_i \longrightarrow F_i$$
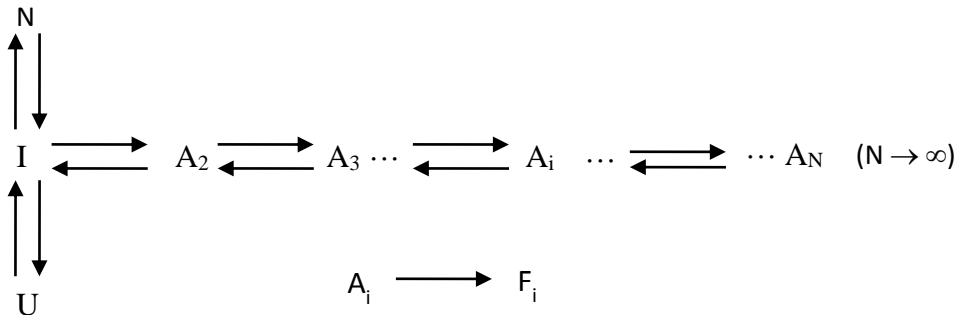
Model description and assumptions:

A partially-unfolded intermediate, I, is in rapid equilibrium with the native, N, and the fully unfolded state, U. The intermediate oligomerizes through a sequential addition of monomers. No limit is imposed to the maximum size of the oligomers, A_i. It is assumed that the conformational equilibria of the monomer species and the oligomerization are fast enough to be pre-equilibrated during the whole process. Amyloid fibril nuclei, F_i, are then formed by a conformational change of the polypeptide chains within the oligomers. Any oligomer can undergo this conformational change and the first order rate constant for this process is equal for all oligomers. We assumed that the formation of amyloid nuclei is essentially irreversible and that further fibril growth by monomer addition does not significantly occur during the early stages of the kinetics, as discussed below.

Mathematical development

The equilibrium constants for the conformational unfolding of the monomer are:

$$K_U = \frac{[U]}{[N]} \qquad K_I = \frac{[I]}{[N]}$$

(1)

And the total concentration of protein monomers at the beginning of the aggregation process:

$$C_0 = [N] + [U] + [I] + \sum_{i=2}^{N} i[A_i]$$

(2)

The fraction of protein in each state is given by:

$$x_N = \frac{[N]}{C_0} \qquad x_I = \frac{[I]}{C_0} \qquad x_U = \frac{[U]}{C_0} \qquad x_{Ai} = \frac{i \cdot [A_i]}{C_0}$$

(3)

Assuming that all equilibrium constants of oligomerization are equal:

$$K_A = \frac{[A_2]}{[I][I]} = \frac{[A_3]}{[A_2][I]} = \frac{[A_i]}{[A_{i-1}][I]}$$

(4)

Using this equation the concentration of any oligomer of size *i* can be related to that of the monomeric intermediate as:

$$[A_i] = K_A[A_{i-1}][I] = K_A^2[A_{i-2}][I]^2 = ... = K_A^{i-1}[I]^i$$

(5)

And the concentration of protein monomers in the intermediate state and in any of the oligomers is given by:

$$[I] + \sum_{i=2}^{\infty} i[A_i] = \sum_{i=1}^{\infty} i[A_i] = \sum_{i=1}^{\infty} i K_A^{i-1}[I]^i$$

(6)

Where $A_1 = I$ in this series. This series is convergent to:

$$\sum_{i=1}^{\infty} i K_A^{i-1}[I]^i = K_A^{-1} \sum_{i=1}^{\infty} i (K_A[I])^i = \frac{K_A^{-1}(K_A[I])}{(1 - K_A[I])^2} \tag{7}$$

Since for $x < 1$:

$$\sum_{i=1}^{\infty} i \cdot x^i = \frac{x}{(1-x)^2}$$

And using the equilibrium constants K_I and K_U:

$$C_0 = [N](1 + K_U) + \frac{[I]}{(1 - K_A[I])^2} \tag{8}$$

$$1 = x_N(1 + K_U) + \frac{K_I x_N}{(1 - K_A C_0 K_I x_N)^2} = A x_N + \frac{K_I x_N}{(1 - B x_N)^2} \tag{9}$$

Where:

$$B = K_A C_0 K_I \quad \text{y} \quad A = 1 + K_U$$

Rearranging this equation we obtain a cubic equation in x_N:

$$AB^2 x_N^3 - (B^2 + 2AB)x_N^2 + (A + 2B + K_I)x_N - 1 = 0 \tag{10}$$

Solving for x_N and using the equilibrium constants we can calculate the concentrations of each state at the time zero of the aggregation process.

The rate of conversion of oligomers A_i into amyloid nuclei F_i is given by:

$$\frac{d[F_i]}{dt} = -\frac{d[A_i]}{dt} = k_{F,i}[A_i]$$
(11)

Where $k_{F,i}$ is the first-order constant of the conformational conversion. Assuming that $k_{F,i}$ is independent of the oligomer size, the initial rate of conversion of protein monomers into amyloid structure is:

$$r_0 = \left(\frac{dc_F}{dt}\right)_{t\to0} = -\sum_{i=2}^{\infty} i\left(\frac{d[A_i]}{dt}\right)_{t\to0} = \sum_{i=2}^{\infty} i k_{F,i}[A_i]_0 = k_F \sum_{i=2}^{\infty} i[A_i]_0 = \frac{k_F}{K_A} \frac{(Bx_N)^2(2-Bx_N)}{(1-Bx_N)^2}$$
(12)

Since it can be easily shown that:

$$\sum_{i=2}^{\infty} i[A_i] = K_A^{-1}\sum_{i=2}^{\infty} iK_A^i[I]^i = K_A^{-1}\sum_{i=2}^{\infty} i(Bx_N)^i = \frac{1}{K_A}\frac{(Bx_N)^2(2-Bx_N)}{(1-Bx_N)^2}$$
(13)

Where we have used the following identity:

$$\sum_{i=2}^{\infty} i \cdot x^i = \frac{x^2(2-x)}{(1-x)^2}$$
(x < 1)

The fraction monomers in each oligomer species A_i is given by:

$$x_{A,i} = \frac{i[A_i]}{C_0} = \frac{i(K_A[I])^i}{C_0 K_A} = \frac{i(Bx_N)^i}{C_0 K_A}$$
(i = 2 ... ∞)
(14)

And the average number of monomers in the oligomeric species can be easily obtained as:

$$\langle A_n \rangle = \frac{\sum_{i=2}^{\infty} i \cdot [A_i]}{\sum_{i=2}^{\infty} [A_i]} = \frac{\sum_{i=2}^{\infty} i \cdot K_A^{i-1} \cdot [I]^i}{\sum_{i=2}^{\infty} K_A^{i-1} \cdot [I]^i} = \frac{\sum_{i=2}^{\infty} i \cdot K_A^i \cdot [I]^i}{\sum_{i=2}^{\infty} K_A^i \cdot [I]^i} = \frac{\dfrac{(Bx_N)^2(2-Bx_N)}{(1-Bx_N)^2}}{\dfrac{(Bx_N)^2}{(1-Bx_N)}} = \frac{(2-Bx_N)}{(1-Bx_N)}$$
(15)

Where we have made use of the above results and of the fact that for x <1:

$$\sum_{i=2}^{\infty} x^i = \frac{x^2}{1-x}$$

Text S2: Model simulations.

Using the equations of the model described in Text S2 we have simulated the initial rates of nucleation as a function of the initial protein concentrations.

1. Amyloid nucleation of a stable partially unfolded amyloidogenic intermediate. In this case the I state is the most stable state. This is equivalent to the linear polymerization model of Oosawa and Kasai [3]. To simulate this case we can asume that K_I is large compared to K_U.

    The following data were calculated for $K_I = 100$, $K_U = 0.12$, and different values of K_A. $k_F = 1$ min^{-1}.
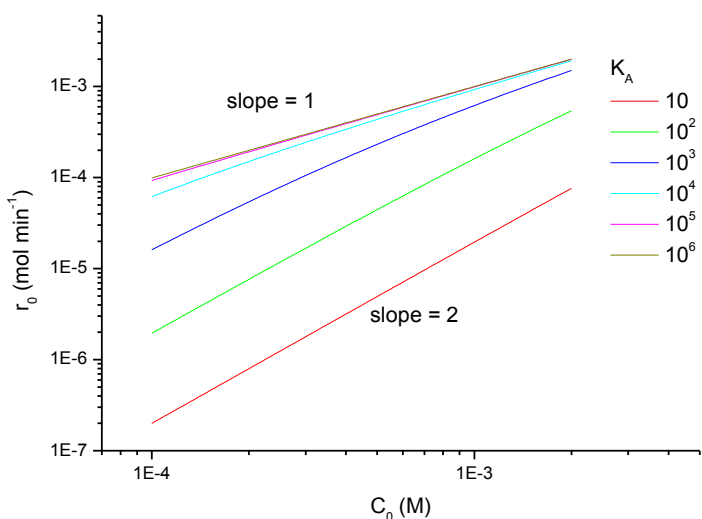
    The slope changes gradually from 2 to 1 as K_A increases. This is logical because for low K_A, the monomer governs the pre-equilibrium but it has to self-associate into dimers to form nuclei. For high values of K_A most of the protein is oligomeric from the beginning of the process and the process appears first order.

2. Amyloid nucleation of a folded protein.

In this case the pre-oligomerization equilibrium is coupled to the folding-unfolding equilibrium. The relative population of I and A_i will be reduced depending on the values of the equilibrium constants K_I and K_U.

a) Effect of K_I and K_A. K_A was varied independently of K_I for $K_U = 0.12$ and $k_f = 1$ min^{-1}.
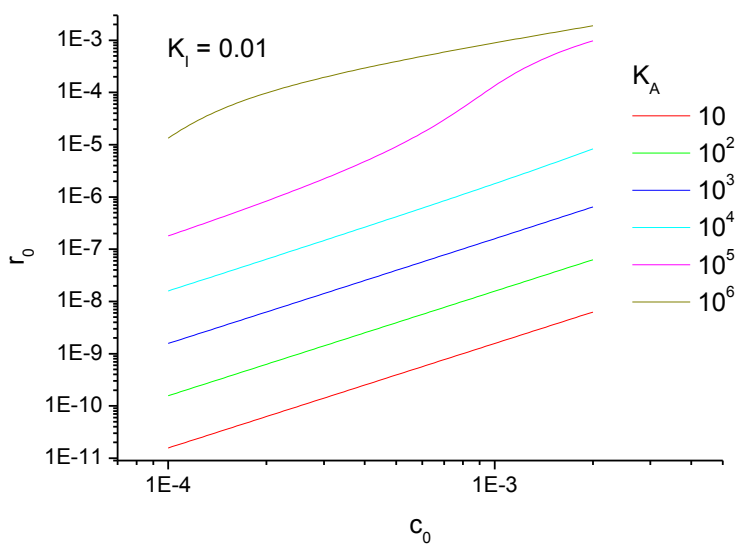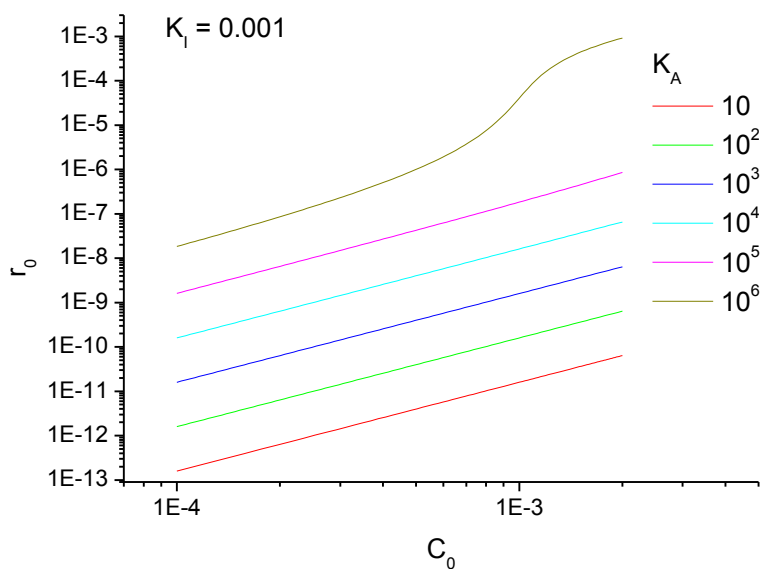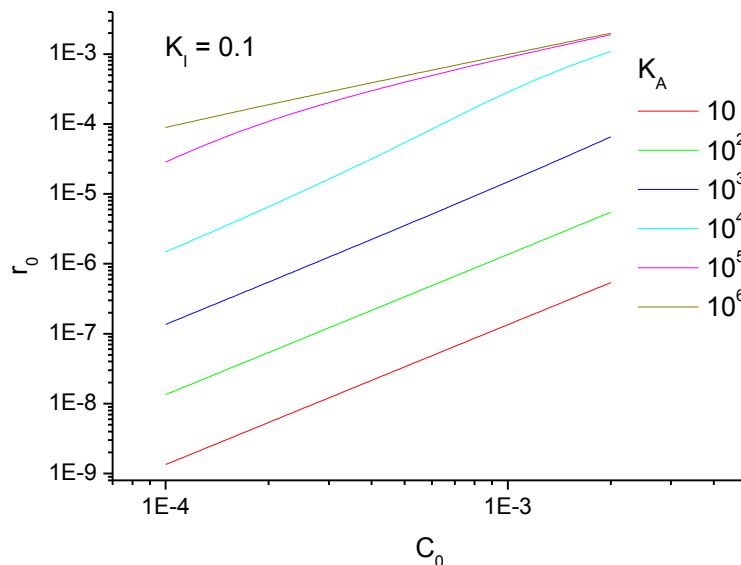
The rate of nucleation depends very strongly on K_A and K_I:

- For $C_0 << (K_A K_I)^{-1}$ the rate of nucleation is very low and scales on the second power of C_0.

- If $C_0 >> (K_A K_I)^{-1}$, the rate tends to a limit imposed by k_F and the nucleation is first order.

- If $C_0 \approx (K_A K_I)^{-1}$, there is a transient increase in the slope of the double logarithmic plot. This is due to an abrupt displacement of the oligomerization equilibrium as C_0 increases. The value $(K_A K_I)^{-1}$ acts as a critical concentration.

b) Next we simulated curves for the same product $K_A K_I = 10^3$ but changing their relative values. K_U and k_F are the same as in a)
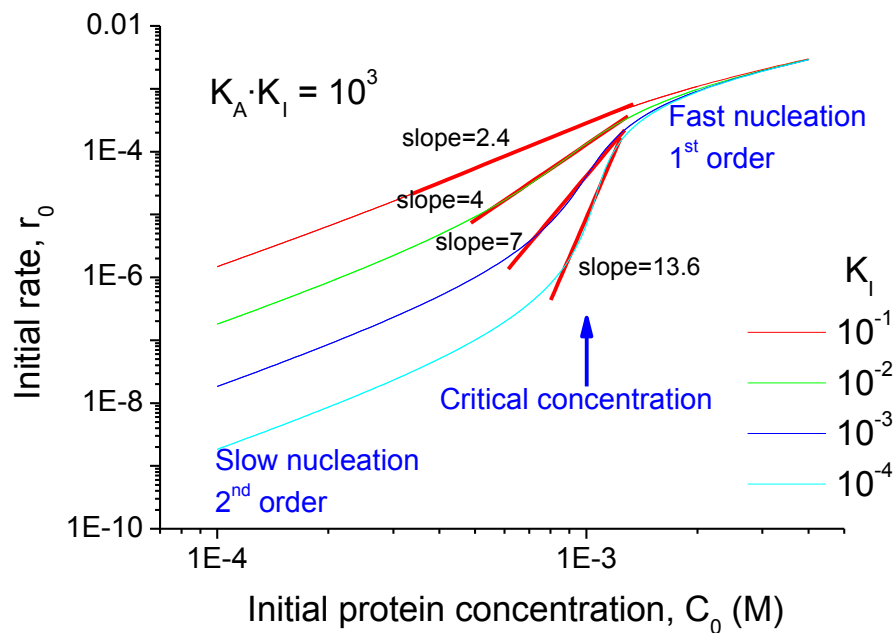
In the región of the critical concentration $C_0 \approx (K_A K_I)^{-1}$ there is a transient slope increase. The slope is higher for higher K_A and lower K_I values.

c) Effect of the global unfolding equilibrium constant K_U:

Simulations were made varying K_U and the resulting values of the unfolding Gibbs energy, ΔG_U. Values of K_A and K_I are as in b)
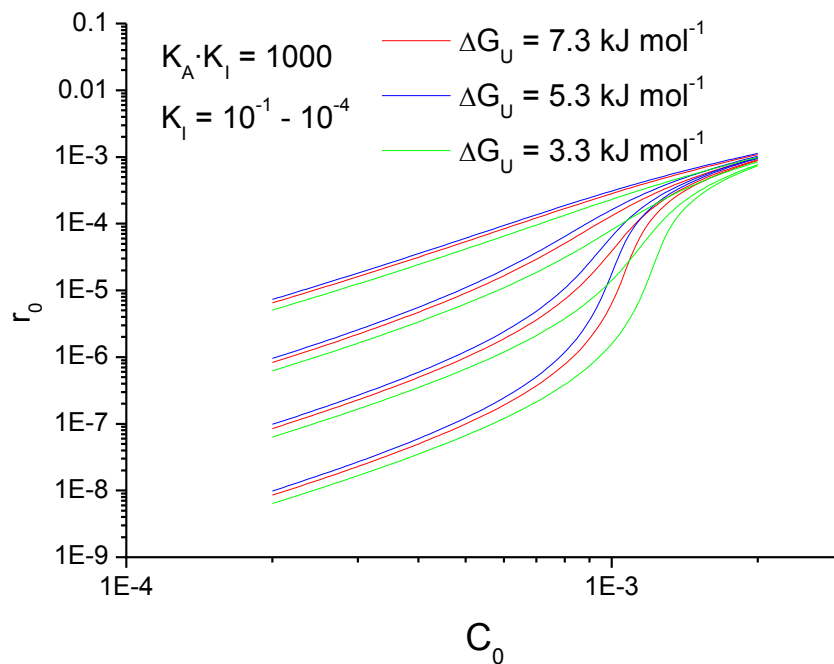
The unfolding Gibbs energy does not have a strong effect on the initial rates because it has a relatively low effect on the population of the amyloidogenic intermediate.

Text S3: Contribution of fibril elongation by monomer addition to the early kinetics.

We consider now the possibility that monomer addition would also contribute significantly to the initial rate of amyloid growth. During the early stages of the kinetics both the nucleation and elongation can be considered essentially irreversible and the concentrations of the monomeric and oligomeric precursors remain approximately constant and equal to the pre-equilibrated concentrations [35]. With these assumptions, the rate of formation of amyloid nuclei is:

$$\frac{dN_F}{dt} = k_F \sum_{i=2}^{\infty} [A_i] = k_F N_A \qquad (16)$$

$$N_F \approx k_F N_A t \qquad (17)$$

Where N_A and N_F are respectively the number concentrations of oligomer and amyloid particles at a particular time. The rate of aggregation at early times is given by:

$$r = k_F C_A + k_E [I] N_F = k_F C_A + k_F k_E N_A [I] t \qquad (18)$$

Here k_E is the elongation rate constant. This equation implies that if monomer addition was important the initial slope of the aggregation kinetics would increase and the kinetics would have an upwards curvature.

The relative contribution of monomer addition to the overall rate is:

$$\frac{r_E}{r_F} = \frac{k_E N_A [I] t}{C_A} = \frac{k_E [I] t}{\langle A_n \rangle} \qquad (19)$$

The following simulations show that an increase in slope with time during the early kinetics due to amyloid growth by monomer addition can only be significant for high k_E. On the other hand, formation of oligomers is favored by high protein concentration, decreasing the concentration of intermediate and reducing the contribution of monomer addition.

In these simulations we used $K_A = 2.5 \times 10^5$, K_I ranging between 10^{-3} and 10^{-1}, and $k_E = 10^3$ and 10^4 M^{-1} min^{-1}.
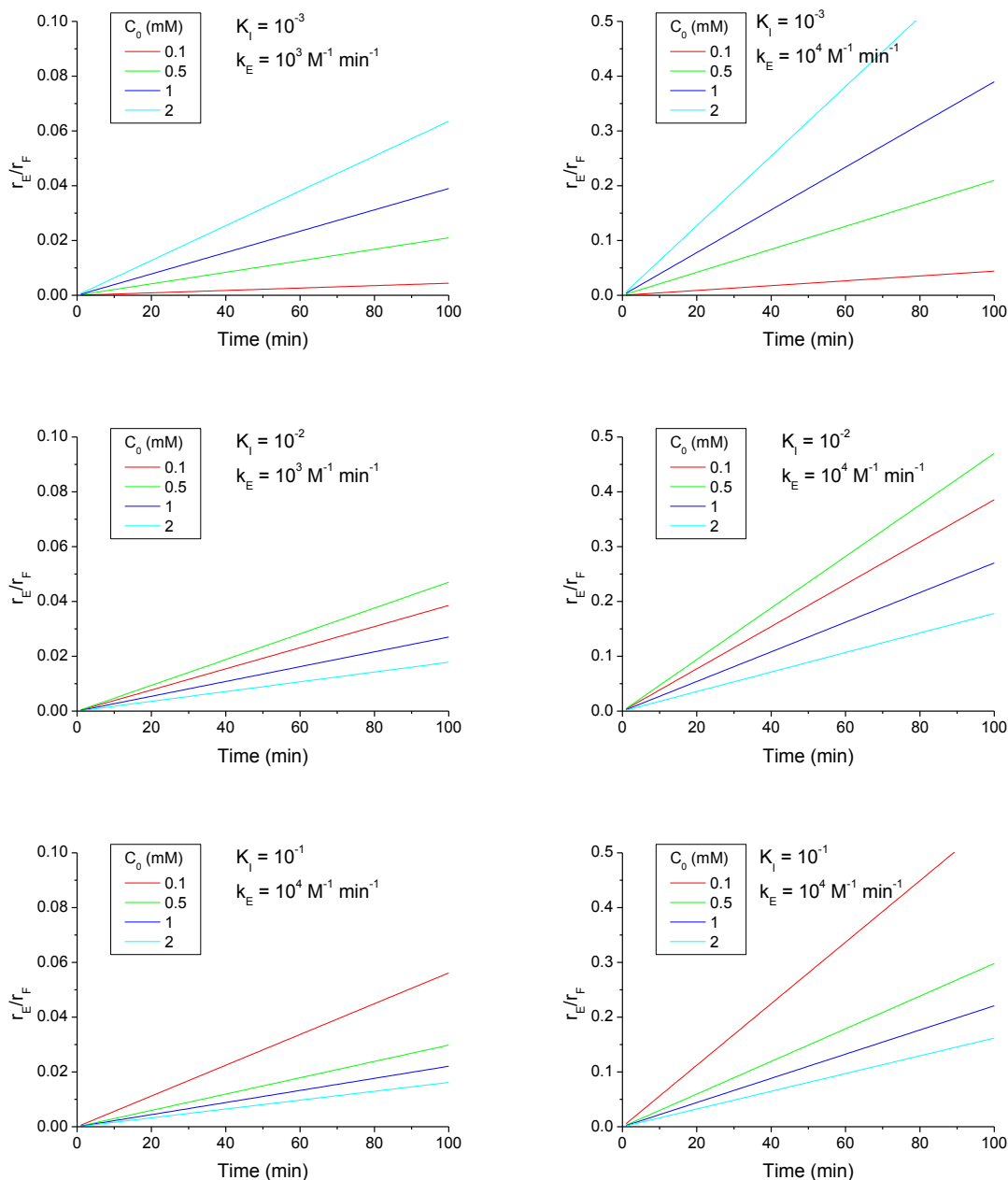
These simulations show that while under most conditions the initial aggregation rates are representative of the formation of nuclei, if the elongation rate constant is high, the contribution of monomer addition can be significant even at short times of aggregation. This problem could be alleviated by using an appropriate extrapolation of the initial rates at time zero.

Chapter 3

MODULATION OF THE STABILITY OF AMYLOIDOGENIC PRECURSORS BY ANION BINDING STRONGLY INFLUENCES THE RATE OF AMYLOID NUCLEATION

(David Ruzafa, Francisco Conejero-Lara and Bertrand Morel)

ABSTRACT

A deep understanding of the physicochemical factors modulating amyloid aggregation of proteins is crucial to develop therapeutic and preventive approaches for amyloid-related diseases. The earliest molecular events of the aggregation cascade represent one of the main targets as indicated by the toxic nature of certain early oligomers. Here, we study how different types of salt ions influence the kinetics of amyloid assembly of the N47A mutant α-spectrin SH3 domain using a battery of techniques. The salts influenced aggregation rates to different extents without altering the overall mechanism and the high apparent order of the experimental kinetics. A quantitative analysis of the initial aggregation rates measured by thioflavine-T fluorescence using a simple nucleation model allowed us to estimate the kinetic and thermodynamic magnitudes of crucial aggregation precursors, as well as evaluating the impact of each type of ion on the earliest amyloid nucleation stages. Whilst cations did not have any noticeable effect under our experimental conditions, anions stabilize an amyloidogenic intermediate state and also increase the rate of the conformational conversion from dynamic oligomers to amyloid nuclei, resulting in a strong acceleration of the nucleation process. Anions appear to act by preferential binding to the amyloidogenic intermediate state, thus enhancing its population and subsequent oligomerization. Overall, our results contribute to the rationalization of the effect of ions on the amyloid nucleation stage and give insight into the properties of the crucial intermediate precursors of amyloid aggregation.

INTRODUCTION

A group of diseases, most of them with tremendous social consequences, is related to the inability of a certain protein or peptide to adopt or maintain its native, functionally active conformation. Despite the existence of exigent mechanisms of control of protein aggregation in the cell, under certain metabolic circumstances (stress, cell aging or the presence of exogenous or infectious agents) some misfolded proteins or peptides form highly organized aggregates, which deposit as fibrils or plaques commonly known as amyloids. To date there are more than 30 diseases, some sporadic and/or hereditary and some transmissible,

associated with amyloid deposits [1]. Among these, there are some of the most devastating neurodegenerative diseases, such as Alzheimer, Parkinson and Huntington diseases. This group of diseases infringes an enormous social and personal damage and it is crucial therefore to understand in detail the molecular mechanisms and the physicochemical factors governing their genesis in order to learn how to treat and prevent them.

The aggregation process leading to amyloid fibrils involves a common pathway generally triggered by protein misfolding, followed by precursors to fibrils [2]. In recent years plenty of evidence has identified soluble oligomers as the main causative agents of cell toxicity [3-6], whereas a controversial debate has arisen about the role of insoluble amyloids as reservoirs rather than sequestering deposits of toxic soluble species [7,8]. These oligomers appear to be relatively disordered initially, but then convert into species containing extensive β-sheet structure [9] that are often capable of stimulating fibril formation [10]. The interest in these types of low-molecular-weight oligomers has increased since these species have been detected in the brains of patients suffering from Alzheimer disease [11,12]. According to the "nucleated conformational conversion" (NCC) model for aggregate formation [10], a group of monomers initially present in solution coalesces to form "molten" oligomers, which subsequently undergo a reorganisation process and eventually give rise to more organised oligomers and fibrils rich in β-sheet structure. Although the nucleated conformational conversion mechanism has been supported by many experimental and theoretical observations [10,13-17], a detailed description of this process at the molecular level remains in large part elusive because it is challenging to describe the early stages of aggregation of polypeptide chains by experiment. This is primarily due to the difficulties in detecting and characterizing the small, structurally heterogeneous, and transient species that are involved. This situation is being considerably alleviated by the progressive emergence of increasingly comprehensive and quantitative formalisms, which have successfully explained the early aggregation kinetics of a number of proteins under a variety of nucleation regimes [18-20].

Recently, we have shown that under conditions of rapid nucleation the quantitative analysis of experimental fibrillation kinetics can provide valuable information about the key precursor states of amyloid nucleation [21]. We have derived a simple mathematical model, which can

account very well for the experimental initial rates of aggregation from the pure monomeric native protein and their dependence with the concentration of protein. The model allowed us the estimation of thermodynamic magnitudes characterizing the highly unstable amyloidogenic intermediate and its oligomers during amyloid aggregation of the Spc-SH3 domain.

It was also shown that environmental conditions such as protein or salt concentrations can strongly affect the stability and population of the precursors, leading to different nucleation scenarios that may in turn result in diverse aggregation pathways and fibril morphologies. Previous studies done on other systems have also highlighted that the amyloid-forming propensity of amyloidogenic peptides/proteins is highly modulated by environmental factors [22,23]. Salts generally speed up fibrillation of many proteins including insulin [24], β2-microglobulin [25], α-synuclein [26], and S6 [27]. A recent study has also revealed that a compact, partially folded conformation of the amyloid beta peptide could be trapped by a variation in the salt concentration [28]. However, in many cases the effects are dependent on the nature of the ions even at low concentrations.

Although the effect of salt ions on protein solubilization/precipitation has been largely investigated [29,30], the influence of salt ions on amyloid fibril formation and particularly on the early stages of the process still remains unclear. Salt ions represent a particularly important group of environmental determinants, as they are ubiquitously present in living cells and have proved to be involved in the aggregation process of system related to diseases, such as amylin (IAPP) [31-33]. Salt ions may in principle promote the aggregation of a polypeptide chain in multiple ways. They may accumulate non-specifically in the proximity of oppositely charged protein groups, causing the electrostatic protein-protein interactions to fall off more rapidly with distance, according to Debye-Hückel screening; this screening reduces repulsive electrostatic interactions and allows forces that favour intermolecular association to prevail. Alternatively, salt ions may interact directly with charged or polar chemical groups of the polypeptide chain, with an efficiency that follows the so-called electroselectivity series [34]. Finally, salt ions can promote protein aggregation by perturbing the hydration shell of the molecule [35]. The efficiency of this "salting out" effect is determined

by the nature of the salt, as described by the Hofmeister series that ranks anions and cations according to their precipitation power [30].

Here, we show that different types of ions strongly influence the kinetics of nucleation of amyloid assembly of the N47A mutant of α-spectrin SH3 domain. The use of such a well-characterized model protein, even though it is unrelated to any known disease, is a potent approach to investigate the mechanisms of formation of amyloid fibrils due to the extended information available about its folding mechanism and conformational stability [36-39]. In addition, proteins related to diseases have been shown to be much more difficult to handle because of their intrinsic properties and high aggregation propensity making it extremely difficult to obtain reproducible quantitative information about the aggregation kinetics.

A range of biophysical techniques (circular dichroism, thioflavine T (ThT) fluorescence, dynamic light scattering, transmission electron microscopy, Fourier-transform infrared spectroscopy) was combined to study the effect of several cations and anions on the rates of amyloid formation. Initial aggregation rates were measured by *in situ* ThT fluorescence at different protein concentrations and fitted using our recently developed kinetic model describing the amyloid nucleation process [21]. The data were analyzed and compared quantitatively in the presence of different salt ions.

With this approach we have estimated thermodynamic magnitudes characterizing the amyloidogenic intermediate and its oligomerization, as well as the rate constants of the conformational change to form the amyloid nuclei, for a set of different salts. The results of these experiments allow us an understanding of how the kinetic phases of nucleation are affected by salt ions. The results strongly suggest that ions act by stabilizing preferentially an amyloidogenic intermediate, which results in enhanced formation of critical oligomers. These effects may likely occur by direct ion binding to the protein groups that may result in an ion-mediated alteration of the hydration shell of the protein.

EXPERIMENTAL SECTION

Protein samples

The N47A mutant Spc-SH3 domain was purified as described elsewhere [40]. For aggregation experiments, the lyophilized protein was rapidly dissolved in the appropriate buffer at 4ºC, centrifuged for 2 min, and filtered through a 0.2 μm filter. Protein concentration was determined by measurement of the absorbance at 280 nm using an extinction coefficient of 15784 $M^{-1}.cm^{-1}$.

Thermodynamic stability of the native state in presence of ions

To evaluate how different salts influence the thermodynamics of stability of the protein, differential scanning calorimetry experiments (DSC) were carried out with a VP-DSC capillary-cell microcalorimeter from MicroCal (Northampton, MA, USA). Calorimetric cells (operating volume 0.134 ml) were kept under an excess pressure of 50 psi to prevent degassing during the scan and also to permit the scans to be performed at a temperature up to 100 ºC. Several buffer-buffer baselines were obtained before each run with the protein solution in order to ascertain proper equilibration of the instrument. Buffer baselines were systematically subtracted from the thermograms of the sample, and the time response of the calorimeter was corrected. Reheating runs were carried out to determine the calorimetric reversibility of the denaturation process. The DSC experiments were performed at a scan rate of 1.5°C.min^{-1} and a protein concentration of 0.2-0.6 mg.mL^{-1}, which is sufficiently low to preclude aggregation during the heating. The partial molar heat capacity curves (Cp) were calculated from the DSC data and analyzed using Origin 7.0 (OriginLab, Northampton, MA) according to the two-state unfolding model. This analysis allowed the determination of the thermodynamic magnitudes of unfolding of the native state under each condition.

Amyloid fibril morphology

The formation of amyloid fibrils in the presence of each salt was monitored by transmission electron microscopy (TEM). Protein samples were incubated during 10 days to allow the

formation of amyloid fibrils under each condition analyzed. The samples were diluted tenfold in the same buffer and a 15 μl aliquot was placed on a formvar-carbon-coated copper grid and left for 4 min. The grid was then washed twice with distilled water and stained with 1% (w/v) uranyl acetate for 1 min. The dry samples were then observed on a Zeiss 902 electron microscope (Zeiss, Oberkochen, Germany) operating at an accelerating voltage of 80 kV and observed at a magnification factor of 50000.

Kinetics of native state depletion during aggregation

The depletion of the native state during amyloid aggregation was specifically followed by near-UV circular dichroism (CD). CD experiments were performed on a Jasco J-715 (Tokyo, Japan) spectropolarimeter equipped with a thermostatted cell holder. Near-UV CD spectra (320–250 nm) of the aggregation solution were measured using a 1 mm cuvette. In aggregation kinetics experiments, the CD signal was monitored at 295 nm as a function of time every 20 seconds and at a constant temperature of 37ºC using a 1 mm path-length cuvette. The kinetic curves were normalized using the initial concentration, C_o, and data were then fitted to an n-order irreversible kinetics to obtain the apparent order and rate constants, as shown in equation 1:

$$[N] = \frac{C_0}{(1 + C_0^{n-1}(n-1)kt)^{\frac{1}{n-1}}} \quad (1)$$

The conversion time of a 25% of the native protein to aggregates, $t_{1/4}$, was calculated as:

$$t_{\frac{1}{4}} = \frac{\left(\frac{4}{3}\right)^{n-1} - 1}{C_0^{n-1}(n-1)k} \quad (2)$$

Initial rates of native state depletion were calculated from the CD curves by fitting the initial region using a double exponential function:

$$y = y0 + A_1 . e^{-k_1 t} + A_2 . e^{-k_2 t} \quad (3)$$

The initial slope is then calculated from the resulting fitting parameters as:

$$r_0 = \left(\frac{dy}{dt}\right)_{t \to 0} = A_1.k_1 + A_2.k_2 \quad (4)$$

This operational extrapolation avoids the assumption of any time interval in the kinetics to define an initial aggregation rate.

Characterization of particle size

To analyze the molecular size of particles and aggregates during the kinetic experiments, DLS measurements were performed with a DynaPro MS-X instrument (Wyatt Technology Corporation, Santa Barbara, CA, USA) using a thermostatized 30 µl quartz cuvette. The protein solutions and the buffer were centrifuged and filtered through 0.02 µm Anotop 10 filters (Whatman plc, Brentford, Middlesex, UK) immediately before measurements. Sets of DLS data at 37°C were acquired every 45 s until saturation of the signal. The laser power was adjusted to avoid early saturation. Dynamics V6 software (Wyatt Technology Corporation, Santa Barbara, CA, USA) was used in data collection and processing. The experimental autocorrelation curves data were analyzed to obtain the particle size distributions using the regularization fit as implemented in Dynamics V6 software.

Secondary structure changes during aggregation

Fourier-transform infrared (FTIR) spectra were recorded from 4000 cm^{-1} to 900 cm^{-1} on a Bruker IFS 66 FTIR spectrophotometer (Brucker, Ettlingen, Germany) equipped with a BIO-ATR-II cell. For each sample, 128 interferograms were co-added and Fourier transformed with a zero filling factor of 4 to yield spectra with a nominal resolution of 2 cm^{-1}. The sample temperature was controlled and set to 25°C by means of a thermostated cell jacket. Then the sample temperature was quickly raised to 37°C and spectra were acquired sporadically during the aggregation process. Solvent spectra were recorded under identical conditions and subtracted from the spectra of the proteins. Spectral contributions from residual water vapour were reduced using the atmospheric compensation filter built in the Bruker OPUS software.

Second derivatives were obtained using the Stavitzky-Golay algorithm with the 13-point smoothing.

Initial rates of formation of amyloid aggregates

Kinetics of amyloid aggregation was monitored in continuous mode by ThT fluorescence using a Cary Eclipse spectrofluorimeter (Varian Inc.). A 500 μM stock solution of ThT was freshly prepared in the desired aggregation buffer (pH 3.2). A 98 μl of protein sample previously prepared in the aggregation buffer was mixed with 2 μl of the ThT stock solution. Fluorescence emission intensity at 480 nm was measured continuously at the desired temperature during the aggregation process in a 3 mm path-length fluorescence cuvette.

Initial rates of formation of amyloid structure were calculated by the same fitting procedure described above for the CD curves.

RESULTS

The kinetics of amyloid aggregation is strongly affected by the presence of different salts

To ascertain how different salts affect the aggregation kinetics of the N47A Spc-SH3 domain, several physical observables were monitored under the experimental conditions previously reported for the formation of amyloid by Spc-SH3 [36,38]. Basically, samples were prepared at a protein concentration of 1.2 mM in different salt ions solutions at a total ionic strength of 0.2 M taking into account the ionization degree of the glycine buffer and of the salt. The salts concentration used in this study are 0.1 M LiCl, 0.1 M KCl, 0.1 M NaCl, 0.025 M $MgSO_4$, 0.1 M $NaNO_3$, 0.1 M KBr, 0.033 M $MgCl_2$ and 0.033 M $CaCl_2$.
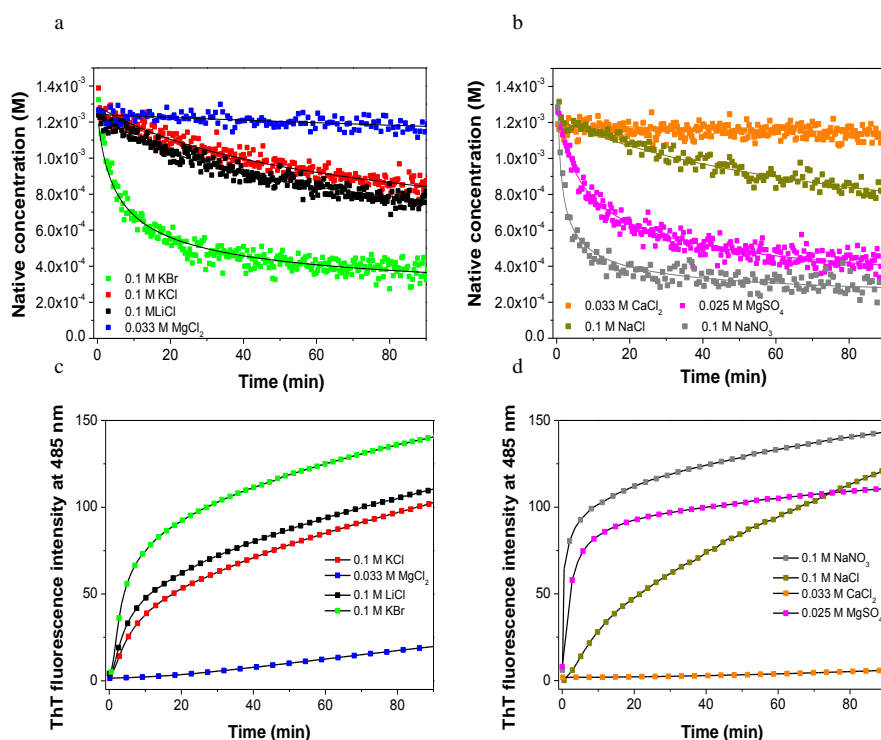
Figure. 1 Effect of different salt ions on the kinetics of the native state depletion of the N47A Spc-SH3 domain followed by near UV CD at 295 nm (a and b) and the formation of amyloid structure followed by ThT fluorescence (c and d). *Experiments were made at 37ºC and the protein concentration was around 8.5 mg mL^{-1} (1.2 mM) in each case. The symbols used are indicated in the graphs.*

The near UV CD signal was used to monitor the disappearance of the native state during aggregation. Near UV CD spectra of the N47A Spc-SH3 domain were recorded at 25°C in the presence of different ions. The similarity of the spectra indicates that the salts added do not alter the tertiary structure of the protein (Supplementary information Figure S1a). The N47A mutant of Spc-SH3 has a characteristic near UV CD spectrum with a positive band at 295 nm. As aggregation progressed, the CD spectrum changed considerably and the positive band at 295 nm, corresponding to the tryptophan signal, disappears for mature amyloid fibrils (Supplementary information Figure S1b).

Aggregation of the N47A Spc-SH3 domain in presence of the different salts at a similar concentration of protein of 1.2 mM was observed by monitoring the near UV CD signal at 295 nm as a function of the incubation time at 37°C. Consequently, we took advantage of the

absence of the CD signal at 295 nm in the near-UV CD spectrum of the amyloid aggregates and we assumed therefore that the CD signal intensity at this wavelength is proportional to the concentration of the native protein monomer during the aggregation process. The normalized signal intensity decay does not follow a first-order kinetics as described previously [21] but could be well fitted using the integrated equation of an irreversible n-order kinetics (Figure 1a and Figure 1b). Individual fittings yielded superior apparent orders ranging between 3 and 4 and the initial rates or aggregation vary by almost three orders of magnitude, depending on the nature of the salt ions in solution (Figure 2a). The apparent rate constants rank roughly in three groups, each one with similar values. The slowest aggregation rates are observed for 0.033 M $MgCl_2$ and 0.033 M $CaCl_2$, then 0.1 M NaCl, 0.1 M LiCl, 0.1 M KCl rank similarly, and finally 0.1 M KBr, 0.025 M $MgSO_4$ and 0.1 M $NaNO_3$ show the highest rate constants.

The influence of the different type of salts ions on the kinetics of formation of amyloid structure was also observed by thioflavin T fluorescence (ThT) under identical conditions. From the data shown in Figures 1c and 1d, it is evident that salt ions have a strong effect on the kinetics of formation of amyloid aggregates. Apart from a short lag observed in the presence of 0.033 M $MgCl_2$ and 0.033 M $CaCl_2$, there is no lag phase in any of the other kinetics, which indicates a rapid formation of amyloid nuclei. According to Figure 2a, the ThT fluorescence early rates of growth correlate quite well with the rate of depletion of native protein. This suggests a direct relationship between the kinetics of formation of amyloid nuclei and that of consumption of native monomers.

To explore the rate of growth of aggregate particles during aggregation of the protein in the presence of different salt ions, the kinetics were also studied by measuring the scattering intensity by DLS (Supplementary information Figure S2a). In the presence of 0.033 M $CaCl_2$ and 0.033 M $MgCl_2$ the development of aggregates, which is related to an increase in the DLS intensity counts, proceeds very slowly during the first 200 minutes and increases rapidly thereafter. In the presence of the other salt ions, much higher rates of particle growth are observed. The initial growth of scattering signal ranks similarly to that of the native state depletion and that of ThT fluorescence for the different salts.

A more detailed analysis of the DLS data allowed us to follow the early distributions of particle sizes during the aggregation process (Supplementary Information Figure S2b and S2c). Before incubation and under all conditions, there were only particles with an apparent hydrodynamic radius (R_h) of ≈1.6 nm corresponding to the monomeric native protein [36,41]. As aggregation progressed, the peak corresponding to the native R_h shifts up to values ranging between 2.8 and 4.0 nm, suggesting the formation and accumulation of small oligomeric nuclei, which become dominant in the DLS size distributions over the smaller monomeric native particles. The apparent R_h of spherical particles is approximately proportional to the 1/3 power of the mass, whereas for coils it scales approximately with the 1/2 power [42]. This implies an average degree of oligomerization of about 3-5 for the observed oligomers, depending on their degree of compactness.

The mean times of the shift in R_h, t_s, associated to formation of these oligomers were estimated by fitting the time dependence of the apparent R_h using a logistic sigmoidal function. The apparent R_h given by the intensity-weighted distributions are mainly representative of the particles dominating the scattering signal. Since the scattering intensity is proportional to the square of the mass particle, the transition of the apparent R_n from that of the native monomer to that of oligomers should occur for an approximate 25% conversion of protein monomers into oligomers. These times correlate well with the corresponding times, $t_{1/4}$, calculated from the near UV CD kinetics (Figure 2b). This supports that formation of amyloid oligomeric species at the expense of native molecules is the dominant event in the early aggregation kinetics of Spc-SH3.

The growth of larger particles, likely amyloid fibrils, is also observable by the presence of a second peak in the distributions, which increases its hydrodynamic radius progressively. Although having similar processes, the speed of this series of events depends markedly on the nature of the salt ions.
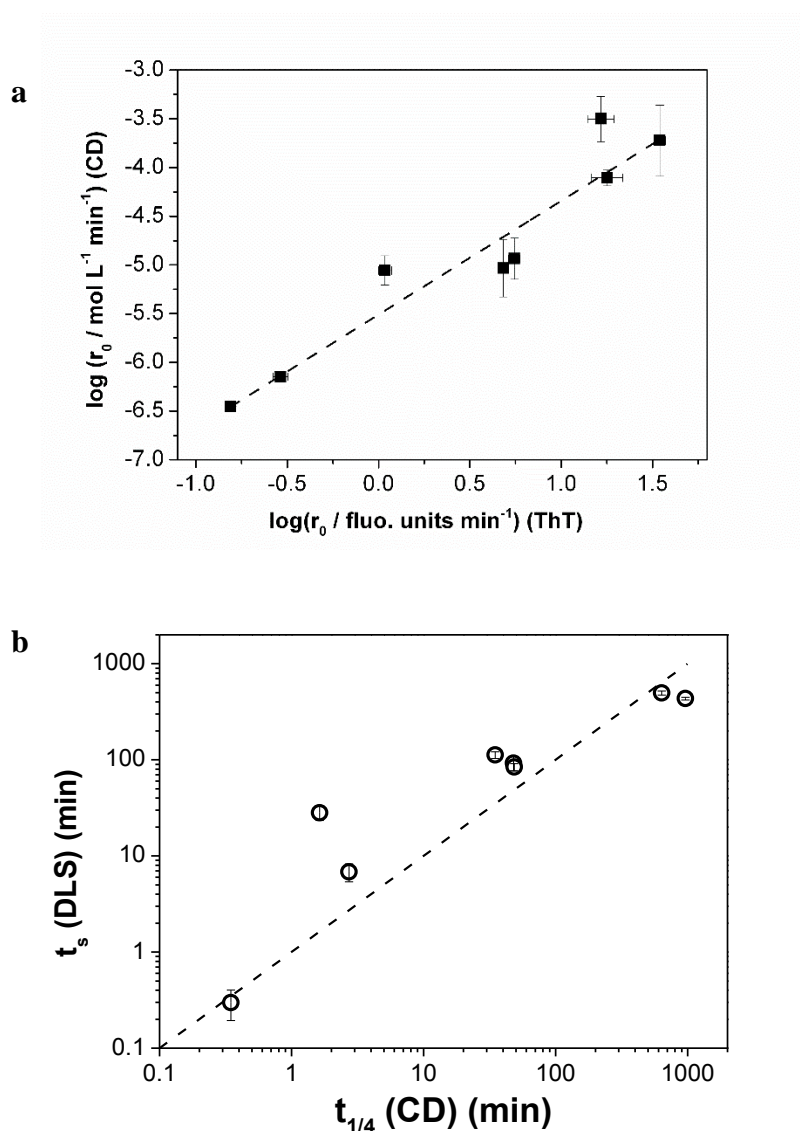
Figure. 2 Correlation between the rates of growth determined using different techniques. Correlation between initial rates obtained with near UV CD and the ThT fluorescence experiments (a). Correlation between the time of oligomers appearance and the conversion time of a 25% of the native protein to aggregates. Correlation coefficients and error bars are indicated in each panel.

The conformational change leading to cross-beta structure accompanying amyloid aggregation was also observed in the presence of the different salt ions by measuring the infrared spectra sporadically during the aggregation process for all the conditions studied. The development of a prominent band at 1622 cm^{-1} indicative of the formation of extended intermolecular β-sheet structure occurs rapidly. After 30 minutes of incubation at 37ºC this

band is present in all spectra (Supplementary information Figure S3), which suggests a similar conformational change in the presence of all the salts. However, the different intensities of the band reflect the different rates of aggregation, as described above.

The fibrillar nature of the aggregates and their overall morphologies are similar for all the salts and also similar to those previously described in the presence of 0.1 M NaCl [38]. As indicated by transmission electron microscopy (TEM) images recorded with samples incubated for 10 days at 37ºC in the presence of the different salts (Supplementary Information Figure S4).

These results show that the different salt ions do not change the series of conformational and oligomerization events along the aggregation pathway but they can have a strong differential effect upon the rates at which these processes occur. Since the ionic strength has been kept constant in these experiments, we can conclude that a Debye-Hückel screening effect is not responsible for these variations.

Quantitative analysis of the initial rates of growth of ThT fluorescence reports about crucial intermediates of amyloid nucleation

We have shown recently that in the absence of lag phase the initial growth of ThT fluorescence could be mainly attributed to a rapid accumulation of small amyloid nuclei and that the dependence of the initial aggregation rates with the initial protein concentration could be analyzed in terms of a simple kinetic model, which allowed us to derive thermodynamic and kinetics magnitudes characterizing the nucleation [21]. For this reason the aggregation kinetics followed by ThT fluorescence were studied at 37°C in the presence of the different salts and at various protein concentrations spanning about one order of magnitude or more depending on the salt. Initial rates of formation of amyloid nuclei were estimated from the slopes of the ThT kinetic traces extrapolated to time zero, as described in Materials and Methods. To fulfil the requirement of rapid nucleation of the model, we used in the analysis only the kinetics without a significant lag phase.

Similarly to the kinetics of native state depletion, the apparent order of the kinetics, derived from the slope of a double logarithmic plot (Figure 3), varies between 3 and 4 depending of the salt present in solution. The high-order kinetics suggests an oligomerization pre-equilibrium preceding the rate-limiting step of amyloid nucleation. This step yields stable oligomeric amyloid nuclei as observed by DLS. However, as reported previously [21], the apparent order of the aggregation kinetics changes significantly with conditions and does not correlate with the degree of oligomerization, suggesting a variety of oligomeric precursors.

We found that the experimental initial rates of amyloid nucleation measured by ThT fluorescence as a function of the protein concentration could be quantitatively accounted for using a simple model for amyloid nucleation (Scheme 1) [21].

Scheme 1
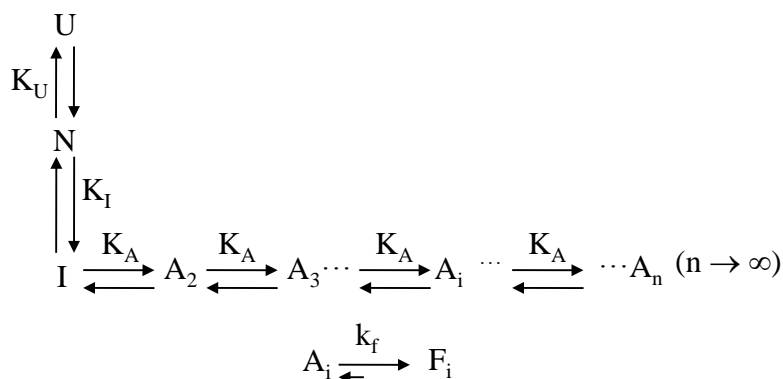
In this analysis we assumed an unrestricted oligomerization pre-equilibrium of a partially unfolded state, preceding the rate limiting step of conformational conversion to amyloid nuclei. The oligomer distribution is only determined by the thermodynamic parameters of the conformational-oligomerization pre-equilibrium and by the concentration of the self-associating species. Only the amyloid nuclei F_i are detected by thioflavin T fluorescence. The theoretical equations of the model depend on four independent fitting parameters (K_A, K_I, K_U and k_F).

The initial rate of aggregation is given by:

$$r_0 = \frac{k_F (Bx_N)^2 (2 - Bx_N)}{K_A (1 - Bx_N)^2} \quad (5)$$

Where the fraction of native protein, x_N, can be obtained for each initial protein concentration, C_0, by solving:

$$1 = Ax_N + \frac{K_I x_N}{(1 - Bx_N)^2} \quad (6)$$

Where $A = 1 + K_U$, and $B = K_I \cdot K_A \cdot C_0$.

The values of K_U (the equilibrium constant between the native and the fully unfolded states) were obtained independently by a set of DSC experiments in the presence of the different salts. These experiments were made in the same buffer used in the aggregation experiments but at a sufficiently low protein concentration to avoid aggregation during thermal unfolding. Under these conditions, all unfolding curves were highly reversible as observed in a second consecutive heating scan and followed very well the two-state unfolding model, from which we obtained the thermodynamic parameters of the unfolded state.

Once fixed the values of K_U, individual fits for all salts tested describe very well the data (results not shown) but the dependency between the three remaining fitting parameters was still high. We found that the fits converged to similar values for K_A (the equilibrium constant of oligomerization) for the different salt ions and the entire set of initial rates could be then globally fitted using a common value for this parameter (Figure 3). This suggests that the oligomerization equilibrium constant has a small dependence on the nature of the salt ions.
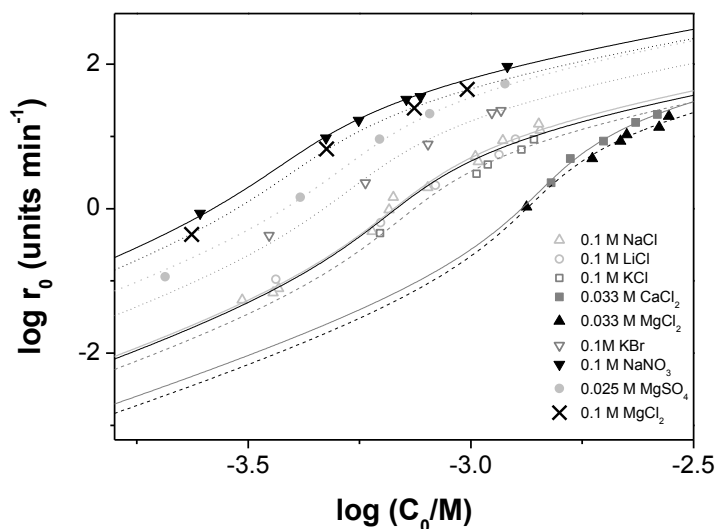
Figure. 3 Double logarithmic plot of the initial rates of amyloid fibrillation of N47A Spc-SH3 versus the initial protein concentration in presence of the different salt ions. *The symbols used are indicated in the graph. Symbols correspond to the experimental rates and continuous lines represent the best fits according to the equation (5) described in Ruzafa et al. [21].*

From the parameters resulting from this global analysis (Table 1) we could conclude that the amyloidogenic intermediate (I in our model) is selectively stabilised in the presence of $MgSO_4$ or KBr and especially $NaNO_3$, in comparison with our standard conditions (0.1 M NaCl). In the presence of LiCl or KCl the thermodynamic parameters are very similar to those obtained with NaCl. In contrast, $CaCl_2$ and $MgCl_2$ produce a destabilization of the amyloidogenic intermediate by about 2 kJ mol^{-1}. Noteworthy, the nature of the cations does not appear to have an effect in this parameter because homologous chlorides have similar effect on the values of ΔG_I.

The first-order rate constant of conformational conversion of dynamic oligomers into amyloid structure (k_f) is almost 10-fold higher in the presence of $NaNO_3$ and $MgSO_4$. The k_f values obtained with all the chlorides are quite similar. This observation suggests that bound ions could participate in the conformational conversion to amyloid structure. Different ions may have a different influence in this conversion.

We have also studied the effect of salt concentration on the nucleation kinetics using $MgCl_2$, which has proved to be one of the less efficient salts to promote aggregation, in comparison with the data obtained for NaCl in our previous study [21,38].

As shown in Figure 3, an increase in $MgCl_2$ concentration accelerates the nucleation and reduces the apparent order of the kinetics from 3.8 ± 0.3 at 0.033 M $MgCl_2$ to 3.2 ± 0.2 at 0.1 M $MgCl_2$. Similar observations were drawn previously for the N47A Spc-SH3 fibrillation upon an increase in the NaCl concentration [21]. The increase in salt concentration also stabilizes the amyloidogenic intermediate relative to the native and unfolded states, thus increasing its population. As shown in Table 1, the rate constant of the conformational conversion of oligomers into amyloid nuclei is also considerably increased with the salt concentration (k_f increases by 7-fold in 0.1 M $MgCl_2$ relative to 0.033 M $MgCl_2$).

In conclusion, while the different cations do not affect the early nucleation stages, anions appear to act at two stages of the nucleation mechanism: firstly, they alter the stability of the amyloidogenic intermediate state, changing its relative population. Secondly, they influence the rate of conformational conversion to amyloid structure within the oligomers.

Table 1 Fitting parameters derived from the analysis of initial nucleation rates at 37°C.

Salt (M)	$\Delta G_u{}^a$ (kJ/mol)	ΔG_a (kJ/mol)	ΔG_i (kJ/mol)	$\log k_F$
0.1 M NaCl	5.52		12.89 ± 0.28	4.26 ± 0.06
0.1 M LiCl	4.54		12.70 ± 0.31	4.19 ± 0.1
0.1 M KCl	4.28		12.81 ± 0.31	4.10 ± 0.09
0.1 M KBr	4.39		12.27 ± 0.29	4.61 ± 0.08
0.1 M NaNO$_3$	3.81		11.32 ± 0.30	5.05 ± 0.07
0.025 M MgSO$_4$	4.70	-31.99 ± 2.89	12.24 ± 0.30	4.92 ± 0.09
0.033 M CaCl$_2$	6.04		14.79 ± 0.32	4.28 ± 0.09
0.033 M MgCl$_2$	6.17		14.69 ± 0.30	4.11 ± 0.07
0.1 M MgCl$_2$	4.65		11.52 ± 0.34	4.93 ± 0.10

^{a}Calculated from the unfolding curves measured by DSC. The value of ΔG_u is fixed in the fitting procedure.

DISCUSSION

The formation of transient oligomers made of partially-unfolded intermediates has been previously reported as a crucial event preceding amyloid fibrillation in many proteins [43-45]. Single-molecule fluorescence methods have also shown a rapid increase in the population of a distribution of oligomeric species of different sizes during the early stages of the N47A Spc-SH3 [46] and PI3–SH3 aggregation [47]. The earliest of these oligomers appeared to be

structurally-unstable and interconverting species with heterogeneous sizes but were described to undergo progressive stabilization as aggregation progresses due to conformational conversion into stable amyloid species [47]. These general characteristics of oligomeric intermediates are in good agreement with our results, confirming that conformational conversion to nucleate amyloid structure takes place from a heterogeneous distribution of oligomeric species as proposed in our model.

The detection of the kinetically-relevant monomeric intermediate proposed in our nucleation model is, however, much more difficult because of its very low stability and population. In fact, our thermodynamic data indicate that this intermediate state is much less populated (0.3%-1%) even than the fully unfolded state (10%-18%) under the different conditions analysed here and it does not manifest in the thermal unfolding curves followed by DSC, which fit very well to a two-state unfolding model. Notwithstanding, the proposal of a partially-unfolded intermediate in our nucleation mechanism is supported by recent findings from a computational analysis using an all-atom Gō model of the equilibrium folding transition of the Spc-SH3 domain and several amyloidogenic mutants (including the N47A mutant analyzed here) [48]. In this study, the authors identify a partially-unfolded, conserved intermediate at a very low population, which is enhanced by the amylodogenic N47A mutation. Moreover, partially folded aggregation-prone intermediates have been detected and characterized structurally in destabilized mutants of the homologous Fyn-SH3 domain using relaxation dispersion NMR spectroscopy[49,50]. Interestingly, both intermediates share some common structural characteristics with significant native-like topology involving β-strands 2, 3 and 4, and structural distortions mainly affecting the interaction between the N- and C-terminal β-strands. These evidences demonstrate the accessibility of a partially-unfolded state in the SH3 folding landscape, which under favourable conditions could trigger the amyloidogenic cascade.

In the present study, we have analyzed in detail how different salt ions affect the kinetic mechanism of amyloid nucleation of the N47A Spc-SH3 domain. We have reported in a previous paper that the environmental conditions, and specially the salt concentration, could modulate the aggregation kinetics[38]. Here, using a recently developed kinetic model for the

amyloid nucleation [21], we have shown that amyloid fibrillation kinetics of the N47A Spc-SH3 domain mutant is highly dependent on the presence of anions, which modulate the stability of the amyloidogenic intermediate state. Our analysis provides important thermodynamic and kinetic magnitudes allowing us rationalizing the nucleation event. This is of chief importance to understand the factors governing the stability of early amyloidogenic species. As shown in Table 1, data obtained differ depending on the nature of the salt ions present in solution.

In electrostatic interactions, if the Debye-Hückel screening effect is alone a predominant factor, then it should depend on the ionic strength regardless of the nature of ions. This is not the case in this study, since different salts produce disparate effects on the aggregation rate despite identical ionic strength. This suggests that the other factors should play an important role in the modulation of the amyloid formation of N47A Spc-SH3 domain.

To understand the effects of dissolved salts on proteins, both B-viscosity coefficients and salt surface tension increments have been suggested as possible indicators of the Hofmeister effect of a salt[51-53]. The Jones-Dole-B coefficient is a measure of the strength of ion-water interactions normalized to the strength of water-water interactions in the bulk solution. Hofmeister series is almost identical to the order of molal surface tension increment (MSTI); i.e., kosmotropes have high MSTI and inversely, chaotropes has low MSTI.

Consequently, the thermodynamic parameters obtained in this study for both unfolded protein and amyloidogenic intermediate, both relative to the native state, were plotted versus the B-coefficient and the MSTI of each electrolyte (Figure 4).

There appears to be a significant degree of correlation between the stability of the amyloidogenic intermediate (ΔG_I) and the lyotropic series. The stability of this intermediate state appears to be higher for kosmotropes ions. It is also found that the energy of the fully unfolded state (ΔG_U) is increased in the presence of kosmotropes ions, as expected. A similar albeit weaker correlation is also observed in the case of the viscosity coefficient B (Figure 4b). Nevertheless, these correlations appear to be just general trends and some inconsistencies are observed. Although $MgSO_4$ is in the middle of these Hofmeister-related series, it produces one of the highest stabilizations of the intermediate. Moreover, $NaNO_3$

produces the strongest stabilization of the intermediate but it is at different positions in these series. Therefore, these results could just qualitatively highlight an implication of the Hofmeister effect as a weak regulator of the early stages of amyloid nucleation, especially in the stabilisation of the intermediate state.

However, recent studies have challenged the original concept of the Hofmeister effect of ions as a water structure "making" and "breaking" effect. Recent advances in understanding the mechanism of the Hofmeister effect have provided valuable insights into the role of several ion-specific phenomena. Experimental evidence clearly shows that changes in bulk water structure by added salts cannot fully explain specific ion effects. Instead, Hofmeister phenomena need to be understood in terms of direct interactions between the ions and macromolecules.

A decade ago Omta and co-workers [54] showed that water structure outside the hydration shell of an ion is not influenced by the ion. As a result, it was concluded that no long-range structure-making or structure-breaking effects for either kosmotropes or chaotropes takes place. These experiments challenged the notion that salt solutions affect bulk water structure. Thermodynamic studies on protein stability also disagreed on the traditional Hofmeister theory [55]. In this study, the authors employed pressure perturbation calorimetry to demonstrate that no correlation can be found between a solute's impact on water structure and its effect on protein stability. A recent study based on isothermal titration calorimetry and NMR spectroscopy has also suggested an important mechanism by which chaotropic anions destabilize protein folds and increase their solubility by preferentially interacting with hydrophobic concavities, which results in a weakening of the hydrophobic effect [56]. All these recent studies have demonstrated that bulk water structure is not central to the Hofmeister effect. Instead, molecular-level models are being developed to explain the Hofmeister series that only involves the ion's direct interactions with macromolecules and their first hydration shell [57].

For this reason, we also have evaluated a potential role of direct ion binding in the early stage leading to amyloid fibrils. The N47A Spc-SH3 domain has a pI of 5.27 and is therefore positively charged at the pH used in this study. This means that if ions bind directly to the

protein surface the anions should be the most probable candidates. Indeed, in Figure 5 we represented the Gibbs energy of the I and U states, relative to the N state, versus the anions activity, which was calculated from the Davies equation [58]. There are clear linear dependences for both ΔG_I and ΔG_U as a function of the logarithm of the activity of chloride anions.
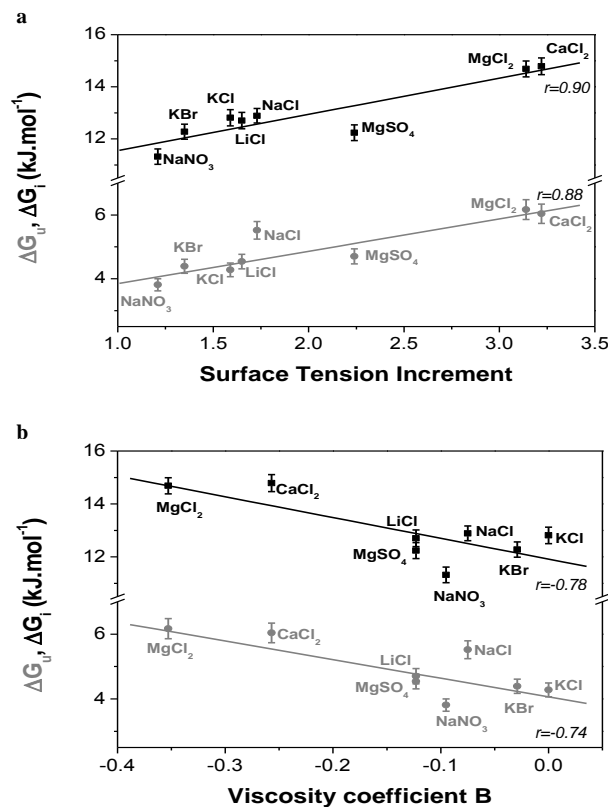
Figure. 4 Correlation of the surface tension increment (a) and the viscosity B coefficient (b) with ΔG_u (grey symbols) and ΔG_i (black symbols). *The continuous lines represent the linear regression. Correlation coefficients are indicated in all cases. Errors bars correspond to the values obtained from the quantitative analyses.*

Thermodynamic linkage between anion binding and conformational stability in proteins was studied two decades ago [59]. In this referential study, preferential anion binding was reported

to be the cause of stabilization of the A-state of cytochrome c and myoglobin, with molten-globule characteristics. The net increment in the number of bound ions X between two states A and B in equilibrium is given by [60]:

$$\Delta v = -RT . \frac{\partial \Delta G_{AB}}{\partial ln a_x} \quad (7)$$

Figure. 5 Dependence with the activity chloride anion of the Gibbs energies of the unfolded state, ΔG_u (grey) and of the intermediate amyloidogenic state, ΔG_i (black) both relative to the native state. Linear regressions are indicated in the graph in both cases.

From the slope of the linear fits of Figure 5 we estimated that an average of 1.1 ± 0.1 chloride anions bind additionally to the intermediate relative to the native state, whereas this preferential binding amounts only of 0.6 ± 0.2 for the unfolded state.

These results indicate that binding of one additional chloride anion relative to the native state stabilizes the amyloidogenic intermediate therefore increasing its concentration.

An interesting observation is the drastic effect of sulfate ions in the aggregation kinetics even at low concentration. Sulfate ions are well known for their ability to strongly promote amyloid aggregation under conditions of acidic pH and increase the stability of the resulting fibrils[25,61-63]. Pedersen and co-workers have shown how sulfate ions stabilize a salt-dependent

type of glucagon fibrils. The stabilization effect was explained by the shape or size of sulfate ions being suitable for interactions with proteins in an amyloid like β-sheet conformation. Sulfate ions were also found to be the most efficient promoter of HypF-N aggregation and structural re-organization in both the monomeric and early-oligomeric states [61]. In this study, sulfate ions revealed to be one of the most effective anions in favoring the formation of amyloid fibrils by stabilising the amyloidogenic intermediate state. Sulfate ions are reported as being kosmotropic ions. The other ions favouring most efficiently amyloid nucleation are usually classified as chaotropes (Br^- and NO_3^-). These results highlight the hypothesized effect of direct ion binding as amyloid modulating factor. We could then hypothesize that the intermediate state -which possess a much more defined structure than the fully unfolded protein and exposes significant hydrophobic patches- would offer considerable surface for binding of anions which consequently compete with interactions between hydrophobic surfaces [56]. It is likely that these effects occur via an alteration of the protein solvation layer that modifies the protein conformational landscape and, as a consequence, alters the energy of the amyloidogenic precursor.

Our thermodynamic results also indicate that the amyloidogenic intermediate, possibly in an anion-bound state, is very prone to oligomerize. Therefore, small changes in concentration of this intermediate induced by environmental factors become strongly amplified by the large energy gain accompanying its self-association, which favours larger and more abundant critical oligomers and finally faster formation of nuclei. The initial rates obtained for the different salts do not allow the identification of any important difference in the association equilibrium constant.

CONCLUSIONS

In this study, we have shown that anions can have a drastic effect on the rate of nucleation of amyloid fibrils of the N47A mutant of the Spc-SH3 domain, whereas cations do not have an important role under the experimental conditions analyzed. The thermodynamic and kinetic contributions to the nucleation derived from the experimental aggregation kinetics have allowed us identifying the specific molecular events of amyloid nucleation that become

modulated by anions. The energy of a low-populated amyloidogenic intermediate is reduced by the activity of anions in solution, increasing its population.

We conclude that preferential anion binding plays a crucial role in stabilizing the precursors of nucleation thus accelerating the subsequent fibrillation processes. These results increase our understanding of the earliest molecular events triggering the amyloid aggregation cascade.

The possibility to control the rate of protein self-assembly and the stability of the species populated during the process are important to understand the pathogenesis of the amyloid-related diseases.

ACKNOWLEDGEMENTS

NOTES

Electronic Supplementary Information (ESI) available: The near UV CD spectra of the protein in different salts are shown in Figure S1. Figure S2 shows the DLS intensity and size distribution in function of the time. Infrared spectra of Spc-SH3 after 30 minutes of incubation are represented in Figure S3. Figure S4 illustrates the morphology of the amyloid fibrils as observed by transmission electron microscopy.

REFERENCES

(1)   Stefani, M.; Dobson, C. M. Protein aggregation and aggregate toxicity: new insights into protein folding, misfolding diseases and biological evolution. *J. Mol. Med.* **2003**, *81*, 678-699.

(2)   Chiti, F.; Dobson, C. M. Protein Misfolding, Functional Amyloid, and Human Disease. *Annual Review of Biochemistry* **2006**, *75*, 333-366.

(3)   Campioni, S.; Mannini, B.; Zampagni, M.; Pensalfini, A.; Parrini, C.; Evangelisti, E.; Relini, A.; Stefani, M.; Dobson, C. M.; Cecchi, C.; Chiti, F. A causative link between the structure of aberrant protein oligomers and their toxicity. *Nat. Chem. Biol.* **2010**, *6*, 140-147.

(4)   Baglioni, S.; Casamenti, F.; Bucciantini, M.; Luheshi, L. M.; Taddei, N.; Chiti, F.; Dobson, C. M.; Stefani, M. Prefibrillar amyloid aggregates could be generic toxins in higher organisms. *J. Neurosci.* **2006**, *26*, 8160-8167.

(5)   Bucciantini, M.; Giannoni, E.; Chiti, F.; Baroni, F.; Formigli, L.; Zurdo, J.; Taddei, N.; Ramponi, G.; Dobson, C. M.; Stefani, M. Inherent toxicity of aggregates implies a common mechanism for protein misfolding diseases. *Nature* **2002**, *416*, 507-511.

(6)   Lajoie, P.; Snapp, E. L. Formation and toxicity of soluble polyglutamine oligomers in living cells. *PLoS One* **2010**, *5*, e15245.

(7)   Koffie, R. M.; Meyer-Luehmann, M.; Hashimoto, T.; Adams, K. W.; Mielke, M. L.; Garcia-Alloza, M.; Micheva, K. D.; Smith, S. J.; Kim, M. L.; Lee, V. M.; Hyman, B. T.; Spires-Jones, T. L. Oligomeric amyloid beta associates with postsynaptic densities and correlates with excitatory synapse loss near senile plaques. *Proc. Natl. Acad. Sci. USA* **2009**, *106*, 4012-4017.

(8)   Haass, C.; Selkoe, D. J. Soluble protein oligomers in neurodegeneration: lessons from the Alzheimer's amyloid beta-peptide. *Nat. Rev. Mol. Cell Biol.* **2007**, *8*, 101-112.

(9)   Calamai, M.; Canale, C.; Relini, A.; Stefani, M.; Chiti, F.; Dobson, C. M. Reversal of Protein Aggregation Provides Evidence for Multiple Aggregated States. *J. Mol. Biol.* **2005**, *346*, 603-616.

(10)   Serio, T. R.; Cashikar, A. G.; Kowal, A. S.; Sawicki, G. J.; Moslehi, J. J.; Serpell, L.; Arnsdorf, M. F.; Lindquist, S. L. Nucleated conformational conversion and the replication of conformational information by a prion determinant. *Science* **2000**, *289*, 1317-1321.

(11)   Roher, A. E.; Chaney, M. O.; Kuo, Y. M.; Webster, S. D.; Stine, W. B.; Haverkamp, L. J.; Woods, A. S.; Cotter, R. J.; Tuohy, J. M.; Krafft, G. A.; Bonnell, B. S.; Emmerling, M. R. Morphology and toxicity of Abeta-(1-42) dimer derived from neuritic and vascular amyloid deposits of Alzheimer's disease. *J. Biol. Chem.* **1996**, *271*, 20631-20635.

(12)   Lue, L. F.; Kuo, Y. M.; Roher, A. E.; Brachova, L.; Shen, Y.; Sue, L.; Beach, T.; Kurth, J. H.; Rydel, R. E.; Rogers, J. Soluble amyloid beta peptide concentration as a predictor of synaptic change in Alzheimer's disease. *Am J Pathol* **1999**, *155*, 853-862.

(13)   Bader, R.; Bamford, R.; Zurdo, J.; Luisi, B. F.; Dobson, C. M. Probing the mechanism of amyloidogenesis through a tandem repeat of the PI3-SH3 domain suggests a generic model for protein aggregation and fibril formation. *J. Mol. Biol.* **2006**, *356*, 189-208.

(14)   Cerda-Costa, N.; Esteras-Chopo, A.; Aviles, F. X.; Serrano, L.; Villegas, V. Early Kinetics of Amyloid Fibril Formation Reveals Conformational Reorganisation of Initial Aggregates. *J. Mol. Biol.* **2007**, *366*, 1351-1363.

(15)   Pellarin, R.; Caflisch, A. Interpreting the Aggregation Kinetics of Amyloid Peptides. *J. Mol. Biol.* **2006**, *360*, 882-892.

(16)   Petty, S. A.; Decatur, S. M. Intersheet rearrangement of polypeptides during nucleation of b-sheet aggregates. *Proc. Natl. Acad. Sci. USA* **2005**, *102*, 14272-14277.

(17)   Plakoutsi, G.; Bemporad, F.; Calamai, M.; Taddei, N.; Dobson, C. M.; Chiti, F. Evidence for a Mechanism of Amyloid Formation Involving Molecular Reorganisation within Native-like Precursor Aggregates. *J. Mol. Biol.* **2005**, *351*, 910-922.

(18)   Cohen, S. I.; Linse, S.; Luheshi, L. M.; Hellstrand, E.; White, D. A.; Rajah, L.; Otzen, D. E.; Vendruscolo, M.; Dobson, C. M.; Knowles, T. P. Proliferation of amyloid-beta42 aggregates occurs through a secondary nucleation mechanism. *Proc. Natl. Acad. Sci. USA* **2013**, *110*, 9758-9763.

(19)   Cohen, S. I.; Vendruscolo, M.; Welland, M. E.; Dobson, C. M.; Terentjev, E. M.; Knowles, T. P. Nucleated polymerization with secondary pathways. I. Time evolution of the principal moments. *J. Chem. Phys.* **2011**, *135*, 065105.

(20)   Knowles, T. P.; Waudby, C. A.; Devlin, G. L.; Cohen, S. I.; Aguzzi, A.; Vendruscolo, M.; Terentjev, E. M.; Welland, M. E.; Dobson, C. M. An analytical solution to the kinetics of breakable filament assembly. *Science* **2009**, *326*, 1533-1537.

(21)   Ruzafa, D.; Morel, B.; Varela, L.; Azuaga, A. I.; Conejero-Lara, F. Characterization of Oligomers of Heterogeneous Size as Precursors of Amyloid Fibril Nucleation of an SH3 Domain: An Experimental Kinetics Study. *PLoS ONE* **2012**, *7*, e49690.

(22)   DeToma, A. S.; Salamekh, S.; Ramamoorthy, A.; Lim, M. H. Misfolded proteins in Alzheimer's disease and type II diabetes. *Chem. Soc. Rev.* **2012**, *41*, 608-621.

(23)   Brender, J. R.; Salamekh, S.; Ramamoorthy, A. Membrane Disruption and Early Events in the Aggregation of the Diabetes Related Peptide IAPP from a Molecular Perspective. *Acc. Chem. Res.* **2011**, *45*, 454-462.

(24)   Nielsen, L.; Khurana, R.; Coats, A.; Frokjaer, S.; Brange, J.; Vyas, S.; Uversky, V. N.; Fink, A. L. Effect of Environmental Factors on the Kinetics of Insulin Fibril Formation: Elucidation of the Molecular Mechanism. *Biochemistry* **2001**, *40*, 6036-6046.

(25)   Raman, B.; Chatani, E.; Kihara, M.; Ban, T.; Sakai, M.; Hasegawa, K.; Naiki, H.; Rao, C. M.; Goto, Y. Critical Balance of Electrostatic and Hydrophobic Interactions Is Required for β2-Microglobulin Amyloid Fibril Growth and Stability. *Biochemistry* **2005**, *44*, 1288-1299.

(26)   Munishkina, L. A.; Henriques, J.; Uversky, V. N.; Fink, A. L. Role of Protein-Water Interactions and Electrostatics in α-Synuclein Fibril Formation. *Biochemistry* **2004**, *43*, 3289-3300.

(27)   Pedersen, J. S.; Christensen, G.; Otzen, D. E. Modulation of S6 Fibrillation by Unfolding Rates and Gatekeeper Residues. *J. Mol. Biol.* **2004**, *341*, 575-588.

(28)   Vivekanandan, S.; Brender, J. R.; Lee, S. Y.; Ramamoorthy, A. A partially folded structure of amyloid-beta(1-40) in an aqueous environment. *Biochem. Biophys. Res. Commun.* **2011**, *411*, 312-316.

(29)   Baldwin, R. L. How Hofmeister ion interactions affect protein stability. *Biophys. J.* **1996**, *71*, 2056-2063.

(30)   Hofmeister, F. Zur lehre der Wirkung der Salze. Zweite Mittheilung. *Arch. Exp. Pathol. Pharmakol.* **1888**, *24*, 247-260.

(31)   Brender, J. R.; Hartman, K.; Nanga, R. P. R.; Popovych, N.; de la Salud Bea, R.; Vivekanandan, S.; Marsh, E. N. G.; Ramamoorthy, A. Role of Zinc in Human Islet Amyloid Polypeptide Aggregation. *J. Am. Chem. Soc.* **2010**, *132*, 8973-8983.

(32)   Salamekh, S.; Brender, J. R.; Hyung, S.-J.; Nanga, R. P. R.; Vivekanandan, S.; Ruotolo, B. T.; Ramamoorthy, A. A Two-Site Mechanism for the Inhibition of IAPP Amyloidogenesis by Zinc. *J. Mol. Biol.* **2011**, *410*, 294-306.

(33)   Brender, J. R.; Krishnamoorthy, J.; Messina, G. M. L.; Deb, A.; Vivekanandan, S.; La Rosa, C.; Penner-Hahn, J. E.; Ramamoorthy, A. Zinc stabilization of prefibrillar oligomers of human islet amyloid polypeptide. *Chem. Comm.* **2013**, *49*, 3339-3341.

(34)   Gjerde, D. T.; Schmuckler, G.; Fritz, J. S. Anion Chromatography with low-conductivity eluents. II. *J. Chromatogr. A* **1980**, *187*, 35-45.

(35)   Collins, K.; Washabaugh, M. The Hofmeister effect and the behaviour of water at interfaces. *Quart. Rev. Biophys.* **1985**, *18*, 323-422.

(36)   Morel, B.; Casares, S.; Conejero-Lara, F. A single mutation induces amyloid aggregation in the alpha-spectrin SH3 domain: analysis of the early stages of fibril formation. *J. Mol. Biol.* **2006**, *356*, 453-468.

(37)   Varela, L.; Morel, B.; Azuaga, A. I.; Conejero-Lara, F. The amyloidogenic mutation N47A in the alpha-spectrin SH3 domain does not enhance aggregation by destabilizing the native state but by increasing the rate of the nucleation event. *FEBS Letters* **2009**, *583*, 801-806.

(38)   Morel, B.; Varela, L.; Azuaga, A. I.; Conejero-Lara, F. Environmental Conditions Affect the Kinetics of Nucleation of Amyloid Fibrils and Determine Their Morphology. *Biophys. J.* **2010**, *99*, 3801-3810.

(39)   Morel, B.; Varela, L.; Conejero-Lara, F. The Thermodynamic Stability of Amyloid Fibrils Studied by Differential Scanning Calorimetry. *J. Phys. Chem. B* **2010**, *114*, 4010-4019.

(40)   Sadqi, M.; Casares, S.; Abril, M. A.; Lopez-Mayorga, O.; Conejero-Lara, F.; Freire, E. The native state conformational ensemble of the SH3 domain from alpha-spectrin. *Biochemistry* **1999**, *38*, 8899-8906.

(41)   Casares, S.; Sadqi, M.; Lopez-Mayorga, O.; Conejero-Lara, F.; van Nuland, N. A. Detection and characterization of partially unfolded oligomers of the SH3 domain of alpha-spectrin. *Biophys. J.* **2004**, *86*, 2403-2413.

(42)   Lomakin, A.; Teplow, D. B.; Benedek, G. B. Quasielastic light scattering for protein assembly studies. *Methods Mol. Biol.* **2005**, *299*, 153-174.

(43)   Ahmad, A.; Uversky, V. N.; Hong, D.; Fink, A. L. Early events in the fibrillation of monomeric insulin. *J. Biol. Chem.* **2005**, *280*, 42669-42675.

(44)   Bitan, G.; Kirkitadze, M. D.; Lomakin, A.; Vollers, S. S.; Benedek, G. B.; Teplow, D. B. Amyloid beta -protein (Abeta) assembly: Abeta 40 and Abeta 42 oligomerize through distinct pathways. *Proc. Natl. Acad. Sci. USA* **2003**, *100*, 330-335.

(45)   Lomakin, A.; Chung, D. S.; Benedek, G. B.; Kirschner, D. A.; Teplow, D. B. On the nucleation and growth of amyloid beta -protein fibrils: Detection of nuclei and quantitation of rate constants. *PNAS* **1996**, *93*, 1125-1129.

(46)   Paredes, J. M.; Casares, S.; Ruedas-Rama, M. J.; Fernandez, E.; Castello, F.; Varela, L.; Orte, A. Early Amyloidogenic Oligomerization Studied through Fluorescence Lifetime Correlation Spectroscopy. *Int. J. Mol. Sci.* **2012**, *13*, 9400-9418.

(47)   Orte, A.; Birkett, N. R.; Clarke, R. W.; Devlin, G. L.; Dobson, C. M.; Klenerman, D. Direct characterization of amyloidogenic oligomers by single-molecule fluorescence. *Proc. Natl. Acad. Sci. USA* **2008**, *105*, 14424-14429.

(48)   Krobath, H.; Estacio, S. G.; Faisca, P. F.; Shakhnovich, E. I. Identification of a conserved aggregation-prone intermediate state in the folding pathways of Spc-SH3 amyloidogenic variants. *J. Mol. Biol.* **2012**, *422*, 705-722.

(49)   Korzhnev, D. M.; Salvatella, X.; Vendruscolo, M.; Di Nardo, A. A.; Davidson, A. R.; Dobson, C. M.; Kay, L. E. Low-populated folding intermediates of Fyn SH3 characterized by relaxation dispersion NMR. *Nature* **2004**, *430*, 586-590.

(50)   Neudecker, P.; Robustelli, P.; Cavalli, A.; Walsh, P.; Lundstrom, P.; Zarrine-Afsar, A.; Sharpe, S.; Vendruscolo, M.; Kay, L. E. Structure of an intermediate state in protein folding and aggregation. *Science* **2012**, *336*, 362-366.

(51)   Broering, J. M.; Bommarius, A. S. Evaluation of Hofmeister effects on the kinetic stability of proteins. *J. Phys. Chem. B* **2005**, *109*, 20612-20619.

(52)   Hirano, A.; Hamada, H.; Okubo, T.; Noguchi, T.; Higashibata, H.; Shiraki, K. Correlation Between Thermal Aggregation and Stability of Lysozyme with Salts Described by Molar

Surface Tension Increment: An Exceptional Propensity of Ammonium Salts as Aggregation Suppressor. *The Protein J.* **2007**, *26*, 423-433.

(53)   Yang, Z.; Liu, X.-J.; Chen, C.; Halling, P. J. Hofmeister effects on activity and stability of alkaline phosphatase. *Biochim. Biophys. Acta - Proteins and Proteomics* **2010**, *1804*, 821-828.

(54)   Omta, A. W.; Kropman, M. F.; Woutersen, S.; Bakker, H. J. Negligible Effect of Ions on the Hydrogen-Bond Structure in Liquid Water. *Science* **2003**, *301*, 347-349.

(55)   Batchelor, J. D.; Olteanu, A.; Tripathy, A.; Pielak, G. J. Impact of Protein Denaturants and Stabilizers on Water Structure. *J. Am. Chem. Soc.* **2004**, *126*, 1958-1961.

(56)   Gibb, C. L. D.; Gibb, B. C. Anion Binding to Hydrophobic Concavity Is Central to the Salting-in Effects of Hofmeister Chaotropes. *J. Am. Chem. Soc.* **2011**, *133*, 7344-7347.

(57)   Zhang, Y.; Furyk, S.; Bergbreiter, D. E.; Cremer, P. S. Specific ion effects on the water solubility of macromolecules: PNIPAM and the Hofmeister series. *J. Am. Chem. Soc.* **2005**, *127*, 14505-14510.

(58)   Davies, C. W.: *Ion Association*; Butterworth & Co: London, England, 1962.

(59)   Goto, Y.; Takahashi, N.; Fink, A. L. Mechanism of acid-induced folding of proteins. *Biochemistry* **1990**, *29*, 3480-3488.

(60)   Tanford, C. Protein denaturation. C. Theoretical models for the mechanism of denaturation. *Adv. Prot. Chem.* **1970**, *24*, 1-95.

(61)   Campioni, S.; Mannini, B.; Lopez-Alonso, J. P.; Shalova, I. N.; Penco, A.; Mulvihill, E.; Laurents, D. V.; Relini, A.; Chiti, F. Salt Anions Promote the Conversion of HypF-N into Amyloid-Like Oligomers and Modulate the Structure of the Oligomers and the Monomeric Precursor State. *J. Mol. Biol.* **2012**, *424*, 132-149.

(62)   Jain, S.; Udgaonkar, J. B. Salt-induced modulation of the pathway of amyloid fibril formation by the mouse prion protein. *Biochemistry* **2010**, *49*, 7615-7624.

(63)   Pedersen, J. S.; Flink, J. M.; Dikov, D.; Otzen, D. E. Sulfates Dramatically Stabilize a Salt-Dependent Type of Glucagon Fibrils. *Biophys. J.* **2006**, *90*, 4181-4194.

SUPPLEMENTARY MATERIALS
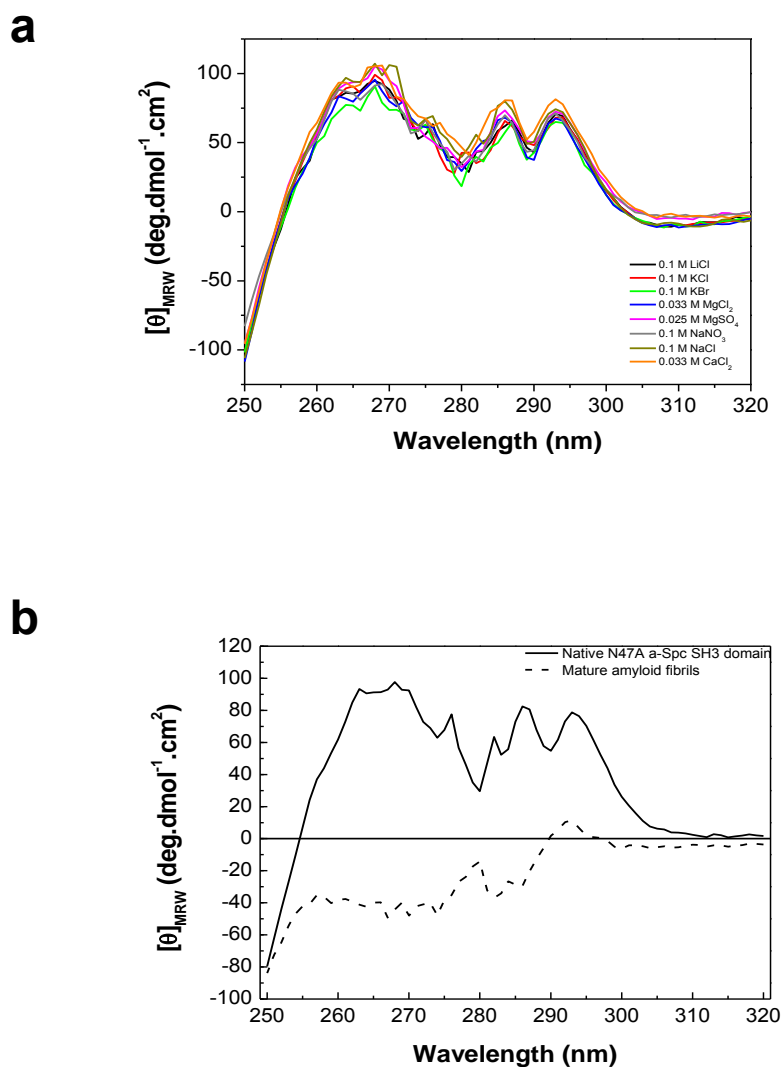
Figure S1. Near UV CD spectra at 25ºC in the presence of different salt ions (a). Near UV CD spectra of N47A Spc SH3 in the native state (continuous line) and amyloid fibrillar state (dashed line) (b). *Spectra were recorded at 25ºC at the same protein concentration in 0.1 M Glycine, 0.1 M NaCl, pH 3.2.*
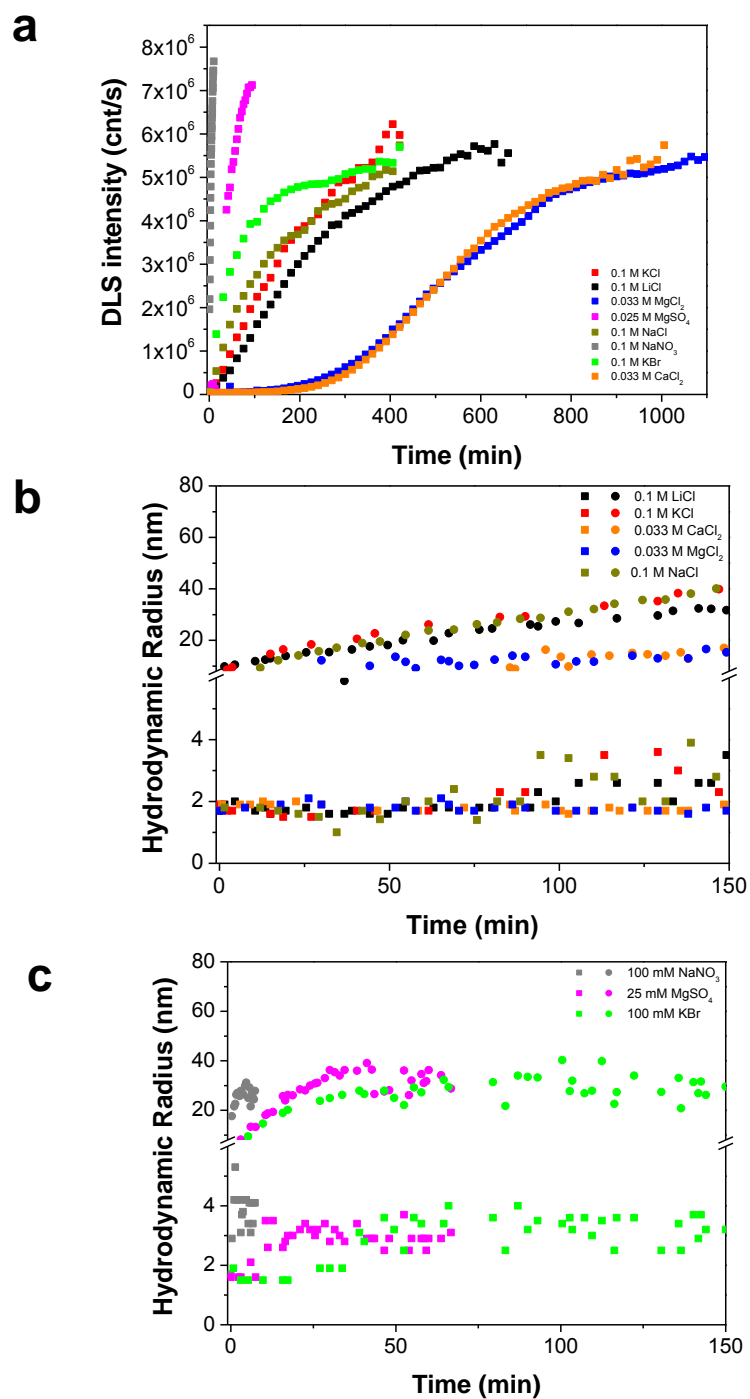
Figure S2. Time course of aggregation of N47A in the presence of different salt ions monitored by DLS. *Time dependence of the scattering intensity (a). Hydrodynamic radii of the two smallest particles visible in the size distributions as a function of the time of incubation (b and c).*
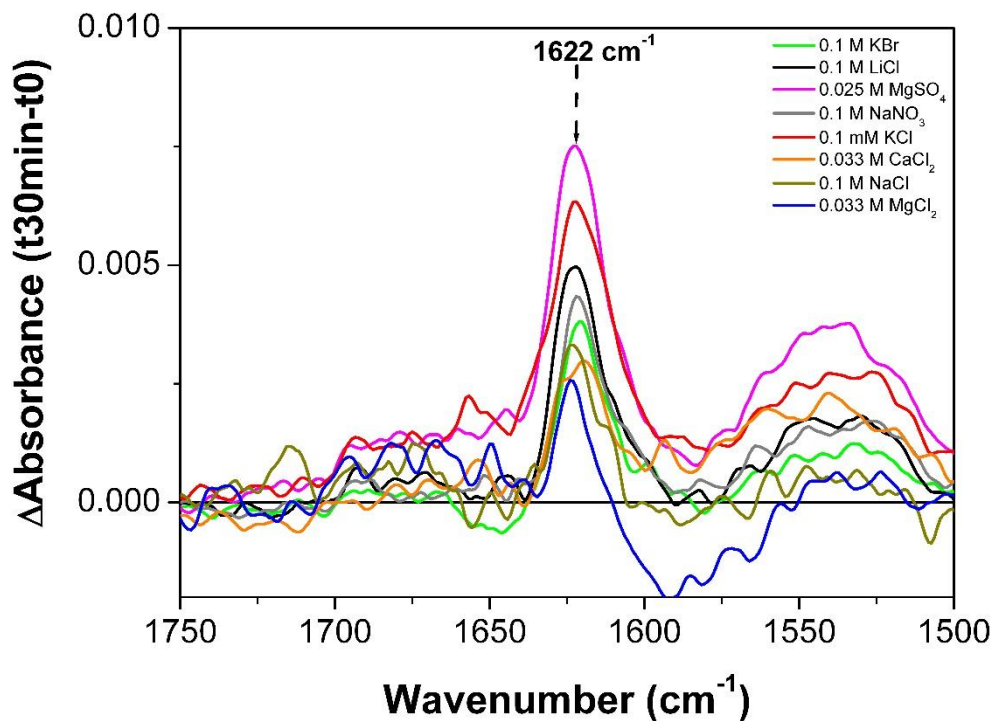
Figure S3. Infrared spectra of N47A Spc SH3 domain*. Spectra of the difference between the FTIR performed at the beginning of the incubation and the spectra obtained after 30 minutes of incubation in the presence of different salt ions.*
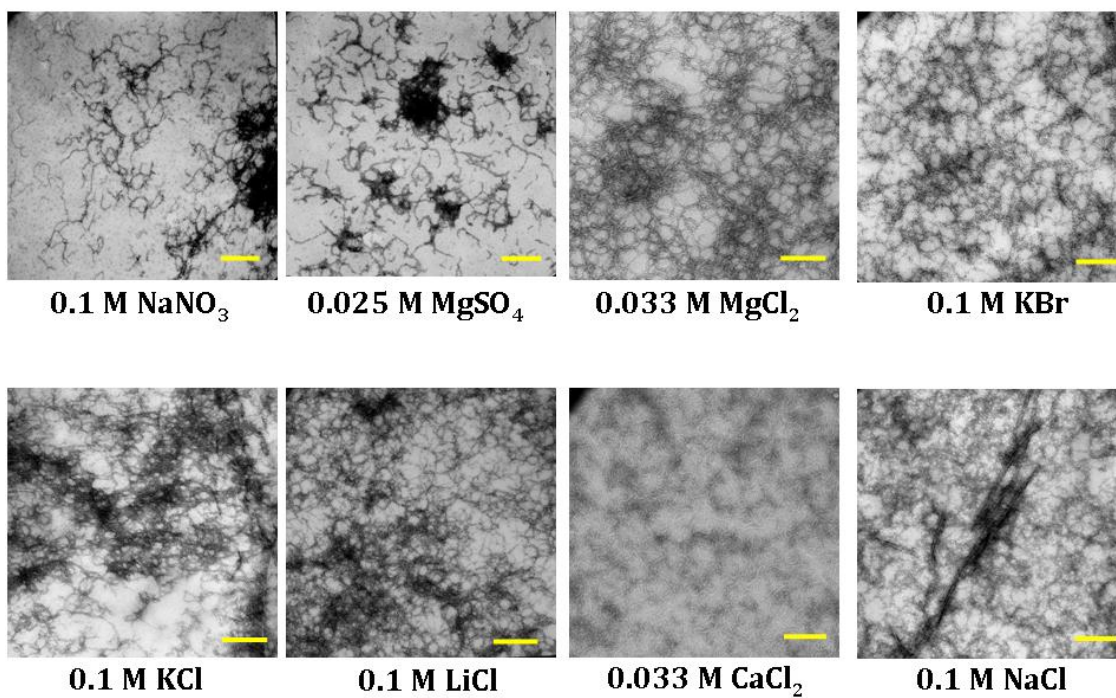
Figure S4. Morphology of amyloid fibrils of N47A α-Spc SH3 domain in the presence of different salts. *The samples were incubated for 10 days at 37°C. The segments represent 200 nm.*

Chapter 4

MAPPING THE STRUCTURE OF AMYLOID NUCLEATION PRECURSORS BY PROTEIN ENGINEERING KINETIC ANALYSIS

ABSTRACT

Understanding the early molecular mechanisms governing amyloid aggregation is crucial to learn how to prevent them. Here, we used a site-directed mutagenesis approach to explore the molecular mechanism of nucleation of amyloid structure in the N47A Spc-SH3 domain. The changes in the native state stability produced by a series of mutations on each structural element of the domain were uncorrelated with those produced on the aggregation rates, although the overall aggregation mechanism was not altered. Analysis of the thioflavin T initial rates based on a simple kinetic model allowed us extracting thermodynamic magnitudes of the precursor states of nucleation and mapping the regions of the protein participating in the structure of the amyloidogenic precursors. This structure differs from that of the folding transition state of the SH3 domains, strongly suggesting that the regions of the conformational landscape leading to amyloid formation are divergent from those leading to the native fold.

INTRODUCTION

Amyloid fibril formation is a multistep process involving a series of intermediate aggregated states [1]. In recent years a large body of evidence has identified soluble oligomers as the main causative agents of cell toxicity [2-7]. It is therefore of great interest to understand the nature of these small oligomers and the reasons of their genesis. However, the lack of a deep understanding of the molecular mechanisms of the early aggregation processes and the factors triggering them comes from their complicated nature, the difficulty in obtaining homogeneous and reproducible samples and data for this type of aggregates and, especially, the scarcity of theoretical formalisms to interpret quantitatively the experimental data. Recently, this situation is being considerably alleviated by the progressive emergence of increasingly comprehensive and quantitative formalisms, which have successfully explained the early aggregation kinetics of a number of proteins in a variety of nucleation regimes [8-10]. Nevertheless, most proteins related to diseases have been shown to be very difficult to handle because of their intrinsic properties and high aggregation propensity, making it extremely difficult to obtain reproducible quantitative information about the aggregation kinetics. For

this reason, the use of well characterized model proteins, even though unrelated to disease, is a potent approach to investigate the mechanisms of formation of amyloid fibrils thanks to the extensive information available about their folding mechanism and conformational stability.

The Spc-SH3 domain is an archetypical two-state folding protein, which has been during decades subject to extensive studies about its folding mechanism, conformational stability and aggregation [11-18]. The folding transition state of this domain is organized around the distal β-hairpin and the subsequent 3_{10}-helix, and the formation of the tight distal β-turn has been described as a compulsory step in the folding pathway [15]. Destabilization of this turn by the N47A mutation promotes the formation of curly amyloid fibrils under mild acid conditions favoured by the presence of salts [19,20]. The amyloidogenic character of this mutation is mainly due to an increase in the rate of formation of amyloid nuclei [21] and recent computational studies have proposed that it favours the population of a partially unfolded intermediate, which may be crucial in triggering the aggregation cascade [14]. It is of great interest therefore to characterize the molecular and physicochemical details of the transition by which a soluble and folded protein converts into amyloid nuclei that further assemble into fibrillar aggregates.

Recently, we have shown that experimental kinetic analysis can report about the kinetic and thermodynamic properties of the precursors of amyloid nucleation [22]. We developed a simple kinetic model that quantitatively accounted for the initial rates of aggregation of the Spc-SH3 domain under conditions of rapid formation of amyloid nuclei. The model perfectly captured the variability of experimental aggregation rates and apparent kinetic orders, and allowed us extracting meaningful kinetic and thermodynamic parameters characterizing the different nucleation steps and more recently we identified the specific role of ions in these nucleation stages [23]. The availability of thermodynamic magnitudes characterizing the critical steps of the nucleation process allows a further exploration of its mechanism by analysing the response of these magnitudes to changes in experimental conditions or to specific mutations. This latter approach has been widely used in investigating the molecular mechanisms of protein folding for more than two decades [24-30]. Mutational studies have also proved to be extremely valuable in the structural and stability characterization of amyloid fibrils and the

process of their assembly [31-35]. Such results indicate that mutational studies have the potential to provide residue-specific structural information on the process of amyloid formation.

Consequently, in this study we have employed a site-directed mutagenesis approach to analyse deeply the molecular mechanisms of amyloid nucleation of the Spc-SH3 domain. Using the single mutant N47A Spc-SH3 as reference, we designed a set of second mutations on selected positions of the polypeptide chain to produce energy changes affecting the different structural elements of the protein. A range of biophysical techniques was combined to study the effect of the mutations on the structure and stability of the native protein, and on the kinetics of amyloid aggregation. Then, initial aggregation rates, measured for all the double mutants by *in situ* ThT fluorescence at different protein concentrations, were analyzed using our recently developed nucleation model [22].

With this approach we evaluated the changes produced by each mutation in the thermodynamic magnitudes characterizing the amyloidogenic intermediate and its oligomerization, as well as in the rate constants of the conformational change to form the amyloid nuclei. The results provided a very detailed description of the molecular events leading to the formation of amyloid nuclei.

EXPERIMENTAL SECTION

Protein samples preparation

The DNA of all the double mutants was obtained by a QuikChange® Site-Directed Mutagenesis kit (Agilent Technologies Inc.) using primers designed to insert the desired mutations in the DNA of the N47A Spc-SH3 mutant, which was used as template. The N47A variant and the double mutants of the Spc-SH3 domain were expressed and purified as described previously [16]. Protein aliquots were dialyzed extensively against pure water and lyophilized for storage at -20ºC. For aggregation experiments the lyophilized protein was dissolved in 0.1 M glycine, 0.1 M NaCl pH 3.2 (unless otherwise stated) at 4ºC, centrifuged for 2 min and filtered through a 0.2 µm filter. The protein concentration was determined by measurement of absorbance at 280 nm using an extinction coefficient of 15784 $M^{-1}.cm^{-1}$.

Thermodynamic stability of the native state

Differential scanning calorimetry (DSC) experiments were carried out with a VP-DSC capillary-cell microcalorimeter from MicroCal (Northampton, MA, USA). Temperature scans were performed between 5ºC and 100ºC at a scan rate of 90°C.h^{-1}. The reversibility of the thermal unfolding was always checked in a second consecutive scan of the same sample. Instrumental baselines were subtracted to the experimental thermograms of the samples and the time response of the calorimeter was then corrected. The partial molar heat capacity curves (C_p) were calculated from the DSC data and analyzed using Origin 7.0 (OriginLab, Northampton, MA) according to the two-state unfolding model. This analysis allowed the determination of the thermodynamic magnitudes of unfolding of each protein variants.

Effect of the mutations on the secondary structure of Spc-SH3

To monitor possible changes in the secondary structure, circular dichroism (CD) experiments were performed on a Jasco J-715 (Tokyo, Japan) spectropolarimeter equipped with a thermostated cell holder. Far UV CD measurements (260-200 nm) were done at a protein concentration of 0.2 mg.mL^{-1} in a 1 mm path length cuvette using a bandwidth of 1 nm, a scan rate of 100 nm.min^{-1}, a response time of 1 s, and an average of 8 scans.

Characterization of particle size

To analyze the molecular size of particles and aggregates during the kinetic aggregation experiments, DLS measurements were performed with a DynaPro MS-X instrument (Wyatt Technology Corporation, Santa Barbara, CA, USA) using a thermostatized 30 µl quartz cuvette. The protein solutions and the buffer were centrifuged and filtered through 0.02 µm Anotop 10 filters (Whatman plc, Brentford, Middlesex, UK) immediately before measurements. Sets of DLS data at constant temperature (37ºC) were acquired every 45 s until saturation of the signal. The laser power was adjusted to avoid early saturation.

Dynamics V6 software (Wyatt Technology Corporation, Santa Barbara, CA, USA) was used in data collection and processing. The experimental autocorrelation curves data were analyzed to obtain the particle size distributions using the regularization fit as implemented in Dynamics V6 software.

Amyloid fibril morphology

The formation of oligomers and amyloid fibrils by each mutant was monitored by transmission electron microscopy (TEM). Protein samples were diluted 10-fold with aggregation buffer (0.1 M glycine, 0.1 M NaCl pH 3.2) and a 15 µl aliquot was placed on a formvar coated copper grid and left for 4 min. The grid was then washed twice with distilled water and stained with 1 % (w/v) uranyl acetate for 1 min. The dried samples were then observed in a Zeiss LEO 906E electron microscope (Zeiss, Oberkochen, Germany), operating at accelerating voltage of 80 kV and observed at a magnification factor between 60000 and 100000 depending on the nature of the aggregates. Particle diameters were determined using ANALYSIS v3.2 LS image analysis software (Olympus Soft Imaging Solutions, GmbH, Germany).

Initial rates of amyloid aggregates formation determined by ThT fluorescence kinetics

Kinetics of amyloid aggregation was monitored in continuous mode by ThT fluorescence using a Cary Eclipse spectrofluorimeter (Varian Inc.). A 500 µM stock solution of ThT was freshly prepared in 0.1 M glycine, 0.1 M NaCl pH 3.2. A 98 µl of protein sample in the aggregation conditions was mixed with 2 µl of the ThT stock solution. Fluorescence emission intensity at 480 nm was measured continuously at 37ºC during the aggregation process in a 3 mm path-length cuvette. Initial rates of growth of amyloid structure were calculated by an operational extrapolation procedure as detailed previously [22,23] and in Supplementary Information (Text S1).

Kinetic model for quantitative analysis of the initial nucleation rates

To understand the observed kinetic effects in terms of a plausible mechanism, we proposed recently a simple model to account quantitatively for the initial rates of amyloid fibril nucleation [22]. This model is based upon previous polymerization models reported in the literature [36-38], in which partial unfolding and/or linear polymerization processes previous to the rate-limiting steps of aggregation were assumed to be pre-equilibrated. The model is summarized in Scheme 1.

Scheme 1
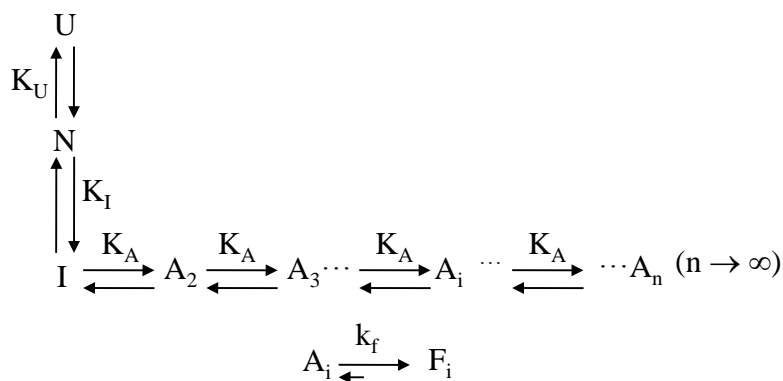
$$U$$
$$K_U \updownarrow$$
$$N$$
$$\updownarrow K_I$$
$$I \underset{\longleftarrow}{\overset{K_A}{\longrightarrow}} A_2 \underset{\longleftarrow}{\overset{K_A}{\longrightarrow}} A_3 \cdots \underset{\longleftarrow}{\overset{K_A}{\longrightarrow}} A_i \cdots \underset{\longleftarrow}{\overset{K_A}{\longrightarrow}} \cdots A_n \ (n \to \infty)$$

$$A_i \underset{\longleftarrow}{\overset{k_f}{\longrightarrow}} F_i$$

In this model, N and U are respectively the native and the unfolded states of the protein. The state I is a monomeric intermediate prone to intermolecular association in equilibrium with the folded and unfolded states. The species A_i are oligomeric aggregates formed by reversible association of intermediate molecules.

The model assumes an unrestricted oligomerization pre-equilibrium of a partially unfolded state preceding the rate limiting step of conformational conversion to amyloid nuclei. The oligomer distribution is only determined by the thermodynamic parameters of the conformational-oligomerization pre-equilibrium and by the concentration of the self-associating species. It is assumed that only the amyloid nuclei F_i are detected by thioflavin T fluorescence. The theoretical equations of the model depend on four independent fitting parameters: K_I (the equilibrium constant between the native and the intermediate states), K_A (the equilibrium constant of oligomerization), K_U (the equilibrium constant between the

native and the fully unfolded states) and k_F (the first order rate constant of conformational conversion of dynamic oligomer into amyloid structure). To reduce the number of parameters to only three, the values of the equilibrium constant between the native and the fully unfolded states (K_U) were obtained independently by the DSC experiments and fixed in the analyses.

The initial rate of aggregation is given by:

$$r_0 = \frac{k_F(Bx_N)^2(2-Bx_N)}{K_A(1-Bx_N)^2} \qquad (1)$$

Where the fraction of native protein, x_N, can be obtained for each initial protein concentration, C_0, by solving:

$$1 = Ax_N + \frac{K_I x_N}{(1-Bx_N)^2} \qquad (2)$$

Where $A = 1 + K_U$, and $B = K_I \cdot K_A \cdot C_0$.

RESULTS

Description of the mutations

Using the N47A Spc-SH3 domain mutant as a reference, a series of second mutations were designed with the aim of producing energy changes at every secondary structural element of the protein (Figure 1a). Mutations to alanine were normally selected except for a few specific cases, in which the mutation to alanine did not produce significant stability change.

The mutations could be classified into three groups: Four mutations were made to probe local stability changes at the loops and turns: R21D, K27A, N38A and D48G. A second group of mutations were designed to probe exposed interactions at secondary structure elements: L10A, T32A, K43A and A56G and finally three mutations affected directly the hydrophobic core of the protein: V46A, V53A and V58A. Intramolecular contacts affected by the mutated residues are detailed in Figure 1b.
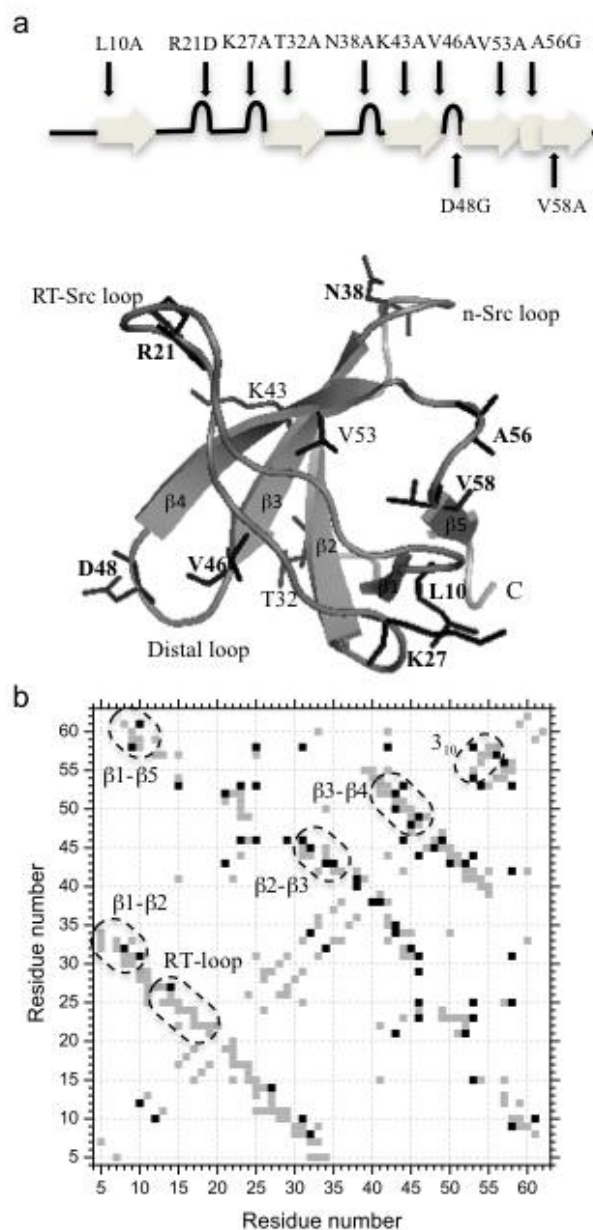
Figure 1. ***Schematic and structural representations showing the locations of the 11 mutations and their intramolecular contacts***. *(a) Schematic representation of the polypeptide chain showing the residues mutated (upper panel) and ribbon diagram of the N47A Spc-SH3 domain structure (PDB code 1QKX) featuring the structural characteristics of the SH3 domain and the mutated residues. Backbone and side chains of the mutated residues are shown in sticks. This graph was generated using Pymol [39]. (b) Intramolecular contact map for the N47A Spc-SH3 structure. Dark dots mark inter-residue contacts affected by the side chain mutations. The dashed lines delimit the secondary structure elements.*

Structure and thermodynamic stabilities of the double mutants

Far-UV CD experiments of the variants at 25°C were carried out to check the conservation of the secondary structure. For most mutants the resulting spectra are very similar to that of the native Spc-SH3 domain except in the case of N47A-K43A, N47A-V53A and N47A-V58A, which exhibit significant differences in the spectra (Figure 2a). Nevertheless, the spectra of these mutants are not characteristic of a fully unfolded Spc-SH3 domain and indicate residual structure, suggesting that they are partially unfolded. The thermodynamic changes in the stability of the protein produced by the mutations were investigated using DSC.
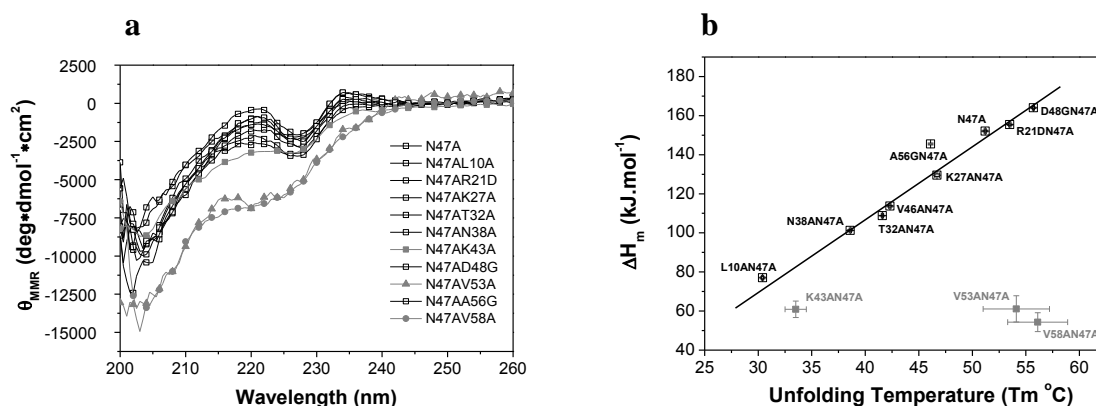
Figure 2. *Structural and thermodynamic stability of the mutants studied by far-UV CD and DSC. (a) Far-UV CD spectra of N47A and the double mutants of the Spc-SH3 domain. Experiments were carried out at 25°C in the presence of 0.1 M glycine, 0.1 M NaCl pH 3.2 at a protein concentration of 0.3 mg/mL. Double mutants showing the largest differences in secondary structure are indicated in grey closed squares (N47A-K43A), grey closed triangles (N47A-V53A) and grey closed circles (N47A-V58A). (b) Enthalpy change of unfolding (ΔH$_m$) versus the unfolding temperature (T$_m$) for all the mutants obtained from the fittings of the DSC thermograms using the two-state model. The line corresponds to the linear regression (r = 0.975) of the data indicated in black. The values obtained for the mutants showing different secondary structure are shown in grey using the same symbol as in (a).*

The experiments were made under the same conditions of the aggregation experiments (i.e. 0.1 M Gly, 0.1 M NaCl pH 3.2) but at low protein concentration (0.2-0.6 mg mL^{-1}) to avoid aggregation during the thermal unfolding (Supplementary information Figure S2). Under

these conditions, the thermal unfolding of all mutants was highly reversible as we observed in a second heating scan (not shown). The thermograms obtained for all mutants could be well fitted using the two-state unfolding model, from which the thermodynamic parameters of the unfolding process were obtained (Table S2). Mutations L10A, K27A, T32A, N38A, V46A and A56G produced destabilizing effects, whereas the R21D and D48G mutations stabilized the protein, as previously described [40]. Noteworthy, mutations K43A, V53A and V58A resulted in very broad unfolding transitions with low unfolding enthalpies, in agreement with a partially unfolded structure of the corresponding mutants.

A plot of the unfolding enthalpies (ΔH_m) versus the unfolding temperatures (T_m), gave a single linear dependence (Figure 2b) for all the mutants that showed cooperative unfolding, excluding the data obtained for N47A-K43A, N47A-V53A and N47A-V58A. This linearity indicates that the changes in enthalpy of unfolding are mainly due, within the experimental error, to its dependence with temperature due to the heat capacity change of unfolding, $\Delta C_p = d\Delta H/dT$, which appears to be common to these mutants, $C_p = 3.67 \pm 0.15$ kJ K^{-1} mol^{-1}. This value is fully consistent with those previously published for the Spc-SH3 domain [17,21], confirming that these mutants conserve the native structure of the N47A Spc-SH3 domain. The fact that the three less structured mutants deviate from this linear regression confirms their partially-unfolded conformation.

Aggregation kinetics of the double mutants

To ascertain how the different mutations affect the early aggregation kinetics of the N47A Spc-SH3 domain, several observables were monitored at 37°C under identical aggregation conditions, i.e., a protein concentration of around 1.2 mM in 0.1 M glycine buffer, 0.1 M NaCl pH 3.2.

The growth of aggregate particles was explored by measuring the scattering intensity by DLS (Supplementary information Figure S3). Surprisingly, the mutants N47A-L10A and N47A-D48G did not show any significant growth in scattering intensity indicating the absence of aggregate particles during the first 250 min of incubation at 37°C. The rest of the mutants

showed considerable differences in the rates of growth of scattering intensity.

A detailed analysis of the DLS data allowed us following the distribution of particles sizes during the early stages of the aggregation process (Supplementary information Figure S4). Although, the speed of changes in the size distributions was markedly different depending on the mutant, the series of events appear globally similar for many of them. In most mutants and similarly to the N47A reference, at the start of the incubation there are only particles with an apparent hydrodynamic radius (R_h) of around 1.6 nm, which is consistent with the value reported for the native Spc-SH3 monomer [11,19]. As aggregation progressed, the peak corresponding to the native R_h shifts up to values ranging between 2.5 nm and 5 nm, suggesting the formation of small oligomers, corresponding to stable amyloid nuclei, which start to dominate the distribution over the native particles. This process is faster for some mutants than others indicating different rates of nucleation.

In agreement with their lack of scattering intensity increases, the mutants N47A-L10A and N47A-D48G presented exclusively particles with an apparent R_h of 2 nm and 1.6 nm respectively during the whole course of the experiment. The R_h of the N47A-L10A mutant at 37ºC is between that of the native monomer and the 2.3 nm value predicted for a fully unfolded monomer [41]. This is consistent with the melting temperature of 30.3ºC measured by DSC for this mutant. In addition, the partially folded mutants (N47A-K43A, N47A-V53A, N47A-V58A) also showed slightly expanded radii right from the beginning of the experiment. In fact, the N47A-K43A variant is present as an oligomer right at the beginning of the incubation at 37°C.

The growth of amyloid fibrils was also observed by the presence of a second peak in the R_h distributions, which increases its hydrodynamic radius progressively. Interestingly, the average rates of fibril elongation, estimated from the slopes of the increase in apparent R_h, were not correlated with the speed of oligomerization described above. In fact, the fastest growing fibrils were observed for the single mutant N47A and the double mutant N47A-A56G. On the opposite side, fibrils elongated more slowly for mutants oligomerizing early and extensively, such as N47A-K43A and N47A-V53A. These observations suggest that heterogeneous oligomeric nuclei can manifest different capacities to seed an efficient fibril elongation [22]. In addition, rapid and extensive formation of oligomeric nuclei and

protofibrillar species for some mutants could deprive the solution from soluble monomers to drive fibril elongation.

The kinetics of formation of amyloid structure at 37°C was also observed by thioflavin T (ThT) fluorescence (Figure 3). Thioflavin T increases its fluorescence upon binding to the ordered amyloid structure. The signal is considered proportional to the total mass of protein in the amyloid aggregates, whereas it is relatively independent of the aggregate particle size [42]. Noteworthy, binding of ThT clearly precedes the light scattering increase, as observed by comparison of the aggregation kinetics obtained by ThT fluorescence (Figure 3) and scattering intensity (Figure S3). This indicates that accumulation of small amyloid particles precedes the formation of large fibrilar aggregates.

All variants except N47A-L10A and N47A-D48G rapidly formed amyloid structure to different extents under this experimental condition. Except for the two non-aggregating mutants, the absolute absence of lag phase in the ThT experiments confirms a rapid formation of amyloid nuclei. Once again, the rate of growth of ThT fluorescence varies strongly between the different mutants. Noteworthy, the initial slopes of the kinetics do not always correspond with higher amplitudes in the ThT fluorescence at late times. This supports that a faster nucleation does not necessarily correlate with a more extensive fibrillation, due to the fact that some oligomeric nuclei may be less competent for an efficient elongation of amyloid fibrils.

More importantly, the initial rates of amyloid nucleation are also uncorrelated with the stability of the native state for the different mutants. For instance, the least stable mutant N47A-L10A did not fibrillate to a significant extent. N47A-T32A and N47A-V46A are also among the least stable mutants but their rates of aggregation are relatively low.

Figure 3d shows a correlation between the initial rates of growth obtained from the ThT experiments and the mean times of the shift in the hydrodynamic radius (t_s). This was obtained by fitting the time dependence of the apparent R_h using a logistic sigmoidal function (Supplementary Information Figure S4). This supports a direct relationship between the initial growth of ThT fluorescence and the rapid accumulation of the small amyloid nuclei. Due to the initial oligomeric nature of the N47A-K43A at 37°C, this variant was discarded

from this analysis.
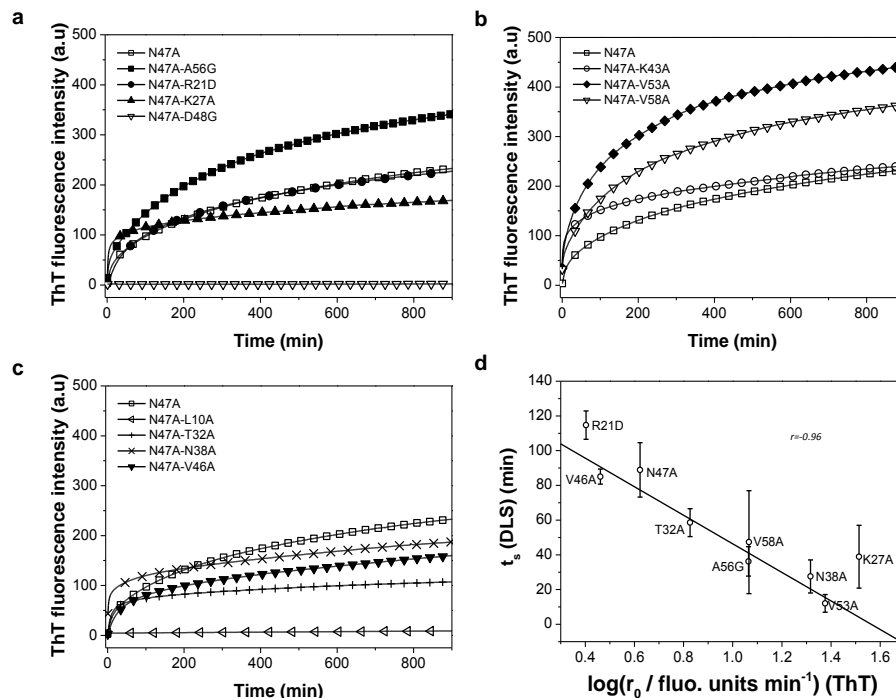
Figure 3. ***Kinetics of formation of amyloid fibrils followed by ThT fluorescence at 37ºC (a, b, c).*** *Protein concentration was about 8.5 mg mL^{-1} (1.2 mM) in each case. The symbols used are indicated in each graph. Correlation between initial rates obtained with the ThT fluorescence experiments and the time of oligomers appearance determined by DLS (d). Correlation coefficient and errors bars are indicated.*

The morphology of the aggregates formed by the double mutants was also explored by transmission electron microscopy (TEM) during the time course of aggregation (Figure 4). At early incubation times (Figure 4 a-d), only aggregates with globular or amorphous shapes could be observed and there are practically no fibrillar aggregates. Although the sizes of the oligomers observed by DLS are in the limit of the microscope resolution, most of the globular particles visible by TEM appear to have a wide distribution of sizes, with radii roughly between 3-6 nm, consistent with the DLS data. After about 840 minutes of incubation, fibrils can be clearly observed for most mutants, except for N47A-L10A and N47A-D48G, which did not evolve towards fibrillar aggregates when incubated at 37ºC under the same conditions. The overall curly morphologies of the fibrils were similar for all variants and also similar to those described previously [19-21].

These results obtained from various biophysical observables showed that most of the studied mutants convert to similar amyloid aggregates. Although the processes occurred at different rates, the mutants have shown to aggregate by a common mechanism.
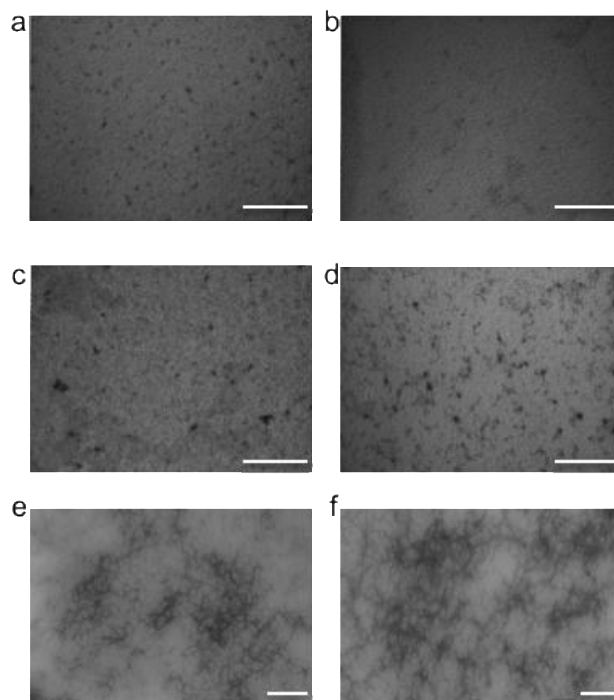
Figure 4. Time course of amyloid fibril formation of variants of Spc-SH3 observed by transmission electron microscopy. TEM images correspond to different times of incubation at 37°C. Representative images correspond to (a) N47A-T32A incubated for 10 minutes, (b) N47A-K43A incubated for 10 minutes, (c) N47A-K27A incubated for 10 minutes, (d) N47A incubated for 30 minutes, (e) N47A-K27A incubated for 1440 minutes, (f) N47A-R21D incubated for 1440 minutes. The white segments represent 200 nm in each panel.

Analysis of the initial rates of growth of ThT fluorescence reports about crucial intermediates of amyloid nucleation

Recently, we developed a simple kinetic model, which has proved to be applicable to the amyloid nucleation mechanism of Spc SH3 domain under different conditions [22,23]. This simple and mathematically affordable aggregation model allowed us to analyze quantitatively the initial rates of amyloid growth derived from ThT fluorescence kinetics and extract kinetic and thermodynamic magnitudes characterizing the key molecular events

preceding the nucleation process. Although the use of Thioflavine T fluorescence to detect oligomers was defined as relatively insensitive [43], in the present study using the Spc SH3 domain, it has shown to be a sensitive probe for the initial growth of amyloid oligomers. Nevertheless, our methodology could also be applied to other techniques used to specifically detect oligomers. Recent studies using solid state NMR [44-48] and also ^{19}F NMR [49,50] have shown to have the ability to resolve individual oligomers and track their formation in real-time.

This model is summarized in the Methods section. Here we made a series of ThT kinetics experiments for all double mutants to measure the initial rates of amyloid growth at different initial protein concentrations (Figure 5). The dependences of the initial rates on the initial concentrations of protein were fitted using the model equations in order to evaluate the impact of each mutation on the amyloid nucleation stages.

In the fitting procedure, we first fixed the values for ΔG_U at 37ºC, obtained independently from the analysis of the thermal unfolding by DSC at low protein concentrations (Table 1) therefore reducing the number of adjustable parameters to just three for each mutant. As shown in Figure 5, the double logarithmic plots of the initial rates versus the protein concentration show a great variability between the different mutants. Individual fittings described very well the data and allowed us to derive the thermodynamic magnitudes corresponding to the stability of the intermediate state (ΔG_I) and its subsequent oligomerization (ΔG_A), as well as the rate constant of the conformational change within the aggregates to yield amyloid nuclei (k_F) (Table 1).

The k_F values are similar in all cases, indicating that the different mutations do not influence to a great extent the rate of conformational change of the protein within the dynamic oligomers to form amyloid nuclei. This suggests that once the polypeptide chains are associated into oligomers, the barrier for their conversion into amyloid structure is almost independent of the mutations. This is in agreement with the concept that amyloid structure is mainly stabilized by main chain interactions. On the other hand, the variability in ΔG_I and ΔG_A is much greater.

Table 1. Fitting parameters derived from the analysis of the initial nucleation rates at 37ºC.

Variant	ΔG_U (kJ/mol)[b]	ΔG_I (kJ/mol)	ΔG_A (kJ/mol)	log k_F
N47A	5.28 ± 0.40	13.08 ± 0.40	-31.80 ± 0.49	4.25 ± 0.06
L10AN47A	-1.97 ± 0.30	-	-	-
R21DN47A	6.33 ± 0.40	16.52 ± 0.95	-34.93 ± 1.01	4.04 ± 0.21
K27AN47A	3.37 ± 0.40	16.70 ± 0.72	-37.93 ± 0.81	4.37 ± 0.09
T32AN47A	1.46 ± 0.30	16.04 ± 0.50	-36.25 ± 0.54	4.11 ± 0.06
N38AN47A	0.50 ± 0.30	15.68 ± 0.95	-37.16 ± 1.08	4.43 ± 0.12
K43AN47A	2.30 ± 0.80	13.91 ± 1.30	-37.12 ± 1.43	4.57 ± 0.09
V46AN47A	1.75 ± 0.30	13.53 ± 1.30	-32.24 ± 1.49	4.39 ± 0.25
D48GN47A	7.34 ± 0.40	-	-	-
V53AN47A	3.80 ± 0.80	10.74 ± 1.61	-32.08 ± 2.04	4.49 ± 0.15
A56GN47A	3.68 ± 0.40	13.11 ± 1.13	-32.45 ± 1.33	4.48 ± 0.12
V58AN47A	3.85 ± 1.00	10.43 ± 0.61	-31.75 ± 0.86	4.33 ± 0.06
N47A[a]	4.64 ± 0.30	11.65 ± 1.28	-32.02 ± 1.68	4.59 ± 0.16
L10AN47A[a]	-0.74 ± 0.30	10.43 ± 1.88	-24.52 ± 7.96	4.42 ± 0.82

[a]Determined from aggregation kinetics studied in presence of 0.2 M NaCl. [b]Calculated from the unfolding curves measured by DSC. Data of N47A Spc-SH3 were taken from reference [15].

In order to interpret the ΔG_I data in terms of a structural characterization of the amyloidogenic precursor, I, we used an approach similar to the ϕ-value analysis of folding transition states [24-30].
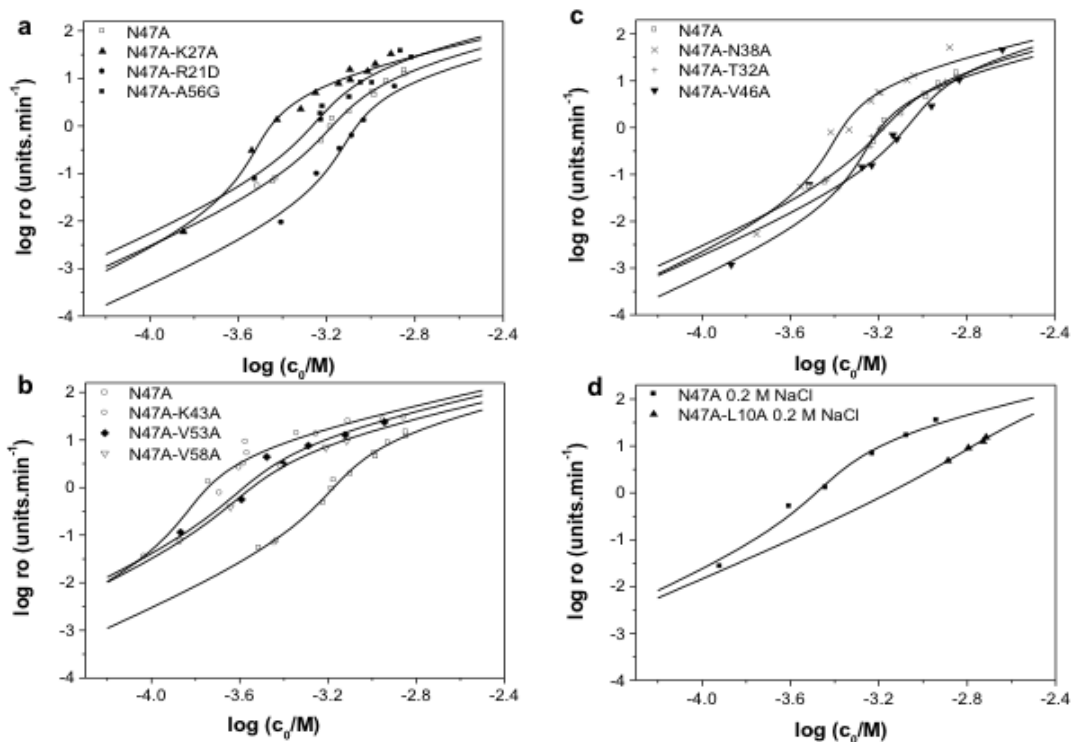
Figure 5. Double logarithmic plot of the initial rates of amyloid fibrillation of N47A Spc-SH3 and the double mutants versus the initial protein concentration. The symbols used are indicated in the graph. Symbols correspond to the experimental rates and continuous lines represent the best fits according to the equation described in Materials and Methods and in Ruzafa et al. [22].

In this type of analyses the ϕ-value is typically calculated as the ratio between the changes produced by a mutation in the energy difference between the transition state and the unfolded state ($\Delta\Delta G_{\ddagger-U}$), relative to the changes produced in the energy difference between the native and the unfolded states ($\Delta\Delta G_{N-U}$).

In our study, ϕ-values characterizing the effect of each mutation on the I state could be similarly obtained as $\Delta\Delta G_{I-U}/\Delta\Delta G_{N-U}$ but some of the values result to be much greater than 1 and others even negative. The reason of this is that some of the mutations strongly altered the native fold and/or its stability and, in addition, the energy changes produced by the different mutations in the native-state stability do not correlate with the changes in the rates of nucleation. In fact, a plot of ΔG_I versus ΔG_{N-U} illustrates this lack of correlation (Supplementary information Figure S5). For this reason, we decided not to use normalized

φ-values but directly compare the ΔG_{I-U} differences between the double mutants, obtained as $\Delta G_I - \Delta G_U$, and the reference N47A single mutant. These values represent the energy cost of formation of the partially-folded amyloidogenic intermediate from the fully unfolded state, in which all interactions are broken and the protein groups are fully exposed and solvated, for each mutant (Figure 6a).

In order to obtain data related to the N47A-L10A mutant, we also studied the aggregation kinetics of this mutant in 0.2 M NaCl, which was previously shown to accelerate amyloid aggregation considerably [20,22]. Under these conditions the N47A-L10A mutant fibrillated faster as shown by an increase in ThT fluorescence intensity. However, the interval of protein concentrations and the range of experimentally accessible initial rates were very limited. Because of these limitations, the initial rates obtained for N47A-L10A in the presence of 0.2 M NaCl were analyzed in conjunction with the similar data obtained with the single mutant N47A under the same conditions. In this fitting the k_F value was shared for the two mutants, since we found that this parameter did not change much between all mutants studied. This gave us a reasonable estimation of the nucleation thermodynamic magnitudes for the L10A mutation, although with significantly higher uncertainties (Figure 5d and Table 1). The thermodynamic magnitudes represented in Figure 6a allow us to globally classify the mutations in two groups: A group of mutations located in the region between R21 and V46 (RT loop, divergent turn and strands β2 and β3), which show significant changes in ΔG_I - ΔG_U relative to the reference N47A mutant.

These changes imply that these mutations destabilize the amyloidogenic intermediate and therefore the affected residues participate in its structure.

In contrast, the ΔG_I - ΔG_U values obtained for the mutation L10A (strand β1) and the mutations V53A, A56G and V58A (3_{10} helix, strands β4 and β5) are very similar to that of the reference mutant N47A. This indicates that these residues do not participate in the structure of the intermediate, because the mutations do not significantly alter its energy relative to the fully unfolded state. Therefore the regions probed by these mutations are unfolded in the intermediate and this implies that the distal β-hairpin formed by strands β3 and β4 must be open before amyloid nucleation. This is striking because these mutations

have profound effects on the stability of the native state and some of these residues are directly implied in the hydrophobic core of the domain.
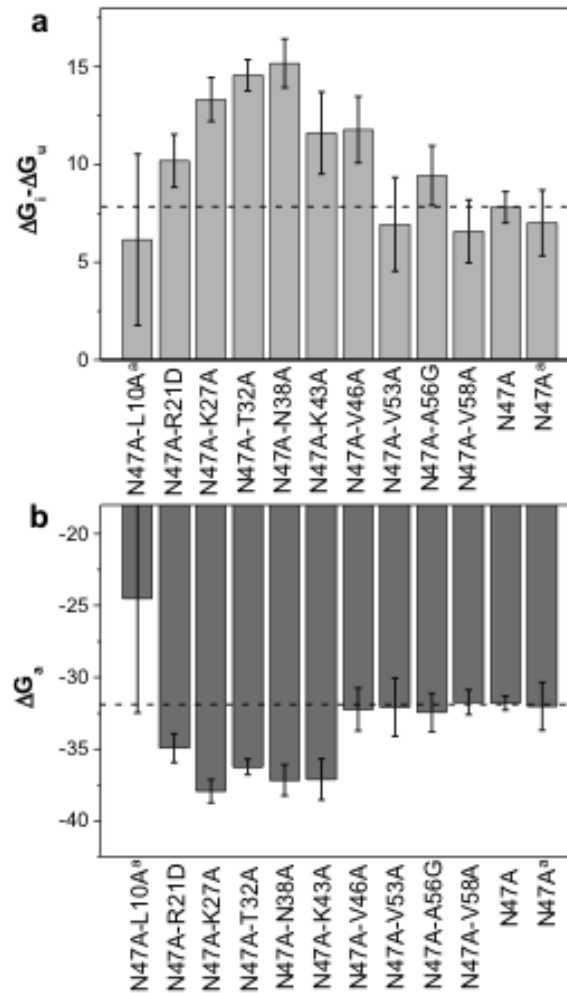
***Figure 6. Changes in the amyloidogenic intermediate stability (a) and its oligomerization energy (b) as a result of the mutations**. [a]Determined from aggregation kinetics studied in the presence of 0.2 M NaCl.*

Interestingly, all the mutations in the 21-43 region (RT loop, divergent turn, strands $\beta 2$ and $\beta 3$) make the oligomerization Gibbs energy, ΔG_A, considerably more negative, therefore increasing the oligomerization propensity of the intermediate (Figure 6b). This indicates a direct participation of these residues in intermolecular interactions mediating dynamic oligomerization. In contrast, mutations V46A, V53A, A56G and V58A do not change in the oligomerization Gibbs energy consistently with the lack of implication of the final region of the sequence in the structure of the intermediate. Moreover, the strong inhibition in the

aggregation process produced by the L10A mutation can be fully attributed to its considerable effect in decreasing Gibbs energy gain associated to oligomerization. This indicates that the strand β1 is fully involved in the oligomerization process. The importance of L10 in the aggregation cascade was also highlighted by the predictions of the aggregation-prone regions of Spc-SH3 domain using Aggrescan [51], TANGO [52] and Zyggregator [53] algorithms. These programs identified the highly hydrophobic region 7-14 as having the highest intrinsic aggregation propensities (Supplementary information Figure S6). These results strongly suggest that oligomerization is mediated by intermolecular interactions between the highly hydrophobic residues of strand β1 and an exposed hydrophobic surface created by the structured elements of the intermediate (residues of the RT loop, divergent turn, β2 and β3 strands).

DISCUSSION

Native-state thermodynamic stability is not correlated with the amyloid nucleation propensity

We have shown here strong changes in thermodynamic stability of the native state produced by different mutations (Table S2) but these changes do not generally correlate with the nucleation and fibrillation propensities of the mutants. The changes on amyloid propensity need to be rationalized on the basis of the specific effects on the nucleation mechanism. In fact, despite their dramatic opposite effects on the stability of the native state, both mutations L10A and D48G essentially abolished fibrillation in the presence of 0.1 M NaCl but this effect takes place at completely different steps of the mechanism. The mutation D48G was reported to stabilize significantly the protein through a local conformational change of the distal turn, facilitating the formation of the distal β-hairpin [15] and therefore promoting native folding. Since amyloid nucleation requires the selective unfolding of the distal β-hairpin, it is not surprising that this mutation inhibits aggregation.

The effect of the mutation L10A is remarkable. This mutation strongly destabilises the native state and at the same time inhibits fibrillation very strongly. Opposite to the distal hairpin,

the strand β1 does not participate in the folding nucleus of the Spc-SH3 domain [15]. Our results show that whilst this region seems to be unfolded in the amyloidogenic intermediate state, it participates in establishing the hydrophobic intermolecular interactions to form dynamic oligomers that precede nucleation. Therefore, the L10A mutation specifically destabilizes these oligomers and reduces their population resulting in a much slower aggregation rate.

As for the rest of mutations, there are two main classes of effects: those mutations at regions participating in the structure of the amyloidogenic intermediate mainly act by altering specifically its stability and also affecting the formation of oligomers. In contrast, the mutations at regions becoming unstructured in the intermediate act exclusively by destabilizing the native state and, therefore, by increasing the population of alternative states, including the amyloidogenic one.

Although many earlier studies based on the elucidation of fibril formation pointed towards a significant inverse correlation between native stability and the propensity to form amyloids [54-58], a more recent mutagenesis study on the fibrillation of the thermophilic protein S6 revealed no correlation between native stability and fibril formation [59]. Instead, the unfolding rates correlated directly with the lag phases of amyloid aggregation suggesting that the nucleation occurs from a quasi-native state. Our results support the importance of local specific intramolecular interactions between certain parts of the domain in the early stages of the fibrillation process. Such hypothesis was also drawn in the study of two amyloidogenic variants of human lysozyme [60], in which transient unfolding of a specific region of the protein including the beta domain and the C-helix is favoured by the mutations. However, we also demonstrate that specific intermolecular interactions could also be determinant in the primary amyloid nucleation events. In some other cases, however, the intermolecular contacts that promote the amyloid conversion may be provided by fibril fragmentation [10] or by non-specific heterogeneous nucleation [61].

Folding and amyloid fibrillation are divergent routes on the conformational landscape

It has been generally assumed that amyloidogenesis is initiated by a change in conformation

of the native structure leading to an intermediate state which is prone to aggregate by exposing an amyloidogenic region that in turn promotes self-association [62].

There is also accumulating evidence that the amyloid-competent species may be a locally-unfolded native-like state that becomes accessible through thermal fluctuations occurring under physiological conditions [63,64]. However, such scenario differs sharply from the conformational change hypothesis [65-67], according to which the early precursor of amyloid results from an unfolding transition involving the crossing of a major energy barrier. Therefore, it is crucial to understand how the folding and aggregation landscapes are related to be able to identify and characterize the conformational states that connect them [68].

Previous kinetic and thermodynamic studies performed on the folding process of the Spc-SH3 domain using a mutagenesis approach identified the residues involved in the folding transition state and also the obligatory steps in protein folding [15,69]. In particular, the formation of the β3-β4-hairpin has been described as an obligatory step during folding of Spc-SH3 [15]. This structural motif is also central in the structure of the folding nuclei of other SH3 domains [70]. In addition, residue V53 has been reported as a key residue in the protein core participating strongly in the folding nucleus of the domain establishing hydrophobic contacts stabilizing the correct topology leading to the native fold. High φ-values characterizing the residues involved in the transition state structure include mainly residues in the distal hairpin and the 3_{10} helix (V44, V46, N47, D48, F52, V53 and A55), whereas other regions contribute little to the transition state ensemble in terms of free energy.

In our study, the residues defined as major contributors to the stability of the amyloidogenic intermediate are located at several structural elements, some of them unrelated with the folding transition state i.e., the RT loop (R21), the diverging turn (K27), strand β2 (T32), the n-src loop (N38) and strand β3 (K43 and V46). In contrast, the amyloidogenic intermediate appears to have strand β1 (L10), strand β4 (V53), the 3_{10}-helix (A56) and strand β5 (V58) mainly unstructured. These results are striking because they indicate that, in order to form the kinetically critical amyloidogenic precursor, the protein needs to acquire a markedly different topology to that found along the native folding-unfolding pathway. Accordingly, native folding and nucleation of the Spc-SH3 domain take place on different regions of the

conformational landscape (Figure 7).
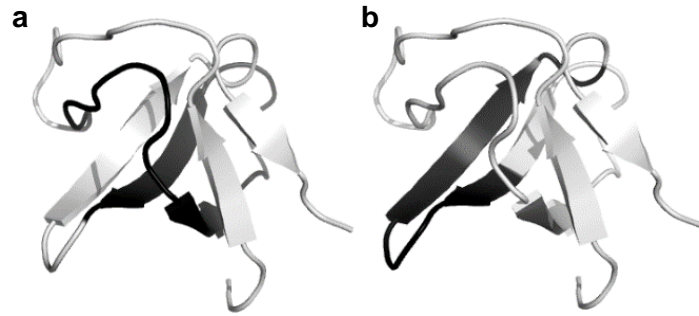
***Figure 7**. **Regions of Spc-SH3 involved in aggregation (a) and folding (b) transition states.** The structure of N47A Spc-SH3 (pdb: 1QKX) is shown in both representations with important structural regions colored in black. The data for aggregation are taken from those shown in Figure 6. The data for the folding process are from ref [69].; only regions with relevant high φ values are colored in black in panel (b). The protein structural representations were done using Pymol [39].*

Other studies performed on other SH3 domain [71,72] agree properly with our main conclusions. PI3-SH3 domain was reported as the very first protein unrelated to disease that was shown to form amyloid-like fibrils in vitro [73]. PI3-SH3 domain shares the same fold and 24% sequence identity with Spc-SH3 [72]. Using protein engineering, Ventura and co-workers reported that the RT loop (residues L11-D23) and the adjacent diverging turn (residues L24-D28) of PI3-SH3 are specific regions influencing the amyloidogenic behavior. More recently, an interesting study based on pulse-labeling hydrogen-deuterium (HD) exchange monitored by mass spectrometry and NMR spectroscopy on amyloid fibrils of PI3-SH3 [71] reinforced the crucial role of residues comprising the RT loop and the diverging turn in the ordered aggregates during fibrillation.

Other studies point toward native-like partially unfolded states as amyloidogenic precursors. Fyn-SH3 has been used recently to elucidate the mechanisms by which intermediates initiate fibrillar aggregation [74]. In this case, the authors stabilized a weakly populated on-pathway intermediate of the SH3 domain via a triple mutant of the protein. The structure of the intermediate was characterized by NMR relaxation-dispersion measurements. The C-terminus (i.e., the last β-strand) is disordered and, therefore, the N-terminal β-strand is solvent exposed; however, the native-like central three-stranded β-sheet remains intact in this

intermediate. A recent computational study by Shakhnovich and co-workers has proposed a conserved aggregation-prone intermediate state in the folding pathway of Spc-SH3 amyloidogenic variants [14]. Although the lack of structure predicted in strand β5 and the potential role of the strand β1 in establishing intermolecular contacts are fully coincident with our results, the intermediate was characterized as having native-like topology, with the central three-stranded β-sheet still formed. However, in this work, the authors used a Gō type algorithm that focuses on the native-like interactions and would not be therefore appropriate for exploring landscape areas containing non-native conformations.

Finally, it is important to emphasize that our methodology provides a selective characterization of the intermediate state that is kinetically relevant to the aggregation process. It is likely that the protein ensemble is exploring other low-populated intermediates over wide regions of the conformational landscape as reported before [75] but many of these states may be unproductive to trigger the amyloidogenic cascade. Therefore, our results strongly support that the sequences of natural proteins may have evolved to favour fast and efficient folding pathways and avoid the amyloidogenic regions of the energy landscape [76].

Implications in disease-related amyloid aggregation

Our kinetic methodology could be expanded to different applications in proteins related to disease. The importance of obtaining the quantitative thermodynamic magnitudes about the amyloidogenic precursors of different proteins resides mainly in the possibility of changing a variety of factors (experimental conditions, sequence mutations, inhibitor compounds etc.) and analyzing how these thermodynamic properties respond to these changes. This may be applicable, for example, to amyloid-beta (1–40), which at low temperature and moderate salt concentration adopts a helical conformation in the central hydrophobic region favoring hydrophobic collapse [77]. Helical intermediates have been predicted to be crucial in amyloid fibrillogenesis [78]. In some cases, oligomers formed during the aggregation process have different toxicity. These are the cases of the rat and human versions of $IAPP_{1-19}$ [79] and also the HypF-N domain [2]. Analyzing the thermodynamic and structural properties of the different

types of oligomers using our approach may shed light on their different cytotoxic properties.

Our kinetic model could also be extended to the study of inhibitor compounds. For example, polyphenols have been shown to alter the aggregation kinetics of many proteins [49,80-82]. However, the mechanism of action is not fully understood. For instance, direct interaction of EGGC with the prostatic acid phosphatase fragment PAP248-286 has been shown to strongly inhibit formation of amyloid SEVI, likely by a shift in the conformational-oligomerization equilibrium towards non-amyloidogenic species [81]. Our approach could be adapted to explore the effect of these inhibitors by inclusion of the corresponding preequilibria in the kinetic scheme. With this methodology, it could be possible to unveil the thermodynamic effects of such chemicals on the nucleation stage.

CONCLUSION

In this study, a mutagenesis analysis of the early aggregation kinetics of the Spc-SH3 domain has allowed us to characterize structurally and energetically the molecular events leading to fibril nucleation.

The combination of DSC and biophysical experiments performed on the series of second mutations made upon the N47A mutant and covering all the structural elements of the protein has highlighted the lack of correlation between the thermodynamic stability of the native state and the propensity to form amyloid fibrils. Instead, our results have demonstrated that the inhibitory or potentiating effect of amyloid formation exerted by the mutations is mainly related to the relative efficiency in the formation of early dynamic oligomers, which precedes the formation of amyloid nuclei.

A robust kinetic and thermodynamic analysis on the basis of a simple model has allowed us the identification of the residues playing an important role in the structure of the amyloidogenic intermediate state and participating in its intermolecular self-association process. It appears that the conformational transition leading to amyloid nucleation follows a completely different pathway to that of the folding-unfolding process and involves partial unfolding of the domain core and intermolecular association mediated by the unfolded N-

terminal strand.

Taken together, these insights provide a deeper understanding of the fundamental forces that control the competition between folding, misfolding and aggregation. Such understanding undoubtedly enriches the framework for the development of rational strategies for the design of therapeutic compounds able to influence steps in the complex self-association processes so as to reduce the risk of misfolding events.

NOTES

Electronic Supplementary Information (ESI) available: Text S1: Determination of the initial rates. Thermodynamic parameters of the equilibrium thermal unfolding of N47A Spc-SH3 and the double mutants measured by DSC are shown in Table S2. DSC experiments of N47A and the double mutants of Spc-SH3 domain (Figure S2). Aggregation kinetics followed by DLS intensity (Figure S3). Figure S4 illustrates the time evolution of the hydrodynamic radii. In Figure S5 ΔG_I versus Δ_{GN-U} is plotted. Aggregation propensity of the primary sequence of N47A Spc-SH3 domain predicted by algorithms (Figure S6).

REFERENCES

(1)   Rochet, J.-C.; Lansbury Jr, P. T. Amyloid fibrillogenesis: themes and variations. *Curr. Opin. Struc. Biol.* **2000**, *10*, 60-68.

(2)   Campioni, S.; Mannini, B.; Zampagni, M.; Pensalfini, A.; Parrini, C.; Evangelisti, E.; Relini, A.; Stefani, M.; Dobson, C. M.; Cecchi, C.; Chiti, F. A causative link between the structure of aberrant protein oligomers and their toxicity. *Nat. Chem. Biol.* **2010**, *6*, 140-147.

(3)   Baglioni, S.; Casamenti, F.; Bucciantini, M.; Luheshi, L. M.; Taddei, N.; Chiti, F.; Dobson, C. M.; Stefani, M. Prefibrillar amyloid aggregates could be generic toxins in higher organisms. *J. Neurosci.* **2006**, *26*, 8160-8167.

(4)   Bucciantini, M.; Giannoni, E.; Chiti, F.; Baroni, F.; Formigli, L.; Zurdo, J.; Taddei, N.; Ramponi, G.; Dobson, C. M.; Stefani, M. Inherent toxicity of aggregates implies a common mechanism for protein misfolding diseases. *Nature* **2002**, *416*, 507-511.

(5)   Lajoie, P.; Snapp, E. L. Formation and toxicity of soluble polyglutamine oligomers in living cells. *PLoS One* **2010**, *5*, e15245.

(6)   Brender, J. R.; Salamekh, S.; Ramamoorthy, A. Membrane disruption and early events in the aggregation of the diabetes related peptide IAPP from a molecular perspective. *Acc. Chem. Res.* **2012**, *45*, 454-462.

(7)   Sciacca, M. F.; Kotler, S. A.; Brender, J. R.; Chen, J.; Lee, D. K.; Ramamoorthy, A. Two-step mechanism of membrane disruption by Abeta through membrane fragmentation and pore formation. *Biophys. J.* **2012**, *103*, 702-710.

(8)   Cohen, S. I.; Linse, S.; Luheshi, L. M.; Hellstrand, E.; White, D. A.; Rajah, L.; Otzen, D. E.; Vendruscolo, M.; Dobson, C. M.; Knowles, T. P. Proliferation of amyloid-beta42 aggregates occurs through a secondary nucleation mechanism. *Proc. Natl. Acad. Sci. USA* **2013**, *110*, 9758-9763.

(9)   Cohen, S. I.; Vendruscolo, M.; Welland, M. E.; Dobson, C. M.; Terentjev, E. M.; Knowles, T. P. Nucleated polymerization with secondary pathways. I. Time evolution of the principal moments. *J. Chem. Phys.* **2011**, *135*, 065105.

(10)   Knowles, T. P.; Waudby, C. A.; Devlin, G. L.; Cohen, S. I.; Aguzzi, A.; Vendruscolo, M.; Terentjev, E. M.; Welland, M. E.; Dobson, C. M. An analytical solution to the kinetics of breakable filament assembly. *Science* **2009**, *326*, 1533-1537.

(11)   Casares, S.; Sadqi, M.; Lopez-Mayorga, O.; Conejero-Lara, F.; van Nuland, N. A. Detection and characterization of partially unfolded oligomers of the SH3 domain of alpha-spectrin. *Biophys. J.* **2004**, *86*, 2403-2413.

(12)   Casares, S.; Sadqi, M.; Lopez-Mayorga, O.; Martinez, J. C.; Conejero-Lara, F. Structural cooperativity in the SH3 domain studied by site-directed mutagenesis and amide hydrogen exchange. *FEBS Lett.* **2003**, *539*, 125-130.

(13)   Espargaró, A.; Castillo, V.; de Groot, N. S.; Ventura, S. The in Vivo and in Vitro Aggregation Properties of Globular Proteins Correlate With Their Conformational Stability: The SH3 Case. *J. Mol. Biol.* **2008**, *378*, 1116-1131.

(14)   Krobath, H.; Estacio, S. G.; Faisca, P. F.; Shakhnovich, E. I. Identification of a conserved aggregation-prone intermediate state in the folding pathways of Spc-SH3 amyloidogenic variants. *J. Mol. Biol.* **2012**, *422*, 705-722.

(15)   Martinez, J. C.; Pisabarro, M. T.; Serrano, L. Obligatory steps in protein folding and the conformational diversity of the transition state. *Nat. Struct. Biol.* **1998**, *5*, 721-729.

(16)   Sadqi, M.; Casares, S.; Abril, M. A.; Lopez-Mayorga, O.; Conejero-Lara, F.; Freire, E. The native state conformational ensemble of the SH3 domain from alpha-spectrin. *Biochemistry* **1999**, *38*, 8899-8906.

(17)   Viguera, A. R.; Martinez, J. C.; Filimonov, V. V.; Mateo, P. L.; Serrano, L. Thermodynamic and kinetic analysis of the SH3 domain of spectrin shows a two-state folding transition. *Biochemistry* **1994**, *33*, 2142-2150.

(18)   Klimov, D. K.; Thirumalai, D. Stiffness of the distal loop restricts the structural heterogeneity of the transition state ensemble in SH3 domains. *J. Mol. Biol.* **2002**, *317*, 721-737.

(19)   Morel, B.; Casares, S.; Conejero-Lara, F. A single mutation induces amyloid aggregation in the alpha-spectrin SH3 domain: analysis of the early stages of fibril formation. *J. Mol. Biol.* **2006**, *356*, 453-468.

(20)   Morel, B.; Varela, L.; Azuaga, A. I.; Conejero-Lara, F. Environmental Conditions Affect the Kinetics of Nucleation of Amyloid Fibrils and Determine Their Morphology. *Biophys. J.* **2010**, *99*, 3801-3810.

(21)   Varela, L.; Morel, B.; Azuaga, A. I.; Conejero-Lara, F. The amyloidogenic mutation N47A in the alpha-spectrin SH3 domain does not enhance aggregation by destabilizing the native state but by increasing the rate of the nucleation event. *FEBS Letters* **2009**, *583*, 801-806.

(22)   Ruzafa, D.; Morel, B.; Varela, L.; Azuaga, A. I.; Conejero-Lara, F. Characterization of Oligomers of Heterogeneous Size as Precursors of Amyloid Fibril Nucleation of an SH3 Domain: An Experimental Kinetics Study. *PLoS ONE* **2012**, *7*, e49690.

(23)   Ruzafa, D.; Conejero-Lara, F.; Morel, B. Modulation of the stability of amyloidogenic precursors by anion binding strongly influences the rate of amyloid nucleation. *Phys. Chem. Chem. Phys.* **2013**, *15*, 15508-15517.

(24)   Matouschek, A.; Kellis, J. T., Jr.; Serrano, L.; Fersht, A. R. Mapping the transition state and pathway of protein folding by protein engineering. *Nature* **1989**, *340*, 122-126.

(25)   Campos, L. A.; Bueno, M.; Lopez-Llano, J.; Jimenez, M. A.; Sancho, J. Structure of stable protein folding intermediates by equilibrium phi-analysis: the apoflavodoxin thermal intermediate. *J. Mol. Biol.* **2004**, *344*, 239-255.

(26)   Crane, J. C.; Koepf, E. K.; Kelly, J. W.; Gruebele, M. Mapping the transition state of the WW domain beta-sheet. *J. Mol. Biol.* **2000**, *298*, 283-292.

(27)   Fersht, A. R.; Matouschek, A.; Sancho, J.; Serrano, L.; Vuilleumier, S. Pathway of protein folding. *Faraday Discuss* **1992**, 183-193.

(28)   Matouschek, A.; Kellis, J. T., Jr.; Serrano, L.; Bycroft, M.; Fersht, A. R. Transient folding intermediates characterized by protein engineering. *Nature* **1990**, *346*, 440-445.

(29)   Neudecker, P.; Zarrine-Afsar, A.; Davidson, A. R.; Kay, L. E. Phi-value analysis of a three-state protein folding pathway by NMR relaxation dispersion spectroscopy. *Proc. Natl. Acad. Sci. USA* **2007**, *104*, 15717-15722.

(30)   Ventura, S.; Vega, M. C.; Lacroix, E.; Angrand, I.; Spagnolo, L.; Serrano, L. Conformational strain in the hydrophobic core and its implications for protein folding and design. *Nat. Struct. Biol.* **2002**, *9*, 485-493.

(31)   Williams, A. D.; Shivaprasad, S.; Wetzel, R. Alanine Scanning Mutagenesis of Aß(1-40) Amyloid Fibril Stability. *J. Mol. Biol.* **2006**, *357*, 1283-1294.

(32)   Margittai, M.; Langen, R. Template-assisted filament growth by parallel stacking of tau. *Proc. Natl. Acad. Sci. USA* **2004**, *101*, 10278-10283.

(33)   Shivaprasad, S.; Wetzel, R. Scanning Cysteine Mutagenesis Analysis of Abeta-(1-40) Amyloid Fibrils. *J. Biol. Chem.* **2006**, *281*, 993-1000.

(34)   Williams, A. D.; Portelius, E.; Kheterpal, I.; Guo, J.-t.; Cook, K. D.; Xu, Y.; Wetzel, R. Mapping Abeta Amyloid Fibril Secondary Structure Using Scanning Proline Mutagenesis. *J. Mol. Biol.* **2004**, *335*, 833-842.

(35)   Ferguson, N.; Becker, J.; Tidow, H.; Tremmel, S.; Sharpe, T. D.; Krause, G.; Flinders, J.; Petrovich, M.; Berriman, J.; Oschkinat, H.; Fersht, A. R. General structural motifs of amyloid protofilaments. *Proc. Natl. Acad. Sci. USA* **2006**, *103*, 16248-16253.

(36)   Andrews, J. M.; Roberts, C. J. A Lumry-Eyring nucleated polymerization model of protein aggregation kinetics: 1. Aggregation with pre-equilibrated unfolding. *J. Phys. Chem.* **2007**, *111*, 7897-7913.

(37)   Morris, A. M.; Watzky, M. A.; Finke, R. G. Protein aggregation kinetics, mechanism, and curve-fitting: a review of the literature. *Biochim Biophys Acta* **2009**, *1794*, 375-397.

(38)   Oosawa, F.; Kasai, M. A theory of linear and helical aggregations of macromolecules. *J. Mol. Biol.* **1962**, *4*, 10-21.

(39)   De Lano, W. L.: The PyMOL Molecular Graphics System. Scientific, D., Ed.: San Carlos, CA, USA, 2002.

(40)   Camara-Artigas, A.; Gavira, J. A.; Casares, S.; Garcia-Ruiz, J. M.; Conejero-Lara, F.; Allen, J. P.; Martinez, J. C. Understanding the polymorphic behaviour of a mutant of the alpha-spectrin SH3 domain by means of two 1.1 A resolution structures. *Acta Crystallogr D Biol Crystallogr* **2011**, *67*, 189-196.

(41)   Wilkins, D. K.; Grimshaw, S. B.; Receveur, V.; Dobson, C. M.; Jones, J. A.; Smith, L. J. Hydrodynamic radii of native and denatured proteins measured by pulse field gradient NMR techniques. *Biochemistry* **1999**, *38*, 16424-16431.

(42)   Wilcken, R.; Wang, G.; Boeckler, F. M.; Fersht, A. R. Kinetic mechanism of p53 oncogenic mutant aggregation and its inhibition. *Proc. Natl. Acad. Sci. USA* **2012**, *109*, 13584-13589.

(43)   Lee, J.; Culyba, E. K.; Powers, E. T.; Kelly, J. W. Amyloid-beta forms fibrils by nucleated conformational conversion of oligomers. *Nat. Chem. Biol.* **2011**, *7*, 602-609.

(44)   Bertini, I.; Gallo, G.; Korsak, M.; Luchinat, C.; Mao, J.; Ravera, E. Formation Kinetics and Structural Features of Beta-Amyloid Aggregates by Sedimented Solute NMR. *Chembiochem* **2013**, *14*, 1891-1897.

(45)   Dupuis, N. F.; Wu, C.; Shea, J.-E.; Bowers, M. T. Human Islet Amyloid Polypeptide Monomers Form Ordered b-hairpins: A Possible Direct Amyloidogenic Precursor. *Journal of the American Chemical Society* **2009**, *131*, 18283-18292.

(46)   Itoh-Watanabe, H.; Kamihira-Ishijima, M.; Kawamura, I.; Kondoh, M.; Nakakoshi, M.; Sato, M.; Naito, A. Characterization of the spherical intermediates and fibril formation of hCT in HEPES solution using solid-state 13C-NMR and transmission electron microscopy. *Physical Chemistry Chemical Physics* **2013**, *15*, 16956-16964.

(47)   Tang, M.; Comellas, G.; Rienstra, C. M. Advanced Solid-State NMR Approaches for Structure Determination of Membrane Proteins and Amyloid Fibrils. *Accounts of Chemical Research* **2013**, *46*, 2080-2088.

(48)   Tay, W. M.; Huang, D.; Rosenberry, T. L.; Paravastu, A. K. The Alzheimer's Amyloid-beta(1-42) Peptide Forms Off-Pathway Oligomers and Fibrils That Are Distinguished Structurally by Intermolecular Organization. *J. Mol. Biol.* **2013**.

(49)   Suzuki, Y.; Brender, J. R.; Hartman, K.; Ramamoorthy, A.; Marsh, E. N. Alternative pathways of human islet amyloid polypeptide aggregation distinguished by (19)f nuclear magnetic resonance-detected kinetics of monomer consumption. *Biochemistry* **2012**, *51*, 8154-8162.

(50)   Suzuki, Y.; Brender, J. R.; Soper, M. T.; Krishnamoorthy, J.; Zhou, Y.; Ruotolo, B. T.; Kotov, N. A.; Ramamoorthy, A.; Marsh, E. N. G. Resolution of Oligomeric Species during the Aggregation of Aß 1-40 Using 19F NMR. *Biochemistry* **2013**, *52*, 1903-1912.

(51)   Conchillo-Sole, O.; de Groot, N.; Aviles, F.; Vendrell, J.; Daura, X.; Ventura, S. AGGRESCAN: a server for the prediction and evaluation of "hot spots" of aggregation in polypeptides. *BMC Bioinformatics* **2007**, *8*, 65.

(52)   Fernandez-Escamilla, A. M.; Rousseau, F.; Schymkowitz, J.; Serrano, L. Prediction of sequence-dependent and mutational effects on the aggregation of peptides and proteins. *Nat. Biotechnol.* **2004**, *22*, 1302-1306.

(53)   Tartaglia, G. G.; Vendruscolo, M. The Zyggregator method for predicting protein aggregation propensities. *Chem. Soc. Rev.* **2008**, *37*, 1395-1401.

(54)   Chiti, F.; Taddei, N.; Bucciantini, M.; White, P.; Ramponi, G.; Dobson, C. M. Mutational analysis of the propensity for amyloid formation by a globular protein. *EMBO J.* **2000**, *19*, 1441-1449.

(55)   Kim, Y.; Wall, J. S.; Meyer, J.; Murphy, C.; Randolph, T. W.; Manning, M. C.; Solomon, A.; Carpenter, J. F. Thermodynamic modulation of light chain amyloid fibril formation. *J. Biol. Chem.* **2000**, *275*, 1570-1574.

(56)   Ramirez-Alvarado, M.; Merkel, J. S.; Regan, L. A systematic exploration of the influence of the protein stability on amyloid fibril formation in vitro. *PNAS* **2000**, *97*, 8979-8984.

(57)   Ramirez-Alvarado, M.; Regan, L. Does the Location of a Mutation Determine the Ability to Form Amyloid Fibrils? *J. Mol. Biol.* **2002**, *323*, 17-22.

(58)   Chiti, F.; Calamai, M.; Taddei, N.; Stefani, M.; Ramponi, G.; Dobson, C. M. Studies of the aggregation of mutant proteins in vitro provide insights into the genetics of amyloid diseases. *PNAS* **2002**, *99 Suppl 4*, 16419-16426.

(59)   Pedersen, J. S.; Christensen, G.; Otzen, D. E. Modulation of S6 Fibrillation by Unfolding Rates and Gatekeeper Residues. *J. Mol. Biol.* **2004**, *341*, 575-588.

(60)   Dumoulin, M.; Canet, D.; Last, A. M.; Pardon, E.; Archer, D. B.; Muyldermans, S.; Wyns, L.; Matagne, A.; Robinson, C. V.; Redfield, C.; Dobson, C. M. Reduced Global Cooperativity is a Common Feature Underlying the Amyloidogenicity of Pathogenic Lysozyme Mutations. *J. Mol. Biol.* **2005**, *346*, 773-788.

(61)   Hartman, K.; Brender, J. R.; Monde, K.; Ono, A.; Evans, M. L.; Popovych, N.; Chapman, M. R.; Ramamoorthy, A. Bacterial curli protein promotes the conversion of PAP248-286 into the amyloid SEVI: cross-seeding of dissimilar amyloid sequences. *PeerJ* **2013**, *1*, e5.

(62)   Kelly, J. W. The alternative conformations of amyloidogenic proteins and their multi-step assembly pathways. *Current Opinion in Structural Biology* **1998**, *8*, 101-106.

(63)   Chiti, F.; Dobson, C. M. Amyloid formation by globular proteins under native conditions. *Nat. Chem. Biol.* **2009**, *5*, 15-22.

(64)   Jahn, T. R.; Parker, M. J.; Homans, S. W.; Radford, S. E. Amyloid formation under physiological conditions proceeds via a native-like folding intermediate. *Nat. Struct. Mol. Biol.* **2006**, *13*, 195-201.

(65)   Clark, P. L. Protein folding in the cell: reshaping the folding funnel. *Trends Biochem. Sci.* **2004**, *29*, 527-534.

(66)   Gsponer, J.; Vendruscolo, M. Theoretical approaches to protein aggregation. *Protein Pept. Lett.* **2006**, *13*, 287-293.

(67)   Jahn, T. R.; Radford, S. E. The Yin and Yang of protein folding. *FEBS J.* **2005**, *272*, 5962-5970.

(68)   Jahn, T. R.; Radford, S. E. Folding versus aggregation: polypeptide conformations on competing pathways. *Arch. Biochem. Biophys.* **2008**, *469*, 100-117.

(69)   Martinez, J. C.; Serrano, L. The folding transition state between SH3 domains is conformationally restricted and evolutionarily conserved. *Nat. Struct. Biol.* **1999**, *6*, 1010-1016.

(70)   Lindorff-Larsen, K.; Vendruscolo, M.; Paci, E.; Dobson, C. M. Transition states for protein folding have native topologies despite high structural variability. *Nat. Struct. Mol. Biol.* **2004**, *11*, 443-449.

(71)   Carulla, N.; Zhou, M.; Arimon, M.; Gairi, M.; Giralt, E.; Robinson, C. V.; Dobson, C. M. Experimental characterization of disordered and ordered aggregates populated during the process of amyloid fibril formation. *Proc. Natl. Acad. Sci. USA* **2009**, *106*, 7828-7833.

(72)   Ventura, S.; Zurdo, J.; Narayanan, S.; Parreno, M.; Mangues, R.; Reif, B.; Chiti, F.; Giannoni, E.; Dobson, C. M.; Aviles, F. X.; Serrano, L. Short amino acid stretches can mediate amyloid formation in globular proteins: The Src homology 3 (SH3) case. *PNAS* **2004**, *101*, 7258-7263.

(73)   Guijarro, J. I.; Sunde, M.; Jones, J. A.; Campbell, I. D.; Dobson, C. M. Amyloid fibril formation by an SH3 domain. *Proc. Natl. Acad. Sci. USA* **1998**, *95*, 4224-4228.

(74)   Neudecker, P.; Robustelli, P.; Cavalli, A.; Walsh, P.; Lundstrom, P.; Zarrine-Afsar, A.; Sharpe, S.; Vendruscolo, M.; Kay, L. E. Structure of an intermediate state in protein folding and aggregation. *Science* **2012**, *336*, 362-366.

(75)   Casares, S.; López-Mayorga, O.; Vega, M. C.; Cámara-Artigas, A.; Conejero-Lara, F. Cooperative propagation of local stability changes from low-stability and high-stability regions in a SH3 domain. *Proteins: Structure, Function, and Bioinformatics* **2007**, *67*, 531-547.

(76)   Dobson, C. M. Protein folding and misfolding. *Nature* **2003**, *426*, 884-890.

(77)   Vivekanandan, S.; Brender, J. R.; Lee, S. Y.; Ramamoorthy, A. A partially folded structure of amyloid-beta(1-40) in an aqueous environment. *Biochem. Biophys. Res. Commun.* **2011**, *411*, 312-316.

(78)   Fezoui, Y.; Teplow, D. B. Kinetic studies of amyloid beta-protein fibril assembly. Differential effects of alpha-helix stabilization. *J. Biol. Chem.* **2002**, *277*, 36948-36954.

(79)   Nanga, R. P.; Brender, J. R.; Xu, J.; Veglia, G.; Ramamoorthy, A. Structures of rat and human islet amyloid polypeptide IAPP(1-19) in micelles by NMR spectroscopy. *Biochemistry* **2008**, *47*, 12689-12697.

(80)   Palhano, F. L.; Lee, J.; Grimster, N. P.; Kelly, J. W. Toward the molecular mechanism(s) by which EGCG treatment remodels mature amyloid fibrils. *J. Am. Chem. Soc.* **2013**, *135*, 7503-7510.

(81)   Popovych, N.; Brender, J. R.; Soong, R.; Vivekanandan, S.; Hartman, K.; Basrur, V.; Macdonald, P. M.; Ramamoorthy, A. Site specific interaction of the polyphenol EGCG with the SEVI amyloid precursor peptide PAP(248-286). *J. Phys. Chem. B* **2012**, *116*, 3650-3658.

(82)   Zhang, T.; Zhang, J.; Derreumaux, P.; Mu, Y. Molecular mechanism of the inhibition of EGCG on the Alzheimer Abeta(1-42) dimer. *J. Phys. Chem. B* **2013**, *117*, 3993-4002.

SUPPLEMENTARY INFORMATION

Text S1:

Determination of initial rates of growth

In this study, initial rates of growth of amyloid structure were calculated by fitting the initial region of the ThT kinetics curves using a double exponential function:

$$y = y_0 + A_1 \times e^{-k_1 t} + A_2 \times e^{-k_2 t} \qquad (1)$$

The initial slope of the ThT curves was then accurately calculated from the resulting fitting parameters as:

$$r_0 = \left(\frac{dy}{dt} \right)_{t \to 0} = A_1 \cdot k_1 + A_2 \cdot k_2 \qquad (2)$$

The fit of the initial ThT curve (Figure S1) is only used for extrapolation purposes and only the initial slope (extrapolated to time zero) is considered. This operational extrapolation procedure allowed us an accurate determination of the initial slopes of the ThT curves and avoided the assumption of any time interval in the kinetics to define an initial aggregation rate.

Another alternative method of the initial slope was also tested by calculating the first derivative of the kinetic trace and extrapolated it to time zero. As shown in Table S1, the results obtained by the two procedures are identical.
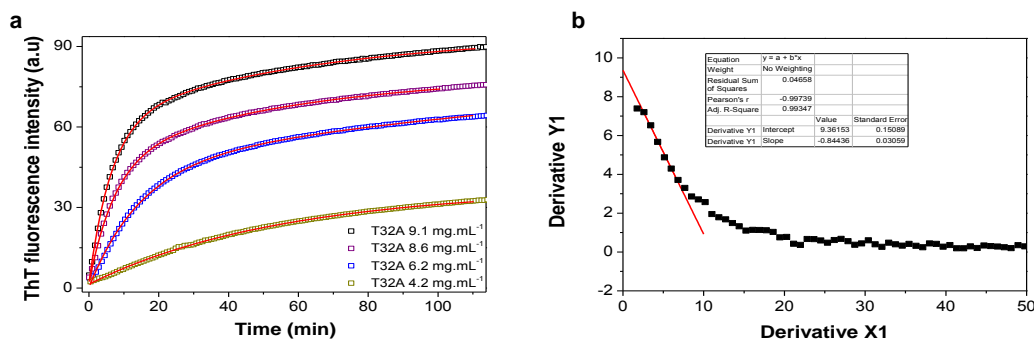
Figure S1: (a) Aggregation kinetics curves of T32A-N47A obtained from ThT fluorescence experiments. Symbols represent the experimental data and the continuous lines correspond to the best fit to equation 1. (b) First derivative of the ThT kinetics curve obtained for T32A-N47A (9.1 mg.mL⁻¹) is represented in black squares. The tangent of the maximum decay is shown as the red line.

Concentration (mg.mL^{-1})	Equation 2	First derivative
9.1	9.80	9.36
8.6	6.70	6.82
6.2	3.28	3.25
4.2	0.65	0.66

Table S1: Initial rates obtained from ThT aggregation kinetics performed at different protein concentrations using the two methods described.

Mutant	T_m (°C)	ΔH_m (kJ.mol^{-1})
N47A[a]	51.2 ± 0.1	152.1 ± 0.4
N47A-L10A	30.3 ± 0.1	77.0 ± 0.5
N47A-R21D	53.5 ± 0.1	155.4 ± 0.3
N47A-K27A	46.7 ± 0.1	129.5± 0.6
N47A-T32A	41.6 ± 0.1	108.8 ± 0.2
N47A-N38A	38.6 ± 0.1	101.3 ± 0.3
N47A-K43A	43.9 ± 1.0	60.9 ± 4.2
N47A-V46A	42.3 ± 0.1	113.7 ± 0.4
N47A-D48G	55.7± 0.1	164.1 ± 0.4
N47A-V53A	54.5 ± 3.1	61.1 ± 6.7
N47A-A56G	46.1 ± 0.1	145.5 ± 0.4
N47A-V58A	56.1 ± 2.8	54.3 ± 4.8

Values of the unfolding temperature (T_m) and enthalpy change (ΔH_m) have been obtained by two-state analysis of the DSC unfolding transitions. The errors have been estimated from the fittings as 95% confidence intervals for each parameter.

[a] : Data taken from Morel *et al.,* [20].

Table S2. Thermodynamic parameters of the equilibrium thermal unfolding of N47A Spc-SH3 and the double mutants measured by DSC in 0.1 M Glycine, 0.1 M NaCl pH 3.2.
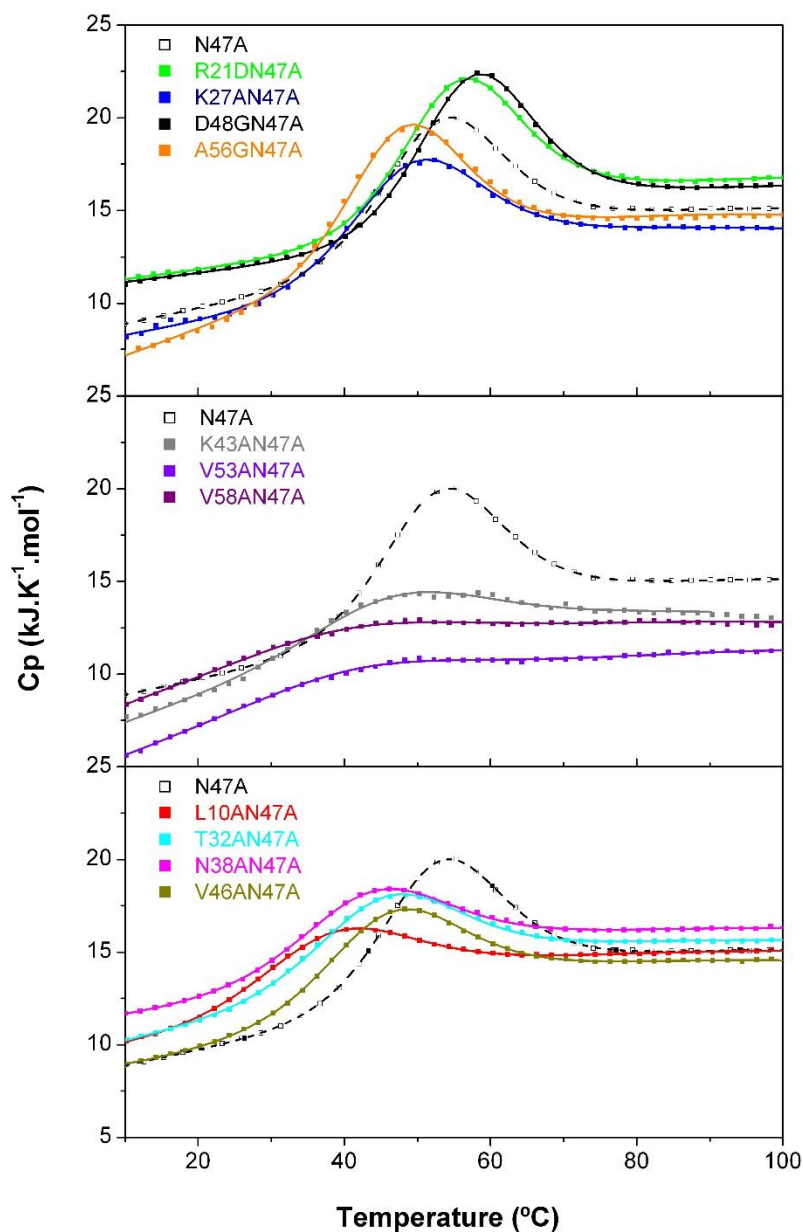
Figure S2. DSC experiments of N47A and the double mutants of Spc-SH3·domain. *Experiments were carried out at low protein concentration in 0.1 M Gly, 0.1 M NaCl pH 3.2. Symbols represent the experimental data and the lines correspond to the best fit using the two-state unfolding model. For sake of clarity, experimental*

data of N47A mutant is shown in open squares and the best fit using the two-state unfolding model in dashed lines.
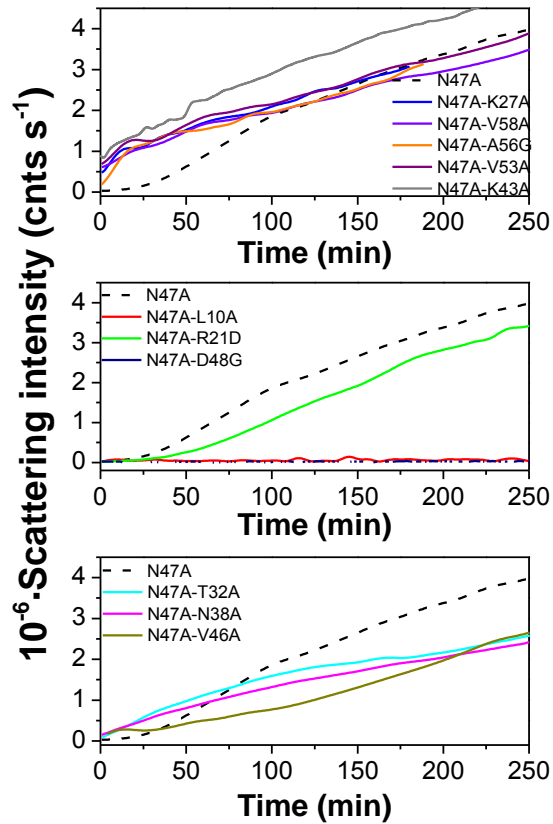
Figure S3. Aggregation kinetics at 37 ºC of the double mutants and the N47A mutant followed by scattering intensity.
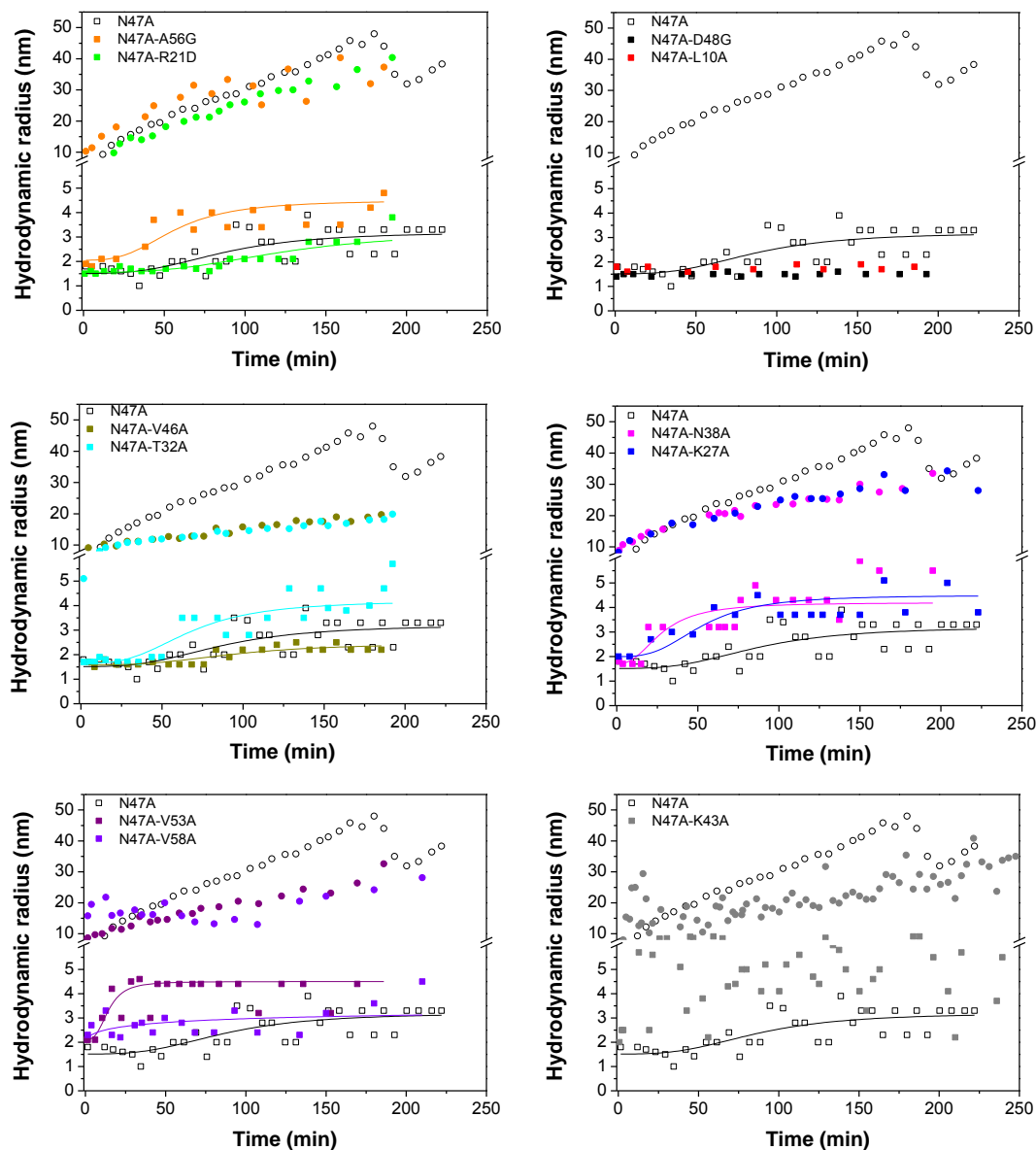
Figure S4. ***Time evolution of the apparent hydrodynamic radii (Rh) for the two smallest peaks in the particle size distributions measured by DLS during the course of fibrillation of the N47A and the double mutants of*** ***α-Spc SH3 domain.*** *The continuous lines represent the best fit of the time dependence of the apparent R_h using a logistic sigmoidal function.*
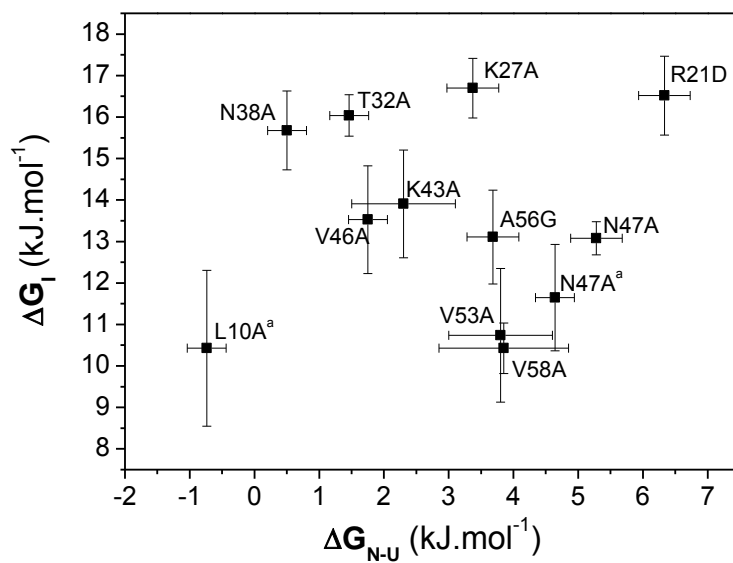
Figure S5. The energy changes produced by the different mutations in the native-state stability do not correlate with the changes in the rates of nucleation. Plot of ΔG_I versus ΔG_{N-U}. [a] Determined from aggregation kinetics studied in the presence of 0.2 M NaCl.
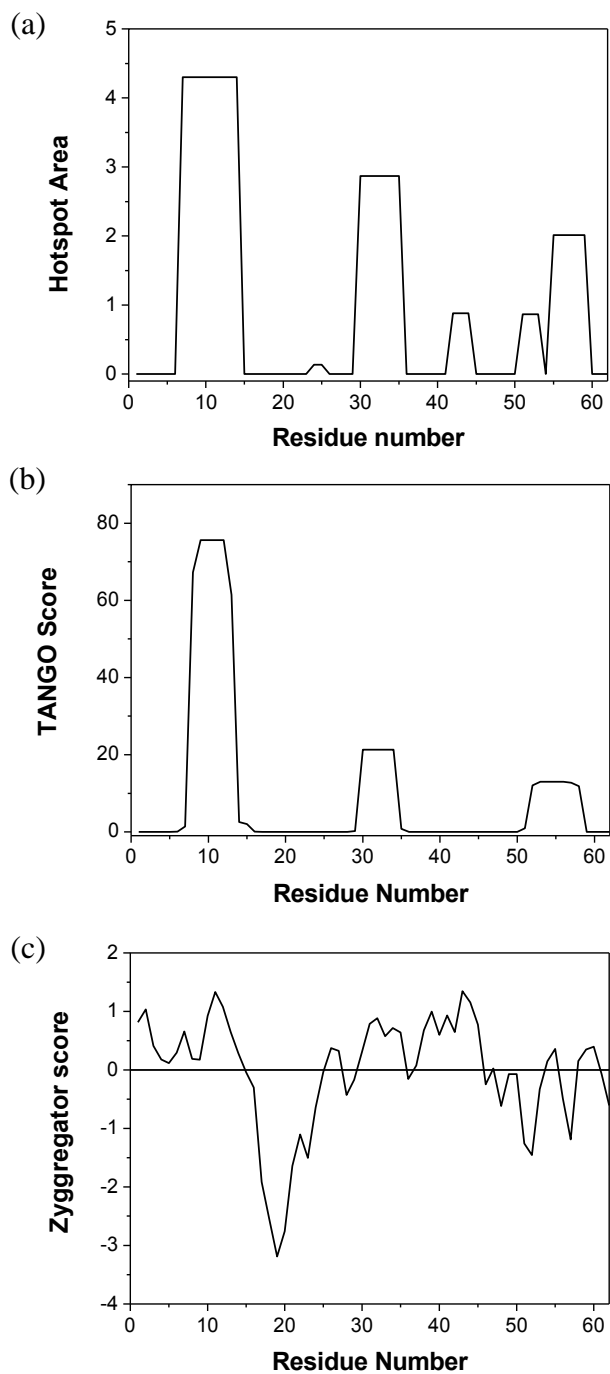
Figure S6. The aggregation propensity of the primary sequence of N47A Spc-SH3 domain predicted by the algorithms (a) Aggrescan [51] (b) TANGO [52] and (c) Zyggregator [53].

Chapter 5

N-TERMINAL ACETYLATION OF α-SYNUCLEIN DECREACES THE POPULATION OF PARTIALLY FOLDED OLIGOMERS AND REDUCES AMYLOID AGGREGATION

ABSTRACT

Parkinson's disease is a neurodegenerative disorder with a high impact in our society. This is one of several diseases related to the oligomerization and aggregation of α-Synuclein (aSyn). The interaction of aSyn with surfactants, lipids and membranes appears to play a key role in its physiological function. The aSyn found in cells presents a post-transcriptional modification consisting of the acetylation of its N-terminus, which appears to affect its behavior and therefore also its function. Sodium dodecyl sulfate (SDS) has been widely used as a simple model for membrane environment and has been reported to accelerate amyloid fibrillation of aSyn *in vitro*. In this study, we compared N-acetylated and unacetylated aSyn in their mode of interaction with SDS and related their different properties with their amyloidogenic propensity. We found that in the presence of sub-CMC concentrations of SDS aSyn forms SDS-associated partially folded oligomers. These oligomers appear to constitute optimal species for spontaneous and efficient formation of amyloid nuclei, which further drive rapid, lag-free amyloid fibrillation. N-acetylation reduces the extent of aSyn oligomerization favoring its interaction with micelles, thereby reducing the rate of formation of amyloid nuclei.

INTRODUCTION

Parkinson's disease (PD) is the most common neuronal motor system disorder. This neurodegenerative disease affects more than 1% of the population aged over 65 [1]. PD is characterized by the loss of dopaminergic neurons in the "*substantia nigra*" and the appearance of intraneuronal inclusions, composed basically by proteins, known as Lewy bodies [2,3]. These Lewy bodies are also implied in the multiple system atrophy and other synucleinopathies, including dementia [4-6,7,8]. The major components of the Lewy bodies are fibrillar aggregates of α-synuclein (aSyn) [9], a 140 amino-acids protein particularly abundant in the presynaptic terminals [10], and its oligomeric forms. These oligomers are believed to play a role in the progress of PD [11] [12].

aSyn has been considered for many years to be an intrinsically disordered protein with high net charge and low hydrophobic content [13]. However, its native state has been described very

recently as a folded tetramer [14,15], although this finding has led to many discussions in the scientific community [16-18]. For this reason, its precise physiological function has yet to be established, although different studies suggest a function related to lipids and membrane . Although aSyn presents a mostly disordered structure in aqueous solution [13], it could adopt α-helical structure when binding to negatively charged membranes [19]. A range of interactions with lipids has been described for the aSyn, such as: transporting and regulating poliunsaturated fatty acids (PUFAs) in dopaminergic neurons[20,21] [22], modulating presynaptic vesicle pool size and vesicle recycling[23], inducing curvature in them[24] and due to its interactions with membranes a type of membrane remodeling function is proposed[25,26]. The interactions of aSyn with small droplets of docohexanoic acid (DHA), which is very abundant in the brain, induce α-helical structure in the protein and protect against proteolysis the N-terminus[27], In addition, exposure of aSyn with high levels of PUFAs, has been described to promote the formation of cytotoxic aSyn oligomers and both *in vivo* [28] [29] and *in vitro* [30] [31].

In general, many studies have suggested that aSyn exists mostly as unfolded monomers but in equilibrium with labile oligomeric forms [32,33]. On the other hand, oligomers with amyloid structure are often observed in coexistence with amyloid fibrils, but many aspects of the relationship between oligomerization and the mechanism of amyloid fibril assembly are not yet understood. It has been evidenced recently that amyloid oligomers are the main toxic species in amyloidogenesis [34-39]. Moreover, these kinetic intermediates have appeared to be highly modified by a change in the protein N-terminus[14,40]. N-α-Acetylation is one of the most common post-translational modifications occurring in eukaryotic cells. It has been suggested that up to 80–90% of mammalian and 40–50% of yeast proteins bear an N-α-acetyl group. Nevertheless, the role of this modification, which affects thousands of proteins, remains poorly understood. This post-transcriptional modification increases the hydrophobicity of the N-terminal section of the protein and also favors protein-protein interactions within the cells[41]. Despite the identification of quantitative N-acetylation of aSyn both as soluble protein and entrapped within Lewy bodies from human PD brains [42], most of the biophysical studies investigating aSyn structural, biochemical, and aggregation

properties in vitro have been relying on recombinant aSyn from *E. coli*, which is not acetylated.

Sodium dodecyl sulfate (SDS) is an anionic surfactant commonly used in biophysical studies to mimic membrane environments for proteins and indeed it has been extensively used with aSyn [43-47] [48]. The SDS interacts with aSyn in a complex pathway, presenting a dual behavior. Firstly, increasing the SDS concentration stabilizes the amyloidogenic conformations until a maximum of amyloidogenic propensity, between 0.5-1 mM SDS. Upon a subsequent increase in SDS concentration, this amyloidogenic propensity decreases concurrently with an increase of the α-helix content [43,45,46]. Moreover, recent reports have described an increase of the affinity of the Nac-aSyn for lipids and physiological membranes and a decrease in its aggregation propensity[49,50]. However, despite the amount of existing information, the link between the conformational effects of N-acetylation on unstructured aSyn, the changes produced on aSyn-surfactant interactions, and the consequences in the formation of amyloidogenic oligomers and fibrils is not well understood.

In this study, we compare the biophysical properties of the N-acetylated (Nac-aSyn) and unmodified (aSyn) synucleins and analyze the effect of SDS on their structure, oligomerization and amyloid aggregation. We demonstrate that low concentrations of SDS (sub-CMC conditions[45]) promote the accumulation partially-folded oligomeric species in aSyn. Moreover, N-acetylation reduces significantly the population of these oligomers and decreases the rate oligomer-mediated amyloid aggregation. These results give insight into the interactions between aSyn and surfactant molecules and help to understand the mechanisms by which this type of interactions may promote conditions favoring amyloid oligomerization and fibrillation and thereby the appearance of cellular toxicity mediated by aSyn oligomers in membrane environments.

MATERIALS AND METHODS

Purification of αSyn WT and WT acetylated

The N-acetylated and unmodified forms of aSyn were produced by overexpression in *E.Coli* modified with the plasmid encoding human aSyn (to obtain the Nac form it is necesary to add the NatB plasmid to the cells and 5 µg/mL chloramphenicol to the LB media[51]). The cells were grown in LB media in the presence of 100 µg/mL of ampicillin at 37ºC with shaking until an optical density at 600 nm of 0.6–0.8. Protein expression was induced by adding isopropyl 1-thio-β-D-galactopyranoside to a final concentration of 50 µg/mL (0.2 mM) for 4 h. The cells were harvested by centrifugation at 2200 g for 10 min at 4 ºC. The pellets were resuspended in buffer (25 mM TRIS, 1 mM EDTA, 0.1 mM DTT, pH 7.4, 1 x protease inhibitor mixture (sigma)) and lysed by ultrasonication. The lysate was ultracentrifuged at 105000 g for 45 min at 4 ºC. The supernatant was filtered (0.45 µm) and applied onto a HiTrap QFF anion-exchange column (GE Healthcare) previously equilibrated in buffer (50 mM TRIS, 0.1 mM DTT, pH 7.4). Protein was eluted with 150 mL of buffer with a gradient of NaCl concentration (0-500 mM) in an Äkta Prime FPLC (GE Healthcare). After analysis by SDS-PAGE, the fractions containing the protein were precipitated with ammonium sulfate at 47.5 % of saturation and ultracentrifuged at 105000 g for 30 min at 4ºC. The precipitate was resuspended (50 mM TRIS, 50 mM NaCl, 8M urea, 0.1 mM DTT,pH 8.3) and injected in a HiLoad 26/60 Superdex 200 column (GE Healthcare). Then, the eluted protein fractions, analyzed by SDS-PAGE, were pooled and dialyzed extensively against the same buffer in the absence of urea. Then, the protein was concentrated (Amicon ultracentrifugal filter units MWCO 3.000, Millipore) and injected in a HiLoad 26/60 Superdex 75 column (GE Healthcare). Pure pooled fractions were dialyzed against 20 mM HEPES, 0.05% NaN3, pH 7.2, lyophilized and kept frozen at -20ºC. N-terminal acetylation was verified by electrospray mass spectrometry giving a molecular weight of 14502.1 Da for Nac-aSyn and 14460.1 Da for aSyn.

Sample preparation

The lyophilized protein was dissolved in 20 mM HEPES pH 7.2, containing 0.05% NaN_3 except for the CD experiments described below. The protein concentration was determined by the measurement of absorbance at 280 nm using 5960 M^{-1} cm^{-1} as molar absorptivity, calculated as described [52].

Thioflavin T Fluorescence

Kinetic experiments were performed to monitor amyloid fibril aggregation at 37°C by continuous measurement of Thioflavin T (ThT) fluorescence [53] as described elsewhere [54]. Fluorescence was recorded using a Varian Cary Eclipse spectrofluorimeter (Agilent Technologies, Santa Clara, CA, USA) equipped with a Peltier-controlled thermostatic cell holder. Stock solutions of 200 μM ThT and 100 mM SDS were prepared in pure water (Milli-Q). Protein samples were freshly prepared in 20 mM HEPES, 0.05% NaN_3, pH 7.2, in an appropriate concentration in order to obtain a final protein concentration of 100 μM. In order to avoid evaporation during the experiments, the cuvette was sealed using a specific stopper.

Differential Scanning Calorimetry

Temperature scans were performed at protein concentrations of 20, 60 and 100 μM in a VP-DSC microcalorimeter fitted with capillary cells (MicroCal, Northampton,MA, USA). DSC scans were run between 5°C and 125°C at a scan rate of 2°C min^{-1}. The reversibility of the thermal unfolding was always checked in a second consecutive scan of the same sample. Several buffer–buffer baselines were obtained before each run with the protein solution in order to ascertain proper equilibration of the instrument. Instrumental baselines were subtracted to the experimental thermograms of the samples and the time response of the calorimeter was then corrected. The partial molar heat capacity curves (Cp) were calculated and analyzed using Origin 7.0 (OriginLab, Northampton, MA, USA).

Determination of hydrodynamic radius by Dynamic Light Scattering

DLS measurements were performed at 25ºC using a DynaPro MS-X instrument (Wyatt Technology Corporation, Santa Barbara, CA, USA) in a thermostated 30 μl quartz cuvette. The protein solutions and the buffer were filtered through 0.02 μm Anotop 10 filters (Whatman plc, Brentford, Middlesex, UK) immediately before the measurements. Sets of DLS data were acquired at 25°C every 10 s until 20 sets of data were obtained. Dynamics V6 software (Wyatt Technology Corporation, Santa Barbara, CA, USA) was used in data collection and processing. The experimental autocorrelation curves data were analyzed to obtain the particle size distributions using the regularization fit as implemented in Dynamics V6 software. Total scattering intensity measurements were also made with the same instrument as a function of the SDS concentration. The intensities changes were normalized using the following expression:

$$I_{norm\ i} = \frac{I_{final} - I_i}{I_{final} - I_{Initial}}$$

Gel-filtration Chromatography coupled to Static/Dynamic Light Scattering

The samples were run at room temperature on a Superdex 200 10/300 GL (GE Healthcare) at a flow rate of 0.5 mL/min coupled with a Zetasizer DLS Malvern instrument (Worcestershire,UK) for simultaneous detection of UV absorption and light scattering. The samples were freshly prepared in the appropriate buffer at a concentration of 100 μM and the column was previously equilibrated in the same buffer. The chromatograms were analyzed by the OmniSEC 4.7 analysis software, using bovine serum albumin as a standard sample for the calibration of the instrument. This technique allows us obtaining simultaneously for each eluted peak the weight-averaged molecular masses (Mw) from static light scattering measurement, as well as the apparent hydrodynamic radius, R_h, by DLS measurements independently of the Ve.

Determination of secondary structure by Circular Dichroism (CD)

Far-UV CD measurements were made at 25ºC in a Jasco J-715 spectropolarimeter (Tokyo, Japan) equipped with a thermostatic cell holder in a 10 mm path length cuvette. The protein samples were prepared and dialyzed using a buffer without NaN_3 due to the intense absorption band that the sodium azide produces (near 210 nm). The protein concentration used was 100 μM. Represented data were the average of 5 scans using a bandwidth of 1 nm and a scan speed of 100 nm/min. The α-helix content was estimated using the mean residue ellipticity value at 222 nm as described elsewhere [55].

Transmission Electron Microscopy (TEM)

A Carl Zeiss LEO 960E (Zeiss, Oberkochen, Germany) transmission electron microscope was used for the analysis of the αSyn aggregates morphology. The samples were incubated in different conditions for 30 and 150 minutes at 37ºC. 10 μL of the incubated solution were placed on a Formvar 300-mesh copper grid (ANAME, Madrid, SP) for 1 minute. The sample was negatively stained with 10 μL of 1% (w/v) uranyl acetate solution for 1 minute. Excess stain was removed with a tissue paper and the grids were air dried before visualization. The samples were observed at a magnification between 60000 and 100000.

RESULTS

α-Synuclein Binds SDS in a Partially Folded α-Helical Conformation

The secondary structures of aSyn and Nac−aSyn at 100 microM were compared by CD in the presence of different SDS concentrations. In the absence of SDS, the far UV CD spectra obtained for both proteins are similar (Figure S1). The resulting spectra show a marked characteristic shape corresponding to random coil structure. These results are in agreement with previous studies reporting the intrinsically disordered nature of aSyn [43,50].

Upon addition of SDS (Figure S2), the progressive development of a minimum at 222 nm indicates that aSyn acquires α-helical structure as a result of interactions with SDS [45] with a value up to ~45% for unmodified aSyn and ~50% for Nac-aSyn reached in the presence of 5 mM SDS. However, the titration experiments over a range of SDS concentrations show different behaviors between Nac-aSyn and unmodified aSyn (Figure 1b). For aSyn the process can be described by two phases, one below about 0.7 mM SDS, where the α-helical content increases linearly up to a 30%, and a second phase above 0.7 mM SDS, where the α-helical structure develops more smoothly with the increase in SDS concentration, until ~5 mM SDS (Figure 1b). Although below 0.7 mM SDS the α-helical growth is quite parallel for both proteins, it appears to be slightly retarded for Nac-aSyn compared to the unmodified aSyn. In addition, for Nac-aSyn the structure develops linearly and steadily until ~1.5 mM SDS, from which the α-helical content remains practically unaltered upon further addition of SDS. Therefore, the structural change induced by SDS in Nac-aSyn appears to be more cooperative than for unmodified aSyn. This could be a result of a higher affinity of Nac-aSyn for SDS micelles [49].
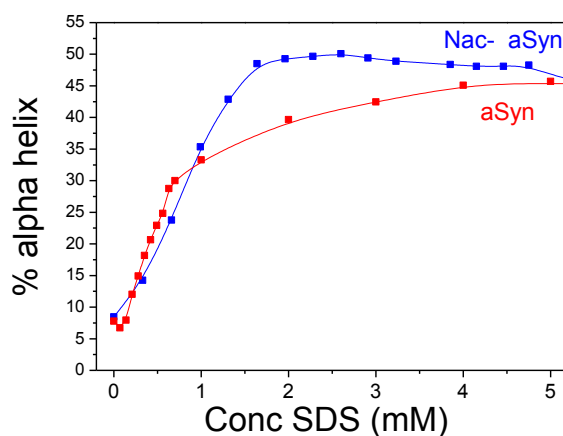
Figure 1. SDS induces α-helical structure in unmodified aSyn and Nac-aSyn. The graph shows the percentage in α-helix as a function of the concentration of SDS. The colors used are red for aSyn and blue for the Nac-aSyn. In splines lines represent the tendencies of the different phases.

The hydrodynamic radius is highly dependent on SDS concentration

As we have shown by far UV CD experiments, the secondary structure of aSyn is highly dependent on the SDS concentration as a result of interactions with the surfactant. This gain in α-helical structure could also be associated to changes in molecular size of the protein, as well as to the formation of micelles and/or oligomerization. For this reason the particle size was analyzed at different concentrations of protein and SDS using dynamic light scattering (DLS).
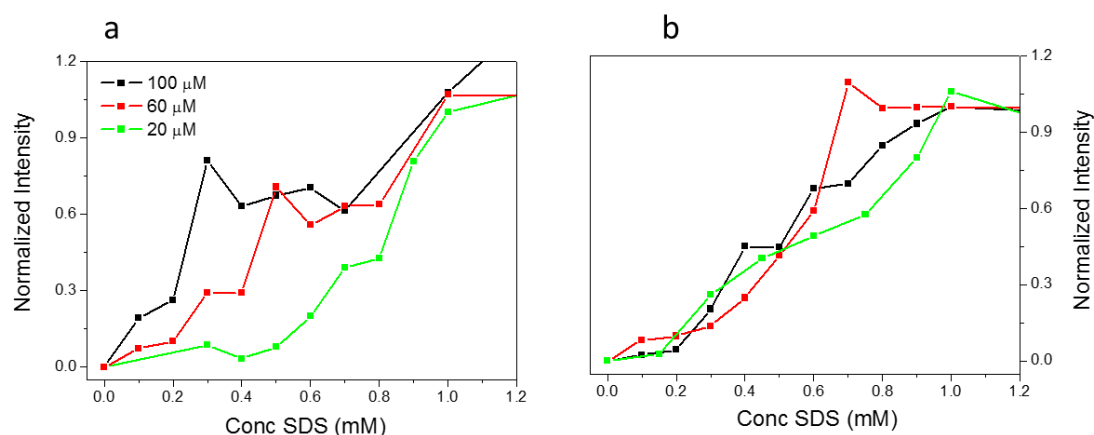
Figure 2. Effect of the SDS concentration on the scattering intensity of aSyn (a) and Nac aSyn (b). *The experiments were performed at the protein concentration indicated in the graphs.*

Firstly, we measured the increase in total scattering intensity associated to the addition of SDS to the buffer. The scattering intensity is correlated to the formation of large particles in solution such as oligomers or micelles. From these data we estimated a critical micellar concentration (CMC) of 7.45 mM for SDS (Figure S2, Supplementary material) in good agreement with the value described elsewhere[43]. Then, we measured the scattering intensity increase produced by SDS addition in the presence of different protein concentrations (Figure 2). According with these data, both protein forms produce a dramatic decrease of the apparent CMC of SDS similarly to previous reports [56]. Moreover, for unmodified aSyn a significant dependence of the intensity growth with the protein concentration can be appreciated at intermediate SDS concentrations, whereas for Nac-aSyn we observed a very similar transition for all the concentrations.
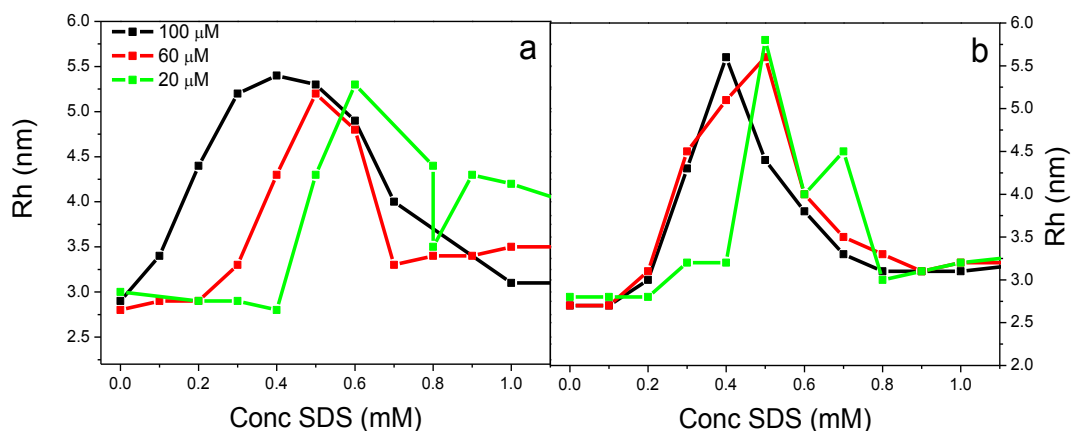
Figure 3. Effect of SDS concentration on the hydrodynamic radius of WT aSyn (a) and Nac aSyn (b). *Experiments were carried out at different protein concentrations as indicated in the graphs.*

In addition to the scattering intensities, the DLS data provide a richer picture about the particle size distributions in the protein-SDS mixtures. In the absence of SDS, both Nac-aSyn and unmodified aSyn have a similar hydrodynamic radius (R_h) of ~2.9 nm. Similar values were previously reported [57] and are in agreement with aSyn being a monomeric largely unstructured protein. Upon SDS addition, the particle size distributions changed progressively. Significant differences between the Nac-aSyn and unmodified aSyn occur at low SDS concentration concomitantly with the appearance of α-helical structure as observed in the far UV CD spectra. This change can be appreciated as an increment in the apparent R_h for the small particles until ~5-6 nm. The range of SDS concentrations at which the maximum R_h values are reached is dependent on the protein concentration and different between the two protein forms. This range is considerably broader for aSyn than for Nac-aSyn. This transitory increment in apparent R_h could be related to an oligomerization of the protein induced by SDS. It would appear then that Nac-aSyn presents a lower effect in the position of the maximum.

Once past this maximum R_h (~0.8-1 mM SDS), a further increase of the SDS concentration produces the progressive decrease of R_h down to ~3.0-3.2 nm. These conditions are over the apparent CMC, and the radius is compatible with a SDS micelle (~2 nm) associated with an

aSyn molecule. That could imply that, concurrent with the increase of structure, shown in the far UV-CD spectra, a transition occurs from aSyn oligomers to aSyn monomers associated with the SDS micelles. The similar R_h values reached at high SDS concentrations indicate the high similarity of the state reached for both protein forms.

aSyn oligomers formed at low SDS concentration can be detected by size exclusion chromatography (SEC)

The apparent oligomerization of aSyn observed by low SDS concentrations may induce a variation of the elution volume (Ve) in SEC experiments. Here, we examined in more detail the potential oligomeric state differences between the aSyn and Nac-aSyn. To this end, we performed analytical SEC coupled to on-line determination of absolute molecular weight by laser light scattering. aSyn and Nac-aSyn were dissolved at a concentration of 100 μM in buffer with or without SDS and injected in a Superdex 200 10/300 GL SEC column at a flow rate of 0.5 mL/min. In absence of SDS, aSyn has a Ve anomalously low for a molecular weight of 14460.1 Da. If aSyn were a globularly folded protein, according to the calibration performed on the column using standard globular proteins, it would elute at around 20.9 mL. This difference can be explained by the fact that aSyn has an expanded random coil structure. Both aSyn and Nac-aSyn proteins eluted at an identical volume of 13.7 ml (Figure 4, Table 1), suggesting that N-acetylation does not have a large impact on the overall hydrodynamic behaviour of aSyn. Furthermore, the molecular weights estimated by light scattering from these eluted peaks for Nac-aSyn (16000 Da) and aSyn (17000 Da) are consistent with a monomeric state.
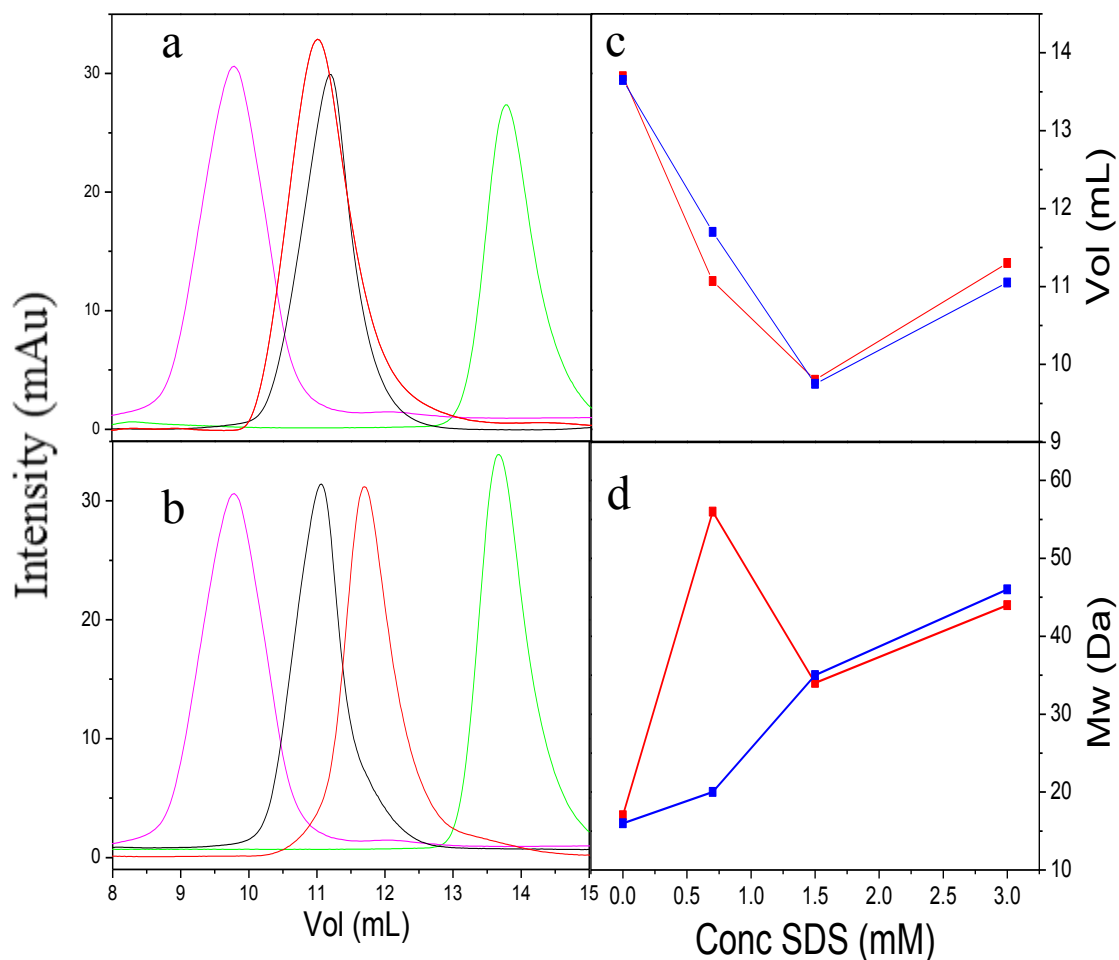
Figure 4. *Effect of SDS in aSyn and Nac-aSyn by size exclusion chromatography. The graphs a and b correspond to the elution profiles of **aSyn and Nac-aSyn** respectively in the presence of different SDS concentrations (0 mM (green); 0.7 mM (red); 1.5 mM (pink) and 3 mM (black)). The graph c represents the Ve of the proteins versus the SDS concentration, and the graph d shows the absolute molecular weight versus the SDS concentration. In both graphs c and d the aSyn and the Nac-aSyn data are represented in red and blue respectively.*

With the addition of SDS a shift to lower Ve is produced in all cases. SEC is a separative technique and therefore produces a dilution of the sample. For this reason, the effective protein concentration of this analysis might be ~20-30 μM. Accordingly, these data would be comparable to the DLS measurements in batch shown above at 20 μM concentration of protein. When the concentration of SDS increases, significant differences exist between the N-acetylated and unmodified forms. At a concentration of 0.7 mM SDS, aSyn elutes

considerably earlier than Nac-aSyn indicating a higher hydrodynamic size. The apparent R_h of the protein eluting in this peak and its absolute Mw indicates an oligomeric state for aSyn associated to SDS molecules under these experimental conditions. In contrast, the R_h and Mw values are considerably smaller for Nac-aSyn, suggesting no detectable oligomerization at 0.7 mM SDS by this technique.

When we increase the SDS concentration until 1.5 mM SDS the shift produced is maximum (Ve ~9.8 mL) and similar for both aSyn forms. According to the column calibration, such Ve corresponds to that of a globular protein of about 200 kDa, meanwhile according to the analysis using the scattering intensity data, the absolute Mw is about 34-35 kDa for both forms (2.4 times the Mw of aSyn). This could be associated with a protein monomer that binds to SDS micelles (made of 50-90 SDS molecules[45]) as we have shown in the scattering measurements (Figure 2). A further increase of the SDS concentration (3 mM), as it has been shown in far UV-CD (Figure 1), produces the appearance of 45% α-helical structure for the aSyn and 50% of the Nac-aSyn form. These highly folded species probably present a more compact structure. The higher Mw might be related to an increase in the number of SDS molecules incorporated into the micelles and/or to the incorporation of another aSyn molecule to the protein-micelle complex. Under these conditions, the Ve for Nac-aSyn is ~11 mL, slightly lower than for the unmodified form (~11.3 mL). This difference could be interpreted as a result of a higher affinity of the N-acetylated protein for the SDS micelle. Nevertheless, the Mw values measured from the elution peaks at each SDS concentration should be interpreted as apparent averages of different protein-SDS complexes coexisting in rapid exchange.

Table 1. *Elution volumes, molecular weights and average hydrodynamic radii at different concentrations of SDS measured by SEC-scattering as represented in Figure 4.*

	Conc SDS (mM)	Ve (mL)	Mw (Da)	Rh (nm)
aSyn	0	13.70	17000	2.7
	0.7	11.07	56000	5.9
	1.5	9.80	34000	4.3
	3	11.30	44000	4.2
Nac-aSyn	0	13.65	16000	3.1
	0.7	11.70	20000	3.5
	1.5	9.75	35000	4.3
	3	11.05	46000	4.4

In summary, N-acetylation appears to reduce the degree of aSyn oligomerization at sub-CMC SDS concentrations. At supra-CMC SDS concentrations, the differences between the aSyn forms are reduced but Nac-aSyn migrates slightly before than the unmodified aSyn, which implies a slightly larger size of the complex aSyn-SDS micelle.

N-acetilation increases the stability of aSyn-SDS mixed micelles and reduces the range of existence of protein oligomers

As it has been already shown, aSyn and Nac-aSyn can interact with SDS differently, with formation of oligomers and mixed protein-SDS micelles to different extents, depending on the conditions and concentrations. These processes are accompanied by acquisition of α-helical structure by both aSyn forms. To understand the energetic changes associated to these processes, the effect of thermal melting of these protein-SDS complexes could be followed by DSC. The DSC thermograms measured at different protein and SDS concentrations are shown for both proteins in Figure 5.

In the absence of SDS, neither aSyn nor Nac-aSyn show any unfolding transition in the DSC thermograms. These results agree perfectly with an unstructured conformation for both

proteins as described in the literature[58,59], and also with our circular dichroism results indicating the lack of specific secondary structure under these experimental conditions.

As the concentration of SDS increases, we could observe the appearance of a faint transition around ~50ºC that further grows and shifts until ~70ºC. Moreover, these transitions show a fully reversible behavior that implies an equilibrium process, therefore susceptible of being analyzed thermodynamically.

This shift and the width of the transition give us an idea of the complexity of the process, which has precluded so far a quantitative analysis of the data. However, a variety of qualitative information can be obtained such as an estimation of thermal stability of the protein-SDS complexes, as indicated by the melting temperature (Tm), an approximation to the amount and level of acquired structure, indicated by the unfolding enthalpy (ΔH) and an idea about the degree of hydration of the hydrophobic surface of the protein and surfactant, estimated by the heat capacity change (ΔCp). Those data are listed in the tables 2 and 3 and represented in Figure 6.

In addition, the emergence of the melting transition in both protein forms appears to be affected by the protein concentration. In the case of the unmodified aSyn, the transition starts to occur at 0.7 mM SDS for 20 μM of protein (5a), at 0.5 mM for 60 μM (5b) and at 0.4 mM SDS for 100 μM (5c). Meanwhile, for Nac-aSyn, the transitions arise at lower SDS concentrations, at 0.6 mM SDS for 20 μM (5d) and at 0.4 mM SDS for both 60 μM (5e) and 100 μM (5f). This could be interpreted as a result of a higher affinity for SDS of the acetylated form.
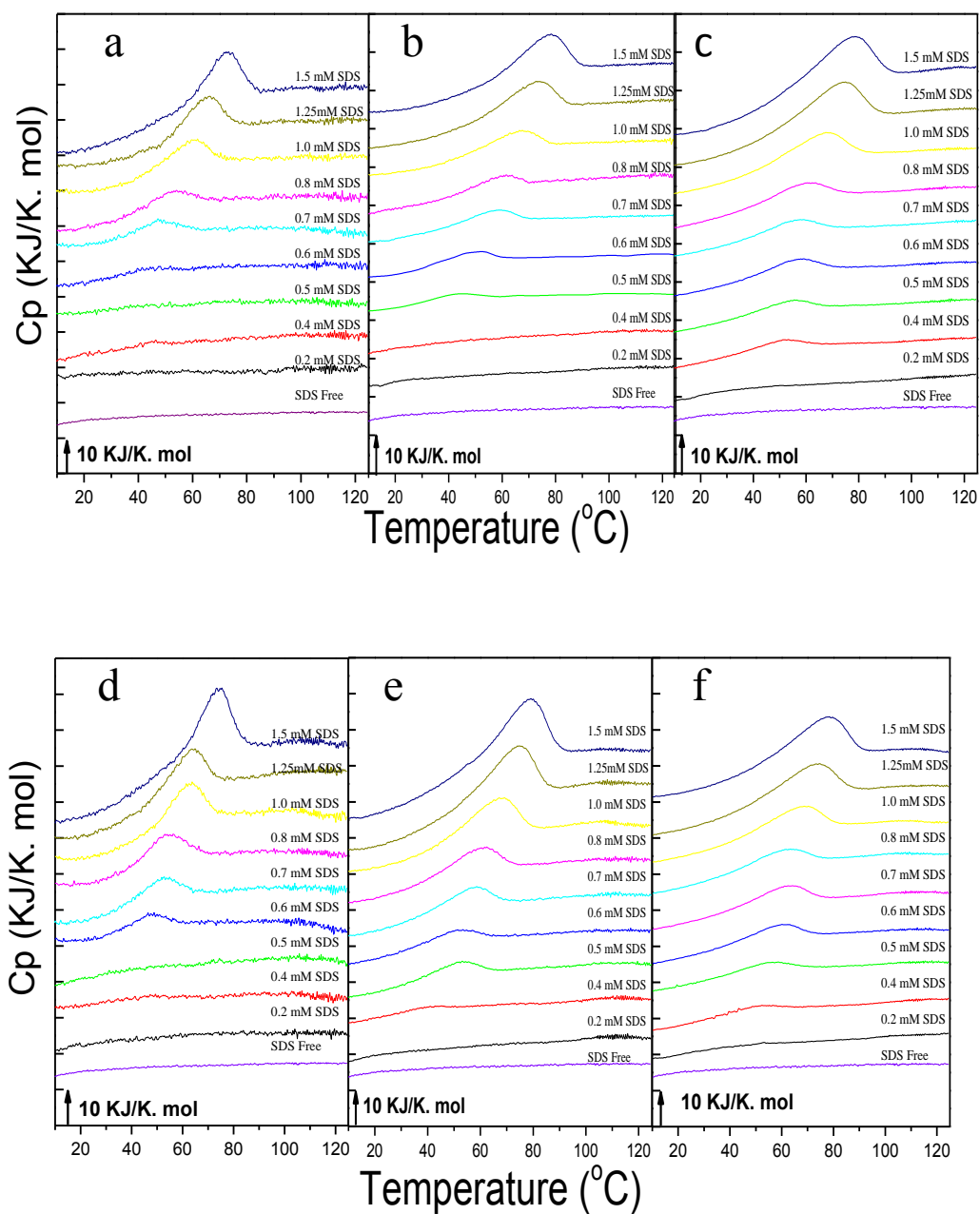
Figure 5. *Effect of SDS concentration on the thermal melting of protein-SDS complexes for the unmodified aSyn (a,b,c) and Nac-aSyn (d,e,f) at different protein concentrations: (a,d) 20 μM; (b,e) 60 μM; (c,f) 100 μM. The scan rate was 2 K/min in all the cases, the buffer used was 20mM HEPES, 0.05% sodium azide, pH 7.2, and the SDS concentrations are shown alongside each thermogram. The thermograms were artificially moved along the ordinate axis for clarity.*

Table 2. Thermodynamic parameters obtained for aSyn from the DSC experiments of the figure 5 and represented in figure 6

	[SDS] (mM)	20 μM			60 μM			100 μM		
		Tm (°C)	ΔH (kJ/mol)	ΔCp$_{20°C}$ (kJ/mol)	Tm (°C)	ΔH (kJ/mol)	ΔCp$_{20°C}$ (kJ/mol)	Tm (°C)	ΔH (kJ/mol)	ΔCp$_{20°C}$ (kJ/mol)
aSyn	0	--	--	0	--	--	0	--	--	0
	0.2	--	--	-0.1	--	--	-0.2	--	--	-0.4
	0.4	--	--	1.9	--	--	0.9	51.8	63	0.9
	0.5	--	--	1.7	43.3	39	1.7	55.8	80	1.5
	0.6	--	--	3.5	50.6	59	2.0	58.3	111	2.0
	0.7	47	83	3.6	58.7	85	3.2	59.6	108	2.8
	0.8	54.6	131	5.2	60.9	77	3.8	61.7	131	3.6
	1	60.2	189	7.1	67.5	145	5.4	68.1	213	4.9
	1.25	66.1	224	9.6	73.6	194	7.2	74.6	314	7.9
	1.5	72.6	298	14.8	78.1	260	8.9	78.6	383	10.6

Table 3. Thermodynamic parameters obtained for Nac-aSyn from the DSC experiments of the figure 5 and represented in figure 6

	[SDS] (mM)	20 µM			60 µM			100 µM		
		Tm (°C)	ΔH (kJ/mol)	$\Delta Cp_{20°C}$ (kJ/mol)	Tm (°C)	ΔH (kJ/mol)	$\Delta Cp_{20°C}$ (kJ/mol)	Tm (°C)	ΔH (kJ/mol)	$\Delta Cp_{20°C}$ (kJ/mol)
	0	--	--	0	--	--	0	--	--	0
	0.2	--	--	1.6	--	--	-0.4	--	--	0.2
	0.4	--	--	1.9	43.7	19	0.5	52.6	70	1.6
	0.5	--	--	1.4	51.9	93	2.6	56.2	79	1.3
Nac-aSyn	0.6	48.0	87	3.6	51.7	95	3.5	61.3	101	2.9
	0.7	51.8	154	6.4	58.3	137	5.1	62.6	125	3.5
	0.8	54.5	165	6.9	60.0	155	6.0	62.7	125	4.5
	1	62.1	228	10.4	67.4	256	8.6	68.5	167	4.8
	1.25	63.1	254	10.3	74.4	339	12.6	73.9	255	6.9
	1.5	74.1	461	16.0	78.9	406	13.0	78	304	7.0

Similarly to what we have seen using other biophysical techniques, the thermograms obtained by DSC describe two distinct phases related to the SDS-protein interaction. The first one includes the SDS concentration range where there is no transition induced yet. This range is approximately coincident for unmodified aSyn with the first phase of partial formation of α-helical structure and with the formation of protein oligomers as observed by DLS. For Nac-aSyn, the SDS concentration range of this phase is narrower.

The second phase occurs when a transition appears and the Tm increases almost linearly along the SDS interval (Figure 6a). This phase could be associated to the thermal melting of mixed protein-SDS micelles that become progressively more stable and abundant as the concentration of SDS increases. As it was previously mentioned, the Nac-aSyn form appears to be more sensitive to the addition of SDS indicating a higher affinity of this form for SDS micelles.

A derived parameter can be calculated from these data, the ΔCp at 20ºC, defined as the decrease of the Cp produced by the SDS presence relative to the unstructured protein in the absence of SDS. To correct for possible uncertainties in baseline position, the Cp curve of aSyn in the absence of SDS was fitted to a polynomial and the parameters obtained were used to fit the right side of each thermogram, once passed the melting transition. This allowed us to estimate by extrapolation the Cp(20ºC) of the unfolded protein at each SDS concentration. The ΔCp values were normalized per mole of protein monomer. Using this parameter the influence of SDS over the Cp of the initial state can be evaluated. This parameter is related to the amount of hydrophobic surface area protected in the protein-SDS micelle complexes that becomes exposed to solvent with the melting. The ΔCp per mole of protein at high SDS concentrations reach very high values (up to 16 kJ K^{-1} mol^{-1}) for a protein of the size of aSyn. Even for highly compact globular proteins, the ΔCp of unfolding per residue ranges between 40 and 75 J K^{-1} mol^{-1} at 20ºC [60], which would give between 5.6 and 10.5 kJ $K^{-1}mol^{-1}$ if aSyn were very compactly folded and forming a well-defined hydrophobic core when interacting with SDS. This is quite unrealistic since, according to the structures availiable, aSyn interacts with micelles in a helical bended conformation without tertiary contacts [61]. Although many aSyn hydrophobic residues become buried at the protein-micelle interface, it is quite unlikely

that they account for these large ΔCp effects. Therefore, besides the contribution of the protein, a large contribution from the hydrophobic surface area of the hydrocarbon chains of SDS that become exposed with the SDS micelle disruption must be adding up to the large ΔCp values observed. The ΔCp presents a similar tendency as the Tm (Figure 6b) and, in general, the ΔCp values are higher for the Nac-aSyn form than for aSyn, which implies a larger hydrophobic surface area buried from water within the core of the mixed protein-SDS micelles. This is once more an indication of a higher number of SDS molecules in the Nac-aSyn-bound micelles. The increase in ΔCp is somehow delayed for aSyn.

In the absence of a mathematical model capable of quantitatively describing the protein-SDS interaction and the thermal melting process, the values of ΔH can only be a gross estimation obtained by rough integration of the area under the transitions. In spite of that, the tendency described is similar to that obtained for ΔCp. A higher affinity of Nac-aSyn for SDS can be deduced from higher values of ΔH generally obtained under most conditions. A greater ΔH value per mole of protein implies a higher number of SDS molecules incorporated into the protein-stabilized micelle.
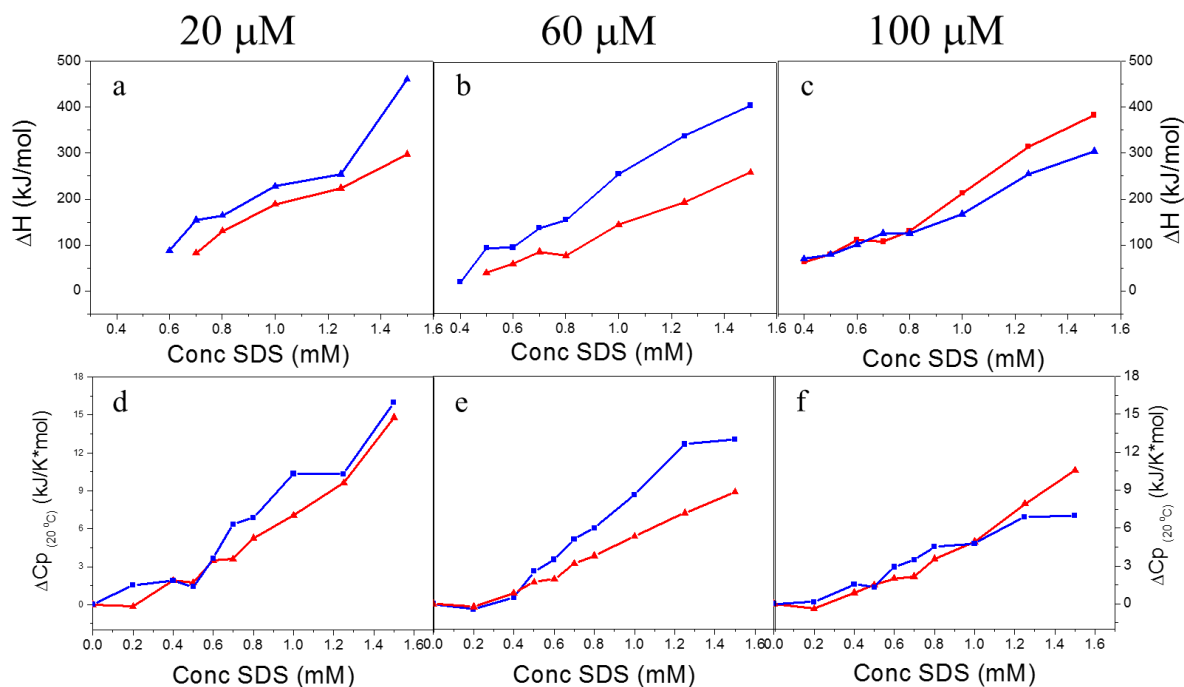
Figure 6. *Effect of the SDS concentration on the ΔH (a,b,c) and ΔCp(20ºC) (d,e,f) for the aSyn (red,solid lines) and Nac-aSyn (blue, dotted lines) at different protein concentration;* The data represented in these figures are included in tables 2 and 3.

In summary, both aSyn forms interact with SDS and reduce its CMC considerably, acquiring α-helical structure. However, the transition from disordered structure to micelle-associated, α-helical structure is more cooperative for Nac-aSyn than for unmodified aSyn. This is related to the fact that at sub-CMC SDS concentrations unmodified aSyn can form high order oligomers with partial helix to a greater extent than Nac-aSyn. In contrast, Nac- aSyn shows a higher affinity for SDS micelles and promotes incorporation of a greater number of SDS molecules.

N-acetilation of aSyn reduces the rate of amyloid aggregation

Once characterized the soluble states of aSyn and Nac-aSyn and its interactions with SDS, we examined their influence on the amyloidogenic propensity of the protein.

To investigate the morphology of the aggregates, a TEM study was performed on 100 µM protein samples incubated at 37ºC in the presence of various concentrations of SDS. In absence of incubation neither fibrils nor oligomers have been detected. After a short time of incubation (~30 min), the two proteins form similar globular or amorphous aggregates of a variety of sizes. No fibrillar material is observed. At longer times (~150 min), most of the aggregated material is still amorphous, although very few aggregates start to show certain fibrillar shape. Very low amount of fibrillar aggregates can be generally seen at these early incubation times. At longer incubation times, curly fibrils appear to develop from the amorphous aggregates at both 0.4 mM and 0.7 mM SDS. At higher SDS concentration (1.5 mM), the protein aggregates remain mayoritarity amorphous for longer incubation times. From these data we cannot extract any important differences between the morphology of the aggregates of aSyn and Nac-aSyn.
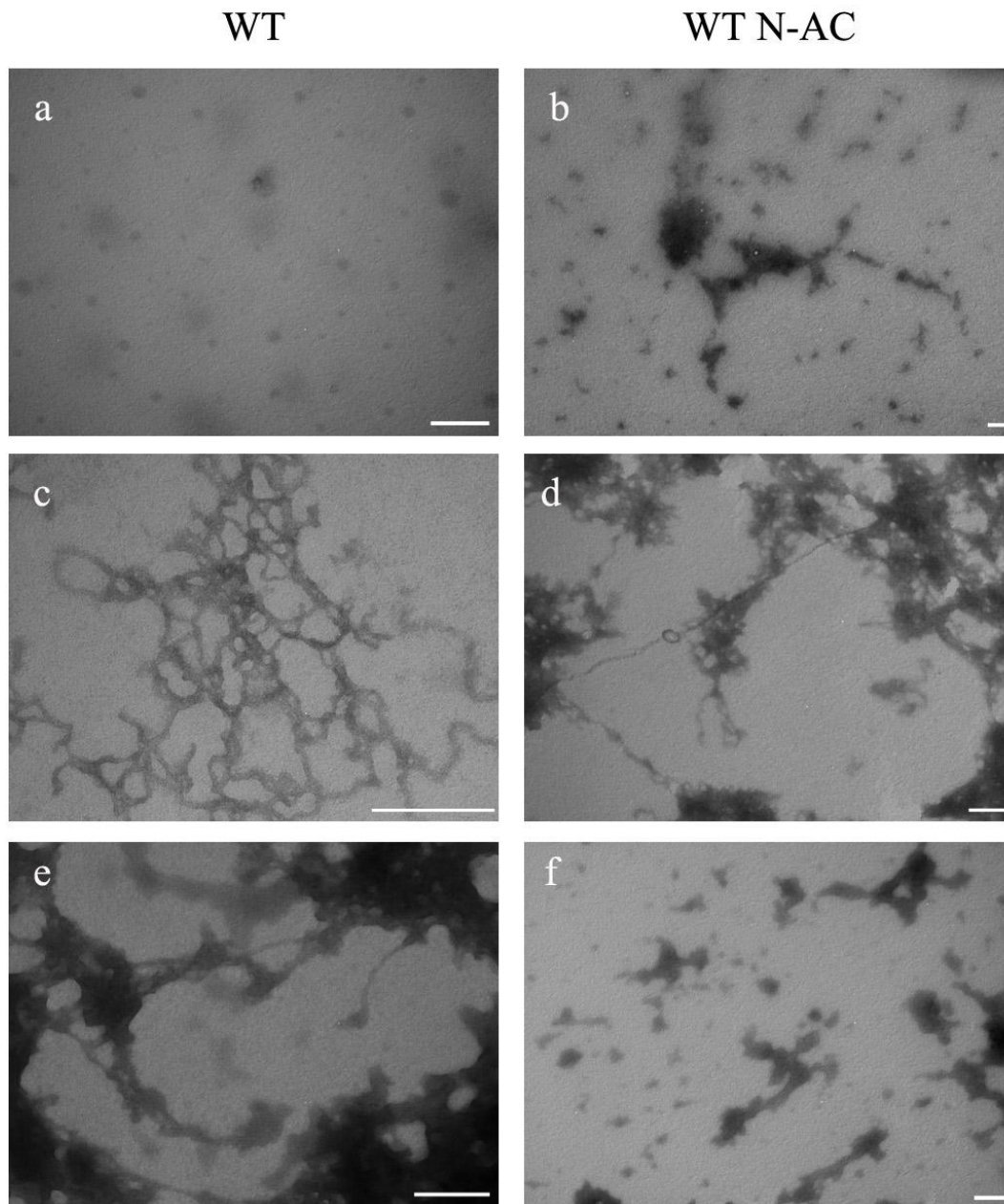
Figure 7. Morphology of amyloid fibrils of aSyn WT (a,c,e) and N-Acetylated(b,d,f) in the presence of SDS. *The samples were incubated at 37°C without shaking for different times. The image a corresponds to 0.7 mM SDS, 30min, the image b corresponds to 0.4 mM SDS, 150min of incubation, the images c and d correspond to 0.7 mM SDS, 12h of incubation and the images e and f correspond to 1.5 mM SDS, 12 h of incubation. The segments represent 200 nm.*

The next step was to study of the influence of the SDS on the kinetics of formation of amyloid structure by Nac-aSyn and aSyn using thioflavin T (ThT) fluorescence.

ThioflavinT is a fluorophore highly sensitive to oligomeric species and fibrils presenting cross-beta amyloid structure. Consequently, ThT can be used to monitor the process of amyloid oligomer formation, nucleation and subsequent fibril elongation. The kinetic aggregation experiments followed by ThT fluorescence were performed at a protein concentration of 100 μM in 20 mM HEPES, 0.05% NaN_3 pH 7.2 buffer at 37ºC without shaking. In the absence of SDS, the protein shows a monomeric state with random coil structure. Under these conditions the aSyn aggregation presents a very long lag phase of several weeks (results not shown). This lag phase could be reduced with the addition of seeds [43,62], salts [63-65], shaking [66] and also the fibrillation rate could be enhanced by the addition of anionic surfactants [49,67-69]. As it has been already mentioned, low SDS concentrations induce a conformational change accompanied by oligomerization prior to the formation of protein-SDS micelles. However, the detailed molecular mechanisms of this fibrillation enhancing activity of surfactants of not well understood., Since the detected oligomers may be able to act as amyloidogenic nuclei, we compared the amyloid aggregation kinetics of aSyn and Nac-aSyn in the presence of different SDS concentrations (Figure 8). Due to its high complexity, we concentrated our study specifically on the early stage of the process where the fibril elongation is nearly inexistent whereas formation of oligomeric aggregates is the predominant process.

For both protein forms the aggregation rates are strongly dependent on the SDS concentration. Moreover, the aggregation kinetics are devoid of detectable lag phase except at high SDS concentrations, where short lag phases of about 100 min are visible. These kinetics are therefore susceptible to be studied by quantifying initial aggregation rates, as we described before [54,70,71].
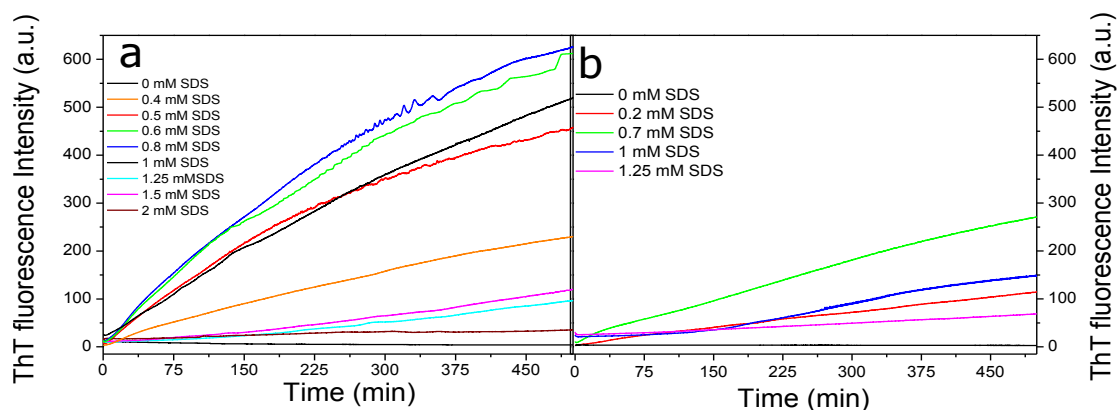
Figure 8. Effect of SDS on the kinetics of formation of amyloid structure for aSyn (a) and Nac-aSyn (b) followed by ThT fluorescence. *Experiments were made at 37ºC and the protein concentration was 100 μM in each case. The colors correspond to different SDS concentrations as indicated in the graphs.*

As it has been recently reported [50], N-acetylation decreases the rate of aggregation of aSyn. Here this different behavior could be quantitatively evaluated in terms of initial aggregation rates using our experimental data sets (Figure 9).

Figure 9. Variation of the ThT initial aggregation rates with the SDS concentration. *The data of the unmodified aSyn are represented in red while those of Nac-aSyn are represented in blue.*

The SDS dependence of the initial aggregation rates can be divided in two phases (Figure 9), similarly to those described above. In a first one, the aggregation rate increases with the SDS concentration reaching a maximum. In a second phase, a progressive decrease in the initial aggregation rate is observed with the appearance of a lag phase and an inhibition of the aggregation process is obtained at SDS concentration above about 1.2 mM.

However, the unmodified aSyn reaches much higher initial rates and ThT intensity values, as can be easily seen in Figure 8. This indicates a faster aggregation and a higher quantity of amyloid structure for the non-acetylated aSyn.

Similarly to the dependence of the hydrodynamic radii with the concentration of SDS (Figure 3), a broader interval of SDS concentration with high aggregation rates appears to be found for the unmodified aSyn, consistently with a higher persistence of its partially folded oligomers with SDS. In contrast, Nac-aSyn presents a higher affinity for SDS micelles at high SDS concentrations and a lower propensity to oligomerize, as described above. These mixed SDS-protein micelles present less propensity to form amyloid structure. In addition, form both proteins at high SDS concentrations, which stabilize protein-micelle complexes, the amyloid aggregation is strongly reduced. Therefore, we can conclude that aSyn oligomeric species that become populated at sub-CMC SDS concentrations constitute the key species necessary to nucleate amyloid formation.

DISCUSSION

Both native monomeric aSyn and Nac-aSyn are intrinsically disordered in solution

In this study, we have shown that aSyn and Nac-aSyn share similar structure and biophysical properties. According from our CD, DLS and DSC experiments, the proteins are monomeric and mainly unstructured. These observations agree perfectly with many previous studies reporting that the deposition of aSyn originates from an intrinsically disordered monomer ensemble that under fibril promoting conditions forms amyloid [72-74]. However, this view was challenged recently [14,15]. In these controversial studies, the authors suggested that the protein

exists in its actual native state as a fibrillation-resistant α-helical tetramers and that these differences in the protein conformation could have arisen from the use of harsh conditions in the purification protocols and/or from molecular differences between the purified samples arising from a modification to the aSyn N-terminus by acetylation. The tetrameric form of the native aSyn has been reported in these studies to be rich in α-helix.

Previous work and this present study have highlighted the propensity of aSyn to adopt α-helical conformation. This conformational change is favored in the presence of surfactants, lipids or other membrane components. The native state of aSyn has been thought to originate from an ensemble of intrinsically disordered monomeric forms, with recognition that the monomers therein are capable of adopting a wide range of accessible conformations depending on solution and environmental conditions [13,63,75-77]. Uversky first spoke of aSyn as the ''protein chameleon'' [72] due to its ability to respond to its environment and binding partners by varying its foldedness and aggregation state.

Our data support a mainly unstructured conformation for both Nac-aSyn and aSyn forms in the absence of external determinants that may induce or select those specific conformations that are encoded in its sequence and thereby its structural propensity to develop its biological functions or to aggregate. This results in a very slow rate of nucleation of amyloid structure and a prolonged lag phase in the aggregation kinetics. Under these conditions, secondary nucleation processes are likely to govern amyloid aggregation [78].

SDS-induced aSyn oligomers and not aSyn bound to micelles are the key precursors of amyloid nucleation

Since we are mainly interested in the early formation of primary oligomeric nuclei and because aSyn function is related to lipids and membranes, we have analyzed the aggregation of aSyn in the presence of SDS, a simple mimetic of membrane environment, which has been described to accelerate the process dramatically. Firstly in our study, we have focused on the effect of SDSon the structures of aSyn and Nac-aSyn. It has been argued that aSyn in the absence of SDS presents dynamic long-range tertiary interactions that limit its aggregation

propensity[79]. This could lead to the proposal that SDS may affect aSyn aggregation by disrupting those interactions. The binding equilibrium of aSyn with SDS follows two different phases as evidenced by our experiments using various biophysical techniques. Our results are in good agreement with the previous similar studies[43], although a more complex process cannot be discarded[45]. A proposed mechanism of aSyn oligomerization and subsequent amyloid aggregation in the presence of SDS is illustrated in Figure 10.

The first transition occurs mainly from 0 to 0.4-0.7 mM SDS depending of the protein concentration. This phase is characterized by a sharp conformational change characterized by an enhancement of the content of alpha helix (~30%), an increment of the hydrodynamic radius and an increase in the molecular weight, accordingly with the scattering measurements, without micellization of SDS. The ΔCp and ΔH of melting remain nearly unaltered from that of the unfolded state. This implies that the resulting structure of aSyn within these SDS-associated oligomers is not cooperative and should be essentially labile and dynamic, still exposing considerable amount of hydrophobic surface area. This stage could be defined by an equilibrium constant, K_1, which defines the oligomer formation of aSyn in presence of SDS. This transition results in an increase in the amyloidogenic propensity, related to the formation of dynamic aSyn oligomers, which can dramatically increase the probability of intermolecular contacts that can rapidly evolve into amyloidogenic nuclei.
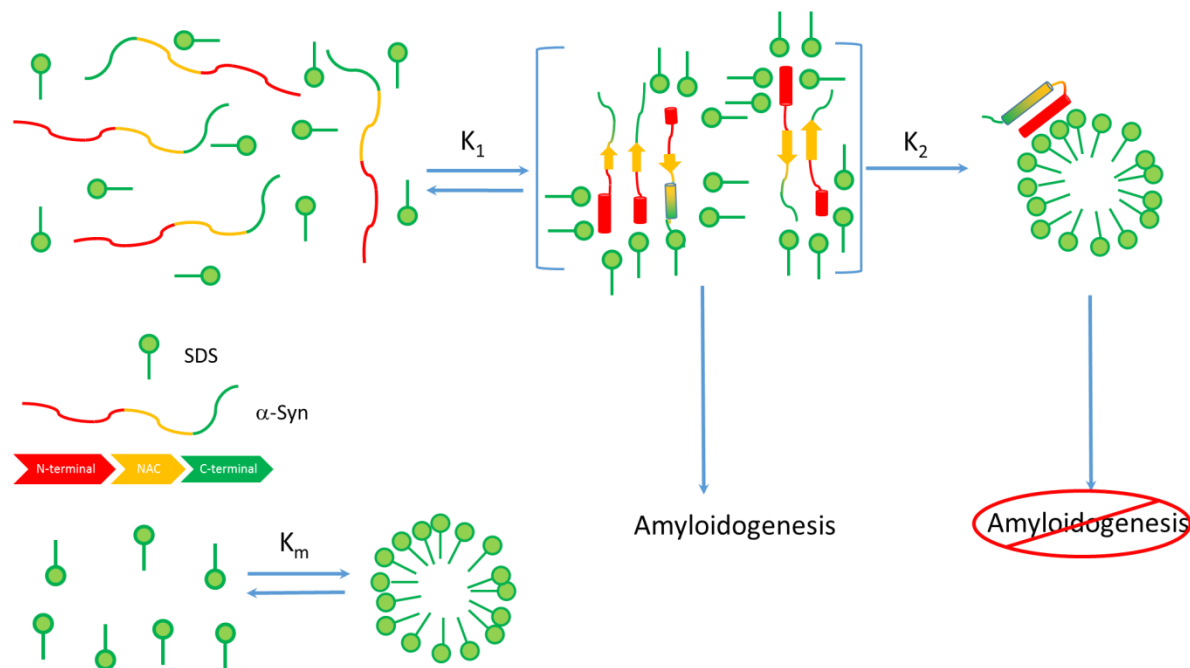
Figure 10. Scheme for SDS-aSyn interaction. *K_1 and K_2 are equilibrium constant that represent the two different phases discussed. Km represents the micellization SDS constant.*

The rate of formation of amyloid aggregates is maximal at the end of this transition, at a SDS concentration of 0.7-0.8 mM. Upon further increase in SDS concentration, a second transition could be observed consisting in the formation of aSyn-bound SDS micelles. In this subsequent stage, the α-helical structural content is increased while the R_h and Mw decreased. In addition, the structure becomes more cooperative and stable as indicated by the large ΔCp and ΔH values observed for their thermal melting. The gain in the system cooperativity also implies a strong reduction of the SDS-promoted amyloid aggregation of aSyn. This second phase could be defined by an equilibrium constant, K_2, which characterizes the formation of folded aSyn bound to SDS micelles from the oligomers.

All the species described in this proposed mechanism are in equilibrium with the SDS micellization process and are at the same time affected by the mass action law, producing a reduction of the critical micelle concentration of the SDS.

As it was previously mentioned, SDS interacts with aSyn in a complex pathway, presenting a dual behavior. A similar model was described by Ahmad and coworkers[43] , although these

authors did not identify the formation of oligomeric aSyn species in their study. Otzen and coworkers also identified similar SDS-induced transitions for aSyn but using a different set of techniques, including small angle x-ray scattering, defined a slightly more complex model for aSyn fibrillation induced by SDS [43,45,46]. Like us, these authors also concluded that SDS can facilitate fibrillation by mediating intermolecular contacts between different aSyn molecules. In addition to these models, Ferreon and coworkers proposed a more complex model for the SDS induced conformational changes of aSyn based on single molecule FRET experiments[38,80,81]. They describe up to five different aSyn conformations including the unfolded state, two different partially helical intermediates (one with an extended conformation and another with a broken-helix hairpin structure) and two micelle associated states (also extended and bent respectively, the latter only attained at very high SDS concentrations). These authors did not define, however, the oligomerization degree of these states, which might also be responsible for reduced FRET distances due to intermolecular contacts. Nevertheless, most of our observations are largely consistent with previous studies in the literature and points directly to SDS-associated, partially-folded aSyn oligomers as critical for nucleating the amyloid aggregation pathway.

N-terminal acetylation protects aSyn from amyloid aggregation by reducing oligomerization and stabilizing the micelle-bound state

The N-terminal acetylation of the aSyn induces a different behavior in presence of SDS. Based on the data presented in this work together with the literature [82,83] we can conclude that the N-acetylation increases the affinity of the aSyn for the SDS micelles. This affinity increase is considered to be related to a stabilizing effect of acetylation of the N-terminal α-helix structure, which is the region responsible of the interaction with surfactants [84,85]. It enhances nearly twice the affinity for anionic lipid surfaces [41,86]. These reasons make trustworthy the suggestion that the function of the N-acetylation is related to a regulatory effect of the aSyn interaction with lipids and surfactants.

We have shown that the formation of the mixed SDS-protein micelles is favored in the case of Nac-aSyn. This could be due to an increase of the equilibrium constant, K_2, coming from

a stabilization of the folded state. This could result in two effects on the aggregation cascade. First, by a mass action effect it reduces the population of the amyloidogenic oligomeric intermediate and the interval of SDS concentrations where it is populated, and second, as Nac-aSyn presents a higher affinity for the SDS and the evolution of the aggregation process would require the dissociation of SDS from the oligomers. Consequently for both reasons, the aggregation rate is limited in the acetylated form compared to the unmodified one. This is in agreement with previous studies showing that aSyn acetylation somehow precludes aggregation or at least decreases the aggregation propensity [14,50,87].

These observations could seem a bit paradoxical because it has been reported that oligomers represent the most toxic species in diseases related to amyloid. Moreover, the deposits found in Parkinson affected-brain are mainly constituted of Nac-aSyn. However, our results could point towards an effect of N-acetylation on the balance between unstructured monomers, dynamic oligomers and micelle-protein complexes. This may result in different structural properties of the amyloid oligomeric species and therefore affect their toxicity of the oligomers obtained from the two forms of aSyn. The different oligomers produced by each aSyn form could also produce an alteration of their amyloidogenic propensity, being more efficient the evolution to amyloid fibrils of the oligomers produced by the unmodified form.

CONCLUSIONS

We have demonstrated that SDS-associated partially-folded and dynamic oligomers of aSyn constitute optimal species for spontaneous and efficient formation of amyloid nuclei, which further drive lag-free amyloid fibrillation. Although N-acetilation of aSyn does not produce significant changes in the unstructured conformation of the protein in solution, we have provided evidence that acetylation increases the affinity for SDS. This results in a decrease in the population of oligomeric species and therefore reduces the amyloidogenic propensity significantly.

A deeper study should be performed in order to increase our knowledge of the system at different SDS and protein concentrations. The SDS-induced aSyn fibrillation kinetics could be amenable to a quantitative analysis using our previously developed nucleation model [54].

We also expect to extend this study to the aSyn mutants related to the development of PD, the missense mutations A30P, E46K ant A53T[88,89], which also fold in presence of fatty acids, as it has been described previously[30].

ACKNOWLEDGEMENTS

REFERENCES

(1)   Moore, D. J.; West, A. B.; Dawson, V. L.; Dawson, T. M. Molecular pathophysiology of Parkinson's disease. *Annual Review of Neuroscience* **2005**, *28*, 57-87.

(2)   Takahashi, H.; Wakabayashi, K. The cellular pathology of Parkinson's disease. *Neuropathology* **2001**, *21*, 315-322.

(3)   Takahashi, H.; Wakabayashi, K. Controversy: is Parkinson's disease a single disease entity? Yes. *Parkinsonism Relat Disord* **2005**, *11 Suppl 1*, S31-37.

(4)   Arima, K.; Ueda, K.; Sunohara, N.; Arakawa, K.; Hirai, S.; Nakamura, M.; Tonozuka-Uehara, H.; Kawai, M. NACP/alpha-synuclein immunoreactivity in fibrillary components of neuronal and oligodendroglial cytoplasmic inclusions in the pontine nuclei in multiple system atrophy. *Acta neuropathologica* **1998**, *96*, 439-444.

(5)   Forno, L. S. Neuropathology of Parkinson's disease. *J Neuropathol Exp Neurol* **1996**, *55*, 259-272.

(6)   Polymeropoulos, M. H.; Lavedan, C.; Leroy, E.; Ide, S. E.; Dehejia, A.; Dutra, A.; Pike, B.; Root, H.; Rubenstein, J.; Boyer, R.; Stenroos, E. S.; Chandrasekharappa, S.; Athanassiadou, A.; Papapetropoulos, T.; Johnson, W. G.; Lazzarini, A. M.; Duvoisin, R. C.; Di Iorio, G.; Golbe, L. I.; Nussbaum, R. L. Mutation in the alpha-synuclein gene identified in families with Parkinson's disease. *Science* **1997**, *276*, 2045-2047.

(7)   Wakabayashi, K.; Yoshimoto, M.; Tsuji, S.; Takahashi, H. Alpha-synuclein immunoreactivity in glial cytoplasmic inclusions in multiple system atrophy. *Neuroscience letters* **1998**, *249*, 180-182.

(8)   Wakabayashi, K.; Hayashi, S.; Kakita, A.; Yamada, M.; Toyoshima, Y.; Yoshimoto, M.; Takahashi, H. Accumulation of alpha-synuclein/NACP is a cytopathological feature common to Lewy body disease and multiple system atrophy. *Acta neuropathologica* **1998**, *96*, 445-452.

(9)   Spillantini, M. G.; Crowther, R. A.; Jakes, R.; Hasegawa, M.; Goedert, M. alpha-Synuclein in filamentous inclusions of Lewy bodies from Parkinson's disease and dementia with lewy bodies. *Proceedings of the National Academy of Sciences of the United States of America* **1998**, *95*, 6469-6473.

(10)   Maroteaux, L.; Campanelli, J. T.; Scheller, R. H. Synuclein - a Neuron-Specific Protein Localized to the Nucleus and Presynaptic Nerve-Terminal. *Journal of Neuroscience* **1988**, *8*, 2804-2815.

(11)   Dauer, W.; Kholodilov, N.; Vila, M.; Trillat, A. C.; Goodchild, R.; Larsen, K. E.; Staal, R.; Tieu, K.; Schmitz, Y.; Yuan, C. A.; Rocha, M.; Jackson-Lewis, V.; Hersch, S.; Sulzer, D.; Przedborski, S.; Burke, R.; Hen, R. Resistance of alpha-synuclein null mice to the parkinsonian neurotoxin MPTP. *Proceedings of the National Academy of Sciences of the United States of America* **2002**, *99*, 14524-14529.

(12)   Lorenzen, N.; Nielsen, S. B.; Buell, A. K.; Kaspersen, J. D.; Arosio, P.; Vad, B. S.; Paslawski, W.; Christiansen, G.; Valnickova-Hansen, Z.; Andreasen, M.; Enghild, J. J.; Pedersen, J. S.; Dobson, C. M.; Knowles, T. P.; Otzen, D. E. The Role of Stable alpha-Synuclein Oligomers in the Molecular Events Underlying Amyloid Formation. *Journal of the American Chemical Society* **2014**.

(13)   Weinreb, P. H.; Zhen, W.; Poon, A. W.; Conway, K. A.; Lansbury, P. T., Jr. NACP, a protein implicated in Alzheimer's disease and learning, is natively unfolded. *Biochemistry* **1996**, *35*, 13709-13715.

(14)   Bartels, T.; Choi, J. G.; Selkoe, D. J. alpha-Synuclein occurs physiologically as a helically folded tetramer that resists aggregation. *Nature* **2011**, *477*, 107-U123.

(15)   Wang, W.; Perovic, I.; Chittuluru, J.; Kaganovich, A.; Nguyen, L. T. T.; Liao, J. L.; Auclair, J. R.; Johnson, D.; Landeru, A.; Simorellis, A. K.; Ju, S. L.; Cookson, M. R.; Asturias, F. J.; Agar, J. N.; Webb, B. N.; Kang, C. H.; Ringe, D.; Petsko, G. A.; Pochapsky, T. C.; Hoang, Q. Q. A soluble alpha-synuclein construct forms a dynamic tetramer. *Proceedings of the National Academy of Sciences of the United States of America* **2011**, *108*, 17797-17802.

(16)   Fauvet, B.; Mbefo, M. K.; Fares, M. B.; Desobry, C.; Michael, S.; Ardah, M. T.; Tsika, E.; Coune, P.; Prudent, M.; Lion, N.; Eliezer, D.; Moore, D. J.; Schneider, B.; Aebischer, P.; El-Agnaf, O. M.; Masliah, E.; Lashuel, H. A. alpha-Synuclein in Central Nervous System and from Erythrocytes, Mammalian Cells, and Escherichia coli Exists Predominantly as Disordered Monomer. *Journal of Biological Chemistry* **2012**, *287*, 15345-15364.

(17)   Burre, J.; Vivona, S.; Diao, J.; Sharma, M.; Brunger, A. T.; Sudhof, T. C. Properties of native brain alpha-synuclein. *Nature* **2013**, *498*, E4-6; discussion E6-7.

(18)   Coelho-Cerqueira, E.; Carmo-Goncalves, P.; Pinheiro, A. S.; Cortines, J.; Follmer, C. alpha-Synuclein as an intrinsically disordered monomer - fact or artefact? *Febs Journal* **2013**, *280*, 4915-4927.

(19)   Trexler, A. J.; Rhoades, E. Alpha-synuclein binds large unilamellar vesicles as an extended helix. *Biochemistry* **2009**, *48*, 2304-2306.

(20)   Sharon, R.; Goldberg, M. S.; Bar-Josef, I.; Betensky, R. A.; Shen, J.; Selkoe, D. J. alpha-Synuclein occurs in lipid-rich high molecular weight complexes, binds fatty acids, and shows homology to the fatty acid-binding proteins. *Proceedings of the National Academy of Sciences of the United States of America* **2001**, *98*, 9110-9115.

(21)   Sharon, R.; Bar-Joseph, I.; Mirick, G. E.; Serhan, C. N.; Selkoe, D. J. Altered fatty acid composition of dopaminergic neurons expressing alpha-synuclein and human brains with alpha-synucleinopathies. *Journal of Biological Chemistry* **2003**, *278*, 49874-49881.

(22)   Golovko, M. Y.; Rosenberger, T. A.; Faergeman, N. J.; Feddersen, S.; Cole, N. B.; Pribill, I.; Berger, J.; Nussbaum, R. L.; Murphy, E. J. Acyl-CoA synthetase activity links wild-type but not mutant alpha-synuclein to brain arachidonate metabolism. *Biochemistry* **2006**, *45*, 6956-6966.

(23)   Darios, F.; Ruiperez, V.; Lopez, I.; Villanueva, J.; Gutierrez, L. M.; Davletov, B. Alpha-synuclein sequesters arachidonic acid to modulate SNARE-mediated exocytosis. *EMBO reports* **2010**, *11*, 528-533.

(24)   Perlmutter, J. D.; Braun, A. R.; Sachs, J. N. Curvature dynamics of alpha-synuclein familial Parkinson disease mutants: molecular simulations of the micelle- and bilayer-bound forms. *The Journal of biological chemistry* **2009**, *284*, 7177-7189.

(25)   Rao, J. N.; Kim, Y. E.; Park, L. S.; Ulmer, T. S. Effect of pseudorepeat rearrangement on alpha-synuclein misfolding, vesicle binding, and micelle binding. *Journal of molecular biology* **2009**, *390*, 516-529.

(26)   Ouberai, M. M.; Wang, J.; Swann, M. J.; Galvagnion, C.; Guilliams, T.; Dobson, C. M.; Welland, M. E. alpha-Synuclein senses lipid packing defects and induces lateral expansion of lipids leading to membrane remodeling. *The Journal of biological chemistry* **2013**, *288*, 20883-20895.

(27)   De Franceschi, G.; Frare, E.; Bubacco, L.; Mammi, S.; Fontana, A.; de Laureto, P. P. Molecular Insights into the Interaction between alpha-Synuclein and Docosahexaenoic Acid. *Journal of molecular biology* **2009**, *394*, 94-107.

(28)   Sharon, R.; Bar-Joseph, I.; Frosch, M. P.; Walsh, D. M.; Hamilton, J. A.; Selkoe, D. J. The formation of highly soluble oligomers of alpha-synuclein is regulated by fatty acids and enhanced in Parkinson's disease. *Neuron* **2003**, *37*, 583-595.

(29)   Assayag, K.; Yakunin, E.; Loeb, V.; Selkoe, D. J.; Sharon, R. Polyunsaturated fatty acids induce alpha-synuclein-related pathogenic changes in neuronal cells. *American Journal of Pathology* **2007**, *171*, 2000-2011.

(30)   Broersen, K.; van den Brink, D.; Fraser, G.; Goedert, M.; Davletov, B. alpha-synuclein adopts an alpha-helical conformation in the presence of polyunsaturated fatty acids to hinder micelle formation. *Biochemistry* **2006**, *45*, 15610-15616.

(31)   De Franceschi, G.; Frare, E.; Pivato, M.; Relini, A.; Penco, A.; Greggio, E.; Bubacco, L.; Fontana, A.; de Laureto, P. P. Structural and morphological characterization of aggregated species of alpha-synuclein induced by docosahexaenoic acid. *The Journal of biological chemistry* **2011**, *286*, 22262-22274.

(32)   Selkoe, D.; Dettmer, U.; Luth, E.; Kim, N.; Newman, A.; Bartels, T. Defining the Native State of alpha-Synuclein. *Neurodegener Dis* **2013**.

(33)   Bartels, T.; Selkoe, D. J. Properties of native brain alpha-synuclein Reply. *Nature* **2013**, *498*, E6-E7.

(34)   Campioni, S.; Mannini, B.; Zampagni, M.; Pensalfini, A.; Parrini, C.; Evangelisti, E.; Relini, A.; Stefani, M.; Dobson, C. M.; Cecchi, C.; Chiti, F. A causative link between the structure of aberrant protein oligomers and their toxicity. *Nature chemical biology* **2010**, *6*, 140-147.

(35)   Baglioni, S.; Casamenti, F.; Bucciantini, M.; Luheshi, L. M.; Taddei, N.; Chiti, F.; Dobson, C. M.; Stefani, M. Prefibrillar amyloid aggregates could be generic toxins in higher organisms. *The Journal of neuroscience : the official journal of the Society for Neuroscience* **2006**, *26*, 8160-8167.

(36)   Bucciantini, M.; Giannoni, E.; Chiti, F.; Baroni, F.; Formigli, L.; Zurdo, J.; Taddei, N.; Ramponi, G.; Dobson, C. M.; Stefani, M. Inherent toxicity of aggregates implies a common mechanism for protein misfolding diseases. *Nature* **2002**, *416*, 507-511.

(37)   Lajoie, P.; Snapp, E. L. Formation and toxicity of soluble polyglutamine oligomers in living cells. *PloS one* **2010**, *5*, e15245.

(38)   Brender, J. R.; Salamekh, S.; Ramamoorthy, A. Membrane disruption and early events in the aggregation of the diabetes related peptide IAPP from a molecular perspective. *Accounts of chemical research* **2012**, *45*, 454-462.

(39)   Sciacca, M. F.; Kotler, S. A.; Brender, J. R.; Chen, J.; Lee, D. K.; Ramamoorthy, A. Two-step mechanism of membrane disruption by Abeta through membrane fragmentation and pore formation. *Biophysical journal* **2012**, *103*, 702-710.

(40)   Trexler, A. J.; Rhoades, E. N-terminal acetylation is critical for forming a-helical oligomer of a-synuclein. *Protein Science* **2012**, *21*, 601-605.

(41)   Scott, D. C.; Monda, J. K.; Bennett, E. J.; Harper, J. W.; Schulman, B. A. N-terminal acetylation acts as an avidity enhancer within an interconnected multiprotein complex. *Science* **2011**, *334*, 674-678.

(42)   Anderson, J. P.; Walker, D. E.; Goldstein, J. M.; de Laat, R.; Banducci, K.; Caccavello, R. J.; Barbour, R.; Huang, J.; Kling, K.; Lee, M.; Diep, L.; Keim, P. S.; Shen, X.; Chataway, T.; Schlossmacher, M. G.; Seubert, P.; Schenk, D.; Sinha, S.; Gai, W. P.; Chilcote, T. J. Phosphorylation of Ser-129 is the dominant pathological modification of alpha-synuclein in familial and sporadic Lewy body disease. *The Journal of biological chemistry* **2006**, *281*, 29739-29752.

(43)   Ahmad, M. F.; Ramakrishna, T.; Raman, B.; Rao Ch, M. Fibrillogenic and non-fibrillogenic ensembles of SDS-bound human alpha-synuclein. *Journal of molecular biology* **2006**, *364*, 1061-1072.

(44)   Veldhuis, G.; Segers-Nolten, I.; Ferlemann, E.; Subramaniam, V. Single-molecule FRET reveals structural heterogeneity of SDS-bound alpha-synuclein. *Chembiochem : a European journal of chemical biology* **2009**, *10*, 436-439.

(45)   Giehm, L.; Oliveira, C. L.; Christiansen, G.; Pedersen, J. S.; Otzen, D. E. SDS-induced fibrillation of alpha-synuclein: an alternative fibrillation pathway. *Journal of molecular biology* **2010**, *401*, 115-133.

(46)   Vandelinder, V.; Ferreon, A. C.; Gambin, Y.; Deniz, A. A.; Groisman, A. High-resolution temperature-concentration diagram of alpha-synuclein conformation obtained from a single Forster resonance energy transfer image in a microfluidic device. *Analytical chemistry* **2009**, *81*, 6929-6935.

(47)   de Laureto, P. P.; Tosatto, L.; Frare, E.; Marin, O.; Uversky, V. N.; Fontana, A. Conformational properties of the SDS-bound state of alpha-synuclein probed by limited proteolysis: unexpected rigidity of the acidic C-terminal tail. *Biochemistry* **2006**, *45*, 11523-11531.

(48)   Pivato, M.; De Franceschi, G.; Tosatto, L.; Frare, E.; Kumar, D.; Aioanei, D.; Brucale, M.; Tessari, I.; Bisaglia, M.; Samori, B.; de Laureto, P. P.; Bubacco, L. Covalent alpha-synuclein dimers: chemico-physical and aggregation properties. *PloS one* **2012**, *7*, e50027.

(49)   Dikiy, I.; Eliezer, D. N-terminal acetylation stabilizes N-terminal helicity in lipid- and micelle-bound alpha-synuclein and increases its affinity for physiological membranes. *The Journal of biological chemistry* **2014**, *289*, 3652-3665.

(50)   Kang, L.; Moriarty, G. M.; Woods, L. A.; Ashcroft, A. E.; Radford, S. E.; Baum, J. N-terminal acetylation of alpha-synuclein induces increased transient helical propensity and decreased aggregation rates in the intrinsically disordered monomer. *Protein science : a publication of the Protein Society* **2012**, *21*, 911-917.

(51)   Johnson, M.; Coulton, A. T.; Geeves, M. A.; Mulvihill, D. P. Targeted amino-terminal acetylation of recombinant proteins in E. coli. *PloS one* **2010**, *5*, e15801.

(52)   Pace, C. N.; Vajdos, F.; Fee, L.; Grimsley, G.; Gray, T. How to measure and predict the molar absorption coefficient of a protein. *Protein science : a publication of the Protein Society* **1995**, *4*, 2411-2423.

(53)   LeVine, H., 3rd. Quantification of beta-sheet amyloid fibril structures with thioflavin T. *Methods in enzymology* **1999**, *309*, 274-284.

(54)   Ruzafa, D.; Morel, B.; Varela, L.; Azuaga, A. I.; Conejero-Lara, F. Characterization of oligomers of heterogeneous size as precursors of amyloid fibril nucleation of an SH3 domain: an experimental kinetics study. *PloS one* **2012**, *7*, e49690.

(55)   Luo, P.; Baldwin, R. L. Mechanism of helix induction by trifluoroethanol: a framework for extrapolating the helix-forming properties of peptides from trifluoroethanol/water mixtures back to water. *Biochemistry* **1997**, *36*, 8413-8421.

(56)   Caetano, W.; Barbosa, L. R.; Itri, R.; Tabak, M. Trifluoperazine effects on anionic and zwitterionic micelles: a study by small angle X-ray scattering. *Journal of colloid and interface science* **2003**, *260*, 414-422.

(57)   Lendel, C.; Bertoncini, C. W.; Cremades, N.; Waudby, C. A.; Vendruscolo, M.; Dobson, C. M.; Schenk, D.; Christodoulou, J.; Toth, G. On the mechanism of nonspecific inhibitors of protein aggregation: dissecting the interactions of alpha-synuclein with Congo red and lacmoid. *Biochemistry* **2009**, *48*, 8322-8334.

(58)   Frimpong, A. K.; Abzalimov, R. R.; Uversky, V. N.; Kaltashov, I. A. Characterization of intrinsically disordered proteins with electrospray ionization mass spectrometry: conformational heterogeneity of alpha-synuclein. *Proteins* **2010**, *78*, 714-722.

(59)   Eliezer, D.; Kutluay, E.; Bussell, R., Jr.; Browne, G. Conformational properties of alpha-synuclein in its free and lipid-associated states. *Journal of molecular biology* **2001**, *307*, 1061-1073.

(60)   Makhatadze, G. I.; Privalov, P. L. Energetics of protein structure. *Advances in protein chemistry* **1995**, *47*, 307-425.

(61)   Ulmer, T. S.; Bax, A.; Cole, N. B.; Nussbaum, R. L. Structure and dynamics of micelle-bound human alpha-synuclein. *The Journal of biological chemistry* **2005**, *280*, 9595-9603.

(62)   Hong, D. P.; Han, S.; Fink, A. L.; Uversky, V. N. Characterization of the non-fibrillar alpha-synuclein oligomers. *Protein and peptide letters* **2011**, *18*, 230-240.

(63)   Uversky, V. N.; Li, J.; Fink, A. L. Metal-triggered structural transformations, aggregation, and fibrillation of human alpha-synuclein. A possible molecular NK between Parkinson's disease and heavy metal exposure. *The Journal of biological chemistry* **2001**, *276*, 44284-44296.

(64)   Munishkina, L. A.; Henriques, J.; Uversky, V. N.; Fink, A. L. Role of protein-water interactions and electrostatics in alpha-synuclein fibril formation. *Biochemistry* **2004**, *43*, 3289-3300.

(65)   Ahmad, A.; Burns, C. S.; Fink, A. L.; Uversky, V. N. Peculiarities of copper binding to alpha-synuclein. *Journal of biomolecular structure & dynamics* **2012**, *29*, 825-842.

(66)   Uversky, V. N.; Eliezer, D. Biophysics of Parkinson's disease: structure and aggregation of alpha-synuclein. *Current protein & peptide science* **2009**, *10*, 483-499.

(67)   Necula, M.; Chirita, C. N.; Kuret, J. Rapid anionic micelle-mediated alpha-synuclein fibrillization in vitro. *The Journal of biological chemistry* **2003**, *278*, 46674-46680.

(68)   Jo, E.; Darabie, A. A.; Han, K.; Tandon, A.; Fraser, P. E.; McLaurin, J. alpha-Synuclein-synaptosomal membrane interactions: implications for fibrillogenesis. *European journal of biochemistry / FEBS* **2004**, *271*, 3180-3189.

(69)   Perrin, R. J.; Woods, W. S.; Clayton, D. F.; George, J. M. Exposure to long chain polyunsaturated fatty acids triggers rapid multimerization of synucleins. *The Journal of biological chemistry* **2001**, *276*, 41958-41962.

(70)   Ruzafa, D.; Varela, L.; Azuaga, A. I.; Conejero-Lara, F.; Morel, B. Mapping the structure of amyloid nucleation precursors by protein engineering kinetic analysis. *Physical chemistry chemical physics : PCCP* **2014**, *16*, 2989-3000.

(71)   Ruzafa, D.; Conejero-Lara, F.; Morel, B. Modulation of the stability of amyloidogenic precursors by anion binding strongly influences the rate of amyloid nucleation. *Physical chemistry chemical physics : PCCP* **2013**, *15*, 15508-15517.

(72)   Uversky, V. N. A protein-chameleon: conformational plasticity of alpha-synuclein, a disordered protein involved in neurodegenerative disorders. *Journal of biomolecular structure & dynamics* **2003**, *21*, 211-234.

(73)   Uversky, V. N.; Fink, A. L. Conformational constraints for amyloid fibrillation: the importance of being unfolded. *Biochimica et biophysica acta* **2004**, *1698*, 131-153.

(74)   Fink, A. L. The aggregation and fibrillation of alpha-synuclein. *Accounts of chemical research* **2006**, *39*, 628-634.

(75)   Bussell, R., Jr.; Eliezer, D. A structural and functional role for 11-mer repeats in alpha-synuclein and other exchangeable lipid binding proteins. *Journal of molecular biology* **2003**, *329*, 763-778.

(76)   Munishkina, L. A.; Fink, A. L.; Uversky, V. N. Accelerated fibrillation of alpha-synuclein induced by the combined action of macromolecular crowding and factors inducing partial folding. *Current Alzheimer research* **2009**, *6*, 252-260.

(77)   Wu, K. P.; Weinstock, D. S.; Narayanan, C.; Levy, R. M.; Baum, J. Structural reorganization of alpha-synuclein at low pH observed by NMR and REMD simulations. *Journal of molecular biology* **2009**, *391*, 784-796.

(78)   Knowles, T. P.; Waudby, C. A.; Devlin, G. L.; Cohen, S. I.; Aguzzi, A.; Vendruscolo, M.; Terentjev, E. M.; Welland, M. E.; Dobson, C. M. An analytical solution to the kinetics of breakable filament assembly. *Science* **2009**, *326*, 1533-1537.

(79)   Palecek, E.; Ostatna, V.; Masarik, M.; Bertoncini, C. W.; Jovin, T. M. Changes in interfacial properties of alpha-synuclein preceding its aggregation. *The Analyst* **2008**, *133*, 76-84.

(80)   Ferreon, A. C.; Deniz, A. A. Alpha-synuclein multistate folding thermodynamics: implications for protein misfolding and aggregation. *Biochemistry* **2007**, *46*, 4499-4509.

(81)   Ferreon, A. C.; Gambin, Y.; Lemke, E. A.; Deniz, A. A. Interplay of alpha-synuclein binding and conformational switching probed by single-molecule fluorescence. *Proceedings of the National Academy of Sciences of the United States of America* **2009**, *106*, 5645-5650.

(82)   Chandra, S.; Chen, X.; Rizo, J.; Jahn, R.; Sudhof, T. C. A broken alpha -helix in folded alpha -Synuclein. *The Journal of biological chemistry* **2003**, *278*, 15313-15318.

(83)   Ducas, V. C.; Rhoades, E. Investigation of intramolecular dynamics and conformations of alpha-, beta- and gamma-synuclein. *PloS one* **2014**, *9*, e86983.

(84)   Jain, N.; Bhasne, K.; Hemaswasthi, M.; Mukhopadhyay, S. Structural and dynamical insights into the membrane-bound alpha-synuclein. *PloS one* **2013**, *8*, e83752.

(85)   Lokappa, S. B.; Suk, J. E.; Balasubramanian, A.; Samanta, S.; Situ, A. J.; Ulmer, T. S. Sequence and Membrane Determinants of the Random Coil-Helix Transition of alpha-Synuclein. *Journal of molecular biology* **2014**.

(86)   Maltsev, A. S.; Ying, J.; Bax, A. Impact of N-terminal acetylation of alpha-synuclein on its random coil and lipid binding properties. *Biochemistry* **2012**, *51*, 5004-5013.

(87)   Savage, M. J.; Lin, Y. G.; Ciallella, J. R.; Flood, D. G.; Scott, R. W. Activation of c-Jun N-terminal kinase and p38 in an Alzheimer's disease model is associated with amyloid deposition. *The Journal of neuroscience : the official journal of the Society for Neuroscience* **2002**, *22*, 3376-3385.

(88)   Uversky, V. N. Alpha-synuclein misfolding and neurodegenerative diseases. *Current protein & peptide science* **2008**, *9*, 507-540.

(89)   Li, J.; Uversky, V. N.; Fink, A. L. Effect of familial Parkinson's disease point mutations A30P and A53T on the structural properties, aggregation, and fibrillation of human alpha-synuclein. *Biochemistry* **2001**, *40*, 11604-11613.

SUPPLEMENTARY MATERIAL

Figure S1. The secondary structure of WT and N-acetylated a-Syn by far UV CD in absence of SDS. *The colors used are red for aSyn and blue for the Nac-aSyn*
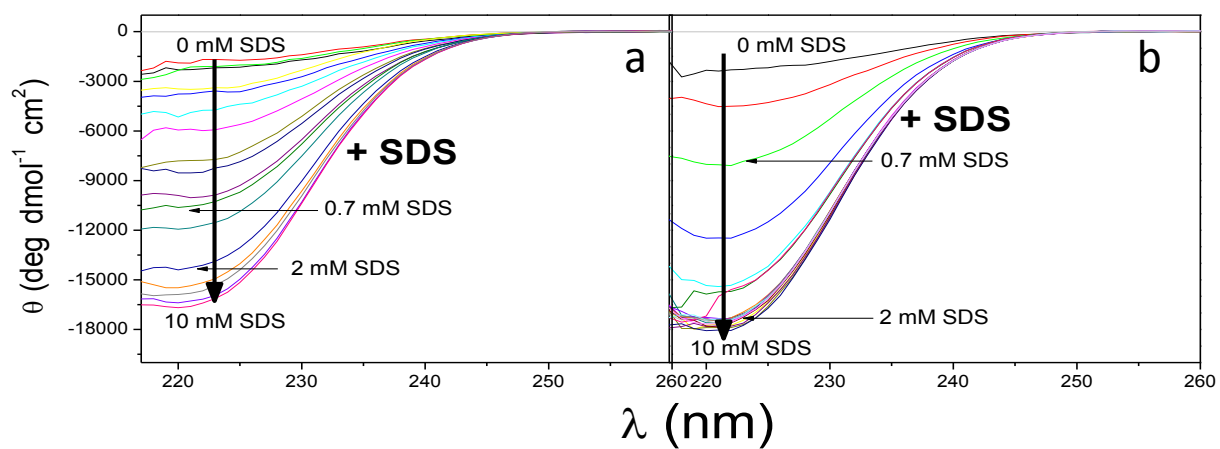
Figure S2. Effect of SDS in the secondary structure of WT and N-acetylated a-Syn by far UV CD. *Experiments were made at 25°C, the protein concentration was 100 μM and the SDS concentration range was 0-10 mM SDS. The spectrum of the experimental buffer is shown in grey.*
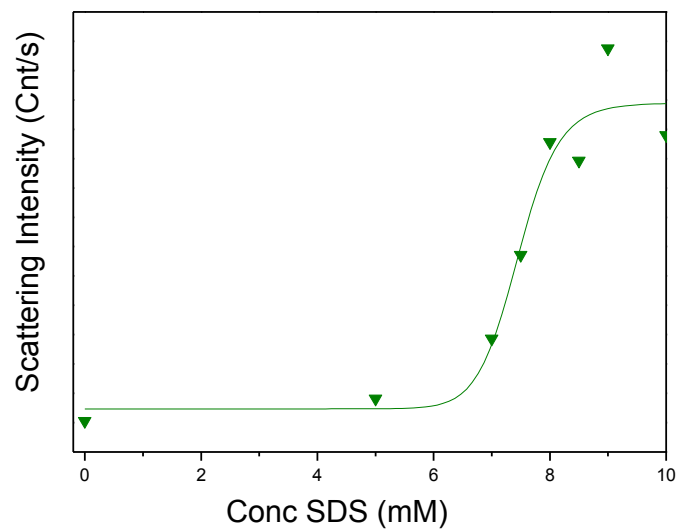
Figure S2. . Effect of the SDS concentration on the scattering of buffer free of aSyn. *The green line corresponds to the best fit to a logistic function*.

The CMC determined is 7.45 ± 0.19 mM SDS.
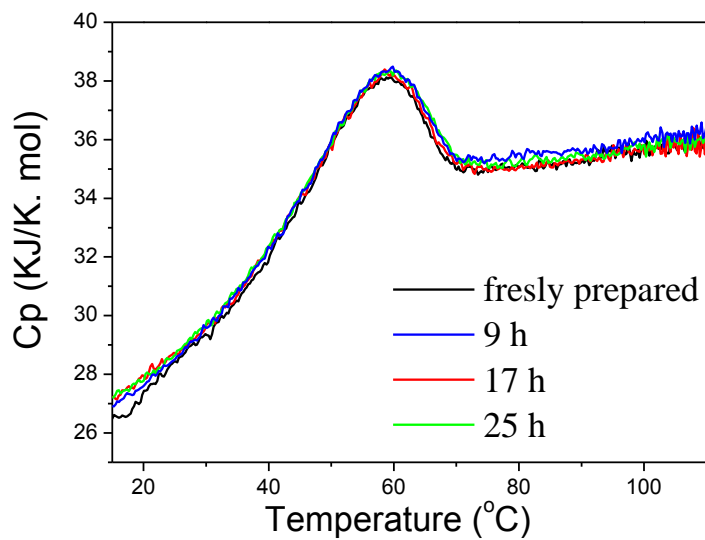
Figure S3. Repetitive DSC experiments of WT α-Syn at 4ºC. *Experiments were carried out at 60 μM protein concentration in 0.7 mM SDS, 20 mM HEPES, 0.05% NaN₃, and pH 7.2 at a scan rate of 120 K/min.*

Chapter 6

SUMMARY AND CONCLUSIONS

RESUMEN Y CONCLUSIONES

SUMMARY

This thesis project can be divided in several successive stages, which are summarized in the next paragraphs.

A first part includes a detailed study of the early stages of aggregation of the Spc-SH3 domain, specifically its N47A mutant. We have shown that the kinetics of amyloid nucleation of the Spc-SH3 domain obeys to a high-order irreversible kinetics. The analysis of the aggregation kinetics by a variety of biophysical methods has allowed us to infer that the earliest stages of amyloid nucleation process imply a pre-equilibrium involving oligomerization of a partially unfolded intermediate followed by a conformational conversion of the polypeptide chain within the oligomers. The latter process leads to formation of the amyloid nuclei. A simple mathematical model can accounts very well for the experimental initial rates of aggregation and their dependence with the concentration of protein. The model has allowed us to derive thermodynamic magnitudes characterizing the highly unstable amyloidogenic intermediate and its oligomers. It is also shown that environmental conditions, such as protein or salt concentration, can strongly affect the stability and population of the aggregation precursors, leading to different nucleation scenarios that may in turn result in different aggregation pathways and fibril morphologies. This kinetic approach might be applicable to characterize the amyloidogenic intermediates and oligomeric precursors of amyloid aggregation in disease-related proteins.

Subsequently, using this model, we have studied the effects of different salts ions on the aggregation kinetics of the N47A mutant of the Spc-SH3 domain. In this work, we have shown that anions can have a drastic effect on the rate of nucleation of amyloid fibrils, whereas cations do not have an important role under the experimental conditions used. The thermodynamic and kinetic magnitudes related to the nucleation process derived from the experimental aggregation kinetics have allowed us identifying the specific molecular events of amyloid nucleation that become modulated by anions. The energy of a low-populated amyloidogenic intermediate is reduced by the activity of anions in solution, increasing its population. We concluded that preferential anion binding plays a crucial role in stabilizing the precursors of nucleation thus accelerating the subsequent fibrillation processes. These

results increase our understanding of the earliest dynamic molecular events triggering the amyloid aggregation cascade. The possibility to control the rate of protein self-assembly by modulating the stability of the species populated during the process is important to understand the pathogenesis of the amyloid-related diseases.

After investigating of the effects of the protein environment on the early aggregation steps, we moved to a study of the effects of protein mutations. A set of residues was mutated in order to produce local stability changes covering all the structural elements of the Spc-SH3 domain. Surprisingly, there is a lack of correlation between the thermodynamic stability of the native state and the propensity to form amyloid fibrils for all the mutants. Instead, our results have demonstrated that the inhibitory or potentiating effect of amyloid aggregation exerted by the mutations is mainly related to the relative efficiency in the formation of early dynamic oligomers, which precedes the formation of amyloid nuclei. A robust kinetic and thermodynamic analysis on the basis of our previously developed nucleation model has allowed us to identify which residues play an important role in the structure of the amyloidogenic intermediate state and later on participate in its intermolecular self-association process. It appears that the conformational transition leading to amyloid nucleation follows a completely different pathway to that of the folding-unfolding process and involves partial unfolding of the domain core and intermolecular association mediated by the unfolded N-terminal strand. Taken together, these insights provide a deeper understanding of the fundamental forces that control the competition between folding, misfolding and aggregation. Such understanding undoubtedly enriches the framework for the development of rational strategies for the design of therapeutic compounds able to influence steps in the complex self-association processes so as to reduce the risk of misfolding events.

Finally, once we have developed a robust methodology to analyse the kinetics and thermodynamic determinants of amyloid nucleation using the Spc-SH3 domain as a model protein, the next logical step was to study a disease-related protein system. In this work we have chosen α-synuclein (aSyn), which is related with Parkinson's disease. Due to the functional involvement of aSyn in interactions with lipids and membranes, we have focused our study on the interaction of α-synuclein with SDS, a well-known surfactant often used as

a membrane mimetic model. To increase even more the biological relevance of our study, since aSyn is found N-acetylated in vivo, a comparison between the N-acetylated and unacetylated forms of the protein was carried out. We have demonstrated that at sub-CMC concentrations SDS stabilizes partially folded and dynamic oligomers of α-synuclein. These oligomers constitute optimal species for spontaneous and efficient formation of amyloid nuclei, which further drive lag-free amyloid fibrillation. In contrast, at higher SDS concentrations, aSyn interacts with SDS micelles, which protect the protein from aggregation. Although N-acetylation of α-Syn does not produce significant changes in the unstructured conformation of the protein in solution, we have provided evidence that acetylation increases the affinity for SDS micelles. This causes a decrease in the population of oligomeric species and, therefore, reduces significantly the amyloidogenic propensity. These results establish a solid basis, on top of which a more extensive analysis of the aggregation kinetics of aSyn can be carried out, similarly to what we have made with the Spc-SH3 domain. The finding of lag-free, rapidly nucleating aggregation kinetics will allow us the application of our nucleation model with the aim of extracting kinetic and thermodynamic magnitudes characterizing the key amyloidogenic precursors.

The potential impact of our methodology of analysis is huge. This is one of the few studies in which thermodynamic properties relevant to aggregation precursors have been provided. This allows us to evaluate how and to what extent these properties become affected when an alteration over the system is produced. In the same way, besides the effects of salt ions and mutations, many other factors can be studied such as pH, solvents (and cosolvents) or the addition of inhibitors/activators. Additionally, as the mathematical complexity of our nucleation model is not excessively high, it allows us to obtain fast results with low computational time.

On the other hand, our methodology has some limitations. A previous extensive analysis of the system is required, particularly in order to find the conditions of lag-free fast nucleation where our model is applicable. This necessary condition also limits the range of analyzable experimental conditions. Despite these limitations, our methodology has revealed as a powerful tool for the study of the aggregation mechanism of disease-related proteins and its

risk factors, in particular to characterize the early oligomeric forms, which are responsible of the cytotoxic effects related to these pathologies.

CONCLUSIONS

Finally, the most relevant conclusions drawn in this thesis are enumerated below:

1- We have been able to elucidate the molecular details of the mechanism of the earliest stages of amyloid fibril formation using the N47A mutants of Spc-SH3 domain as a model system. The aggregation kinetics obey to a high-order process that can be explained by the presence of a fast oligomerization preequilibrium followed by a conformational conversion that leads to amyloid nucleation.

2- On the basis of the mechanistic information obtained, we have developed a mathematical model that describes quantitatively the initial aggregation rates of the Spc-SH3 domain. The model has allowed us to derive thermodynamic magnitudes characterizing the highly unstable amyloidogenic intermediate and its dynamic oligomers.

3- We have determined that anions play a drastic effect on the rate of nucleation of amyloid fibrils of the Spc-SH3 domain. Preferential binding of anions decreases the energy of an amyloidogenic intermediate stabilizing the precursors of nucleation, thus accelerating the subsequent fibrillation processes, whereas cations do not have an important role under the experimental conditions analyzed.

4- Using mutations covering all the structural elements in the protein, we have demonstrated that their effect on amyloid formation is mainly related to the relative efficiency in the formation of early dynamic oligomers, which precedes the formation of amyloid nuclei.

5- The analysis of the initial rates based on our kinetic nucleation model allowed us to extract thermodynamic magnitudes of the precursor states of nucleation and map the structure of the amyloidogenic precursors. This structure differs from that of the folding transition state of the SH3 domains.

6- We have demonstrated that at sub-CMC concentrations SDS interacts with α-synuclein stabilizing partially-folded and dynamic oligomers that constitute optimal species for spontaneous and efficient formation of amyloid nuclei, which further drive lag-free amyloid fibrillation. In contrast, binding of aSyn to SDS micelles protects aSyn from amyloid aggregation.

7- N-acetilation of α-synuclein increases the affinity for SDS micelles, causing a decrease in the population of oligomeric species and, therefore, reducing the amyloidogenic propensity.

Future Work

This thesis has establish a solid basis to continue with the research in amyloid aggregation of a disease-related protein, such as aSyn, in particular in the application of our nucleation model to SDS-induced aSyn aggregation with the aim of further understanding the kinetics and thermodynamics conformational and oligomerization steps that are crucial to the primary nucleation process. In this respect, we would like to continue several further work lines:

On the one hand, we will continue the investigation of the interactions between SDS and aSyn (both in acetylated and non acetylated forms), increasing the amount and variety of experimental data at different SDS and protein concentrations.

The SDS-induced aSyn fibrillation kinetics could be amenable to a quantitative analysis using the nucleation model developed in this thesis. We also expect to extend this study to the study of aSyn mutants related to the early development of Parkinson's disease.

On the other hand, it would also be interesting for us to study other factors that affect over the amyloid aggregation such as, the interactions with other lipids or surfactant molecules, the inhibition/activation (using peptides and small molecules) or the effect of other environmental factors (pH, polarity of the solvent, different salt ions), looking specifically at their effects on the thermodynamics and mechanism of the process.

Complementary training activities

In January 2011, a short training period of a month was carried out under the supervision of Dr. Kerensa Broersen in the SWITCH Laboratory (Brussels, Belgium), centered on learning the purification and preparation protocols of α-synuclein and several mutants related to early-onset Parkinson's disease,.

A three-month period (April-June 2013) was also spent at Yale University (USA) in the research group of Professor Andrew Miranker. The main research topic was the study of the capacity of the oligomeric forms of the unmodified and N-acetylated α-synuclein variants to induce pores in membranes.

This thesis project has presented the work carried out during the last 4 years as holder of a grant "Formación de Profesorado Universitario (FPU)" awarded by the Spanish Ministry of Education, Culture and Sport.

RESUMEN

Este proyecto de tesis se puede dividir en varias etapas sucesivas, que se resumen en los siguientes párrafos.

Una primera parte de este trabajo incluye un estudio detallado de los estados iniciales de agregación del dominio Spc-SH3, concretamente empleamos su mutante N47A. Hemos mostrado que las cinéticas de nucleación del dominio Spc-SH3 obedecen a una cinética irreversible de orden superior. El estudio las cinéticas de agregación, empleando multitud de

métodos biofísicos, nos ha permitido deducir que los estados iniciales del proceso de nucleación amiloide implica un pre-equilibrio que incluye la oligomerización de intermedios parcialmente plegados seguida de una conversión conformacional de las hebras polipeptídicas entre los oligómeros. Este último proceso conduce a la formación de núcleos amiloides. Un modelo matemático simple puede describir muy bien los resultados experimentales de velocidad inicial de agregación y su dependencia con la concentración de proteína. El modelo nos ha permitido obtener magnitudes termodinámicas para caracterizar el altamente inestable intermediario amiloidogénico y sus oligómeros. También se ha mostrado que las condiciones ambientales, como la concentración de proteína y la concentración de sal, pueden afectar fuertemente en la estabilización y población de los precursores de la agregación, dando lugar a las diferentes condiciones de nucleación que pueden producir dos distintos mecanismos de agregación y asimismo producir las diferentes morfologías de las fibras. La aproximación cinética presentada aquí puede ser aplicable para caracterizar los intermedios amiloidogénicos y los precursores oligoméricos de la agregación amiloide en proteínas relacionadas con enfermedades.

Subsecuentemente, empleando este modelo, nos embarcamos al estudio del efecto de las sales en las cinéticas de agregación del mutante N47A del dominio Spc-SH3. En este estudio mostramos que los aniones presentaban un efecto drástico en la velocidad de nucleación, mientras que los cationes no presentaban un papel importante en las condiciones del estudio. Las magnitudes relacionadas con la termodinámica y cinética en el proceso de nucleación obtenidas de las cinéticas de agregación nos permiten identificar que se ven moduladas por los aniones. La energía de un estado intermediario amiloidogénico poco poblado se ve reducida por la actividad de aniones en disolución, aumentando su población, acelerando subsecuentemente el proceso de fibrilación. Este resultado incrementa nuestro conocimiento de los dinámicos estados tempranos implicados en el desencadenamiento de la cascada de agregación amiloide. Este control sobre la velocidad de agregación ejercida por la modulación de la estabilidad de las especies pobladas mediante el uso de sales nos brinda la posibilidad aumentar nuestro conocimiento de la patogénesis de las enfermedades relacionadas con amiloides.

Una vez investigados los efectos ambientales en las etapas iniciales de la agregación, pasamos a estudiar los efectos de las mutaciones en la proteína. Para ello empleamos un conjunto de mutaciones a lo largo de todos los elementos estructurales del dominio Spc-SH3 para producir cambios locales en la estabilidad. Sorprendentemente, existe una notable falta de correlación entre la estabilidad termodinámica del estado nativo y la tendencia a formar fibras amiloides para todos los mutantes. En su lugar encontramos que la inhibición y la potenciación de la agregación amiloide ejercida por las mutaciones se produce principalmente a nivel de una modificación en la eficiencia efectiva en la formación de los dinámicos oligómeros iniciales que preceden al proceso de formación de núcleos amiloide. Un análisis robusto de las cinéticas y de la termodinámica, y basándonos en el modelo de nucleación que previamente habíamos desarrollado, nos ha permitido identificar los residuos que juegan un papel importante en la estructura del estado intermediario amiloidogénico y participan en su proceso de auto-asociación intermolecular. Parece que la transición conformacional que da lugar a la nucleación amiloide sigue un mecanismo completamente diferente al que se produce en los procesos de plegamiento-desplegamiento e implica el desplegamiento parcial del núcleo del dominio y que la asociación intermolecular se produce vía el extremo N-terminal de la cadena. Tomados juntos, estos indicios proporcionan un profundo entendimiento sobre las fuerzas fundamentales que controlan la competición entre plegamiento, plegamiento erróneo y agregación. Esta comprensión indudablemente enriquece el conocimiento fundamental para el desarrollo de estrategias racionales para el diseño de compuestos terapéuticos capaces de interferir en los complejos procesos de auto-asociación, de tal forma que se reduzca el riesgo de que se produzca plegamiento erróneo en las proteínas.

Finalmente, una vez desarrollada una robusta metodología para analizar las cinéticas y la termodinámica que determina la nucleación de amiloides usando el sistema Spc-SH3 como proteína modelo, el siguiente paso lógico era estudiar un sistema en la que la proteína esté relacionada con el desarrollo de enfermedades. En este trabajo hemos seleccionado la α-Sinucleina (aSyn), una proteína relacionada con el mal de Parkinson. Debido a las implicaciones funcionales de la aSyn en interacción con lípidos y surfactantes aniónicos, hemos centrado nuestro estudio en la interacción de la aSyn con SDS, un conocido

surfactante empleado como modelo mimético de una membrana. Para darle aún más relevancia biológica a nuestro estudio, dado que la aSyn se encuentra N-acetilada *in vivo,* hemos comparado las formas N-acetilada y sin modificar de la aSyn. Hemos demostrado que a una concentración sub-CMC de SDS se estabiliza una forma oligomérica y parcialmente plegada de aSyn. Estos oligómeros constituyen especies óptimas para la formación espontánea y eficiente de núcleos amiloides, que conducen a una fribrilación amiloide rápida, libre de tiempo de espera de nucleación. En contraste, a una concentración mayor de SDS, la aSyn interactúa con micelas de SDS, que evitan que se produzca la agregación. Aunque la forma N-acetilada de la aSyn no produce cambios significativos en la forma desplegada en disolución, hemos mostrado evidencias de que la acetilación incrementa la afinidad por las micelas de SDS. Esto produce una disminución de la población de oligómeros y, asimismo, reduce significativamente la tendencia a formar amiloides. Estos resultados establecen una base sólida sobre la que un análisis más extenso de las cinéticas de agregación puede ser llevado a cabo, de forma similar al que hemos realizado con el dominio Spc-SH3. El encuentro de unas condiciones en las que se produce una cinética de agregación en condiciones de nucleación rápida, libres de tiempos de espera de nucleación, nos permite aplicar nuestro modelo de nucleación con el objetivo de extraer magnitudes cinéticas y termodinámicas que caractericen los precursores clave en la amiloidogénesis.

El impacto potencial que tiene el desarrollo de esta metodología es enorme. Este es uno de los pocos estudios que proporcionan propiedades termodinámicas relevantes de los precursores de la agregación. Esto permite evaluar cómo y a qué nivel se producen las alteraciones sobre las propiedades del sistema. De la misma forma, además del efecto de las sales iónicas y las mutaciones, muchas otras variables se podrían evaluar, como son el pH, el efecto del disolvente (cosolventes) o la adición de compuestos inhibidores o activadores. Asimismo la complejidad matemática de nuestro modelo de nucleación no es excesiva y permite la obtención rápida de información con un bajo tiempo cómputo.

Por otro lado, nuestra metodología presenta algunas limitaciones. Es necesaria una importante cantidad de información previa a nivel de preparación de las muestras para estar en las condiciones de nucleación rápida, sin tiempos de espera de nucleación, en las que

nuestro modelo sea aplicable. Esto mismo limita el rango de condiciones experimentables analizables. A pesar de estas limitaciones, nuestra metodología se revela como una potente herramienta para el estudio del mecanismo de agregación de proteínas relacionadas con enfermedades y sus factores de riesgo, en especial para caracterizar sus formas oligoméricas iniciales que, como ya hemos mencionado, son las responsables de los efectos citotóxicos relacionados con esas patologías.

CONCLUSIONES

Finalmente, para resumir, presentamos las conclusiones principales del proyecto de tesis:

1- Hemos sido capaces de elucidar los detalles moleculares del mecanismo de formación de fibras amiloides en sus etapas más tempranas usando el sistema modelo, el dominio Spc-SH3. Las cinéticas de agregación obedecen a las de un proceso de orden superior que puede ser explicado por la presencia de un rápido pre-equilibrio de oligomerización seguido por una conversión conformacional que da lugar a la nucleación de amiloides.

2- Usando la información mecanística obtenida, hemos desarrollado un modelo matemático que describe cuantitativamente las velocidades iniciales de agregación del dominio Spc-SH3. El modelo nos permite obtener magnitudes termodinámicas para caracterizar los intermediarios amiloidogénicos altamente inestables y sus dinámicos oligómeros.

3- Hemos determinado que los aniones presentaban un efecto drástico en la velocidad de nucleación de las fibras amiloides del dominio Spc-SH3. La unión preferente de los aniones disminuye la energía de un estado intermediario amiloidogénico, aumentando su población, y acelerando subsecuentemente el proceso de fibrilación,

mientras que los cationes no presentaban un papel importante en las condiciones del estudio

4- A través de mutaciones a lo largo de todos los elementos estructurales de la proteína modelo, hemos demostrado que los efectos sobre la agregación amiloide se producen principalmente a nivel de una modificación en la eficiencia efectiva en la formación de los dinámicos oligómeros iniciales que preceden al proceso de formación de núcleos amiloide.

5- El análisis de las velocidades iniciales basado en nuestro modelo cinético de nucleación nos permite extraer magnitudes termodinámicas de los estados precursores de la nucleación y caracterizar la estructura de los precursores amiloidogénicos. Esta estructura difiere de la que se produce en el estado de transición durante el proceso de plegamiento del dominio Spc-SH3.

6- Hemos demostrado que las concentraciones sub-CMC de SDS interaccionan con α-Sinucleina estabilizando los estados parcialmente plegados y oligómeros dinámicos, que constituyen especies óptimas para la formación espontánea y eficiente de núcleos amiloides, que conducen a una fibrilación amiloide rápida libre de tiempo de espera de nucleación. Por el contrario, la unión de α-Sinucleina a micelas de SDS evita que se produzca la agregación amiloide.

7- La forma N-acetilada de la α-Sinucleina incrementa la afinidad por las micelas de SDS produciendo una disminución de la población de oligómeros y, asimismo, reduciendo la tendencia a formar amiloides.

Trabajo futuro

Esta tesis ha establecido una base sólida para continuar con la investigación en la agregación de amiloides sobre proteínas relacionadas con enfermedades, como la α-Synucleina, en

particular en la aplicación de nuestro modelo de nucleación a la agregación de aSyn inducida por SDS con el objetivo de obtener un mayor conocimiento de las cinéticas y termodinámicas conformacionales y de las etapas de oligomerización, que son cruciales en las primeras etapas del proceso de nucleación. A este respecto, nos gustaría continuar con varias líneas de trabajo:

Por un lado, continuaremos con la investigación de la interacción entre el SDS y la aSyn (en su forma acetilada y sin modificar), lo que implica aumentar la cantidad y la variedad de los datos experimentales a diferente concentración de SDS y proteína.

Las cinéticas de fibrilación de aSyn inducida por SDS pueden ser susceptibles para llevar a cabo el análisis cuantitativo empleando el modelo de nucleación desarrollado en esta tesis. También esperamos extender este estudio a los mutantes relacionados con el desarrollo precoz del mal de Parkinson.

Por otro lado, también esta propuesto el estudio de otros factores que afectan al proceso de agregación como la interacción con otros lípidos o surfactantes, la inhibición/activación (usando péptidos y pequeñas moléculas) o la modificación de otros factores ambientales (pH, polaridad del disolvente, diferentes sales), mirando específicamente sus efectos termodinámicos y mecanísticos sobre el proceso.

Actividades complementarias de formación

En enero de 2011, durante un mes se realizó un corto periodo de apredizaje bajo la supervisión de la Dra. Kerensa Broersen en el SWITCH Laboratory (Bruselas, Bélgica), centrado en el aprendizaje de la purificación y protocolos de preparación de α-Sinuclein y varios mutantes relacionados con el desarrollo precoz del mal de Parkinson.

Una estancia de tres meses (abril a junio de 2013) fue realizada en la universidad de Yale (USA) en el laboratorio del Prof. Andrew Miranker. El tema principal de la investigación fue un estudio sobre la capacidad de los oligómeros de α-Synuclein sin modificar y de su variante N-acetilada para inducir poros en membranas.

En este proyecto de tesis presentamos el trabajo realizado durante los últimos 4 años durante los que he disfrutado de beca Formación de Profesorado Universitario (FPU) concedida por el Ministerio de Educación, Cultura y Deporte.

APPENDIX A: ABBREVIATIONS

ThT	Thioflavin T
ANS	1-Anilino-8-Naphthalene Sulfonate
E. coli	Escherichia coli
Spc-SH3	SH3 domain of α-Spectrin
UV	Ultraviolet
CD	Circular dichroism
NMR	Nuclear Magnetic Resonance
WT	Wild Type
DLS	Dynamic light scattering
ATR-FTIR	Attenuated total reflectance Fourier-transform infrared
DSC	Differential scanning calorimetry
C_p	Partial molar heat capacity curves
SEC	Size-exclusion chromatography
FPLC	Fast protein liquid chromatography
TEM	Transmission electron microscopy
t	Time
R_h	Hydrodynamic radii
C_0	Total protein concentration
N	Native monomeric state
I	Intermediate monomeric state
U	Unfolded monomeric state
F_i	Oligomeric amyloid nuclei
C_F	Concentration of protein monomers in amyloid states
A_i	Oligomers of i size
r_0	Initial rate
ΔG_U	Unfolding Gibbs energy related to the native state
ΔG_I	Gibbs energy of the intermediate related to the native state
N_A	Concentration of oligomer at a particular time
N_F	Concentration of amyloid particles at a particular time

K_I	Equilibrium constant between the native and the intermediate states.
K_U	Equilibrium constant between the native and the fully unfolded states
K_A	Equilibrium constant of oligomerization
k_E	First order rate constant of conformational conversion of the dynamic oligomer into the amyloid structure
MSTI	Molal surface tension increment
DNA	Deoxyribonucleic acid
HEPES	4-(2-Hydroxyethyl)-1-piperazineethanesulfonic acid
aSyn	α-Synuclein
SDS	Sodium dodecyl sulfate
PD	Parkinson's disease
NCC	Nucleated conformational conversion
Nac	N-Acetylated
Ve	Elution volume
CMC	Critical Micellar Concentration